Genesis, Phototoxicity and Degradation of Retinal Lipofuscin

Matthew Davies

A thesis submitted to Cardiff University in accordance with the requirements for the degree of Doctor of Philosophy in the disciplines of Biochemistry and Cell Biology

Visual Neuroscience and Molecular Biology Group
School of Optometry and Vision Sciences
Cardiff University

ProQuest LLC
789 East Eisenhower Parkway
P.O. Box 1346
Ann Arbor, MI 48106-1346

Form: PGR_Submission_200701

NOTICE OF SUBMISSION OF THESIS FORM: POSTGRADUATE RESEARCH

APPENDIX 1:
Specimen layout for Thesis Summary and Declaration/Statements page to be included in a Thesis

DECLARATION

This work has not previously been accepted in substance for any degree and is not concurrently submitted in candidature for any degree.

Signed .....M Davis..... (candidate) Date .....24/4/09....

STATEMENT 1

This thesis is being submitted in partial fulfillment of the requirements for the degree of .....PhD.....(insert MCh, MD, MPhil, PhD etc, as appropriate)

Signed .....M Davis..... (candidate) Date ....24/4/09....

STATEMENT 2

This thesis is the result of my own independent work/investigation, except where otherwise stated. Other sources are acknowledged by explicit references.

Signed .....M Davis..... (candidate) Date .....24/4/09..

STATEMENT 3

I hereby give consent for my thesis, if accepted, to be available for photocopying and for inter-library loan, and for the title and summary to be made available to outside organisations.

Signed .....M Davis..... (candidate) Date .....24/4/09...

Acknowledgments

Acknowledgments

Reaching this stage of my PhD seems to have taken a long time, and has required a lot of hard work and dedication. Without the considerable support and good advice that I have received during this time I would not have reached this point.

Firstly, I would like to heartily thank my supervisor Prof. Mike Boulton for his patience, wisdom and wicked sense of humour. Each were ever present when in Cardiff and later from the US. Equally, I admire him for always being gracious in defeat (Wales vs England '05, '07 and '08) and managing to convince me that I was having fun whilst spending the past three years of my life chained to a lab bench. Secondly, I would also like to thank my other supervisor, Dr. Malgorzata Rozanowska, for her advice throughout and continued faith in me.

I have had the opportunity to work with many gifted people, too numerous to mention in one short page, during this project. My gratitude goes out to all that have assisted me along the journey. In particular, I would like to mention Dr. K-P Ng and Dr. John Crabb from the Cole Eye Institute, Cleveland, Drs.Alison Paul and Simon Richardson from the Welsh School of Pharmacy and Dr. Anthony Hann from Cardiff Biosciences. Also, I wish all the best to those from the School of Optometry in Cardiff who have spared the time to pass on their knowledge, including: Drs. Jun Cai, Andrew Hollins, Rob Young, BoP and Peter Wu. A special mention goes out to Dr. Stuart Gordon Jarrett who it was my pleasure to work with and buy a beer for (regularly).

A big thanks is due to all the post-grad members of room 2.64 in Redwood and those scattered around the 'New Building' for their support and ideas, but essentially for making my time in Cardiff so pleasurable. I would particularly like to thank: Jack, Miguel, Rishi, Phil, Jen, Debs, Llinos, Kat, Flick, Diti, Bablin, Aihua and Gosia for all their intellectual and moral support and great sense of humour. I should also single out Yadan for her encouragement, advice and unique attitude. Thanks also to the School staff who are always ready to help, in particular Steve, Sue, Rob, John and Phil.

A special thank you to my monthly meeting pals, Kinga Handzel, for bringing an air of elegance to proceedings and Linda Bakker, for providing me with hard-hitting wisdom and technical know-how, but more importantly always being there to help, seemingly without being asked.

I would like to thank my parents, sister and brother for their encouragement and support that provided the motivation for me to get through even the hardest days, for this I will always be grateful.

Finally, I would like to thank Kath for being my constant pillar of reassurance or composure according to the situation and for always being there when needed.

Abstract

Retinal lipofuscin (RLF) is an intra-lysosomal accumulating waste product thought to be composed of oxidatively modified lipids and proteins. The substrates are proposed to be derived from old or damaged organelles and phagocytosed photoreceptor outer segments (POS). The material that is not degradable by retinal pigment epithelium (RPE) lysosomes accumulates within the cell and has the capacity to photogenerate reactive oxygen species. Consequently, the accumulation of RLF within RPE cells has been linked to cell dysfunction and the onset of age-related macular degeneration (AMD) and other retinal degenerative diseases. This study sought to gain important insights into RLF composition and formation, to analyse the efficacy of optical filters in reducing photoexcitation of RLF and develop a nanomedicine with the potential to prevent RLF accumulating and/or degrade RLF accrued within RPE cells.

Ex vivo RLF granules were isolated and analysed by mass spectrometry to determine their protein content, and Western blotting to probe for oxidatively modified components. RLF was found to contain a number of molecules adducted to lipid peroxidation products and minimal protein. *In vitro* models of RLF formation were designed and their physio-chemical characteristics analysed using: spectrophotometry/fluorometry, SDS-PAGE, Western blotting, HPLC and singlet oxygen production measurements. The *in vitro* models shared a number of characteristics with *ex vivo* RLF including: the presence of species adducted to lipid peroxidation products, a protein smear on an SDS-PAGE gel and the ability to photogenerate singlet oxygen. The capability of yellow-tinted optical filters to reduce the blue-light hazard of RLF towards RPE cells was analysed using cell viability assays and fluorescence microscopy. Results showed yellow-tinted filters provided significant protection to RLF-loaded RPE cells when irradiated with blue-light compared to a UV blocking filter or no filter. The suitability of a potential nanomedicine for use in abolishing RLF from RPE cells was assessed using: fluorescence and transmission electron microscopy, cell viability assays and flow cytometry. The study succeeded in identifying a carrier molecule that was localised to the lysosomes of RPE cells and an active component capable of degrading POS. When conjugated, the nanomedicine displayed the ability to degrade accumulated RLF.

The findings presented within this study have enhanced our understanding of RLF composition and the key substrates involved in its formation. This has lead to proposals of how lipofuscin is associated with the onset of AMD. Studies conducted using UV and blue-light blocking optical filters may assist in the future design of intraocular lenses and aid ophthalmologists in advising cataract patients of the most appropriate lens for surgery. Preliminary work has been undertaken to develop a nanomedicine which has been demonstrated to eliminate RLF from the RPE *in vitro*. providing the basis for further development of a therapeutic strategy.

Abbreviations

A2E	2-[2,6-dimethyl-8-(2,6,6-trimethyl-1-cyclohexen-1-yl)-1E,3E,5E,7E-octotetraenyl]-1-(2-hydroxylethyl)-4-[4-methyl-6-(2,6,6-trimethyl-1-cyclohexen-1-yl)-1E,3E,5E-hexatrienyl]-pyridinium
A2PE	*N*-retinylidene-*N*-retinylphosphatidylethanolamine
A2PE-H2	dihydro-N-retinylidene N-retinyl phosphatidylethanolamine
ABCA4	ATP-binding cassette, sub-family A (ABC1), member 4
ABCR	ATP-binding cassette transporter
AMD	age-related macular degeneration
AMO	advanced Medical Optics
ANOVA	analysis of variance
Anti-CEP	2-(ω-carboxyethyl)pyrrole antibody
AREDS	age-related eye disease study
ARM	age-related maculopathy
ARMS2	age-related maculopathy susceptibility 2
ATCC	American Type Culture Collection
ATP	adenosine tri-phosphate
ATR	all-trans-retinal
ATR-dimer	all-trans-retinal dimer
BCA	bicinchoninic acid
BDMA	benzyldimethylamine
BHT	butylated hydroxytoluene
BM	basal medium
BSA	bovine serum albumin
BSA-TxR	bovine serum albumin Texas red
°C	degrees Celsius
CDNB	chloro-dinitro benzene
CEP	2-(ω-carboxyethyl)pyrrole
chOOH	oxidised cholesterol
CNV	choroidal neovascularisation
D_2O	heavy water
Da	Dalton
DAB	diaminobenzidine
DDSA	dodecenylsuccinic acid
dex-GST	dextrin - Glutathione s transferase
DHA	docosahexaenoic acid
DIEA	diisopropylethylamine
DMAP	4-Dimethylaminopropanol
DMF	*N,N'*-dimethyl formamide
DMSO	dimethylsulphoxide
DNA	deoxyribonucleic acid
DTT	dithiothreitol
EDC	*N*-ethyl-*N'*-(3-dimethylaminopropyl)carbodiimide
EDTA	ethylenediaminetetraacetic acid
EEA1	early endosomal associated
ELOVL4	elongation of very long chain fatty acids
EtOH	ethanol
FACS	Flow assisted cell sorting

FCS	fetal calf serum
FITC	fluorescein isothiocyanate
FTIR	fourier transform infrared spectroscopy
FPLC	fast-protein liquid chromatography
G	gauge
GA	geographic atrophy
GSH	glutathione
GST	glutathione s transferase
H_2O	water
HNE	4-hydroxynonenal
HPLC	high performance liquid chromotography
HPMA	*N*-(2-hydroxypropyl)methacrylamide
HRP	Horse-radish peroxidase
HSP	heat shock protein
HSA	human serum albumin
HTRA1	HtrA serine peptidase 1
hv	light
IgG	imunnoglobulin G
IOL	intra-ocular lenses
IRBP	interphotoreceptor retinoid binding protein
iso[4]LGE_2	iso[4]levuglandin E_2
iso-A2E	iso-2-[2,6-dimethyl-8-(2,6,6-trimethyl-1-cyclohexen-1-yl)-1E,3E,5E,7E-octotetraenyl]-1-(2-hydroxylethyl)-4-[4-methyl-6-(2,6,6-trimethyl-1-cyclohexen-1-yl)-1E,3E,5E-hexatrienyl]-pyridinium
LAMP1	lysosomal associated membrane protein
LC MS/MS	liquid chromatography mass spectrometry mass spectrometry
Lyso	lysosome
mAb	monoclonal antibody
MCT1	monocarboxylate transporter 1
MCT3	monocarboxylate transporter 3
MDA	malondialdehyde
MeOH	methanol
MerTK	mer tyrosine kinase
mins	minutes
Mito	mitochondria
MTT	3-(4,5-Dimethylthiazol-2-yl)-2,5-diphenyltetrazolium bromide
NAC	*N*-acetyl cysteine
NHS	*N*-hydroxysulfosuccinimide
NRPE	retinylidine-PE
NEM	*N*-ethyl morpholine acetate
Nd:YAG	neodymium-doped yttrium-aluminium-garnet
nY	nitrotyrosine
OG	oregon green
pAb	polyclonal antibody
PBS	phosphate buffered saline
PDT	photodynamic therapy
PE	phosphatidylethanolamine
PEDF	pigment epithelial-derived factor
PEG	poly(ethyleneglycol
POS	photoreceptor outer segment

PUFA	polyunsaturated fatty acids
PVDF	polyvinyldene fluoride
QTOF2	quadrupole time-of-flight
RCS	Royal College of Surgeon
ROI	reactive oxygen intermediates
ROS	reactive oxygen species
RPE	retinal pigment epithelium
SCX	strong cation exchange
SD	succinoylated dextrin
SDS	sodium dodecyl sulphate
SDS-PAGE	sodium dodecyl sulphate polyacrylamide gel electrophoresis
sec	seconds
SF10PF	special formula 10 photosensitiser free
SNP	single nucleotide polymorphism
SOD1	super oxide dismutase 1
SOD2	super oxide dismutase 2
TBST	tris-buffered saline Tween-20
TEM	transmission electron microscopy
TEMED	*N,N,N′,N′*-Tetramethylethylenediamine
TFA	trifluoroacetic acid
TIF	tagged image files
TLC	thin layer chromotography
TxR-BSA	texas-red bovine serum albumin
UA	uranyl acetate
UV	ultraviolet
UV-VIS	ultra-violet - visible
VEGF	vascular endothelial growth factor
VMD2	vitelliform macular dystrophy type 2

Chapter 1

General Introduction

1. The Retinal Pigment Epithelium

1.1 Structure

The retinal pigment epithelium (RPE) is a monolayer of post-mitotic cells found in the neural retina below the photoreceptor layer and overlying the Bruchs' membrane (Figure 1.1). The cells are cuboidal when viewed by cross-section, hexagonal when viewed from above and have a characteristic orange/red colour arising from the high density of pigment present. There is geographic variation in the size and shape of RPE cells throughout the retina, with cells located in the macula being columnar and roughly 10-14 μm in diameter, then growing broader and flatter towards the periphery with diameters around 60 μm (Marmor, 1998). Despite these variations in size, the number of photoreceptor outer segments (POS) opposing each RPE cell remains at approximately 45 throughout the retina, emphasising also the variation in POS density between the macula and periphery (Newsome, 1983).

RPE cells are polarised into two physiologically and biochemically separate regions, the apical and basal portions. The apical portion faces the overlying photoreceptor layer and has numerous extending microvilli. The microvilli can be distinguished into two separate types. The most numerous are those that are approximately 5-7 μm in length and function to increase surface area and thus enhance transepithelial transport. The other group of microvilli are often referred to as photoreceptor sheaths; these have two variants, one that interacts with rods, the other cones. The basal portion of the cell has a membrane that opposes the choroid. This membrane has many deep infoldings that increase the surface area of the membrane to maximise the absorption of nutrients and disposal of waste.

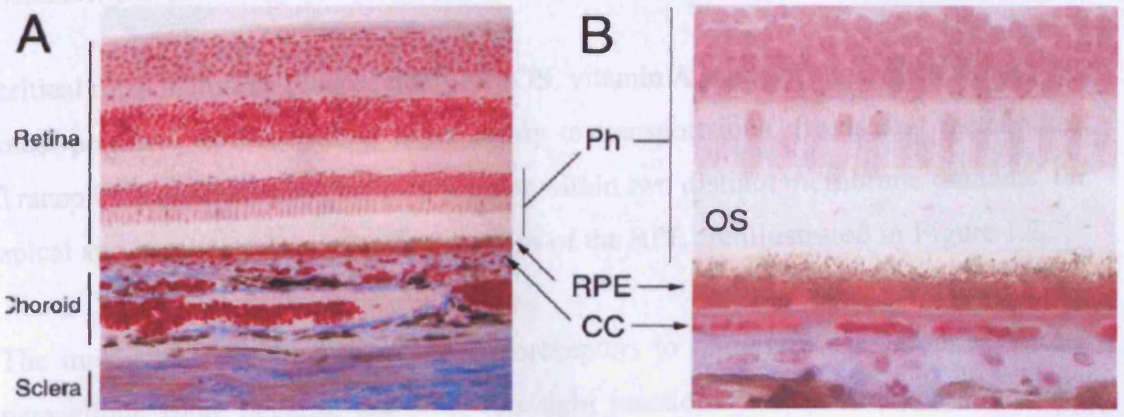

Figure 1.1. Low magnification haematoxylin and eosin image of a human eye showing the positioning of the RPE between the photoreceptor layer (Ph) and choroid (A). The higher magnification image details the microvilli that extend from the RPEs' apical side into the outer segment layer (OS) and the high density of blood vessels, the choriocapillaries (cc), present below the basal side of the RPE (**B**). (Source: (Marmorstein, 2001)

Each RPE cell is differentiated internally, with a varied distribution of organelles throughout the cell (Marmorstein, 2001). The apical section of the cell cytoplasm contains many microtubules and microfilaments and is where the greatest concentration of melanin granules accumulate. The nucleus together with the many mitochondria are located in the mid-section of the cell (Marmorstein, 2001). Lipofuscin granules progressively accumulate in the basal to mid-section of the cell (Feeney-Burns *et al.*, 1980).

The apical and basal membranes of the RPE are also differentiated with respect to the ion channels present in both (Bok, 1993). For instance there are ion pumps such as the Na+ -K+ -ATPase located on the apical membranes that are not present on the basal membrane (Defoe *et al.*, 1994). This assists transepithelial transport of molecules and metabolites to and from the blood and photoreceptors.

1.2 Function

1.2.1 Transepithelial transport

The health of neuronal cells is regulated by accessory cells such as the RPE. The RPE plays a central role in regulating the microenvironment of the photoreceptors with

critical roles including phagocytosis of POS, vitamin A transport and metabolism, but, most pertinent to this section is its ability to transport ions, fluids and metabolites. Transport is generated by proteins present within two distinct membrane domains, the apical and basal membranes. The functions of the RPE are illustrated in Figure 1.2.

The movement of water from the photoreceptors to the choroid is blocked via the paracellular route because the RPE has tight junctions. Its movement through the transcellular route is thought to be assisted by the presence of aquaporin-1 that has been detected in the RPE (Stamer *et al.*, 2003).

Transepithelial transport is important in the removal of lactic acid that is largely generated by the photoreceptors from the cells. Removal requires efficient regulation of intracellular pH and lactic acid is removed from the subretinal space by the Lactate-H+ co-transporter MCT1 and excreted from the basal membrane to the choroid by the MCT3 co-transporter (Philp *et al.*, 1998).

Essentially, the RPE transports electrolytes and water from the subretinal space to the choroid and it supplies the photoreceptors and neurons with glucose and other nutrients including docosahexaenoic acid (DHA). To achieve the transport of glucose the RPE contains a number of glucose transporters in the apical and basal membranes with both GLUT1 and GLUT3 transporters being highly expressed in the RPE (Ban and Rizzolo, 2000).

Another important function of the RPE is the transport of retinol to ensure that retinal is supplied to the photoreceptors. Most retinal is cycled between the photoreceptors and the RPE, however, the vitamin A (all-*trans*-retinol) taken up from the blood stream does add a small quantity to this process. Uptake occurs in a receptor mediated process with recognition by a serum retinol-binding protein/transthyretin complex (Pfeffer *et al.*, 1986; Ottonello *et al.*, 1987).DHA uptake into the RPE is a third type of transport into the cells. DHA is a major component of the membranes of neurons and photoreceptors as well as photoreceptor disks and cannot be synthesised by neuronal tissue, therefore, a regular supply is of great importance (Bazan *et al.*, 1990; Wang *et al.*, 1992)

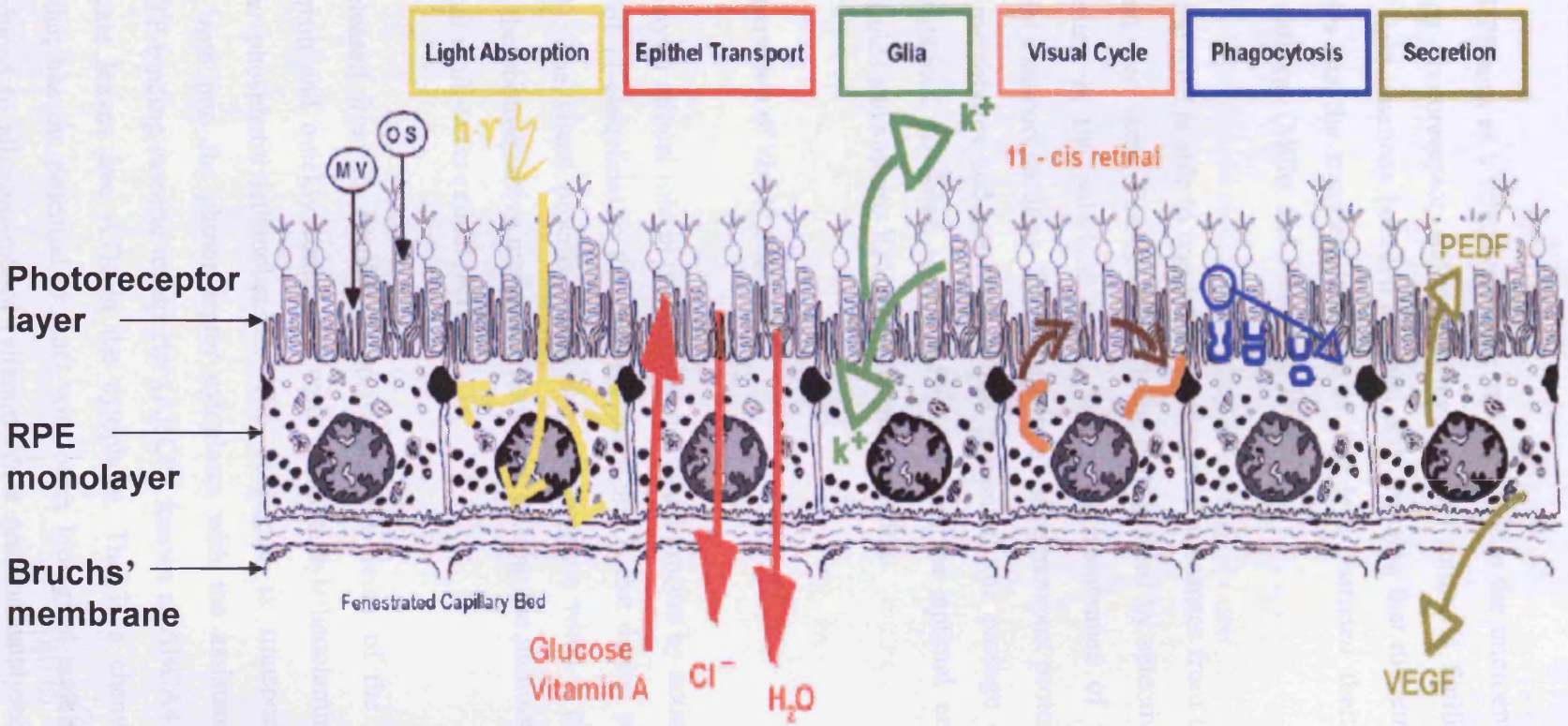

Figure 1.2 Summary of RPE cell functions. The above figure highlights the movements of; salts, nutrients, visual cycle components and signalling molecules. Also of interest are the phagocytic and light absorbing roles played by the RPE. MV = microvilli, OS = outer segment, PEDF = pigment derived epithelial factor, VEGF = vascular endothelial growth factor, K+ = potassium ion, H2O = water, Epithel transport = epithelial transport (adapted from Strauss O, 2005)

1.2.2 Blood Retinal Barrier

The RPE acts as a selective barrier and regulator to the microenvironment of the over-lying photoreceptor and neural layers. This action is facilitated by the existence of tight junctions between adjacent cells meaning that movement of fluids and molecules via the transcellular route is 10x less restricted than through the paracellular pathway (Miller and Steinberg, 1977).

In this way the RPE is able to regulate the passage of substances from the choroid to the retina and vice versa. Passage through the cell is aided by selective transporter proteins present in the polarised apical and basal membranes of the cell (see transepithelial transport section). The selectivity of these transport proteins allows the transfer of metabolites and nutrients, whilst preventing the passage of potentially harmful substances. In doing so the RPE maintains the optimal composition of intraocular fluids and sustains RPE/photoreceptor function.

1.2.3 Regeneration of visual pigment

The RPE plays a critical role in maintaining the visual process by acting to replenish the supply of 11-cis-retinal to the photoreceptors that is lost during photoactivation (Figure 1.3). The visual process begins in photoreceptors when a photon of light reacts with the photosensitive molecule, rhodopsin, causing the photoisomerisation of 11-*cis*-retinal to all-*trans*-retinal (ATR).

ATR is released from its binding to opsin after the decay of the light activated metarhodopsin and quickly conjugates with phosphatidylethanolamine to form N-retinylidine phosphatidylethanolamine. The conjugate is transported from the intradiscal area into the photoreceptor cytoplasm with the assistance of a retina specific ATP-binding cassette transporter (ABCR), known as ABCA4. Hydrolysis of the conjugate leaves free ATR in the cytoplasm. This is a chemically unstable molecule that has the potential to react with other biological material, hence it is quickly reduced to all-*trans*-retinol (vitamin A), a reaction catalysed by all-retinol dehydrogenase (Palczewski *et al.*, 1994).

The resultant all-*trans*-retinol must then be transferred to the RPE so that regeneration of the visual pigment and thus the visual process can continue. The exact method for shuttling vitamin A to the RPE from the photoreceptors is unknown, however, it is believed to be assisted by a transport protein named interphotoreceptor retinoid binding protein (IRBP) (Gonzalez-Fernandez *et al.*, 2007). The function of IRBP is a matter of dispute, as the all-trans-retinol is able to diffuse across cellular membranes with relative ease for a hydrophobic alcohol, so IRBP is possibly not there to aid kinetics. It is postulated that perhaps IRBP adds directionality to the movement of vitamin A, or is there to prevent its degradation (Dingle and Lucy, 1965; Rando, 2001).

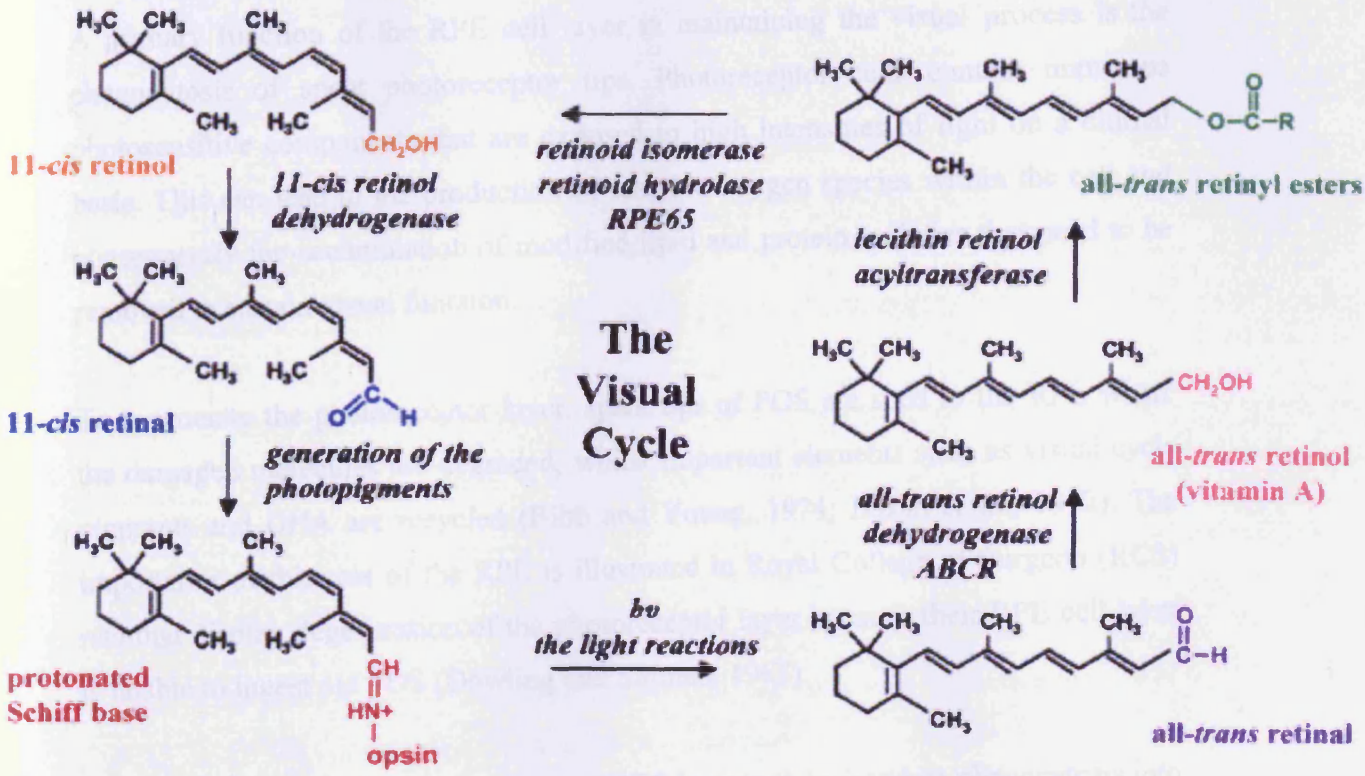

Figure 1. 3. Schematic of the reactions of the visual cycle involved in the interconversion of vitamin A and 11-*cis* retinal (Thompson and Gal, 2003).

Once inside the RPE, vitamin A is bound to a cellular retinol binding protein and undergoes esterification to form retinyl esters, a process catalysed by the action of lecithin:retinol acyl-transferase (Batten *et al.*, 2004). Initially, it was thought that this process was assisted by the chaperone RPE65 and that the retinol esters were isomerised by an unknown enzyme termed isomerohydrolase (Moiseyev *et al.*, 2003).

However, recent work has indicated that RPE65 is responsible for the isomerisation of all-trans-retinyl ester to 11-*cis*-retinol (Jin *et al.*, 2005; Moiseyev *et al.*, 2005; Jin *et al.*, 2007).

Finally, 11-*cis*-retinol is oxidised to the aldehyde, a reaction step requiring 11-cis-retinol dehydrogenase before being transported to photoreceptor cells for re-attachment to opsin, thus, completing the retinoid cycle.

1.2.4 Phagocytosis of photoreceptor outer segments

A primary function of the RPE cell layer in maintaining the visual process is the phagocytosis of spent photoreceptor tips. Photoreceptor cells contain numerous photosensitive components that are exposed to high intensities of light on a diurnal basis. This can lead to the production of reactive oxygen species within the cell and consequently the accumulation of modified lipid and protein moieties that need to be removed to sustain visual function.

To regenerate the photoreceptor layer, spent tips of POS are shed to the RPE where the damaged molecules are degraded, whilst important elements such as visual cycle pigments and DHA are recycled (Bibb and Young, 1974; Bazan *et al.*, 1992). The importance of this role of the RPE is illustrated in Royal College of Surgeon (RCS) rats that display degeneration of the photoreceptor layer because their RPE cell layer is unable to ingest old POS (Dowling and Sidman, 1962).

It has been proposed that the presence of POS is enough to instigate phagocytosis into the RPE (Boulton and Marshall, 1986). However, other evidence suggests an involvement of a number of receptors, ligands and messenger molecules, plus the onset of light and circadian rhythms have been implicated in initiating and regulating phagocytosis (Basinger *et al.*, 1976; LaVail, 1980; Fisher *et al.*, 1983; LaVail, 1983; Nandrot *et al.*, 2004).

It is thought that oxidised phospholipids within POS can act as ligands for CD-36-mediated phagocytosis of POS and that the protein, MFG-E8, acts as a ligand for $\alpha_v\beta_5$-integrin, the sole intergrin receptor at the RPE – photoreceptor interface that is

responsible for promoting RPE phagocytic signalling (Sun *et al.*, 2006; Nandrot *et al.*, 2007).

$\alpha_v\beta_5$-integrin activates focal adhesion kinase which in turn phosphorylates Mer tyrosine kinase (MerTK) that initiates a second messenger cascade that leads to internalisation of POS (Finnemann *et al.*, 1997; Finnemann, 2001; Finnemann *et al.*, 2003; Strauss, 2005). Cells lacking MerTK have the ability to bind POS but not to ingest them, indeed, it is mutations leading to MerTK being absent from the RPE of RCS rats that result in their photoreceptor degeneration. (Feng *et al.*, 2002a; Feng *et al.*, 2002b).

Once ingested into the RPE cell the POS are degraded via a sequential pathway (Figure 1.4). The process of POS degradation begins when shed photoreceptor discs are phagocytosed into the RPE where microfilaments and microtubules are activated that endocytose the POS. The spent tips are then wrapped in a membrane forming a phagosome, which next merges with a lysosome to form a secondary lysosome. RPE lysosomes contain many hydrolytic enzymes thought to be specific to the degradation of POS, of particular importance are the Cathepsin family of enzymes (Rakoczy *et al.*, 1997; Rakoczy *et al.*, 1999). The POS are enzymatically degraded into smaller constituents until they can diffuse out into the cytoplasm. Here they are either recycled back to the photoreceptor layer, stored in the RPE for future use or excreted to the blood stream. However, the process of degradation appears to be inherently flawed as not all substrates are degraded leading to the slow accumulation of a cellular waste product known as lipofuscin. This process is further described in section 1.3.1. Within a human life-time the volume of lipofuscin accrued in RPE cells can account for up to 20% of the cytoplasmic area. (Feeney-Burns *et al.*, 1984).

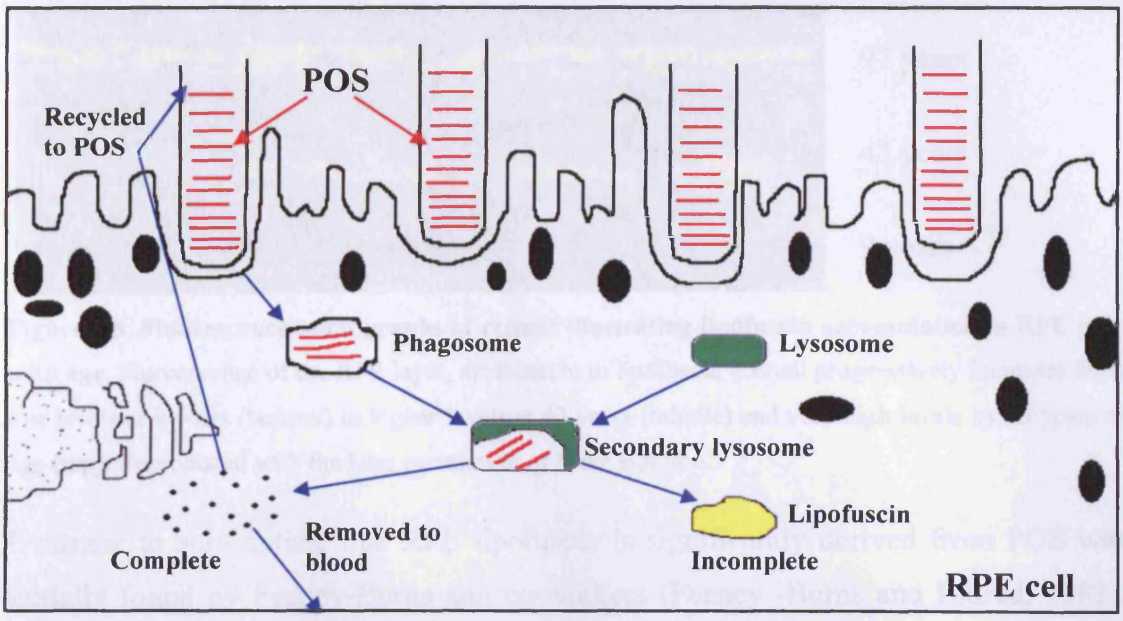

Figure 1.4. Schematic of the phagocytosis of POS and digestion within RPE. (Adapted from Kennedy et al 1995).

1.3 Retinal lipofuscin

1.3.1 Retinal Lipofuscin formation

Lipofuscins are cellular waste products that accumulate in the lysosomal machinery of many post-mitotic cells as a function of age (Terman and Brunk, 2006). The term lipofuscin is derived from the Greek word for fat, *lipo*, and the Latin for dark, *fuscus*. However, lipofuscins are often referred to as 'age-pigment' or 'wear and tear' pigment, emphasising their occurrence in aging cells and the fact they are derived from spent or damaged organelles. Lipofuscins that form in cells such as neurons and heart myocytes are primarily derived from the autophagy of organelles present in those cells. However, lipofuscin that progressively accumulates in RPE cells is unusual as its components are also derived from material phagocytosed into the cell from the overlying photoreceptor outer segments (Wihlmark *et al.*, 1996b). The accumulation of the fluorescent material is highlighted in Figure 1.5 which shows an increase in fluorescence levels in the RPE at the three age stages.

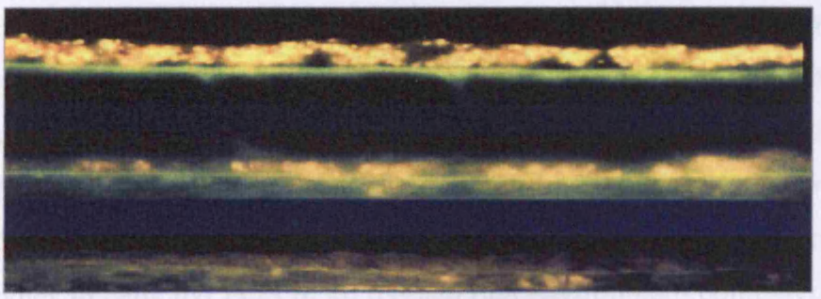

Figure 1.5. Fluorescence micrographs of retinas illustrating lipofuscin accumulation in RPE cells with age. Fluorescence of the RPE layer, attributable to lipofuscin accrual progressively increases from low levels at 9 years (bottom) to higher levels at 43 years (middle) and very high levels by 93 years of age (top). Reproduced with the kind permission of Mike Boulton.

Evidence to substantiate that RPE lipofuscin is significantly derived from POS was initially found by Feeney-Burns and co-workers (Feeney -Burns and Eldred, 1983). They discovered that the RPE contains inclusion bodies that have ultrastructural features of both lipofuscin and phagosomes derived from POS. This suggests there is a pathway that starts with POS, continues through the phagosome and can result in the formation of lipofuscin. Further evidence was compiled by Boulton *et al* (1989) who showed that prolonged feeding of POS to RPE cells *in vitro* resulted in the accumulation of inclusion bodies with lipofuscin-like properties (Boulton *et al.*, 1989). *In vivo* work has shown that RCS rats who fail to phagocytose POS have substantially diminished levels of RPE lipofuscin, as do rats with hereditary photoreceptor degeneration who accumulate lipofuscin at much slower rates than age matched controls (Katz *et al.*, 1986). Equally, the topographical nature of lipofuscin distribution throughout the retina indicates that POS phagocytosis plays an important role in its formation with areas of greatest lipofuscin accumulation mirroring those with the greatest POS density (Feeney-Burns *et al.*, 1984; Delori *et al.*, 2001).

As described in section 1.2.4, a primary function of the RPE is the phagocytosis of POS, with each RPE cell opposing on average greater than 45 POS and over 10% of each being phagocytosed daily (Young, 1967; Newsome, 1983). This invariably places a huge demand on the degradative systems of the RPE cell; however, the lysosomes are equipped with over 40 hydrolytic enzymes to deal with this demand (Boulton *et al.*, 1994; Kennedy *et al.*, 1994). A probable cause of the inefficiency of the acidic vacuolar apparatus in breaking down phagocytosed POS tips is that the constituents are modified in a manner that renders them non-degradable once they

reach the RPE. The environment of the POS and RPE is conducive to the formation of reactive oxygen intermediates (ROI) due to the high oxygen tensions and the diurnal influx of light that is a source of high energy. The influence of oxidative stress on lipofuscin formation in the RPE is demonstrated in studies by Wihlmark *et al* (1996) (Wihlmark *et al.*, 1996a,b). They showed a rapid increase in lipofuscin-like inclusion bodies in cells fed POS in an oxygen rich environment compared to those maintained in normabaric conditions. This is an effect that can be reduced by the presence of antioxidants (Sundelin and Nilsson, 2001).

ROI, such as singlet oxygen and hydroxyl radicals, can interact with the numerous polyunsaturated fatty acids (PUFA) that are present within the lipid bi-layers of POS membranes (Bazan *et al.*, 1990) (Figure 1.6). Initially, free radicals act by removing a hydrogen atom from a carbon atom of a PUFA creating a carbon-centred radical that may undergo conformational rearrangement. This facilitates the reaction with diatomic oxygen to form a lipid peroxyl radical, which due to their close proximity, can interact with an adjacent PUFA instigating a chain-reaction.

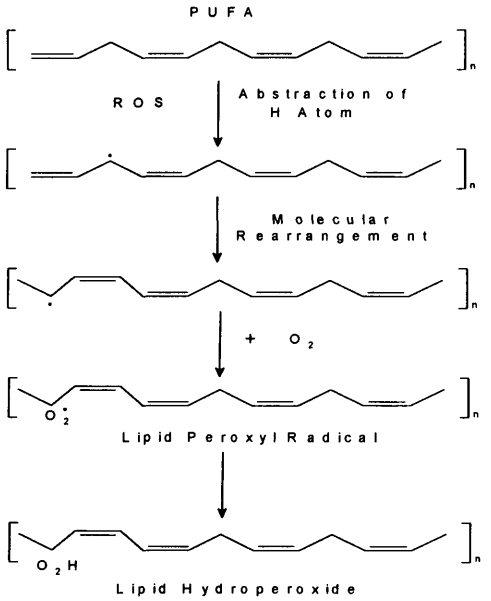

Figure 1.6. The oxidation of PUFAs

The end products of the lipid peroxidation chain reaction are a series of reactive secondary aldehydes that are able to diffuse from their site of origin and react with other molecules. The aldehydes are reactive due to an electron deficient carbon atom that will readily react with nucleophilic amines, thereby forming adducts. Of great importance to the formation of retinal lipofuscin are the aldehydes 4-hydroxynonenal

and 4-hydroxyhexenal, derived from arachidonic and docosohexanoeic acid respectively (Dei *et al.*, 2002; Schutt *et al.*, 2003a). Both of these fatty acids are present in POS in extremely high quantities (Bazan *et al.*, 1990). It appears that the products of lipid peroxidation could have at least a dual role in lipofuscinogenesis. Firstly, they adduct to biomolecules rendering them non-degradable, secondly, they have been shown to induce the mis-sorting and inhibition of lysosomal enzymes (Schutt *et al.*, 2003a; Kaemmerer *et al.*, 2007). Numerous other oxidative modifications have been shown to be present within the lipofuscin granules including nitrotyrosine, isolevuglandin-2 and carboxyethylpyrrole, underlining the importance of oxidative stress and adduction of biomolecules in lipofuscinogenesis (Ng *et al.*, 2008).

1.3.1.1 Vitamin A derivatives in the formation of retinal lipofuscin

Together with products of lipid peroxidation, retinoid derivatives are also involved in the formation of retinal lipofuscin. The significance of these components was initially highlighted by the insightful work of Katz *et al* who noted diminished levels of fluorescent material in the RPE of rats fed diets lacking precursors of 11-cis-retinal (Katz *et al.*, 1985; Katz *et al.*, 1987). This work has been substantiated using Rpe65 knockout mice, in which 11-cis and all-trans-retinal (ATR) are absent and where lipofuscin fluorescence is markedly reduced (Katz and Redmond, 2001).

To date, the retinoid derivatives from the visual cycle that have been identified include A2E, iso-A2E (plus other minor isomers) and all-trans-retinal dimer phosphatidylethanolamine (see figure 1.7) (Parish *et al.*, 1998; Ben-Shabat *et al.*, 2002b; Fishkin *et al.*, 2004). A2E formation is light dependent, with mice reared in dark maintained conditions accumulating very little A2E compared to age matched controls reared in cyclic light/dark conditions (Mata *et al.*, 2000). A2E formation begins in the photoreceptors and the sequence of reactions that are needed to result in its accumulation are described below and illustrated in Figure 1.8.

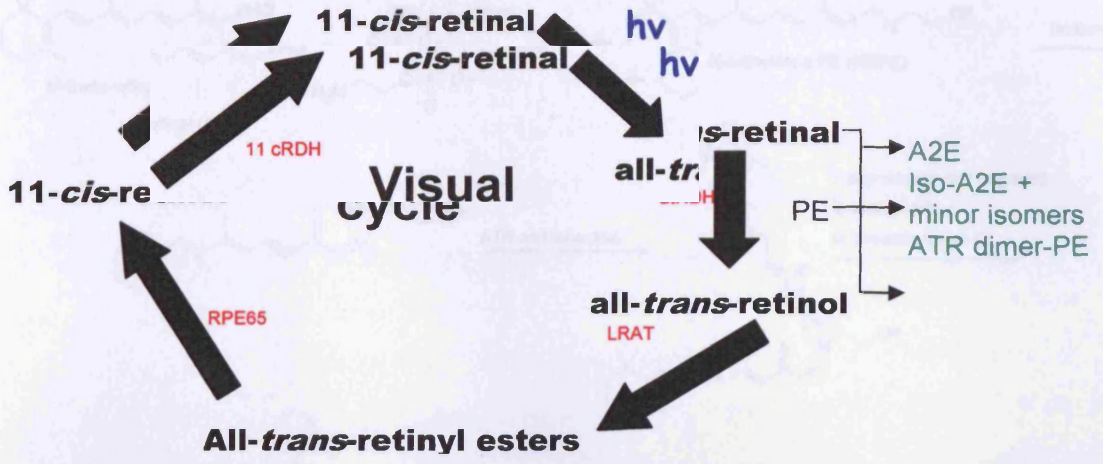

Figure 1.7 RPE lipofuscin fluorophores form as a by-product of the retinoid visual cycle. In a normal functioning visual cycle any all-trans-retinol that is not reduced can react with phosphatidylethanolamine (2:1), ultimately leading to the accumulation of lipofuscin fluorophores; A2E, iso-A2E, other minor isomers of A2E, all-trans-retinal dimer-PE and possibly other as yet unidentified fluorophores. 11cRDH = 11-cis retinol dehydrogenase, atRDH = all-trans retinol dehydrogenase, LRAT = Lecithin Retinol acyl transferase (Sparrow and Boulton, 2005).

The initial stage is a non-enzymatic and random condensation reaction between a single ATR molecule and phosphatidylethanolamine (PE), resulting in N-retinylidine-PE (NRPE). If NR-PE undergoes a further condensation reaction with a second ATR molecule, dihydro-N-retinylidene N-retinyl phosphatidylethanolamine (A2PE-H_2) is formed. This is a particularly unstable species that promptly autooxidises to form A2-PE the immediate precursor to A2E.

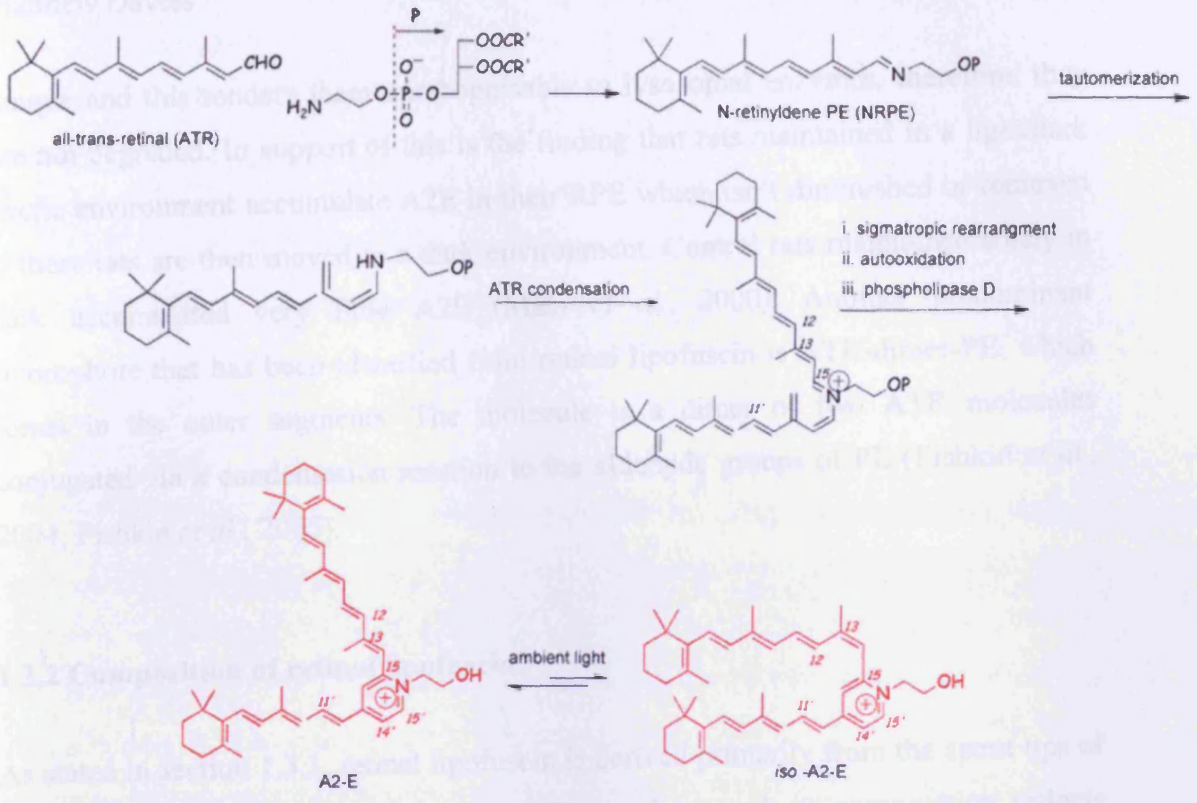

Figure 1.8. Biosynthesis of A2E and iso-A2E. In outer segments after photobleach, PE and ATR are transiently available for conjugation via a condensation reaction to form NRPE. After tautomerisation the resulting secondary amine may condense with another molecule of ATR. Subsequent (3,3) sigmatropic rearrangement of the bis-retinoid product results in the formation of A2PE-H_2, an irreversible step. Oxidation of A2PE-H_2 to A2PE occurs within the RPE phagosomes. Finally, A2E is formed on acid hydrolysis of the phosphate ester by phospholipase D and release of phosphatidic acid (Parish *et al.*, 1998; Fishkin *et al.*, 2003)

To yield A2E, A2PE must undergo enzymatic hydrolysis, a reaction that predominantly takes place within the RPE (Ben-Shabat *et al.*, 2002b). However, it also seems likely that phosphodiesterase activity within the POS creates some A2E even before POS have been phagocytosed by the RPE (Fishkin *et al.*, 2004). In the RPE A2E can undergo photoisomerisation forming *iso*-A2E. Biologically, A2E and iso-A2E are found in a roughly 4:1 ratio. *Iso*-A2E differs from the wholly all-*trans* configuration of A2E by the presence of a *cis* olefin between carbons 13 and 14 on one of its side arms. The carbon-carbon double bonds present within the side-arms of the A2E molecule lend themselves to the formation of numerous structural isomers. Some of these isomers have been identified and deemed to be minor constituents of retinal lipofuscin. The structure of A2E and its isomers are thought to be biologically

unique and this renders them unrecognisable to lysosomal enzymes, therefore, they are not degraded. In support of this is the finding that rats maintained in a light/dark cyclic environment accumulate A2E in their RPE which isn't diminished or removed if these rats are then moved to a dark environment. Control rats maintained solely in dark accumulated very little A2E (Mata *et al.*, 2000). Another predominant fluorophore that has been identified from retinal lipofuscin is ATR-dimer-PE, which forms in the outer segments. The molecule is a dimer of two ATR molecules conjugated via a condensation reaction to the aldehyde groups of PE (Fishkin *et al.*, 2004; Fishkin *et al.*, 2005).

1.3.2 Composition of retinal lipofuscin

As stated in section 1.3.1, retinal lipofuscin is derived primarily from the spent tips of POS and old or damaged cellular organelles, and, as such its composition reflects these origins. Much of our knowledge of the composition, spectral qualities and photoreactivity of retinal lipofuscin comes from chloroform: methanol extraction of the granules with subsequent analysis focusing primarily on the chloroform soluble fraction (Bazan *et al.*, 1990; Rozanowska *et al.*, 1998). However, the chloroform soluble fraction may represent only a small proportion of the lipofuscin granule, and certainly one that diminishes with age relative to the insoluble fraction (Rozanowska *et al.*, 2002).

Early histochemical data of retinal lipofuscin granules revealed them to be predominantly lipidic in nature (Kennedy *et al.*, 1995). Bazan *et al* (1990) conducted a comprehensive review of the lipid component and noted that there was a considerable increase in lipid content with age per eye (Bazan *et al.*, 1990). The study also stated that the predominant fatty acids present in retinal lipofuscin granules were palmitic, arachidonic and oleic acids, largely dissimilar to the major fatty acids the study identified in POS and neural retina.

It is proposed that retinal lipofuscin is composed principally of products of lipid peroxidation that have adducted to other biomolecules and have formed largely modified structures that are no longer recognised by the degradative machinery of the

cells. Lipid peroxidation products have demonstrable ability to inhibit the action of lysosomal enzymes and are often not recognised by them and thus not degraded (Burcham and Kuhan, 1997; Zamora and Hidalgo, 2001). Indeed, studies of lipofuscin components have shown the presence of biomolecules such as proteins adducted to aldehydes derived from lipids that are present in abundance in POS (Tanito *et al.*, 2005). These include; proteins modified by malondialdehyde, 4-hydroxynonenal and 4-hydroxyhexenal plus advanced glycation end products (Schutt *et al.*, 2003a). One of these studies was an annex to a further study that attempted to identify the protein components of retinal lipofuscin (Schutt *et al.*, 2003b). This study, together with a more recent proteomic analysis of retinal lipofuscin, stated that granules were composed of proteins derived either from the POS or from cellular organelles (Warburton *et al.*, 2005). However, each of these studies was marred by apparent contamination of the sample used for analysis with debris that co-localises with lipofuscin during the isolation procedure. Therefore, caution must be used when drawing any conclusions from these results. Both studies noted that proteins present had undergone a considerable increase in mass indicating that the proteins had undergone oxidative damage, cross-linking, or adduction to other molecules.

Lipidic derived components may be the primary source of retinal lipofuscin granules, but other components present do indeed confer some unique properties upon the granules. These unique properties include the golden-yellow fluorescence characteristic to retinal lipofuscin. This distinct feature cannot be attributed to lipid derived aldehydes adducted to amines as these fluoresce in the blue-green region of the spectrum. The most likely cause of this fluorescence is the vitamin A derivatives that are present. Eldred and Katz isolated at least 10 fluorophores from the chloroform soluble fraction of RPE cells (Eldred and Katz, 1988). Of these, 3 fluorophores; A2E, iso-A2E and ATR-dimer-PE have been clearly identified and defined as components of retinal lipofuscin.

To date, some interesting and insightful studies have been conducted with regard to elucidating the components of retinal lipofuscin and thus our knowledge of retinal lipofuscin is continually expanding, however, there is still much to learn and clarify. A number of oxidatively modified molecules have been identified as components of retinal lipofuscin, but it is the authors' opinion that this list is far from exhaustive and

further research would lead to the identification of other oxidatively modified molecules derived from different adduction pathways.

1.3.3 The absorbance and fluorescence characteristics of retinal lipofuscin

Retinal lipofuscin is one of the dominant fluorescent species present within the fundus. It has a characteristic golden-yellow fluorescence when excited with UV light and is strongly fluorescent when excited with light of all visible wavelengths (Docchio *et al.*, 1991; Marmorstein *et al.*, 2002). Indeed, the fluorescence of retinal lipofuscin can be used as a non-invasive method to measure its levels throughout the retina (Delori *et al.*, 1995a; Delori *et al.*, 1995b; Spaide, 2003).

When excited with 364 nm wavelength light, retinal lipofuscin exhibits a broad fluorescent emission. There are a number of factors that influence the emission profile of retinal lipofuscin including; age of donor, wavelength of excitation light and whether granules are measured singularly or en mass (Boulton *et al.*, 1990; Haralampus-Grynaviski *et al.*, 2001; Haralampus-Grynaviski *et al.*, 2003).

Boulton *et al* (1990) noted that there were four main regions of spectral interest when comparing emission spectra of lipofuscin granules from different age groups. These included; a principal peak at 600-610 nm, a blue-green shoulder present in retinal lipofuscin from younger donors that diminishes to nothing with older samples, a yellow-green shoulder at 550 nm and a red shoulder at approximately 680 nm that increases with age of donor (Boulton *et al.*, 1990). Also, with increasing age of donor there is a relative increase in the emission and excitation peaks of isolated retinal lipofuscin when compared to that isolated from younger donors (Boulton *et al.*, 1990; Docchio *et al.*, 1991). Altering the excitation wavelength from 532 to 400 nm when irradiating retinal lipofuscin in bulk leads to a broadening of the emission spectrum (Haralampus-Grynaviski *et al.*, 2003). This most probably occurs due to the photoexcitation of additional fluorophores that emit in this region with the lower wavelength, higher energy light. The changes seen with higher energy excitation light, however, have no effect on the red-edge of the spectrum, possibly because there is one dominant fluorophore that emits in this region. Comparing the emission spectrum

of individual retinal lipofuscin granules highlighted a large degree of variability between granules (Haralampus-Grynaviski *et al.*, 2001; Haralampus-Grynaviski *et al.*, 2003). The wavelength at which emission maxima were found was spread over a 101 nm range, emphasising the heterogeneity of retinal lipofuscin granules.

1.3.4 Phototoxicity of RPE lipofuscin

The autofluorescent characteristics of retinal lipofuscin when excited with short wavelength light indicate that it contains photo-oxidative compound(s) that have the capacity to stimulate oxygen in close proximity (Wihlmark *et al.*, 1997). The opportunity for photosensitisation of oxygen molecules are at much increased rates in the retina due to the favourable conditions for free radical formation consisting of: high oxygen tensions and intense light exposure.

Boulton *et al* (1993) first demonstrated that lipofuscin was photoreactive and that it had the capacity to generate super oxide anions in a light intensity and wavelength dependant manner. Later, the light-induced production of singlet oxygen and hydroxyl radicals by retinal lipofuscin were reported (Gaillard *et al.*, 1995; Rozanowska *et al.*, 1995). These studies showed that the production of reactive species by lipofuscin showed a wavelength dependence, with singlet oxygen production being 10x greater when irradiated with 420 nm light than 520 nm (Rozanowska *et al.*, 1998).

Some of the free radical species generated by lipofuscin have lifetimes that are sufficiently long so as to allow their movement away from their area of origin. They can thus cause damage to biomolecules in other areas of the cell including modification of important cellular components, such as: lipids, proteins and DNA (Boulton *et al.*, 2001). Indeed, levels of products of lipid peroxidation in RPE cells that have been loaded with lipofuscin and irradiated with short wavelength light have been shown to increase (Davies *et al.*, 2001). These products, including malondialdehyde (MDA) and 4-hydroxynonenal (HNE), have been noted as being toxic to RPE cells (Choudhary *et al.*, 2005). Other consequences of irradiating RPE cells containing lipofuscin with short wavelength light have been noted as: protein oxidation, loss of lysosomal integrity, cytoplasmic vacuolation and membrane

blebbing (Davies *et al.*, 2001). The consequence of these actions eventually being cell death. Additionally, irradiation of lipofuscin has been shown to inhibit lysosomal and anti-oxidant enzyme activity in RPE cells (Wassell *et al.*, 1999; Shamsi *et al.*, 2001). This is an effect that can be reduced by the presence of anti-oxidants, implicating that oxidative stress is a cause of these changes.

With an increase in age of the donor from whom lipofuscin is isolated there is a corresponding increase in the photoreactivity of lipofuscin (Rozanowska *et al.*, 2004). Retinal lipofuscin can be separated into chloroform soluble and insoluble fractions using Folchs' extraction (chloroform: methanol 2:1 v/v) (Rozanowska *et al.*, 2004). It was noted that neither the chloroform soluble or insoluble fraction displayed increased photoreactivity with age (Rozanowska *et al.*, 2004). However, there was a significant increase in the chloroform insoluble fraction with age that could possibly account for increased photoreactivity.

Studies involving lipofuscin have shown it to be a photoreactive molecule that has the capacity to photogenerate ROI and increase oxidative stress within the cell. Consequences of this include: DNA lesions, lipid peroxidation and lysosomal dysfunction that could eventually lead to cell atrophy. Lipofuscin is likely to be a contributor to diseases of the retina including age-related macular degeneration (AMD), however, this is a multi-faceted disease and other factors such as genetics and environmental stressors are also likely to play a role.

1.3.4.1 Is A2E responsible for lipofuscin phototoxicity?

One of the lipofuscin components that has been suggested as being responsible for its photoreactivity is A2E (Sparrow *et al.*, 2003b). Initial interest arose as it was noted the molecule absorbs light in the blue region and emits in the yellow-region. Later, *in vitro* studies using RPE cells loaded with A2E and irradiated with short wavelength light demonstrated that A2E was capable of causing cell death (Schutt *et al.*, 2000).

Studies into the photoreactivity of A2E concluded that when photoactivated, A2E could produce singlet oxygen, however, the yields were very low (Cantrell *et al.*, 2001; Lamb *et al.*, 2001; Kanofsky *et al.*, 2003; Gaillard *et al.*, 2004; Lamb and

Simon, 2004). When the photoconsumption of oxygen by ATR, one of the precursors of A2E, was compared with that of A2E, ATR was found to consume 20.6 times more oxygen than A2E (Pawlak *et al.*, 2003).The same study showed that A2E was capable of peroxidising cholesterol with 5-α ChOOH and 7-α/β ChOOH products being formed (Pawlak *et al.*, 2003). 5-α ChOOH is a product formed specifically by interaction with singlet oxygen, whilst the 7-α/β ChOOH product is indicative of free radical formation, but may also derive from the breakdown of 5-α ChOOH. All three of the cholesterol hydroperoxides were formed in low yields, whereas ATR peroxidised cholesterol via the type II singlet oxygen specific pathway in much higher yields (Pawlak *et al.*, 2003). A2E is able to quench singlet oxygen at rates comparable to endogenous singlet oxygen quenchers such as α-tocopherol and ascorbic acid (Roberts *et al.*, 2002; Gaillard *et al.*, 2004). This action is thought to be due to A2E's long conjugated structure which resembles that of dietary carotenoids. However, it was also noted that the use of singlet oxygen scavengers reduced the photocytotoxic effect of A2E (Sparrow *et al.*, 2002). Ben-Shabat *et al* (2002), noted that during illumination with blue light a species of higher molecular mass than A2E was detected using fast atom bombardment mass spectrometry, with the mass of the species increasing in increments of 16 (Ben-Shabat *et al.*, 2002a). Singlet oxygen is known to add across double bonds giving epoxides. Irradiation of A2E in D_2O, in which singlet oxygen has a longer half-life than H_2O, showed that A2E undergoes photooxidation producing epoxide rings (Sparrow *et al.*, 2003c; Gaillard *et al.*, 2004).

The epoxides formed could result from singlet oxygen self-generated by A2E. however, as stated previously this is an inefficient process and it is more probable that A2E epoxides are generated by other chromophores present within lipofuscin. It is possible the A2E epoxides are responsible for blue-light induced damage caused to A2E-laden RPE cells that includes; DNA base lesions, modification of proteins, increase in vascular endothelial growth factor and complement activation (Sparrow *et al.*, 2003a; Gaillard *et al.*, 2004; Zhou *et al.*, 2005; Zhou *et al.*, 2006).

Together with the light induced effects, A2E loaded into RPE cells has been shown to affect other cellular functions. Bergmann *et al* (2004) found that A2E laden cells displayed reduced capacity for the phagocytosis of POS. Finnemann *et al* (2002) who conducted a similar study over a shorter time period noted that phagocytosis was not

disrupted by A2E loading, but that degradation of phagocytosed particles was. The disruption of lysosomal processes by A2E correlates with the earlier work of Schutt *et al* (2001), who described the effect as not being a result of direct inhibition of lysosomal enzymes by A2E. Therefore, a secondary mechanism involving a shift in lysosomal pH was assessed. One action of A2E that could cause a change in lysosomal pH has been suggested to be inhibition of the lysosomal proton pump (Bergmann *et al.*, 2004). A2Es structure means it can act as a detergent towards lysosomal membranes. The lysosomal proton-translocating ATPase represents an integral protein complex whose conformational structure and hence its activity may be influenced by its microenvironment in the membrane. It is possible that once A2E is integrated within the membrane it could interact directly with the proton pump thereby inhibiting its activity.

Substantial evidence has been collected in studies researching the effects of A2E on RPE cells. It has been noted that A2E is phototoxic to RPE cells, most probably through the formation of epoxides, and has the capacity to up-regulate vascular endothelial growth factor (VEGF) and complement factor (Zhou *et al.*, 2005; Zhou *et al.*, 2006). However, A2E is likely to be only a minor component of the retinal lipofuscin granule. A2E is extracted into the chloroform soluble fraction of lipofuscin, a fraction that accounts for at most 35% of lipofuscin granules. It is highly likely that other components of the chloroform soluble and larger insoluble fraction of this complex aggregate play important roles in the effects of lipofuscin upon RPE cell function as well.

1.3.5 The association of retinal lipofuscin with retinal disorders

Despite extensive research into the physical and bio-reactive properties of retinal lipofuscin, its relationship with retinal disorders is based largely on circumstantial evidence. There are a number of factors that have led to the association of retinal lipofuscin with retinal diseases, in particular AMD. These include the greatest density of lipofuscin accumulation being in the perimacular region, mirroring the densest population of rod outer segments (Feeney-Burns *et al.*, 1984; Marshall, 1987). This is of interest as lipofuscin accumulation increases with age in this area, a region that

concomitantly has a preferential loss of rods with age and the onset of AMD (Curcio *et al.*, 1996). Areas with high levels of fundus autofluorescence have been deemed more at risk for AMD, whilst high levels of lipofuscin appear to precede cell death in geographic atrophy (Holz *et al.*, 2001; Lois *et al.*, 2002). Other incidental evidence includes studies that have shown A2E induces elevated levels of VEGF and complement factor, implicated in the onset of AMD, and pigment granules being observed in drusen, a prerequisite for AMD (Hageman *et al.*, 2001; Zhou *et al.*, 2005; Zhou *et al.*, 2006). Some of the strongest evidence supporting the role of retinal lipofuscin in being involved in inducing the onset of AMD has come from recent work identifying the presence of carboxyethylpyrrole (CEP)-adducted molecules in lipofuscin granules (Ng *et al.*, 2008). CEP-adducted molecules have been recorded at elevated levels in patients suffering from AMD and been shown to provoke choroidal neovascularisation (CNV) in a chick model system (Ebrahem *et al.*, 2006).

Lipofuscin accumulates at an increased rate in the RPE of sufferers of the juvenile onset macular degenerative diseases Best's and Stargardts'. The patterns of accumulation coincide with areas of greatest cell loss, however, to date no causative association has been found between lipofuscin accumulation and the onset of these diseases (Allikmets, 1997; Wabbels *et al.*, 2006; Bakall *et al.*, 2007; Gerth *et al.*, 2007).

Considering the evidence presented so far it is tempting to speculate lipofuscin that accumulates as a result of oxidative stress within the retina can cause further damage to this tissue via a number of the mechanisms discussed above. However, as yet no complete link between lipofuscin and the onset of retinal dystrophies has been illustrated and so the question remains as to whether lipofuscins' accumulation in the RPE is the cause or the result of retinal dysfunction.

1.3.5.1 Age-related Macular degeneration

AMD is the leading cause of irreversible vision loss in developed nations, affecting more than 50 million people world wide. AMD is an affliction of the aged, primarily affecting those over the age of 55, with its prevalence increasing with age. As this demographic is the fastest growing in first world countries, the number of those

affected is predicted to increase dramatically unless an effective cure or preventative measure is introduced.

AMD is characterised by a deterioration of the macular region of the retina; showing RPE dysfunction and photoreceptor cell degeneration. Consequently, patients experience reduced central vision with an impaired ability to drive, read or recognise faces (Figure 1.9). AMD is a multifactorial disease with risk factors including: genetic predisposition, environmental stimuli (e.g. smoking and light exposure), dietary intake, sex and race.

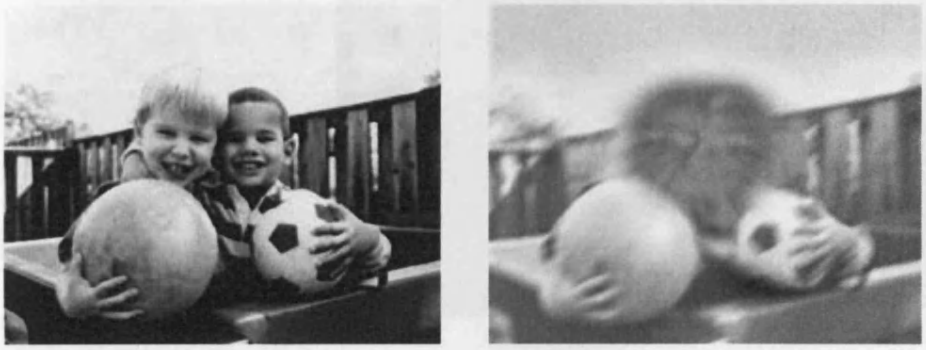

Figure 1.9 The two pictures above represent the same image as would be seen through a normal eye (left) and the image as seen by a patient suffering from AMD (right). Source: National Eye Institute.

AMD is a progressive disease that can be broadly separated into wet and dry forms. Dry AMD has 3 further sub-classes; early, intermediate and advanced. Early dry AMD is characterised by the presence of small to medium sized drusen that result in no vision loss, but this can progress to intermediate dry AMD where medium sized drusen coalesce to form larger soft drusen, possibly resulting in a slight blurring of vision. Late stage or advanced dry AMD is often referred to as geographic atrophy (GA) (Figure 1.10). GA is present when there is a relatively large area of well demarcated hypopigmented RPE. Cells surrounding these areas often have increased pigmentation, possibly arising from the phagocytosis of melanin and lipofuscin released from other cells. GA progresses slowly as photoreceptors gradually shorten and broaden. The initial stage of vision loss is believed to be atrophy of RPE cells, followed by degeneration of photoreceptors and choriocapillaries. The cause of RPE cell death is as yet unknown, but has been associated with excessive lipofuscin accumulation within the cells (Holz *et al.*, 2001; Schmitz-Valckenberg *et al.*, 2006).

Dry AMD is the most prominent form of the disease, which in some cases progresses to the wet form. Currently, the pathogenesis of dry AMD is poorly understood and as such there is no treatment available to combat its progression.

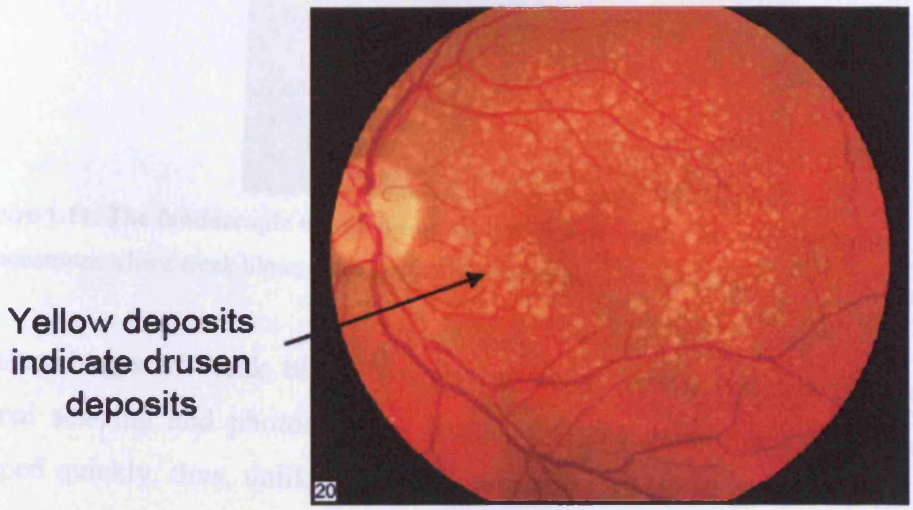

Figure 1.10. The fundoscopic image shows an eye with advanced dry form AMD. The many yellow deposits are the drusen that have accumulated.

Wet AMD is also known as exudative or neovascular AMD. The term neovascular is used as this form of AMD is characterised by the growth of new blood vessels arising from breaks in Bruchs' membrane that continue into the sub-retinal space. The blood vessels are quickly and poorly formed so are susceptible to damage and leakage resulting in haemorrhaging within the retina (Figure 1.11). Under normal conditions the balance between vascular inhibitory factors such as pigment epithelial-derived factor (PEDF) and VEGF remain balanced. However, in eyes suffering from choroidal neovascularisation (CNV) there is a tilt in the PEDF:VEGF ratio, in favour of VEGF. VEGF is a potent stimulator of new blood vessel formation and advances the changes seen during CNV, however, the exact causes for the elevation in VEGF levels are unclear. Hypoxia and ischemia have both been associated with the changes whilst significant increases in VEGF levels have been noted to be stimulated by the presence of ROI (Kannan *et al.*, 2006). Most recently, photoexcited components of lipofuscin granules have been shown to induce up-regulation of VEGF in RPE cells, a factor that could be very important in inducing AMD (Zhou *et al.*, 2005).

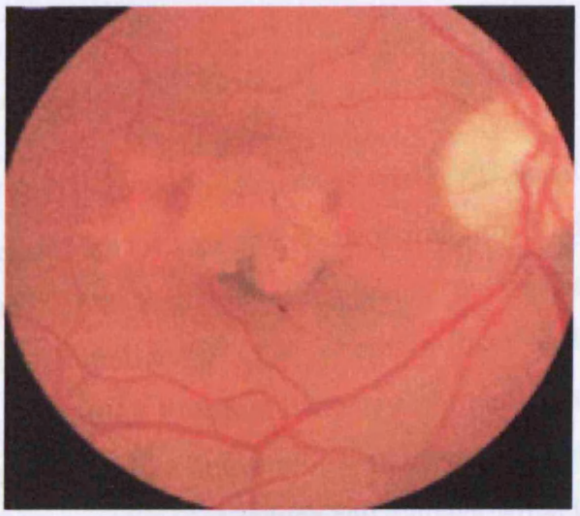

Figure 1.11. The fundoscopic image shows an eye with choroidal neovascularisation. The grey area demonstrates where weak blood vessels have haemorrhaged into the retina.

Haemorrhages of weak blood vessels can cause vision loss via RPE detachment, retinal scarring and photoreceptor death. RPE detachment caused in this way can happen quickly, thus, unlike the slowly progressing dry form, wet AMD can be fast acting.

It should be noted that haemorrhages are not the exclusive cause of RPE detachment. Accumulation of lipids within Bruchs' membrane is thought to be another causative element as this inhibits the movement of fluids from the RPE/photoreceptor complex to the choroid through the mesh-like structure of the membrane (Starita *et al.*, 1995). The accumulation of fluid in the sub-RPE space increases pressure on the adhesive forces between RPE and Bruchs' that may result in detachment of one from the other.

Wet AMD accounts for fewer cases than the dry form (between 10-20%), however, it is estimated to cause around 80% of the severe vision loss attributable to AMD. Patients with wet AMD in one eye have a 4-12% chance of developing it in the fellow eye. Recent advances in treatment of AMD have all focused on the wet form of the disease by attempting to prevent further neovascularisation or stabilising the weak blood vessels that have already formed. The primary current treatments available for AMD are discussed below.

1.3.5.1.1 Treatment of AMD

Photodynamic therapy (PDT) in the treatment of wet AMD involves an intravenous injection of a photosensitiser, for example benzoporphyrin, trade name Visudyne, which is activated upon reaching the retina using a non-thermal laser set at wavelength 689 nm. Excitation of the photosensitiser halts progression of neovascularisation by generating ROI that damage the endothelial cells of unwanted proliferating blood vessels. Unlike conventional photocoagulation therapy, the laser used in photodynamic therapy does not induce cell damage when used on its own, and so theoretically, tissue surrounding the weak blood vessels should not be damaged during surgery. Drawbacks of PDT include that it may serve only to stabilise existing weak vessels and does not prevent the formation of new vessels that could potentially haemorrhage and that it has the potential to damage functional vessles. Indeed, some studies have suggested that the laser used in PDT treatment may even induce the production of VEGF (Schmidt-Erfurth *et al.*, 2003). This has led to trials of combination therapy using both PDT and the VEGF agonists described below (Kim *et al.*, 2006).

Macugen is the trade name for the anti-VEGF aptamer named pegaptanib. Aptamers are macromolecules composed of chemically synthesised single-stranded nucleic acids. Pegaptanib has a high binding affinity for the VEGF165 iso-form and once bound, pegaptanib prevents the VEGF molecule binding to its receptor. Thereby further angiogenesis is prevented which halts a key stage in the wet form of AMD (Fraunfelder, 2005; Ng *et al.*, 2006). Initial *in vitro* studies were useful in demonstrating that the aptamer was effective in inhibiting the action of VEGF and led to clinical trials of pegaptanib (Jellinek *et al.*, 1994). 3 years after FDA approval of pegaptanib for clinical use its ocular and systemic safety and its effectiveness in slowing the progression of wet AMD have been confirmed (Quiram *et al.*, 2007). However, some authors have stated that the success of Macugen was limited and have recorded re-growth of vessels in some patients (Pieramici and Rabena, 2008).

Another anti-angiogenic treatment available to sufferers of wet AMD is ranibizumab, trade name Lucentis. Lucentis is a fragment of a monoclonal antibody that has a high affinity towards VEGF binding. Lucentis is derived from the full length monoclonal

antibody used in fighting colorectal cancer, bevacizumab (Avastin), a drug that has itself been shown to be effective in treating wet AMD when used in an 'off-label' manner (Levy *et al.*, 2008; Melamud *et al.*, 2008). Both Lucentis and Avastin have a mechanism of action similar to Macugen and thus work to prevent further growth of leaky blood vessels, which eliminates the potential for haemorrhaging.

The anti-VEGF treatments have been shown to be effective in the treatment of wet AMD, but due to their administration via intravitreal injection, local side-effects have been noted including: inflammatory reactions, infections, elevated intraocular pressure and in some patients (1.6%) RPE tears that led to severe vision loss (Kiss *et al.*, 2007). To date all treatments available for AMD focus on the wet form of the disease and are only applicable to patients that have progressed to quite a late stage. The development of a therapeutic agent that could act in a preventative way for people who have been identified at risk for the disease would be a significant progression in the battle against AMD. Equally a treatment that addresses the issues faced by patients that present the dry form of the disease could possibly increase their quality of vision and consequently life.

Much of the work contained in this thesis is concerned with the dry form of AMD and therefore it seems pertinent to feature the proposed means of preventing this form also. Currently, the method of treating dry AMD that has generated the most interest is the use of nutritional supplements.

The role of nutritional supplementation in the prevention and treatment of dry AMD is a contentious subject with antioxidants being the most widely hypothesised supplement to have a beneficial effect. The influence of anti-oxidants upon the RPE is theorised to work by reducing the impact of normal metabolic functions which generate ROI on a daily basis (Beatty *et al.*, 2000). Indeed, *in vitro* work using animal models showed that supplementation of lutein, zeaxanthin, lycopene or α-tocopherol to RPE cells maintained under normobaric conditions or loaded with POS resulted in significantly lower lipofuscin-like levels than controls without anti-oxidant supplementation (Sundelin and Nilsson, 2001).

As discussed previously, the eye is an ideal environment for the generation of reactive oxygen species and as such the retina is equipped with numerous anti-oxidant systems, including: enzymatic anti-oxidants such as: superoxide dismutase and glutathione peroxidase, as well as non-enzymatic anti-oxidant nutrients like; vitamin E and certain carotenoids. However, with age the efficiency with which these protective mechanisms act is thought to deteriorate (Winkler *et al.*, 1999). Thus, hypothetically replenishing the supply of anti-oxidants could help maintain the health of the tissue.

Numerous trials have been conducted into the effects of anti-oxidant supplementation in AMD progression (Cangemi, 2007; Jones, 2007; SanGiovanni *et al.*, 2007). Of particular interest is the Age-related eye disease study (AREDS). The AREDS investigated the effect of a high dose of vitamins E and C, beta-carotene and zinc supplements on AMD progression and noted that a group supplemented with anti-oxidants who were deemed high risk for drusen accumulation showed significantly less progression to later stage AMD. However, vitamin E supplementation appeared to have no impact on the development of drusen. Other anti-oxidants that have generated interest are lutein and zeaxanthin (Seddon, 2007). The protective action of these carotenoids could be two-fold. Lutein and zeaxanthin filter blue-light reducing the excitation of photoreactive chromophores, plus they are capable of quenching singlet oxygen and possibly other reactive oxygen species (Edge *et al.*, 1997; Cantrell *et al.*, 2003). Indeed, it has been reported that a high intake of vegetables rich in lutein can lower the risk of exudative AMD by 40% (Seddon *et al.*, 1994).

However, not all studies have reported a beneficial impact of anti-oxidant supplementation in preventing the onset or progression of AMD (West *et al.*, 1994; Evans and Henshaw, 2008; Zhao and Sweet, 2008). This leaves the extensive literature upon the subject inconclusive and contradictory (Tan *et al.*, 2008). Therefore, further research into therapeutic strategies aimed at alleviating the progression of dry AMD is needed.

1.3.5.1.2 Risk Factors for AMD

AMD is a complex disease whose onset can be induced by a combination of factors. As previously noted, the greatest risk factor for developing AMD is age; people over the age of 90 years have approximately ten times the risk of developing the disease as those aged 50 years (Evans, 2001). As discussed in section 1.3.5 lipofuscin has been associated with AMD for a number reasons including; inducing up-regulation of VEGF, activation of complement factors and generation of free radicals leading to cell atrophy, each highlighted in preceding AMD. To prevent repetition this section features other factors besides lipofuscin that have also been deemed risks for the onset of AMD.

Clinical studies have also shown that whites and women are more susceptible to developing AMD (Evans, 2001; Leske *et al.*, 2006). However, it is well established that women live longer than men and, as incidence of AMD increases with age, the distinction as to whether there is a genetic predisposition in women that makes them more susceptible to the disease than men, or, simply that they live longer and are, therefore, at greater risk has not yet been adequately addressed (Evans, 2001).

A number of environmental stimuli have been associated with AMD, including: high dietary fat intake, smoking, sunlight exposure and a low level of anti-oxidant intake. High levels of fat in the diet my have a bimodal influence in determining the onset of AMD. Raised levels of cholesterol may increase the likelihood of developing atherosclerotic plaques, another systemic factor associated with onset of AMD (Fraser-Bell *et al.*, 2008). Alternatively, excess fat in circulation could lead to fatty deposits in Bruchs' membrane that would disrupt the flow of fluids between the choroid and RPE, with consequences described in section 1.3.5.1 earlier. However, no consistent relationship between AMD and dietary fat intake has been found. Equally, conflicting reports with regard to cholesterols' contribution to AMD are to be found in the literature (Cruickshanks *et al.*, 1997; Klein *et al.*, 1997; Rudolf *et al.*, 2004; McGwin *et al.*, 2005). Indeed, an increased level of fish in the diet may proffer an advantageous effect against the onset of AMD, so rather than levels, the type of fat present in the diet may be of importance.

Smoking is a risk that may have two possible mechanisms by which it affects the onset of AMD; a direct impact upon choroidal circulation or, it may decrease levels of plasma anti-oxidants. The influence of smoking in the aetiology of AMD is evident by the dose-responsive relationship between smoking and developing AMD (Christen *et al.*, 1996). Heavy smokers (greater than 20 cigarettes per day) are at greater risk than lighter smokers (less than 20 cigarettes per day) with an odds ratio of 2.4 versus 1.26. Like high dietary fat, if the association between smoking and AMD is true, this is of particular importance as it is a risk factor that can be removed.

The effect of light exposure on the incidence of AMD has been addressed by a number of studies, however, difficulty in accurately assessing exposure levels and identifying the key periods of exposure has ensured that few correlations were made with regard to AMD prevalence (Hyman *et al.*, 1983; Rosenthal *et al.*, 1991). However, a positive correlation between blue-light exposure and the incidence of AMD was reported by Taylor *et al* (1990), whilst Cruickshanks *et al* (1993) noted that the use of sun hats and sunglasses reduced the impact of sunlight exposure as a causative factor in the onset of AMD (Taylor *et al.*, 1990; Cruickshanks *et al.*, 1993).

Increased prevalence of AMD in smokers, together with the apparent association between light exposure and the disease, suggests that oxidative stress may play a role in its onset. Further support for oxidative stress being instrumental in retinal degeneration is that Superoxide dismutase 1 (SOD1) knockout and SOD2 knockdown results in an AMD-like phenotype in rodents (Justilien *et al.*, 2007; Hashizume *et al.*, 2008) As discussed previously, it has been proposed that the presence of anti-oxidants in the retina could protect against AMD by reducing the impact of free radicals in damaging the RPE, a key initial stage of the disease (Beatty *et al.*, 2000). Indeed, *in vitro* studies have shown that supplementation of anti-oxidants such as α-tocopherol reduce the effect of oxidative stressors on the RPE, whist *in vivo* studies have shown that α-tocopherol is found in lower levels in AMD sufferers than age-matched controls (West *et al.*, 1994; Lu *et al.*, 2006). Thus, it is highly likely that oxidative stress is involved in the onset of AMD, however, continued research is needed into methods of reducing its impact.

The familial associations and race bias indicate that genetic predispositions may play a significant role in determining whether or not someone will be afflicted by AMD. Early studies attempted to link AMD with other known genetic disorders that manifested as macular degeneration including; ABCA4 and ELOVL4 (Tuo *et al.*, 2004; Traboulsi, 2005). However, recent research has focused upon particular genes whose variants appear to pre-dispose the carrier to AMD.

Of particular interest are variants of genes located on chromosomes 1q32 and 10q26. The region of 10q26 has highlighted two genes whose variants could potentially pose a high risk for developing AMD. It has been noted that a single nucleotide polymorphism (SNP) in the promoter region of HtrA serine peptidase 1 (HTRA1) is significantly more prevalent in the eyes of AMD patients than in non-sufferers (Dewan *et al.*, 2006; Yang *et al.*, 2006; Chen *et al.*, 2008). The other gene; age-related maculopathy susceptibility 2 (ARMS), also located on chromosome loci 10q26 has been affiliated with the onset of AMD (Francis *et al.*, 2008; Fritsche *et al.*, 2008). Contradictory studies have shown that both HTRA1 and ARMS2 may play a role in determining the risk of developing AMD (Rivera *et al.*, 2005; Francis *et al.*, 2008). However, convincing experiments conducted by Kenda *et al* claim that variants in ARMS2, that encode for an unknown protein, are the actual risk factors involved with 10q26 (Haines *et al.*, 2007; Kanda *et al.*, 2007).

Hageman *et al.*, 2001 studied the eyes of patients suffering from AMD and compared them to age matched controls, finding that AMD sufferers had proteins involved in inflammation and the immune response present around drusen. These proteins included members of the complement system, later to be deemed important when a variant of the gene Y402H on chromosome 1q32, encoding for complement factor H, a protein involved in regulating the complement system, was identified by four separate groups to be involved in increased risk of developing AMD (Edwards *et al.*, 2005; Hageman *et al.*, 2005; Haines *et al.*, 2005; Klein *et al.*, 2005). The link between complement factors and AMD was strengthened when variants in the gene encoding for complement factor B, a protein involved in the activation of the complement system, was identified in AMD patients (Gold *et al.*, 2006; Hageman *et al.*, 2006).

Factors proposed to be responsible for initiating the inflammation response have included infection and oxidative stress. Recent work by Hollyfield *et al* proposed a link between CEP adducts (an oxidation product of DHA that has been identified in lipofuscin and drusen), and the development of lesions within the RPE that mimic those seen in geographic atrophy (Crabb *et al.*, 2002; Hollyfield *et al.*, 2008). Thus, providing a further association of retinal lipofuscin with AMD.

1.3.5.2 Stargarts disease

Stargardts' disease is an autosomal recessive disease that is characterised by rapid accumulation of the lipofuscin fluorophore, A2E, within the RPE. Stargardts' disease is the most common early onset disease of inherited macular degeneration. It primarily affects juveniles, with disease symptoms usually manifesting by 20 years of age, however, some people may not be aware they have a problem until 30 or 40 years into their life-time.

Sufferers of the disease have been noted to accrue up to 7 times the quantity of lipofuscin as age-matched controls (Birnbach *et al.*, 1994). Despite no causal link between lipofuscin accumulation and Stargardts being established, it is believed that the enhanced accumulation of A2E plays a role in the development of macular degeneration, causing a reduction in central visual acuity (Sun and Nathans, 2001).

The gene associated with development of Stargardts is ABCA4, a gene that encodes for a photoreceptor specific ATP-binding protein. *In vitro* work with purified ABCA4 and *in vivo* work using ABCA4 knock-out mice has indicated that ABCR transports ATR from the photoreceptor disc lumen into the cytosol where it is exposed to all-*trans* retinol dehydrogenase for its reduction to all-*trans* retinol (Sun *et al.*, 1999; Ahn *et al.*, 2000; Mata *et al.*, 2000). It is believed that reduced levels of all-trans-retinol transport across the membrane results in increased ATR levels in the photoreceptor discs and an increased probability of A2E forming. The increased levels of A2E being phagocytosed into the RPE are likely to increase its susceptibility to photo-oxidative stress and possibly result in atrophy within these cells. To date, no treatment is available for sufferers; however, identification of the gene responsible and its function

will assist future endeavours in combating the disease. Equally, if a mechanistic link is formed between lipofuscin accumulation and the onset of Stargardts, a therapeutic agent that could either prevent its accretion or degrade the lipofuscin already there would possibly be beneficial to Stargardt disease sufferers.

1.3.5.3 Bests disease

Bests' Disease is a rare, bilateral dominantly inherited condition that results in slowly progressive macular dystrophy. Onset of symptoms usually occurs in early childhood, but sometimes this is delayed until teenage years. Like Stargardts', Bests' is characterised by a rapid accumulation of lipofuscin within and beneath RPE cells (Petrukhin *et al.*, 1998). Accumulation of lipofuscin within the RPE has been associated with degeneration of RPE and subsequently, the overlying photoreceptor layer, both of which are key stages in Bests' disease that lead to central vision loss (Allikmets *et al.*, 1999; Wautier and Schmidt, 2004).

Variants in the gene termed VMD2 that is located on chromosome 11q13 have been identified as being responsible for predisposing carriers to Bests' disease (Petrukhin *et al.*, 1998). Bestrophin is the product of this gene and is a protein that localises in the basolateral membrane of RPE cells and is thought to be a chloride and/or calcium channel that has also been linked to regulation of intraocular pressure (Marmorstein *et al.*, 2000; Yu *et al.*, 2000; Bakall *et al.*, 2008).

Bests' disease shares a number of features that are clinically similar to AMD; however, studies into the VMD2 gene, which is responsible for Bests' disease, found that its occurrence in AMD sufferers was not significantly different from that of age-matched controls (Allikmets *et al.*, 1999). Similar to Stargardts' disease, no treatment has yet been established for sufferers of Bests' disease. Again, identification of the gene responsible and the possible function of the gene product should aid development of therapeutic strategies against the disease. Equally, if a functional link between lipofuscin accumulation and the onset of the disease can be verified and lipofuscin is found to be a causative element in the disease, strategies to prevent lipofuscin accumulation or enhance its degradation may be advantageous to those afflicted by Bests' disease.

1.3.6 Diseases related to lipofuscin accumulation in other post-mitotic cells

The focus of this project is based primarily on the affect of lipofuscin accumulation in the RPE cells of the eye and mechanisms of preventing its formation or degradation once there. However, it would seem naïve to simply ignore lipofuscins that develop in other cells, particularly as the pathways of formation have many similarities (Brunk and Terman, 2002). Some conditions that correlate with excessive lipofuscin accumulation in other tissues are described below.

1.3.6.1 Cardiac hypertrophy

Cardiac hypertrophy is a thickening of the heart muscles that occurs in response to increased stress on the heart. It is related to a weakening of individual muscle fibres, meaning the fibres then need to work harder to pump blood and become thickened over time. Biopsy of hypertrophied papillary muscle of human heart reveals that the larger sized cells are packed with mitochondria, lysosomes and heavy aggregates of lipofuscin granules (Dalen *et al.*, 1987; Dolara *et al.*, 1996)

1.3.6.2 Cirrhosis of the liver

Cirrhosis of the liver develops due to chronic damage resulting in scar tissue slowly replacing normal functioning liver tissue, progressively diminishing blood flow through the liver. As normal tissue is lost the functional efficiency of the liver is lowered, therefore, nutrients, hormones, drugs and poisons are not processed effectively.

Induction of liver cirrhosis in Male F-344 rats resulted in enlarged cells that contained high levels of lipofuscin, while large deposits of lipofuscin accumulating in liver have been suggested as a diagnostic indicator of underlying liver diseases (Szende *et al.*, 1988; Hubscher and Harrison, 1989).

1.4 Hypothesis

In light of the literature reviewed above it appears that lipofuscin which forms within the RPE may have a deleterious effect upon the ageing retina and may be involved in the onset of age-related retinal diseases. To gain a greater understanding of retinal lipofuscin the genesis and composition of the granules were investigated. Equally, we propose that reducing the potential for photoexcitation of retinal lipofuscin would have a beneficial impact upon RPE cell function. It is proposed that the use of blue-light blocking filters would have a beneficial impact upon RPE cells laden with lipofuscin when irradiated with blue-light compared to conventional UV-blocking filters. Equally, reducing the levels of lipofuscin that form or accumulate in the RPE may have a beneficial impact upon the deterioration of these cells. It is hypothesised that supplementing RPE cells with a novel nanomedicine would assist in the degradation of retinal lipofuscin substrates and of granules accrued within the cells.

1.5 Aims

The aims of this project are broad in nature; however, all are linked by the common theme of retinal lipofuscin. The projects interests are based around lipofuscin formation, degradation, composition and in reducing its phototoxicity to RPE cells.
Specifically the project aspires to:

1) Undertake a systematic analysis of the proteomic composition of purified retinal lipofuscin to improve on those that have been undertaken previously, but were potentially contaminated with extra-granular debris.
2) Design and create *in vitro* models of retinal lipofuscin formation using what are believed to be its primary substrates and compare the physical characteristics of the model with those of *ex vivo* human retinal lipofuscin.
3) Develop a methodology to reliably measure the ability of IOLs to reduce the phototoxicity of lipofuscin to RPE cells. Using the novel method to compare the action of yellow-tinted lenses and UV-blocking lenses.

4) Quantitatively measure the phototoxic effect of increasing retinal lipofuscin concentration within RPE cells. Also, record the impact of light intensity on the impact of the phototoxicity of retinal lipofuscin loaded into RPE cells.
5) Analyse a potential nanomedicine consisting of a carrier molecule that can be localised to RPE cell lysosomes and an active component that has the capacity to degrade lipofuscin substrates and/ or lipofuscin accrued in RPE cells. Later, conjugate the two components and determine their ability to remove or degrade retinal lipofuscin in RPE cells.

Chapter 2

General Materials and Methods

This chapter contains details of techniques that are used in more than one chapter in the thesis to prevent repetition. Techniques described within the General Materials and Methods will be referenced in the experimental design of chapters in which they are used, together with any variation of the technique.

2.1 Isolation of RPE cells and retinal lipofuscin

Donors eyes were received from Bristol Eye Bank with the cornea removed for transplantation and permission given for research use. Donors were anonymised before receipt. Donor information included: age, sex and cause of death. Dissection began with the separation of the anterior segment of the eye by circumferential incision immediately posterior to the ora serrata. The vitreous was gently detached and the neuroretina removed from the underlying RPE by dissection of the optic disk. The remaining eye cup was washed with 1 ml of phosphate buffered saline (PBS). RPE cells were detached by gently washing the RPE/choroid complex with a fine camel hair brush and 1 ml of fresh PBS. The process was repeated once and the cell suspension transferred to a cryovial (Nalgene, Rochester, NY, USA) using a sterile pastette (Copan Innovations, Murrieta, CA, USA) before being stored at -80°C until needed for further use.

Lipofuscin granules were isolated from the RPE cell extracts as described by Boulton and Marshall (Boulton and Marshall, 1985). When needed RPE cell suspensions were thawed, removed from the cryovials and pooled. Each cryovial was washed with PBS to ensure all RPE cells were collected.

The suspensions were homogenised through a 25 G needle (BD Microlance, Oxford, UK) attached to a plastic 10 ml syringe into 15 ml centrifuge tubes (Sterilin, Staffs, UK), before being centrifuged at 100 *g* (Boeco U-32R, Hamburg, Germany) for 7 mins at 4°C to remove cellular debris. The resultant supernatant was kept on ice whilst the pellet was further homogenised through a 25 G needle attached to a plastic 10 ml syringe and the centrifugation repeated at 100 *g*, 7 mins and 4°C. The supernatant was centrifuged at 7000 *g* (Sorvall Ultra-Pro 80) for 10 mins at 4°C to

create a pellet of pigment. The pigment was resuspended in 0.25 M sucrose and homogenised with a 25 G needle attached to a plastic 10 ml syringe, before being layered on a discontinuous sucrose density gradient (1.0, 1.2, 1.4, 1.5, 1.6, 1.8 and 2.0 M). The gradient was centrifuged at 103000 *g* for 1 hr at 4°C. Lipofuscin accumulating at the 1.2 and 1.4 M interphase was isolated using a sterile Pasteur pipette. The granules were diluted in PBS and washed twice at 7000 *g*, 10 mins and 4°C. The resulting pellet was re-suspended in 0.25 M sucrose and further homogenised through a 25 G needle attached to a plastic 10 ml syringe. The suspension was layered onto a modified discontinuous density sucrose gradient (1.0, 1.2, 1.4 and 1.5 M sucrose) and the centrifugation and washing steps repeated.

The final pellet was resuspended in the minimum volume of PBS and yield determined by counting on a haemocytometer (Bürker, Sigma, UK). Lipofuscin granules were stored in cryovials at -80°C until needed.

2.2. Cell culture

The ARPE -19 cell line was used as a model of the RPE in cell culture experiments carried out in this thesis. The cell line was obtained from the American Type Culture Collection (ATCC), and is an immortalised cell line which originates from cells cultured from a 19 year old donor. ARPE-19 cells have been shown to have many structural and functional characteristics of human RPE cells (Dunn *et al.*, 1996).

2.2.1 Cell Culture Media and Conditions

ARPE-19 cells were maintained in a 37 °C humidified atmosphere containing 5% CO_2 / 95% air and cultures were grown in 75cm^2 flasks (Triple Red, UK). The cell culture medium used was Ham's F10 nutrient medium which was obtained from Gibco-BRL, UK, and is the medium specifically recommended to allow optimum growth conditions by the ATCC data sheet. In addition, all cell growth media contained antibiotics (100 μg/ml streptomycin, 100 μg/ml kanamycin and 60 μg/ml penicillin, all of which were purchased from Sigma, UK) and 2% v/v fungizone (Gibco-BRL, UK). The culture media was further supplemented with 10% fetal calf

serum (FCS) (Bio-West, UK) until the cell monolayer had reached confluence. Once confluent, cells were maintained in culture medium that was supplemented with 2% FCS (basal medium) until needed for experimental procedures. Cells were used between passage 23 and 26.

2.2.2 Maintenance of Cell Cultures

Routine cell culture involved splitting the cells approximately every 7 days. This was achieved by removal of the cell culture medium by aspiration and washing the monolayer with sterile PBS. Cells were dissociated from the flask using a 0.25% trypsin/0.02% EDTA solution for approximately 2 min. Detached cells were pelleted by centrifugation at 700 *g* for 5 min, 4°C. The supernatant was discarded while the pellet was re-suspended in pre-warmed Hams F-10 culture medium supplemented with 10% FCS. At this point, the cells were spilt in a 1:3 ratio and seeded in further 75cm^2 flasks and stored at 37°C with 5% CO_2 / 95% air in a humidified incubator. Cells needed for experimental procedures were split into the wells of 24-well plates. For microscopy work a glass slide was placed within the 24 well plate upon which the cells were grown. Cells were maintained in culture medium containing 10% FCS until confluent. At the point of confluence, medium was changed to that supplemented with 2% FCS and the cells maintained in this basal medium for a further 7 days. These cell cultures were then used for subsequent experiments.

2.2.3 Liquid nitrogen storage of cell cultures

After trypsinisation as described above, the detached cells were pelleted by centrifugation at 700 *g* for 5 min, 4°C. The supernatant was discarded and the pellet was resuspended in 10% v/v dimethylsulphoxide (DMSO) (Sigma, UK) prepared in FCS (Bio-West, UK). Cells were gradually frozen to -80°C using an isopropanol cryostorage box (Nalgene, UK) to prevent the formation of ice crystals in cells. Once frozen, cells were stored in a liquid nitrogen refrigeration chamber for later use.

2.3 Extraction of bovine retina

Retinas of bovine eyes were extracted by removing the anterior portion of the eye by circumferential incision, gently discarding the vitreous then detaching the retina by cutting at the optic nerve.

2.3.1 Isolation of photoreceptor outer segments form bovine retina

Photoreceptor outer segments (POS) were isolated from bovine retinas using a method adapted from that originally described by Papermaster (Papermaster, 1982). Initially, 25 retinas were added to 15 ml of homogenisation medium (Table 2.1) and a Teflon hand-held (Fisher Scientific, UK) homogeniser passed through the homogenisation media three times. The homogenate was decanted into a cold centrifuge tube then back into the homogenisation tube and the homogenisation repeated. The homogenate was centrifuged at 1500 *g* for 4 min at 4°C (Boeco U-32R).

Table 2.1. Homogenisation media for isolation of POS

	Fresh retina (34% w/w)
42% Sucrose	191g
1 M NaCl	13ml
0.1 M $MgCl_2$	0.4ml
1.0 M Tris-acetate	1.0ml
Add H_2O to:	230g

The resultant supernatant was decanted into ice-cold centrifuge tubes and the pellet re-homogenised with a further 15 ml of homogenisation medium. The centrifugation step was repeated as before with the supernatant kept in ice-cold centrifuge tubes and the pellet discarded. The volume of the supernatant was determined before being transferred to an ice-cold 500 ml conical flask. Two volumes (relative to supernatant)

of 0.01 M Tris-acetate buffer (pH 7.4) were added slowly to the conical flask whilst stirring. The POS were then pelleted at 1500 *g* for 4 min at 4°C (Boeco U-32R).

The pellet was re-suspended in 1.10 g/ml sucrose solution and passed through an 18 G needle rapidly ejecting the homogenised solution against the wall of the plastic tube and re-homogenising as above. Sucrose gradients were prepared using ice-chilled 1.15 g/ml, 1.13 g/ml and 1.11 g/ml solutions. The crude POS suspended in 1.10 g/ml sucrose was then gradually and gently layered onto the gradient. The gradients were then spun at 50000 *g* for 30 min at 4°C (Sorvall Ultra-Pro 80). POS were located between the 1.11/1.13 g/ml and 1.13/1.15 g/ml interfaces. The POS were removed using a sterile Pasteur pipette and recovered as a pellet after dilution in 0.01 M Tris-acetate and sedimentation by centrifugation at 45000 *g* for 20 min (Sorvall Ultra-Pro 80). The POS pellet was re-suspended in the minimum volume of PBS and the yield determined by counting on a haemocytometer (Bürker, Germany). POS in PBS were then stored at -80°C until needed for future experiments.

2.4. Measurement of mitochondrial activity as an indicator of cell viability using the MTT assay

Immediately subsequent to the experimental procedure where measurement of cell viability was required the MTT assay was undertaken (Schutt *et al.*, 2000). The MTT assay was used to provide a reliable technique for measuring levels of cell viability in test and control cultures. The MTT assay uses the ability of a mitochondrial dehydrogenase enzyme from viable cells to cleave the tetrazolium rings of the pale yellow MTT and form dark blue formazan crystals that are largely impermeable to cell membranes, thus resulting in its accumulation within healthy cells. The intensity of the product colour is directly proportional to the reductive capacity of cells which can be used to measure the number of living cells in the culture. To undertake the MTT assay, medium was aspirated from the wells containing cells and 250 µl of PBS containing dissolved MTT (1 mg/ml. Sigma, UK) was gently added into each well. The cells were incubated with MTT solution for 3 hours at 37 °C, after which the MTT was aspirated, and 250 µl of acidified iso-propanol (containing 0.04 M HCl. Acros Organics, UK) was added to solubilise the reduced blue formazan crystals.

Aliquots were transferred to a 96-well plate (Triple Red, UK) and absorbance measured at 590 nm, with a reference measured at 690 nm using a 96-well plate reader (Multiskan Ascent, Labsystems, UK). Results were analysed using the following equation: Viability as a percentage of control = (absorbance of sample cells/absorbance of control cells) x 100.

2.5 Flow cytometry

Flow cytometry is a technique based upon the principles of light scattering, light excitation and emission of fluorochrome molecules to generate information about the physical and chemical characteristics of a population of cells, recording the features of one cell at a time.

To generate the multiparameter data about cells in a population the sample is hydro-dynamically focused in sheath fluid before intercepting an optimally focused light source, usually a laser beam. As each cell passes through the light source it scatters the light in some way and fluorochromes present within the cells are elevated to higher energy states. The scatter of light and resultant photons of light, generated by energy loss from excited fluorochromes, are detected by the flow cytometer and used to produce data on the cell population. Flow cytometers also contain a number of detectors that measure the forward scatter and side scatter of light caused by the cell. The forward scatter produced by a cell relates to the volume of the cell, whereas the side-scatter gives information on the complexity of the cell with respect to parameters such as granularity.

The procedure for using flow cytometry in this study is as follows; cells were cultured as described in Section 2.2.1. and 2.2.2. Experimentation was carried out as described in the relevant chapter section.

After experimentation, when cells were ready for analysis, they were washed three times by the gentle addition of PBS. After the third PBS wash cells were detached from the wells by exposure to a 0.25% (w/v) trypsin solution (Sigma, UK) containing 0.02% EDTA (w/V) made up in PBS and incubated for 2 min (37°C, 95% air, 5%

CO_2). Trypsin was inactivated by the addition 1 ml of Hams-F10 medium containing 10% FCS. Cell suspensions were removed from their wells and centrifuged at 700 *g*, 4°C for 5 min (U-32R, Boeco, UK) to create a pellet. The medium was gently aspirated from the centrifuge tube and replaced with 1 ml of PBS. The pellet of cells was then washed twice in PBS by centrifugation at 700 *g*, 4°C for 5 min. After the final wash cells were re-suspended in 300 µl of PBS and transferred to a FACs tube (Falcon, UK). FACs tubes containing cell suspensions were taken on ice to the flow cytometer (FACSCaliber, BD Life Sciences, UK) for analysis. The fluorescence levels of ARPE-19 cells were measured using flow cytometery by exciting the cells with a 15 mW 488 nm air cooled argon-ion laser. The emission of the samples was detected using high performance, high dynamic range photomultipliers with a 530 nm (FITC) filter. The forward and side scatter generated by the cells was recorded as a measure of cell size and complexity, respectively.

2.5.1 Flow Cytometry Data Analysis

Data collected from the FACSCaliber was analysed using WinMDI 2.8 Software (Perdue University, USA). The programme was used to calculate the geometric mean fluorescence of cells in experimental populations, to create histograms of cellular fluorescence and dot-plots of the size and granularity of cells within populations. Results generated using the WinMDI 2.8 Software were presented using Excel (Microsoft, USA).

2.6 Transmission Electron Microscopy

Transmission electron microscopy (TEM) works in a similar manner to conventional light microscopes, however, TEM does not have the same theoretical limitations as light microscopy and can be used to view specimens in higher resolution. TEM uses a focused stream of electrons that are accelerated towards an ultra-thin sample using a positive electrical potential. The sample affects the flow of the electrons and these changes are detected and used to form an image of the sample.

The procedure for using TEM in this study is as follows; cells in 24-well plates were washed three times by the gentle addition of PBS. After the third PBS wash cells were detached from the wells by exposure to a 0.25% (w/v) trypsin solution (Sigma, UK) containing 0.02% EDTA (w/V) made up in PBS and incubated for 2 mins (37°C, 95% air, 5% CO_2). Trypsin was inactivated by the addition 1 ml of Hams-F10 medium containing 10% FCS. Cell suspensions were removed from their wells and centrifuged at 700 *g*; 4°C for 5 min (U-32R, Boeco, UK) to create a pellet. The medium was gently aspirated from the centrifuge tube and replaced with 1 ml of PBS. The pellet of cells was then washed twice in PBS by centrifugation at 700 *g*, 4°C for 5 min. After the final wash PBS was gently removed and replaced with 1 ml of a mixture of glutaraldehyde (the working solution of 2.5% glutaraldehyde was created by diluting the stock 25% solution in PBS) and osmium tetroxide (1% w/v generated by disolving 0.1 g of osmium tetroxide crystals 10 ml of 1x PBS over-night with stirring in a foil wrapped beaker) buffered with imidazole (0.05 M). Cells were fixed in this mixture for 1 hour at 4°C. After this time the pellet had turned black. The pellet was centrifuged at 1500 *g* for 2 min at room temperature, and then washed once in PBS containing 0.05 M imidazole.

The fixed pellet was then embedded in agar 5% (w/v, dissolved in ddH_20 by heating and allowed to cool) to protect the pellet. The pellet was scraped from the side of the eppendorf tube to ensure the whole pellet was embedded in agar. The agar embedded pellets were then washed 4 times in de-ionised water, for 10 min each time, to remove any residual fixative.

Pellets were then stained with uranyl acetate (UA) (0.5% created by diluting a 2% stock solution in ddH_2O) for 60 min at 4°C. After staining with UA, pellets were dehydrated with a graded series of ethanol solutions: 30%, 50%, 70%, 80%, 90% for 10 mins each, then 3 x 10 min exposures to 100% ethanol. Pellets were further dehydrated with 2 incubations with propylene oxide for 10 min each.

Following dehydration, the pellet of cells was infiltrated in a solution of 50% propylene oxide (Sigma, UK) 50% araldite mix (composed of 5 g araldite CY212: 5 g dodecenylsuccinic acid (DDSA): 0.15 g benzyldimethylamine (BDMA) overnight at

room temperature. Samples were clearly labelled then embedded in araldite mix at 60°C for 48 hours.

Once embedded ultra-thin sections (about 60 nm, light gold in colour) were cut using an ultracut microtome (Reichert-Jung E, Austria) and sections were mounted onto pioloform coated copper grids. Mounted sections were then counterstained using UA (2%) for 10 min and washed three times in de-ionised water. This was followed by further counterstaining using lead citrate (produced by dissolving 2.66 g lead nitrate in 30 ml H_2O which is mixed with 2.52 g of sodium citrate dissolved in a further 30 ml of ddH_2O. The two solutions were mixed for 30 mins with stirring in a foil covered beaker. After mixing, 16 ml of 1 N sodium hydroxide was added with a further 24 ml of ddH_2O. The lead citrate was prepared on the day of use) for 5 min and two more washes in de-ionised water.

Sections were examined using a TEM (Philips EM 208, Philips, UK) operated at 80 kV accelerating voltage with an appropriate magnification. EM images were recorded on film plates (Kodak film 4489, Kodak, UK) and developed in a Kodak D19 developer (Kodak, UK).

Chapter 3

An Analysis of Retinal Lipofuscin Composition

3.1 Introduction

Retinal lipofuscin is a cellular waste product that accumulates with increasing age in the retinal pigment epithelial (RPE) cells of the eye (Feeney-Burns *et al.*, 1984). It has a characteristic golden-yellow colour and is autofluorescent when excited with short wavelength light (Boulton *et al.*, 2004).

Retinal lipofuscin is thought to be primarily derived from the phagocytosis of spent tips of photoreceptor outer segments (POS) that have not been completely degraded (Boulton *et al.*, 1989; Wihlmark *et al.*, 1996b). However, the incomplete degradation of exhausted or old organelles during autophagy is also likely to contribute to its accretion (Brunk *et al.*, 1992; Terman *et al.*, 2006).

Conditions within the retina provide an ideal environment for the generation of reactive oxygen intermediates (ROI), with high oxygen concentrations and diurnal exposure to high energy light. Therefore, it is likely that many of the precursors for lipofuscin are derived from lipids that have undergone oxidative modification and/ or adduction to other biomolecules and are no longer recognised as substrates by lysosomal enzymes in the RPE (Kopitz *et al.*, 2004b; Tanito *et al.*, 2005; Tanito *et al.*, 2006; Kaemmerer *et al.*, 2007). Indeed, the contribution of oxidative stress in the process of lipofuscinogenesis is highlighted by its reduced rate in the presence of anti-oxidants (Robison *et al.*, 1980; Sundelin and Nilsson, 2001). Vitamin A derivatives involved in the visual cycle also play an important role in the formation of retinal lipofuscin, with some reports estimating that up to 90% of lipofuscin constituents could originate from retinoid conjugates (Katz *et al.*, 1985; Katz and Gao, 1995; Wassell and Boulton, 1997; Sparrow *et al.*, 2003b). The contribution of retinoid derivatives in lipofuscin formation is exemplified using RPE65 knockout mice. These mice do not generate 11-*cis*-retinal and do not accumulate significant amounts of lipofuscin (Katz and Redmond, 2001). The presence of retinoids in large quantities is unique to retinal lipofuscin, which together with the environment in which it resides, makes retinal lipofuscin granules distinctive amongst lipofuscins found in the body.

Despite extensive research interest resulting in numerous publications in recent decades, the exact mechanisms of retinal lipofuscin formation and its composition are still poorly understood (Katz, 1985,1989; Yin *et al.*, 1995; Katz *et al.*, 1996; Yin, 1996; Schutt *et al.*, 2002a; Warburton *et al.*, 2005). What is known of retinal lipofuscin granules suggests that there is heterogeneity between and within granules and that the constituent biomolecules have undergone considerable modification (Haralampus-Grynaviski *et al.*, 2001; Simon *et al.*, 2002; Schutt *et al.*, 2003a; Holz *et al.*, 2004).

Much of the interest surrounding retinal lipofuscin is due to its ability to photogenerate ROI when excited with blue-light (Boulton *et al.*, 1993; Nilsson *et al.*, 2003). Blue-light is of a wavelength that has the capacity to penetrate the cornea and lens, reaching the retina and, thus, stimulate lipofuscin in RPE cells (van den Berg and Spekreijse, 1997). ROI have the capacity to seriously disrupt cellular function and cause RPE cell death, indeed, numerous studies using RPE cells *in vitro* have shown a loss in cell viability after light exposure in cells loaded with lipofuscin (Wassell *et al.*, 1999; Schutt *et al.*, 2000; Davies *et al.*, 2001). This is important as RPE atrophy is a key feature in the pathogenesis of AMD.

In early studies Eldred and Katz identified at least 10 fluorophores in the RPE (Eldred and Katz, 1988). Further research then ensued into these fluorophores and to date A2E, iso-A2E and all-*trans*-retinal dimer phosphatidylethanolamine have been identified as constituents of retinal lipofuscin (Eldred and Lasky, 1993; Parish *et al.*, 1998; Fishkin *et al.*, 2005). Of these the most widely studied is A2E. A2E has been shown to induce DNA lesions and apoptosis in RPE cells when illuminated with blue-light, most probably through the formation of A2E-epoxides, whilst other oxidation products of A2E have been associated with complement activation, a process implicated in the aetiology of AMD (Ben-Shabat *et al.*, 2002a; Sparrow *et al.*, 2003c; Zhou *et al.*, 2006).

Thus, retinal lipofuscin and its constituent parts have been associated with AMD. together with other diseases affecting the macular including Bests' disease and Stargardts' disease (Dorey *et al.*, 1989; Lopez *et al.*, 1990; Solbach *et al.*, 1997;

Bakall *et al.*, 2007). However, to date no molecular mechanisms have been determined to form a causative link.

The aim of this study was to enhance the knowledge of lipofuscin components and improve our understanding of the proteomic nature of retinal lipofuscin granules. Isolation of retinal lipofuscin using a sucrose density gradient results in an enriched fraction of lipofuscin granules that invariably contains extra-granular debris of similar density. Previous studies looking into the protein content and oxidative modifications present within retinal lipofuscin included an extensive quantity of the extra-granular debris in their analysis, but failed to state whether their findings were present in the granules, the debris or both (Schutt *et al.*, 2002a; Schutt *et al.*, 2003a; Warburton *et al.*, 2005). Equally, many *in vitro* studies using *ex vivo* retinal lipofuscin include the extra-granular debris in their preparations loaded into cells. Thus, it is important to identify whether the bioactivity associated with lipofuscin from these studies comes from the granules themselves or the co-localised debris.

Accordingly, we set out to achieve a purified sample of lipofuscin granules that was free from contaminating debris and could be characterised with respect to its proteomics, oxidative modifications and bioactivity. The purified sample was then compared to the 'crude' sample of lipofuscin granules with respect to the above characteristics. It was believed the complex problem of identifying the proteomic components of retinal lipofuscin would be best suited to a multi-disciplinary approach so as to prevent a repetition of the mistakes made in previous attempts by other groups. As such a collaboration with the Crabb laboratory based in the Cole Eye Institute, Cleveland was established as members of this group have considerable expertise in dealing with proteomic analysis of related material having published a well received article on the proteomic content of drusen (Crabb *et al.*, 2002). During this study I was fortunate enough to visit the Crabb laboratory and assist in a number of experiments related to this project.

3.2 Materials and Methods

3.2.1 RPE Lipofuscin Isolation and Purification

RPE cell and lipofuscin isolation took place in the School of Optometry and Vision Sciences, Cardiff University, Cardiff. The purification of granules took place in Cole Eye Institute and Lerner Research Institute, Cleveland Clinic Foundation, Cleveland. Isolation of RPE cells and retinal lipofuscin was conducted as described in the General Materials and Methods, Section 2.1. Additional to the method described in Section 2.1, the final lipofuscin pellet was further purified by centrifugation on a third discontinuous density sucrose gradient (1.0, 1.2, 1.4 and 1.5 M sucrose) and the centrifugation (103000 *g* for 1 hr at 4°C) and washing steps (7000 *g*, 10 mins and 4°C) repeated. The third step was added after viewing TEM images of lipofuscin granules that had been isolated using a method that employed just two density gradients which showed considerable debris between lipofuscin granules (Figure 3.2).

Lipofuscin isolated using discontinuous sucrose density gradients were termed 'crude' lipofuscin. Three crude lipofuscin samples were analysed in this study, Preparation 1, from 65 donors, (130 eyes) mean age 70 years $\pm$ 10 years; Preparation 2, from 30 donors (60 eyes), mean age 65 years $\pm$ 8 years; Preparation 3, from 41 donors (82 eyes), mean age 76 years $\pm$ 11.

To purify the crude lipofuscin samples aliquots were either (i) washed 6x in 15 mM N-ethyl morpholine acetate (NEM) pH 8.3, 2 mM EDTA, 100 mM BHT, 0.2% SDS; or (ii) digestion with proteinase K (10 µg/µl, 24 hours/ room temperature) in 15 mM NEM pH 8.3, 2 mM EDTA, 100 mM BHT, 0.2% SDS.

Quantification of each of the lipofuscin samples was conducted by counting on a haemocytometer and also measuring dry weight using a Sartorius Model SE2 microbalance (Data Weighing System Inc. IL, USA).

3.2.2 Light, Transmission and Confocal Fluorescent microscopy

TEM analysis was conducted initially to analyse the purity of lipofuscin granules. This was undertaken in Cardiff using the method described in Section 2.6 of the General Materials and Methods Chapter. Variations from the method described were: no cells were involved so there was no need for detachment from culture plates. Instead, lipofuscin granules were centrifuged at 4000 *g*, 3 min at 4°C in a cooled micro-centrifuge (Sorvall Pico, Sorvall, UK) to create a pellet. The pellet was then treated as cells were in Section 2.6, with the exception that the lipofuscin pellet was not embedded in agar.

Initial fluorescence microscopy analysis of retinal lipofuscin granules was conducted within the School of Optometry and Vision Sciences, Cardiff University. The procedure was as follows; 25 µl of retinal lipofuscin suspended in PBS was gently loaded onto a glass slide (Lamb RA, Sussex, UK) and a glass coverslip (VWR International, UK) applied. The sample was immediately viewed using a fluorescence microscope (Leica CTR 6000, Leica, Milton Keynes) equipped with a band-pass filter to detect FITC and a DFC359 FX camera (Leica, Milton Keynes). Images were analysed using Microsoft Picture Manager (Microsoft, USA).

Retinal lipofuscin granules underwent further microscopic analysis to compare the inter-granular debris present between crude and purified samples. This took place in the Cole Eye Institute and Lerner Research Institute, Cleveland Clinic Foundation, Cleveland. For analysis of both crude and purified lipofuscin granules by TEM and light microscopy samples were prepared initially in the same way. Granules were fixed in 2% glutaraldehyde and 1% paraformaldehyde, post-fixed in 1% osmium tetroxide, dehydrated in a graded series of ethanol concentrations before further dehydration in propylene oxide. The dehydrated pellets were then embedded in epon/araldite and polymerised for 48 hrs at 60°C.

Semi-thin sections of the embedded pellet were cut using a diamond histotech knife, ready for light microscopy. Sections were dried and stained with toluidine blue before

being imaged on a Zeiss Axiophot microscope equipped with a Hamamatsu digital camera.

For TEM, thin sections were taken from each of the samples using an RMC, MT-XL (Tucson, AZ) ultramicrotome. Sections were stained with uranyl acetate and lead citrate before being viewed using a Tecnai 20, 200 kV digital electron microscope equipped with a Gatan image filter.

Before the fixing process an aliquot was taken for each sample (~10^8 granules) for immuno-TEM. The crude and purified granules were incubated in PBS containing 2.5 μg of anti-carboxyethylpyrrole (CEP) monoclonal antibody (mAb) and 1% BSA for 1 hr at room temperature. The pellets were washed thrice in ice cold PBS containing 1% BSA and 0.1% Triton X-100 before incubation with horseradish peroxidise-conjugated rabbit anti-mouse imunnoglobulin G (IgG) for 1 hr at room temperature. Three more washes ensued after which diaminobenzidine (DAB) was added to 0.5 mg/ml and incubated until a brown colour formed (~ 20 mins). The pellet was washed twice then prepared as described above for TEM. Negative controls were included that contained no primary anti-body. A Leica laser scanning confocal microscope (TCS-SP2, Leica) using a high magnification, oil immersion objective lens was used for confocal microscopy. Images were collected sequentially in the green, red and differential contrast channels, through the entire sample using a 1μm step-size.

3.2.3 Morphometric Analysis

Morphometric analysis took place in the Cole Eye Institute and Lerner Research Institute, Cleveland Clinic Foundation, Cleveland. Comparisons of the two samples of lipofuscin granules were carried with respect to area, roundness, aspect ratio, perimeter and mean diameter. To do this, TEM images of both the crude and washed samples were analysed using a semi-automated batch-processing routine generated in Image-Pro Plus 6.2 (Media Cybernetics)

3.2.4 HPLC Analysis of Bisretinoids

HPLC analysis of the bisretinoid components of the crude and purified lipofuscin granules took place in the Department of Ophthalmology, Columbia University, New York. Crude and purified granule samples were extracted using Folchs extraction (chloroform:methanol 2:1 v/v), filtered initially through cotton, then through a C18 Sep-Pak cartridge (Millipore, Bedford, MA) in methanol containing 0.1% TFA and dried under Argon. The extracts were re-dissolved and analysed on an Alliance HPLC system (Waters Corp, Milford, MA) equipped with a 2695 Separation module, a 2996 Photodiode Array Detector (with monitoring at 430 and 510 nm), Empower® software, and Atlantis® dC18 column (3μm, 4.6 x 150 mm, Waters, USA) and using aqueous acetonitrile/ 0.1% of TFA gradients with a flow rate of 0.8 ml/min as described previously (Parish *et al.*, 1998). A2E, iso-A2E and all-*trans*-retinal dimer-phosphatidylethanolamine were identified and quantified based on UV-visible absorbance spectra and elution times that correspond to authentic synthetic compounds.

3.2.5 Phototoxicity Assay

The phototoxicity assays were carried out in the School of Optometry and Vision Sciences, Cardiff University, Cardiff. ARPE-19 cells were grown to confluence in 24-well plates (Orange Scientific, UK) as described in Section 2.2. of the General Materials and Methods chapter. After 7 days at confluency cells were exposed to equal amounts (measured by granule count, 300 granules/cell) of either crude or washed granules for 24 hrs. Control cells were maintained on the same plates but contained no lipofuscin. Cells were then maintained in basal medium as described for a further 7 days (Schutt *et al.*, 2000). Immediately prior to light exposure basal medium was replaced with a custom-made culture medium (SF10PF, Gibco, UK) based on Hams F-10 medium, however, the photosensitisers: phenol red, tyrosine, riboflavin, tryptophan and folic acid were removed. Cells were then exposed to blue-light (400-500 nm 2.8 mW/cm^2), generated by a sunlight simulator (SOL 1200, Holne UV Technology, Munich, Germany), at 37°C for 48 hours. A dark maintained control consisted of cells, with and without lipofuscin, wrapped in black foil and placed atop

the lamp. The cell viability was then measured using the MTT assay as described in the General Materials and Methods, Section 2.4. The MTT assay was used to provide a reliable technique for measuring levels of cell viability (Schutt *et al.*, 2000). Each experiment was carried out in triplicate and repeated four times.

3.2.6 SDS-PAGE and Western Analysis

SDS-PAGE and Western analysis was conducted in the Cole Eye Institute and Lerner Research Institute, Cleveland Clinic Foundation, Cleveland. Prior to Western blot analysis the crude and purified lipofuscin preparations under went Folchs extraction. The chloroform soluble and insoluble fractions were separated, with the chloroform insoluble fraction being sonicated and then boiled in SDS sample buffer containing 0.1 M DTT. Approximately 20 μg of this material was then applied to a polyvinyldene fluoride (PVDF) membrane (Millipore, Bedford, MA) using a slot blot apparatus (Bethesda Research Laboratories HS-1878) and probed with either; mouse anti-nitrotyrosine mAb (1 μg/ml in 5% low fat milk in PBS, Upstate Biotechnology, Lake Placid, NY, USA), mouse anti-CEP mAb (0.2 μg/ml in 5% low fat milk in PBS), or rabbit polyclonal (pAb) anti-iso[4]LGE_2 (1 μg/ml in 5% low fat milk in PBS). All secondary antibodies were HRP conjugated (0.1 μg/ml in 5% low fat milk in PBS, Santa Cruz Biotech, USA). ECL Western blotting detection system (GE Healthcare, USA) was used as substrate.

3.2.7 Protein Identification by LC MS/MS

Protein identifications were carried out in the Cole Eye Institute and Lerner Research Institute, Cleveland Clinic Foundation, Cleveland. Crude and proteinase K treated lipofuscin (~170 μg dry weight each) were sonicated then boiled 5 mins in Laemmli SDS-PAGE sample buffer and subjected to 10% SDS-PAGE and stained with colloidal Coomassie blue (Gel Code Blue, Pierce Chemical Co.). Gel slices were excised from the top to the bottom of the lane, in-gel proteins were reduced with DTT (10 mM), alkylated with iodoacetamide (55 mM), and digested in situ with trypsin, then peptides were extracted for LC MS/MS. LC MS/MS was performed with a

QTOF2 instrument (Waters) using a Cap LC system (Waters), a 0.3 x 5-mm trapping column (C18 Pepmap 100, LC Packings), a reverse phase separating column (75 μm x 5 cm Vydac C18), and a flow rate of 250 nl/min (Crabb *et al.*, 2002). Gradient LC separation was achieved with aqueous formic acid/acetonitrile solvents. The QTOF2 mass spectrometer was operated in standard MS/MS switching mode with the three most intense ions in each survey scan subjected to MS/MS analysis.

Alternatively, equal amounts (by dry weight) of crude or SDS washed lipofuscin preparations were subjected to overnight tryptic digestion in 30mM NEM acetate pH 8.6, 0.05% SDS containing 0.3 μg trypsin and soluble components fractionated by strong cation exchange (SCX) chromatography using a PolySulfoethyl A column (1.0 x 150 mm, 5 μm particle size; 200 Å pore size), a flow rate of 50 μl/min and a gradient of 0-600 mM KCl in 25% acetonitrile, 10 mM KH_2PO4, pH 3 with fractions collected at 10, 1 min intervals. SCX fractions were analysed by LC MS/MS on a QTOF2 mass spectrometer as described above.

Protein identification from QTOF2 MS data utilised MASSLYNX 4.1 software (Waters), the Mascot search engine (Matrix Science, version 2.1), and the Swiss-Protein sequence database (August 21, 2007, version 54.1). The Swiss Protein database search parameters included all human entries (~17K total sequences), 1 missed tryptic cleavage site allowed, precursor ion mass tolerance = 0.8 Da, fragment ion mass tolerance = 0.8 Da, and protein modifications for Met oxidation and Cys carboxyamidomethylation. A minimum Mascot ion score equal to 25 was used for accepting all peptide MS/MS spectra. A minimum of 2 unique peptides per protein was required for all protein identifications.

3.2.8 Amino Acid Content Analysis

Amino Acid analysis was performed at the Cole Eye Institute and Lerner Research Institute, Cleveland Clinic Foundation, Cleveland. Approximately 1 – 2 μg of sample (proteins or peptides) were dried before HCl (6 N, 300 μl) and a crystal of phenol (~ 1 – 2 mg) was added. Air was removed from the sample by flushing with argon gas. The vial was heated at 150 °C for 1 hour, followed by the release of pressure and

cooling of the sample to room temperature. The sample was then flushed with argon and stored at –20 °C until ready to perform phenylthiocarbamyl derivatisation of the amino acids. Phenylthiocarbamyl derivatisation makes amino acids UV visible. The acid from the hydrolysis was neutralised with the base diisopropylethylamine (DIEA) in methanol and dried. Once dried, samples were analysed immediately. For HPLC, the samples were dissolved in transfer buffer (29 mM sodium acetate, pH 5.2, 0.025 % K_3EDTA). Typically, 14 µl of transfer buffer solution was added to hydrolysed and derivatised lipofuscin granules and 8 µl of this solution was injected for analysis. HPLC was performed with an Agilent 1100 HPLC system, Spheri-5 PTC, 5 µ, C18, 220 x 2.1 mm column (Perkin Elmer, Wellesley, MA) and with solvent A (50 mM sodium acetate buffer, pH ~5.4) and solvent B (70 % acetonitrile, 32 mM sodium acetate, pH ~6.1). The gradient (flow rate of 300 µl / min) was from 20 – 68 % B for 20 mins, and then to 100 % B in five mins and dropped to the initial condition of 20 % B in 2 mins. Standard amino acids (Standard H, Pierce) were used. Standard H (300 pmol) was derivatised and separated using the above chromatographic method. The average peak area was calculated for each amino acid from multiple samples of standard H and an analysis response factor was calculated for each amino acid by dividing the average peak area by the pmole of each amino acid. This was used to create a calibration file for each amino acid. The amount of the unknown samples was obtained by dividing the peak area from each amino acid by the response factor. For pure proteins of known composition and molecular weight, the concentration of the protein can be calculated. For mixtures of proteins of unknown mass and sequence, the total mole percentages of each amino acid were determined.

3.3 Results

3.3.1 Purification of Lipofuscin Granules

The isolation of retinal lipofuscin granules from RPE cells using a discontinuous sucrose density gradient is an established method that has been used in many studies involving analysis of retinal lipofuscin (Boulton and Marshall, 1985; Davies *et al.*, 2001; Schutt *et al.*, 2003b). However, this method consistently yields a population of granules surrounded by a considerable amount of extragranular debris of similar density.

After isolation, the retinal lipofuscin granules were viewed by fluorescence microscopy. The granules isolated after three discontinuous sucrose density gradients display the characteristic autofluorescence associated with retinal lipofuscin (Figure 3.1).

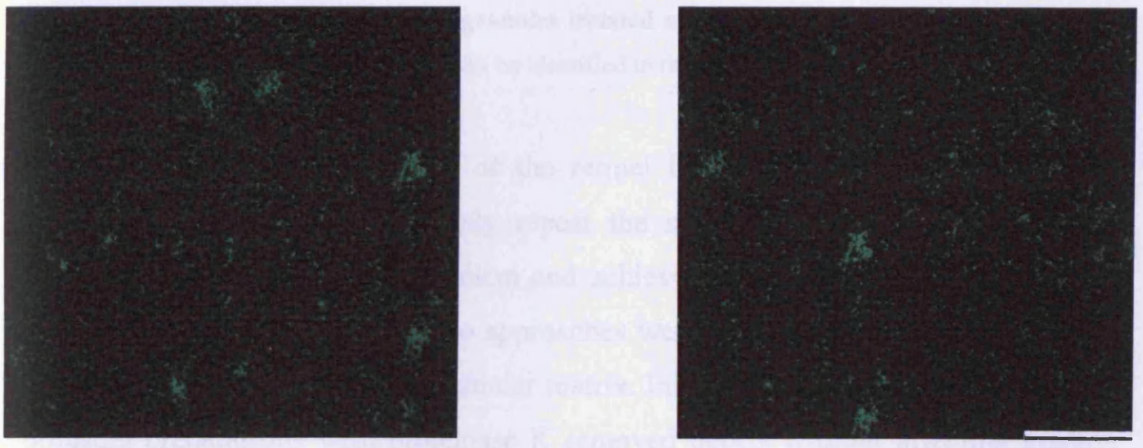

Figure 3.1 Fluorescence microscopy of retinal lipofuscin granules isolated after 3 discontinuous sucrose density gradients. The granules display the characteristic autofluorescence associated with retinal lipofuscin. Scale bar is equivalent to 75 μm.

TEM images of retinal lipofuscin illustrates that the isolation of granules using a discontinuous sucrose density gradient produces an enriched fraction of granules that are surrounded by debris of similar density (Figure 3.2). Repeating the isolation step with a third discontinuous sucrose density step resulted in a sample of granules that were less contaminated with debris (Figure 3.3), however, this method of enrichment

resulted in a loss of granules. It could be speculated that a fourth or fifth sucrose gradient would have resulted in a more pure sample, but the amount of lipofuscin recovered would possibly have been too small to conduct any further analysis.

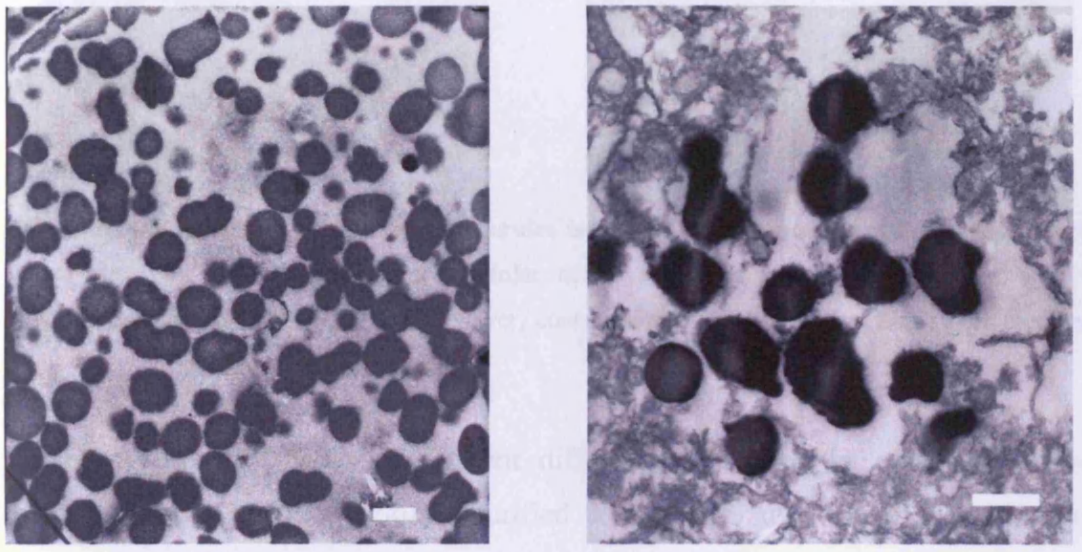

Figure 3.2. TEM images of lipofuscin granules isolated after 2 discontinuous sucrose gradient steps. Considerable inter-granular debris can be identified in the images. Scale bars represent 1 μm.

To conduct a proteomic analysis of the retinal lipofuscin granules sample when surrounded by debris would simply repeat the studies that had previously been undertaken. To overcome this problem and achieve a purified sample for structural and functional characterisation, two approaches were taken to purify the sample and remove the debris from the extragranular matrix. Initially it was found washing crude lipofuscin preparations with proteinase K removed debris without affecting granule structure (Figure 3.4. G, H, J). Secondly, simply washing the preparations in 0.2% SDS without proteinase K resulted in an extra-granular free granule population (Figure 3.4. B, D, L).

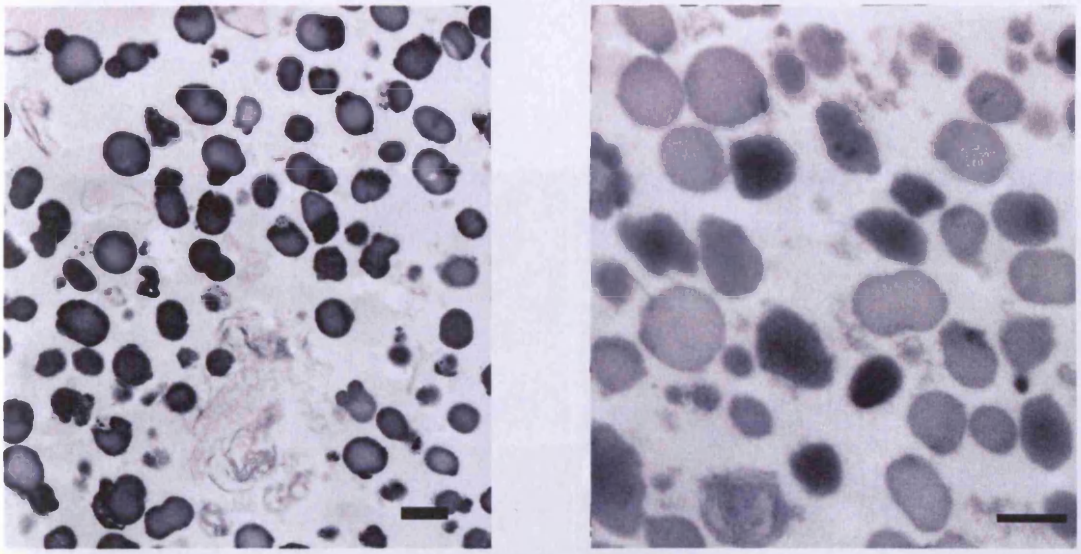

Figure 3.3 TEM images of lipofuscin granules isolated after 3 discontinuous sucrose gradient steps. There is a reduction in inter-granular debris compared to granules isolated with two discontinuous sucrose gradient steps; however, contaminants are still present. Scale bars represent 1 μm.

There was no statistically significant difference identified in either the granule diameter (crude, 0.74 ± 0.24μm; purified 0.76 ± 0.20 μm, p=0.12) or circularity (aspect ratio crude, 1.23 + 0.81; purified 1.25 + 0.18, p= 0.06) when analysed using morphometric TEM images. However, morphometric analysis revealed that crude granules had a smoother surface than those that had been washed (crude, 1.06 + 0.09, purified, 1.08 + 0.09, $p < 0.0001$). However, this difference has been concluded to not be significant and most likely the result of virtual corners created by the analysis software when separating touching granules in the more tightly packed pure lipofuscin sample.

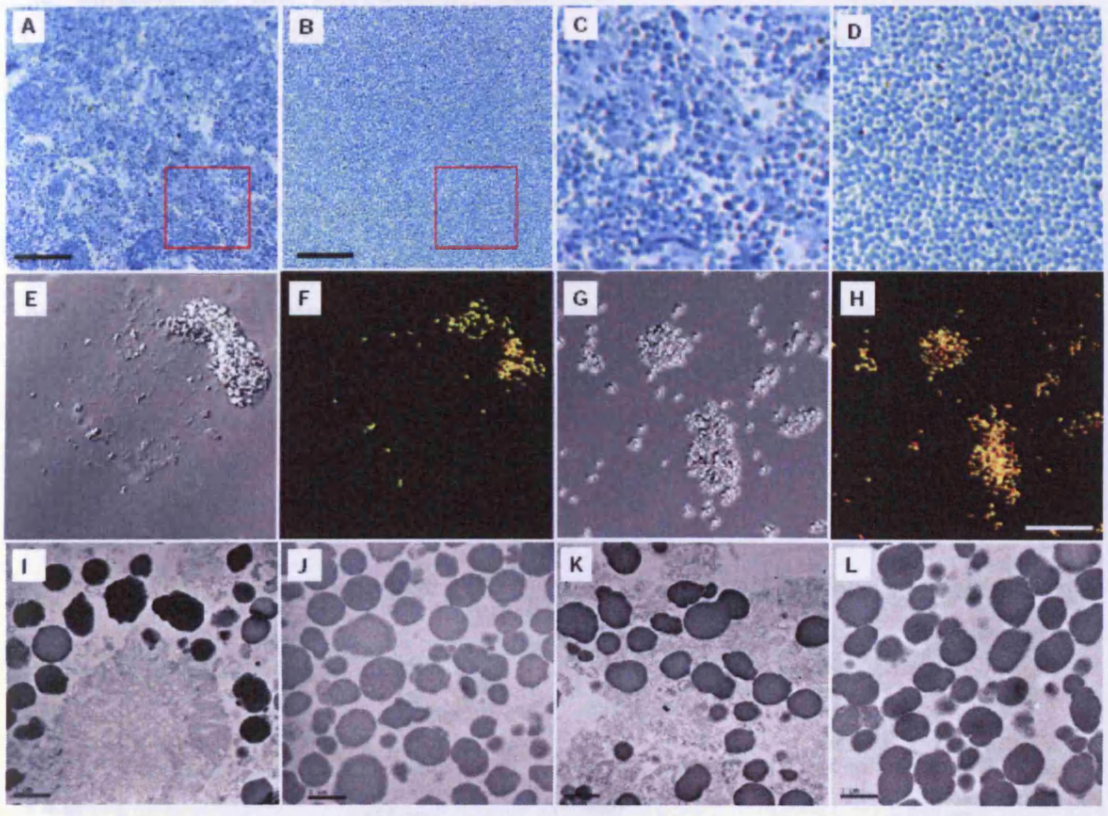

Figure 3.4. Light, Fluorescent Confocal and Transmission Electron Microscopy of Lipofuscin. Light microscopy of (A) crude lipofuscin and (B) SDS washed lipofuscin granules stained with toluidine blue. Bar scale equals 20 μm in (A) and (B). Magnified view of boxed region is shown in (C) crude lipofuscin and (D) SDS washed granules. Confocal microscopy of crude lipofuscin (E, F) and proteinase K treated lipofuscin granules (G, H). Differential interference contrast (DIC) images (E, G) and corresponding laser-excited autofluorescence are shown (F, H). Bar scale equals 16 μm in (E-H). Transmission electron micrographs of (I, K) crude lipofuscin, (J) lipofuscin granules after proteinase K treatment, and (L) SDS washed lipofuscin granules. Bar scale equals 1 μm in (I-L). Significant extra-granular debris is apparent in crude lipofuscin but is absent in the SDS washed or proteinase K treated lipofuscin granules.

3.3.2 Bisretinoids in RPE lipofuscin

The quantity of the bisretinoids A2E, iso-A2E and all-trans-retinal dimer – phosphatidylethanolamine were examined by HPLC in both the crude and purified lipofuscin samples. Equal amounts of granules (by granule count) from the crude and purified samples underwent extraction with chloroform and methanol and were then analysed using reverse-phase HPLC (Figure 3.5).

There was no significant difference in the fluorophore levels in either the crude or purified sample when the 15.1% error in counting is considered. These results are consistent with the hypothesis that the vitamin A derived moieties are localised within the granules.

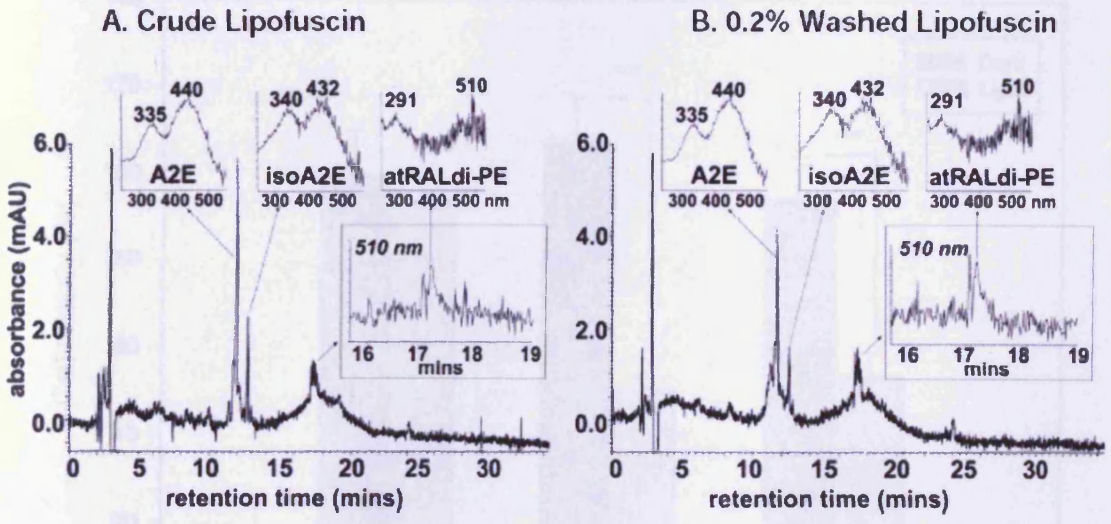

Figure 3. 5. Quantitation of Bisretinoid Pigments in RPE Lipofuscin.

Reverse phase-HPLC analysis of chloroform/methanol extracts of equal amounts (~5.5 x 10^7 granules) of (A) crude lipofuscin and (B) SDS washed lipofuscin granules. Chromatograms obtained with 430 nm monitoring. Top inserts, UV-visible spectra of A2E, isoA2E, and all-*trans*-retinal dimer phosphatidylethanolamine in acetonitrile/water. Lower right inserts, monitoring at 510 nm, the detection wavelength favouring all-trans-retinal dimer phosphatidylethanolamine, with chromatogram expanded between retention times 15.5-19 min. The total amount of A2E and isoA2E recovered was ~380 pmol from the crude and ~328 pmol from the purified granules; the total amount of all-*trans*-retinal dimer-PE was ~201 pmol and ~187 pmol, respectively. These values are within experimental error of being equal given the 15.1% relative standard deviation of the mean granule count.

3.3.3 Phototoxicity of RPE lipofuscin

The phototoxicity of crude and purified lipofuscin granules was assessed by loading ARPE-19 cells with equal quantities of either crude or SDS-washed granules (by granule count) before exposing them to intense blue-light. Control cells included those that were maintained in the dark with and without lipofuscin and those not fed lipofuscin and exposed to light. There was no significant loss in viability of cells maintained as controls. However, cells loaded with either the crude or SDS-washed lipofuscin granules displayed an approximately 50% loss in viability (Figure 3.6). These results signify that the photoreactive species associated with retinal lipofuscin are unlikely to be protein moieties and are intrinsic to the granules and not the extra-granular debris.

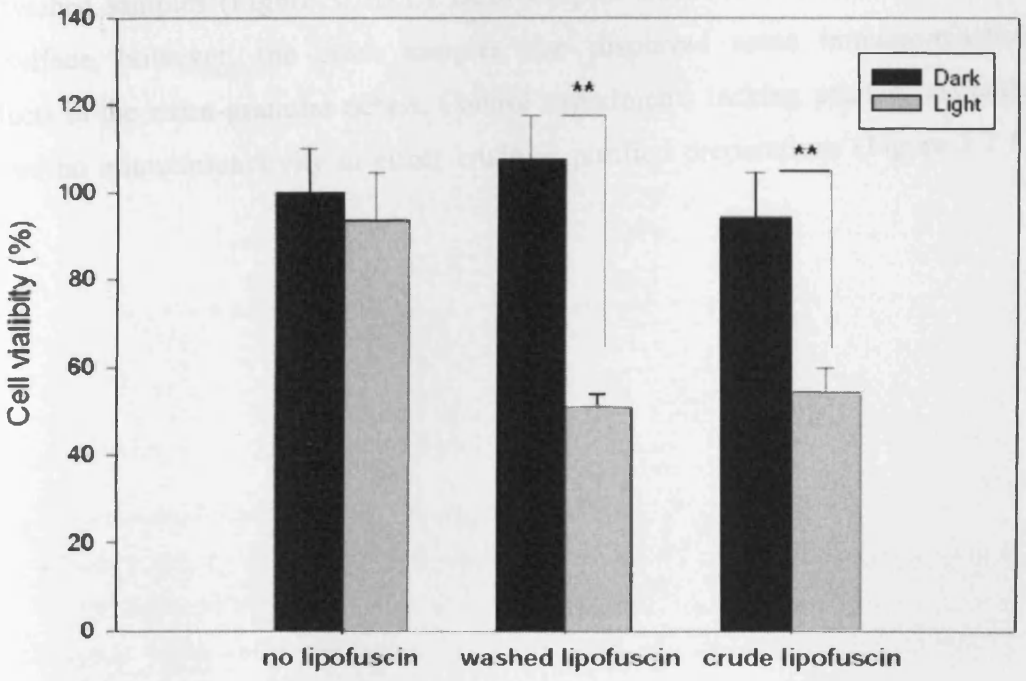

Figure 3.6. Phototoxicity of Lipofuscin.

Cultured ARPE-19 cells were assayed for viability by MTT after treatment with equal amounts (300 granules/cell) of SDS washed lipofuscin or crude lipofuscin, with or without exposure to intense blue light for 48 hrs. Viability was calculated with reference to control cells not fed LF and maintained in the dark (set to 100%). Debris-free lipofuscin reduced ARPE-19 cell viability by the same amount as crude lipofuscin, namely ~50%. **$p<0.0001$, one-way ANOVA.

3.3.4 Oxidative modifications in RPE Lipofuscin

Western slot blot analysis was used to determine if either the crude or SDS washed lipofuscin granules contained constituents modified by either nitrotyrosine, 2-(ω- CEP or iso[4]LGE_2. Nitrotyrosine is a molecule deemed to be an indicator of cell damage and the production of nitric oxide. Nitrotyrosine has also been linked to inflammatory conditions such as atherosclerotic plaques. CEP and iso[4]LGE_2 are the downstream products of oxidative damage to docosahexaenoyl and arachidonyl containing lipids, respectively. Both samples displayed immunoreactivity for nitrotyrosine, CEP and iso[4]LGE_2 (Figure 3.7.A, B, C).

CEP-immunoreactivity was confirmed with Immuno-TEM analysis of both the crude and washed samples (Figure 3.7.D,E). Both samples exhibited immunoreactivity on the surface, however, the crude samples also displayed some immuno-reactive products in the extra-granular debris. Control experiments lacking primary antibody showed no immunoreactivity in either crude or purified preparations (Figure 3.7 F, G).

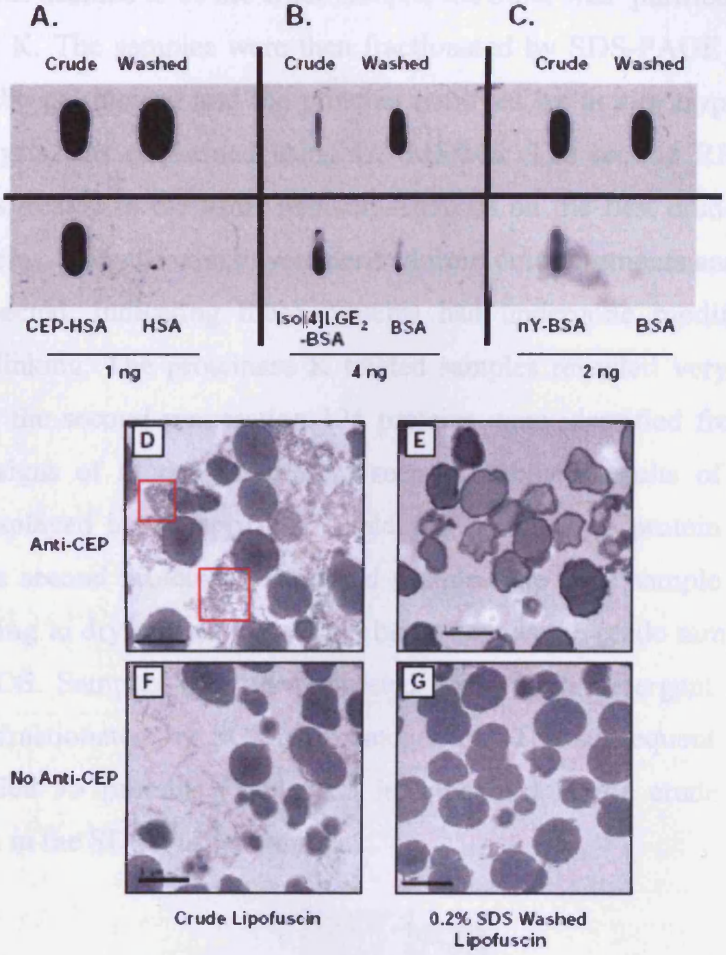

Figure 3.7. Oxidative Modifications in Lipofuscin.

Slot blot Western analyses of crude and SDS washed lipofuscin (~4 x 10^7 granules applied per blot) are shown for immunoreactivity to (A) CEP adducts, (B) iso[4]LGE_2 adducts, and (C) nitrotyrosine. Controls include CEP modified and unmodified human serum albumin (HSA), iso[4]LGE_2 modified and unmodified BSA and nitrotyrosine modified and unmodified BSA with the applied amounts indicated. Analyses by TEM of crude (D) and SDS washed (E) lipofuscin for CEP immunoreactivity with anti-CEP primary antibody, HRP-conjugated secondary antibody and diaminobenzidine (DAB) detection. TEM control analyses with secondary antibody and DAB but no primary antibody are shown for crude lipofuscin (F) and SDS washed granules (G). Intense CEP immunoreactivity is apparent on the granule surface (panels D, E) and in regions of the extragranular debris (boxed in panel D).

3.3.5 Identification of proteins present in RPE lipofuscin granules

Three RPE lipofuscin isolation preparations were used in the determination of its protein components. The first was divided equally (according to dry mass) into two samples. One was deemed to be the crude sample, the other was 'purified' by washing with proteinase K. The samples were then fractionated by SDS-PAGE (Figure 3.8), with slices of the gel incised and the proteins removed by *in situ* tryptic digestion. Proteomic analysis was performed using LC MS/MS. The second RPE lipofuscin preparation was treated in the same manner. Analysis on the first crude preparation yielded 77 proteins, many of which were derived from outer segments and with higher mass than expected, indicating these proteins had undergone modifications and possibly cross-linking. The proteinase K treated samples revealed very few protein components. In the second preparation 124 proteins were identified from the crude aliquot, again signs of modification were seen (Combined results of two protein analyses are displayed in the appendix Table A.2). Very little protein content was identified in the second proteinase K treated sample. The third sample was divided equally (according to dry mass), one aliquot being kept as the crude sample the other washed with SDS. Samples were then digested using dilute detergent solution and peptides were fractionated by SCX chromatography. The subsequent LC MS/MS analysis identified 75 proteins (Table A.3 in appendix) in the crude sample and minimal protein in the SDS washed sample.

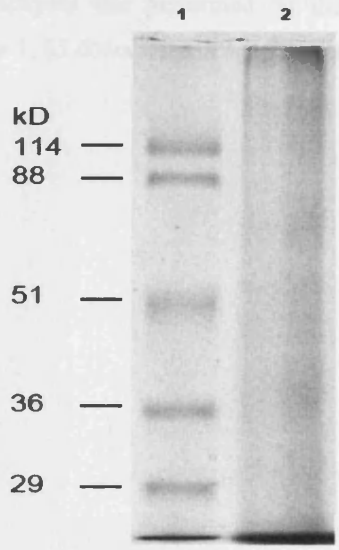

Figure 3.8. SDS-PAGE and Western analysis of crude lipofuscin. The chloroform insoluble fraction of crude lipofuscin (Preparation 2, average. age 65 years) was separated by 10% SDS-PAGE. Lane 1, molecular weight standards; lane 2, crude lipofuscin ~2.0 μg.

3.3.6. Amino acid content of RPE lipofuscin

Amino acid analysis of each of the preparations was used to quantify the protein content. Replicate amino acid analyses identified that there was a five-fold greater protein content in crude samples than in proteinase K or SDS treated samples (Table 3.1).

Crude preparations contained 10-12% of protein (w/w) that can be degraded to amino acids. Proteinase K or SDS treated samples were found to contain very little protein that could be degraded to amino acids (~2% w/w) and there was no significant difference in the amino acid content of these samples. Differences in the amino acid composition in donor group preparations did occur, highlighting the heterogeneous make-up of lipofuscin populations.

Table 3.1. Summary of Amino Acid content of HCl-Hydrolysate from lipofuscin preparations

Preparation	Number of Analyses	% Amino Acid (w/w)	Average % Amino Acid (w/w)
Crude-Preparation 1	3	9.2	10.8
Crude-Preparation 3	3	12.3	
Proteinase K-Preparation 1	3	1.9	2.2
SDS Washed-Preparation 3	3	2.5	

Phenylthiocarbamyl amino acid analysis was performed on the above lipofuscin preparations as describe in the methods. Preparation 1, 65 donors, mean age 70 years and preparation 3, 41 donors, mean age 76 years.

3.4.Discussion

This study set out to obtain a purified sample of lipofuscin granules that were free from extragranular debris. The purified sample was then compared with the crude isolate in respect to bisretinoid components, bioreactivity towards RPE cells, oxidative modifications present and proteomic components.

The isolation of retinal lipofuscin from RPE cells involves separating the granules from other cell constituents using a discontinuous sucrose gradient (Boulton and Marshall, 1985). However, retinal lipofuscin granules are not unique within the RPE with respect to their density. Using TEM micrographs we have shown that the isolation procedure results in an enriched fraction of granules that is surrounded by a considerable amount of other material (Figure 3.2). To reduce the amount of extra-granular material surrounding the sample we extended the isolation procedure by introducing further sucrose density gradients. Consequently, we have demonstrated that the amount of extra granular material is reduced with successive purifications using discontinuous sucrose density gradients (Figure 3.3); unfortunately, there is also a concomitant loss in granules with the increase in purity. To ensure that enough retinal lipofuscin remained for further analysis another method of removing the extra-granular debris that would leave a pure sample of granules was sought.

A purified sample of granules was achieved by washing the isolates with either SDS or proteinase K. Both samples were then compared using microscopy techniques to determine the extent of extragranular contamination present. Aliquots of crude granules showed extensive contamination (Figure 3.4. A, C, I, K), whereas the purified sample showed no contamination (Figure 3.4. B, D, J, L). However, the granules in the purified sample appear to lose their outer membrane. Removal of the surrounding material would allow for a more accurate characterisation of granular proteins than in previous studies that contained high levels of co-isolated debris in their samples (Schutt *et al.*, 2003b; Warburton *et al.*, 2005).

TEM images of the granules underwent morphometric analysis that indicated washing granules with SDS or proteinase K left them intact. This is supportive of there being

no significant difference in mean diameter or circularity between the crude and purified samples, with the average diameter for both samples agreeing well with those previously cited (Haralampus-Grynaviski *et al.*, 2003). However, the granules in the crude sample were found to have a significantly smoother surface than the washed granules. This could possibly be the result of surface associated molecules being removed during the washing process, or of analysis software limitations.

The two samples were analysed for the presence of the bisretinoids; A2E, iso-A2E and the all-*trans*-retinal dimer phosphatidylethanolamine. These bisretinoids, in particular A2E, have undergone intensive scrutiny with respect to the role they play in lipofuscin phototoxicity and the adverse effects they have on cell function (Schutt *et al.*, 2000; Sparrow and Cai, 2001; Schutt *et al.*, 2002; Zhou *et al.*, 2006). The two samples that were analysed in this study were found to have equivalent levels of each of the bisretinoids in samples of equal size (according to granule count) (Figure 3.5.). This suggests that the bisretinoid components are present within the core of the granule and are not surface associated or easily removed. Similarly, the pure and crude samples were found to be equally bioreactive when loaded into ARPE-19 cells and exposed to high intensity blue-light (Figure 3.6.). Thus, signifying that the bioreactive component of lipofuscin is indubitably associated with the granules and not the surrounding debris.

The major difference recorded between the two sample sets was the proteins identified in the two. Granules that were washed with SDS or proteinase K showed limited Coomassie blue reactivity when analysed using SDS-PAGE and few positive protein identifications when processed using conventional mass spectrometric methods. However, from the crude sample, including extragranular material, a total of 186 proteins were identified, many of which had higher apparent mass than predicted indicating that they had undergone some sort of modification. Approximately 40% of the proteins identified in the crude sample have been previously described by others in reports on the protein content of retinal lipofuscin (Schutt *et al.*, 2003b; Warburton *et al.*, 2005). This is symptomatic that many of the proteins identified in these studies may have arisen from the extragranular debris. Of the proteins identified many originated from the POS, including rhodopsin and the RPE, such as RPE65.

An important aspect of this study was the comparison of photoreactivity of retinal lipofuscin samples and their effect on RPE cells when irradiated with blue-light. Many studies analysing the photoreactivity of retinal lipofuscin and its effect upon RPE cells have used the discontinuous sucrose gradient method for obtaining a sample from RPE cells, and would, therefore, have obtained a sample that was also contaminated with inter-granular debris. We have demonstrated that the photoreactivity of retinal lipofuscin and its deleterious impact upon RPE cells when excited with blue-light is not affected by the removal of the co-isolated debris. Equally, this section of the study has demonstrated that if proteins are removed from the granular-surface, or from below the lost membrane, during the purification steps the proteins removed are not intrinsic to the damaging effect that photoexcited retinal lipofuscin has on RPE cells and appear to play no role in the bioreactivity of the lipofuscin molecules.

Oxidative stress has long been hypothesised to play a role in lipofuscinogenesis, with the suggestion that compounds become adducted or crosslinked to each other and are, therefore, no longer recognisable by lysosomal enzymes (Schutt *et al.*, 2003b; Kaemmerer *et al.*, 2007). Using Western slot blot techniques crude and purified lipofuscin granules showed positive immunoreactivity towards products of lipid peroxidation including CEP and iso[4]LGE_2. Another marker of oxidative stress, nitrotyrosine, was also observed in both samples. This is indicative that oxidative stress in the POS and probably the RPE plays a significant role in the formation of lipofuscin granules.

Nitrotyrosine adducts are formed in the presence of nitric oxide which is a free radical that reacts readily with other free radicals. This often results in the formation of species that are more reactive than their precursors. Particular research interest has focused on the reaction between nitric oxide and the superoxide anion to form peroxynitrite (Halliwell *et al.*, 1999). Peroxynitrite has the potential to react with DNA and proteins producing modifications that can affect protein function (Halliwell, 2001). Nitration of tyrosine in proteins has been shown to increase *in vivo* during oxidative stress, to be elevated in rats experiencing ocular inflammation, to be associated with a number of inflammatory related diseases and to cause an increase in

the expression of VEGF in retinas when present in high levels (El-Remessy *et al.*, 2003; Koeck *et al.*, 2004; Adithi *et al.*, 2005; Aslan *et al.*, 2006).

Iso[4]LGE_2 is a member of the family of isolevuglandins that are reactive γ-ketoaldehydes generated by free radical oxidation of arachidonate containing lipids, of which there are many within POS (Bazan *et al.*, 1990). Like nitrotyrosine, Iso[4]LGE_2 is a marker of oxidative stress and has also been demonstrated to have the ability to adduct to DNA and proteins (Iyer *et al.*, 1989; Murthi *et al.*, 1993). Adduction by iso[4]LGE_2 has been shown to inhibit the function of proteins (Salomon, 2005). Even once adducted to proteins and DNA the levuglandins can continue to react with other proteins and DNA forming crosslinked molecules that cannot be degraded. Elevated levels of iso[4]LGE_2 have been noted in patients affected by atherosclerosis (Salomon *et al.*, 2000; Poliakov *et al.*, 2004).

CEP-adducts are a family of 2-(ω-carboxyalkyl)pyrrole adducts derived from the easily oxidised fatty acid docosahexaenoic acid (DHA), which is found in high quantities in POS (Bazan *et al.*, 1990). CEP-modified proteins have been measured at high levels in the Bruchs membrane of patients suffering from AMD and been shown to induce angiogenesis in chick chorioallantoic membrane whilst they intensify choriodal neovascularisation in a mouse model (Ebrahem *et al.*, 2006). This, taken together with its presence in drusen, a high risk factor in the progression of AMD, suggests that CEP-adducted molecules could play a role in the onset of AMD (Crabb *et al.*, 2002; Combadiere *et al.*, 2007). Indeed, a recent paper documented lesions forming in the RPE-layer of mice that had been exposed to CEP-adducted proteins (Hollyfield *et al.*, 2008). The lesions were reminiscent of those seen with the onset of AMD and this could provide a link between oxidative stress in the retina and AMD.

Characterisation of granules in this study has demonstrated that retinal lipofuscin contains many molecules that have undergone extensive modification. Previous studies have also described such an occurance including proteins that have been adducted to malondialdehyde, 4-hydroxynonenal and advanced glycation end-products (Schutt *et al.*, 2003a; Schutt *et al.*, 2003b; Kaemmerer *et al.*, 2007). Such thorough post-translational modifications of proteins within lipofuscin granules may prevent tryptic digestion or render them unidentifiable by LC MS/MS. Our results

suggest that previous reports characterising the protein content of retinal lipofuscin may be largely based around the proteins associated with the extra-granular material that is co-isolated with granules (Schutt *et al.*, 2002a; Warburton *et al.*, 2005).

This study has succeeded in producing a sample of granules that are free from debris and has shown that these purified granules contain little if any protein. The study has clearly shown that the photoreactivity associated with lipofuscin is inherent to the granules and not the extragranular debris that is co-isolated. The unstable nature of the lipids and retinoids present in high quantities in the POS and their susceptibility to free radical attack, suggests that lipofuscin granules are composed mainly of conjugates of these molecules. Together these undegradable waste products form an agglomerate that has the capacity to generate free radicals and singlet oxygen, disrupt lysosomal enzyme function and inhibit the anti-oxidant enzymes of the RPE, each having a negative impact on RPE cell viability (Rozanowska *et al.*, 1995; Rozanowska *et al.*, 1998; Shamsi *et al.*, 2001). These factors taken together with the ability of A2E to activate complement and CEP-adducts to cause RPE lesions and initiate CNV (Zhou *et al.*, 2006; Hollyfield *et al.*, 2008), form a strong link between oxidative stress, lipofuscin formation and the onset of AMD. The findings of this study can hopefully assist the further research that is needed to elucidate the connections involved in multifaceted diseases of the retina.

Chapter 4

Development and Analysis of an *In Vitro* Model of Retinal Lipofuscin

4.1 Introduction

As described in Chapter 1 above, lipofuscin is an intra-lysosomal waste product composed primarily of oxidatively modified lipids and post-translationally modified proteins. These waste products gradually accumulate in post-mitotic cells with time. Indeed, in Chapter 3 we identified a number of post-translational adductions present in lipofuscin-granules derived from lipid peroxidation products. Retinal lipofuscin has characteristic fluorescence and absorbance spectra that differ from those seen in lipofuscins that are found in other post-mitotic cells (Boulton *et al.*, 1990; Nilsson and Yin, 1997). Retinal lipofuscin also has demonstrable phototoxic properties and has been shown to produce a number of reactive oxygen species, including: singlet oxygen and superoxide (Boulton *et al.*, 1993; Gaillard *et al.*, 1995; Rozanowska *et al.*, 1995; Rozanowska *et al.*, 1998).

It was of interest to this project to ascertain which components involved in retinal lipofuscin formation gave the granules their characteristic traits. To do so, we developed 6 *in vitro* models of retinal lipofuscin formation using enrichments of cell components we believed to play the most important role. Previous studies have identified POS as being the major substrate of retinal lipofuscin, bestowing it with a number of unique features including the presence of retinoid derivatives such as A2E, (Eldred, 1998; Boulton *et al.*, 2004) however, the presence of retinoids in lipofuscin found in liver cells has also been recorded (Szweda, 1994). Some authors believe that the autophagy of old or damaged organelles, in particular mitochondria, within the RPE play a role that is as equally important as POS in the formation of retinal lipofuscin (Burke and Skumatz, 1998; Terman *et al.*, 2007).

As described previously, retinal lipofuscin has been associated with a number of retinal degenerative diseases (Beatty *et al.*, 2000; Nowak, 2006a; Holz *et al.*, 2007). Therefore, interest in retinal lipofuscin is driven by the strive for greater understanding of how it affects the function of RPE cells with age. A broader knowledge of the substrates and mode of genesis of retinal lipofuscin could be important as this has the potential to assist in the development of novel strategies in either preventing its formation, or, aiding its degradation. Preventing the formation of

retinal lipofuscin or instigating the degradation of retinal lipofuscin that has accumulated in RPE cells has potential therapeutic implications. With this in mind, the *in vitro* lipofuscin formation models were designed and analysed in a manner that will enhance our understanding of the contribution made by both POS and mitochondria in the formation of retinal lipofuscin and how they influence its characteristics.

4.2 Experimental design

4.2.1 Collection of components of the *in vitro* lipofuscin models

4.2.1.1 Isolation of POS from bovine eyes.

POS were isolated from bovine eyes as described in the General Materials and Methods chapter, Section 2.3. One variance to the technique described in Section 2.3 was that POS designated POS (dark) in the results section were isolated under dim red light to preserve the rhodopsin present in the outer segments.

4.2.1.2 Isolation of a lysosomal enzyme enriched fraction from bovine liver

Bovine liver was obtained from a local abattoir with tissue being transported on ice and all preparations undertaken immediately upon arrival. A lysosomal enzyme enriched fraction was obtained by sub-cellular fractionation involving the bovine liver being homogenised in Homogenising medium (0.25 M sucrose, 5 mM TRIS-HCl, 1 mM EDTA) using an electronic homogeniser (Kenwood, UK) to create smaller pieces of liver. The liver was further homogenised using a handheld homogeniser (Fisher Scientific, UK). The sample was subjected to four centrifugation steps all at 4°C: (i) 700 *g*, 10 mins (Boeco U-32R, Hamburg, Germany), (ii) 11 300 *g*, 3 mins, (iii) 27 200 *g*, 7 mins, and (iv) 141 500 *g*, 60 mins (Sorvall Ultra-Pro 80, Sorvall, USA), retaining 1.5 ml samples and noting the volume of both the supernatant and pellet after each step. The lysosomal enriched fraction was identified by determining the specific activity of three lysosomal enzymes; acid phosphatase, N-acetyl β-D-glucosaminidase and Cathepsin D, in each fraction using methods adapted from that of Cabral *et al* (1988) (Section 4.2.1.2.2). The fraction identified as being enriched in lysosomes was disrupted using a dismembranator (Sartorius Stedin Biotech, France). Samples were transferred to a stainless steel shaking flask containing a ball-bearing and frozen in liquid nitrogen. The frozen shaker flask was then quickly inserted into the dismembranator and shaken at 3000 shakes per minute for 60 sec. The sample was transferred to a sample tube and maintained on ice. The process aimed to disrupt the

lysosomal membranes and create a lysosomal enzyme cocktail that was sterilised by sequential filtration.

4.2.1.2.1 Protein determination of lysosomal fraction

Protein levels were determined using a BCA assay (Pierce Biotechnology, USA). The BCA protein assay is a routinely used laboratory technique used for the quantification of protein and was undertaken according to the manufacturers guidelines. The assay employs bicinchoninic acid (BCA) for the colourimetric quantification of protein and is based around the reduction of Cu^{2+} to Cu^{1+} by proteins under basic conditions.

A calibration curve was created using standards of known protein content ranging from 0 to 2000 µg/ml. The calibration curve was then used to calculate the protein content of the unknown sample. The volume of working reagent needed for each protein determination was calculated using the following formula: number of triplicates of the standard plus number of triplicates of the test sample plus three (pipetting error) times the volume of working reagent for each sample. The working reagent was prepared by mixing BCA reagent A and BCA reagent B in a ratio of 50:1. 10 µl of each standard in triplicate or test sample in triplicate were added to the 96-well plate (Orange scientific, UK). 200 µl of working reagent was added to each well and incubated at 37°C for 30 mins. The plate was cooled to room temperature before measuring the absorbance at 570 nm on a microplate reader (Multiskan Ascent. Labsystems, UK).

The standard curve was created by plotting the average measurement of each dilution of BSA standard into a regression of linear fit (Graphpad, Prism). Concentration of the total protein was determined by reference to the standard curve (Graphpad, Prism).

4.2.1.2.2 Lysosomal enzyme marker assays

Enzyme assays were carried out using a modification of the techniques described by (Cabral *et al.*, 1990). 25 µl of the sample being analysed for lysosomal enzyme activity was solubilised by exposure to 25 µl of 0.2% Triton-X 100 (1:1 dilution) for 5

mins on a plate shaker (R-100 Rotatest Shacker, Luckham). After solubilization, buffer and substrates were added to the lysosomal isolates. Each sample was run in at least triplicate.

(i) Acid phosphatase assay

5 mM p-nitrophenol-phosphate was used as substrate, giving a final volume of 100 µl of 0.1 M acetate buffer (pH 4.5). The reaction was allowed to proceed for 30 mins at 37°C before being stopped by the addition of 100 µl of 200 mM NaOH (pH 10.5, final concentration 100 mM).

(ii) N-acetyl β-D- glucosaminidase

5 mM p-nitrophenol –β-D –glucosaminide in 0.1 M citrate buffer (pH 4.5) was used as substrate, in a final volume of 100 µl. The reactions were allowed to proceed for 45 mins at 37°C and were stopped with the addition of 100 µl 0.8 M glycine NaOH (pH 10.5; final concentration 0.4 M).

The reaction product for the acid phosphatase and N-acetyl β-glucosaminidase assay (p-nitrophenol) was measured spectrophotometrically at 405 nm (Multiskan Ascent, Labsystems, UK). The concentration of p-nitrophenol was expressed in nanomoles by reference to a calibration curve. The activity of these enzymes was then expressed as nM p-nitrophenol/ min / µg protein.

Data for the p-nitrophenol calibration curves were obtained by aliquoting 100 µl p-nitrophenol standards (Sigma, UK) of increasing concentration in 0.1 M acetate buffer (pH 4.5) into different wells of a 96-well plate. 100 µl of 200 mM NaOH was added to each well and the resultant absorbance was measured at 405 nm with a Multiskan Ascent multi-well plate reader. Wells used as blanks contained an identical concentration of acetate and NaOH but did not contain p-nitrophenol.

(iii) Cathepsin D

50 µl of 2% (w/v) haemoglobin in 0.25 M formate buffer (pH 3.3) was used as substrate to give a final volume of 100 µl. The reaction was allowed to proceed for 60 mins at 37°C before being stopped with the addition of 250 µl of 3% TCA. The

eppendorf tubes containing sample were centrifuged at 220 *g* for 10 mins (Micro Centaur, MSE). 25 µl of the supernatant was transferred to a 96-well plate and the protein quantified as described in Section 4.2.1.2.1, using tyrosine of known concentrations to create a calibration curve.

The coloured reaction product of the Cathepsin D assay was measured spectrophotometrically at 570 nm using a 96-well plate reader (Multiskan Ascent, Labsystems, UK). The absorbance values were converted to tyrosine equivalents using a calibration curve. The activity of Cathepsin D is expressed as ng of Tyrosine equivalents/ min/ µg protein. The calibration curve for tyrosine equivalents were created using 25 µl aliquots of tyrosine (Sigma, UK) in 0.25 M formate buffer (pH 3.3) of varying concentrations that were introduced to different wells of a 96-well plate. Protein content was determined using the BCA assay as described in section 4.2.1.2.1 Wells used as blanks did not contain tyrosine.

Controls for each of the assays were established by running in tandem with the assay (a) wells that contained no sample only buffer, but with substrate present (b) wells containing no substrate only buffer, with sample present. The absorbance values of these wells were subtracted from the sample values when determining the activity of the enzymes of samples to account for light scattering, background absorbance and spontaneous hydrolysis of the substrate.

4.2.1.3 Isolation of mitochondria from bovine liver

Isolation of mitochondria took place using a technique adapted from that described by; Johnson, and Lardy, 1967 (Johnson and Lardy. 1967). To isolate mitochondria. firstly, 500 g of bovine liver was dissected into ~25 mm sections. The bovine liver sections were next added to 1.5 volumes of mitochondria buffer (See Table 4.1 below) before being homogenised in a mechanical blender (Kenwood. UK) in 15 sec bursts until smooth. At this point the pH of the solution was adjusted to 7.8 using 1 M Tris base. The liver tissue was further disrupted by homogenising with a hand-held pestle and mortar (Fisher Scientific, UK) on ice. Next, the homogenate was centrifuged at 1000 *g* for 10 mins at 4°C (Boeco U-32R, Hamburg, Germany), discarding the pellet and retaining the supernatant. The supernatant was filtered through cheesecloth before

undergoing a further centrifugation at 1000 *g* for 15 mins, 4°C. The pellet of this centrifugation was discarded with the supernatant undergoing a further spin; 12000 *g* for 15 mins at 4°C (Sorvall Ultra-Pro 80, Sorvall, USA). The resultant pellet was retained and washed in 4 volumes of mitochondria buffer containing a protease inhibitor cocktail consisting of: 1 M phenylmethanesulphonyl fluoreide, 1 mg/ml leupeptin, 1 mg/ml pepstatin (all from Sigma-Aldrich, UK) at 12000 *g* for 15 mins at 4°C. The washing step was repeated three times in total before the mitochondrial sample was suspended in a small volume of mitochondria buffer with an aliquot being used to determine the presence of Hsp60 and protein content (Section 4.2.1.2.1) by Western blot analysis (Section 4.2.1.3.1). The mitochondria were then re-suspended in either PBS (pH 7) or citrate buffer (pH 4.5) to be used as components of the *in vitro* lipofuscin models.

Table 4.1 Mitochondrial buffer used for the isolation of mitochondria from bovine liver.

EDTA	0.2 mM
Sucrose	0.25 M
Tris. HCl (pH 7.8)	10 mM

4.2.1.3.1 Western blot to determine if mitochondria were present in the enriched fraction

The mitochondria (1/10 dilution in PBS) were suspended in sample loading buffer, boiled at 100°C for 10 mins, separated by 8% SDS–PAGE and blotted on a 0.2 μm nitrocellulose membrane (350 A) (Bio-Rad). The membrane was blocked for 1 hour with 5% milk in 0.1% TBST (0.1% Tween 20 in TBS). Next the membrane was probed for 1 hour at room temperature with primary mouse monoclonal Hsp60 antibody [LK-2] (Abcam) (1:1000 dilution), washed four times in 0.1% TBST for 10 mins each. Washing was followed by a 1 hour incubation with goat anti-mouse horse-radish peroxidase (HRP) secondary antibody (1:10 000 dilution; Jackson ImmunoResearch Laboratories). After four washes in 0.1% TBST the signal on the blot was detected with enhanced chemiluminescence with HRP as substrate. (Pierce, UK).

4.2.2 *In vitro* lipofuscin model maintenance conditions

Isolated mitochondria were re-suspended in either citrate buffer (pH 4.5) or PBS (pH 7) and mixed with the lysosomal enzyme cocktail at the same pH. POS isolated either under dim red-light or full light conditions were suspended in either citrate buffer or PBS (pH 4.5 and 7, respectively) and mixed with the lysosomal enzyme cocktail at the same pH. Each model was maintained at 37°C in a humidified atmosphere containing 5% CO2 / 95% air for four months. An initial volume of 18 ml was used for each model then 1 ml (~1 x 10^7 POS/ml) of light or dark isolated POS or 1 ml (~500 µg/ml protein content) of mitochondrial enriched sample plus 500 µl (~800 µg/ml protein content) of lysosomal enzyme cocktail was added every 14 days to give a final sample volume of 30 ml. For controls that consisted of single components of the model, the volume was corrected to that of the models by the addition of either PBS for the controls at pH 7 or citrate buffer for the controls at pH 4.5.

4.2.3 Analysis of rhodopsin levels in POS

Analyses of rhodopsin levels in dark and light isolated POS were carried out using the U-2800 UV-VIS Spectrophotometer (Hitachi) with UV Solutions software. The absorbance spectra was measured between 400-600 nm with a characteristic peak at 500 nm present in samples containing rhodopsin which disappeared with exposure of the sample to light for 6 mins. Samples that contained little or no rhodopsin did not show the peak at 500 nm.

4.2.4 Isolation of *ex vivo* lipofuscin for comparison with the in vitro models of lipofuscin

Lipofuscin was isolated from human donor eyes as described in the General Materials and Methods Chapter, Section 2.1.

4.2.5 Analysis of *in vitro* models and comparison with ex-vivo retinal lipofuscin

4.2.5.1 Absorption and fluorescence spectra of in vitro models and their components

Absorbance spectra of samples were measured for wavelengths between 260-700 nm in a 1 cm path length quartz cuvette using a U-2800 UV-VIS Spectrophotometer (Hitachi) with UV Solutions software. For each set of absorbance readings a buffer-only reading was taken to ensure the cleanliness of the cuvette, this spectrum was also used as a buffer baseline and subtracted from sample readings by the software. 500 µl of sample was made up to 3 ml with the appropriate buffer.

Fluorescence spectra were measured using a F4500 Fluorescence Spectrophotometer (Hitachi) with FL Solutions Software. Emission spectra of samples were measured using 364 nm and 476 nm as the excitation wavelength. These values were chosen as they are wavelengths cited in previous studies detailing the emission spectra of retinal lipofuscin (Boulton *et al.*, 1990). The fluorescence spectra of buffers alone were measured and the background removed from samples using Microsoft Excel (Microsoft, USA). No fluorescence spectra were corrected for the loss in sensitivity of fluorescence detection at longer wavelengths.

4.2.5.2 SDS-PAGE analysis

SDS-PAGE is an analytical tool designed to examine proteins by denaturing them to their polypeptide constituents. SDS is an anionic detergent that denatures proteins and leaves them with an overall negative charge. The protein sample can then be fractionated using a polyacrylamide gel according to size, since all polypeptides will have an identical mass to charge ratio, with smaller proteins moving quickest through the gel. SDS-PAGE can be used to estimate the molecular mass of proteins as well as to analyse the purity of sample and determine if any post-translational modifications have affected the sample.

Table 4.2. Solutions for casting a 10% resolving and 5% stacking gel for SDS-PAGE

	Resolving gel (10%) (10 ml)	Stacking gel (5%) (3 ml)
Distilled H2O	4.0 ml	2.1 ml
30% acrylamide mix	3.3 ml	500 µl
1.5 M Tris/HCl pH 8.8	2.5 ml	-
1.0 M Tris/HCl pH 6.8	-	380 µl
10% SDS	100 µl	30 µl
10% APS	100 µl	30 µl
TEMED	4.0 µl	3.0 µl

A 10% (w/v) resolving gel with a 5% (w/v) stack gel (See Table 4.2 above) was used to separate the peptides in the samples prepared for the targets of interest. Samples were mixed with an equal volume of 2x electrophoresis sample buffer (sc-24945, Bio Rad laboratories Ltd, Herts, UK) and incubated at 95°C for 5 minutes. Equal amounts of protein at a volume of 15-20 µl/well were loaded and the gel was run at 30 mA in 1x Laemmli buffer (Bio Rad laboratories Ltd, Herts, UK) until the dye approached the bottom of the gel. The gel was analysed by Coomassie blue staining for the protein profile. To ascertain the molecular weights of protein species detected with Coomassie blue staining, 5 µl of a pre-stained molecular weight standard (Precision Plus Protein Standards, range 7.2 – 250 kDa; Bio Rad laboratories Ltd, Herts, UK) was applied to the gel.

4.2.5.2.1 Visualisation of protein profile by Coomassie brilliant blue staining

After electrophoresis, gels were immersed in an acidic alcoholic solution of the Coomassie brilliant blue staining solution (MeOH and acetic acid in a ratio of 4.5:1. and Coomassie brilliant blue R250, 2.5 mg/ml). This denatures the proteins, fixes them in the gel and allows the dye to bind to them. Subsequently, the gel was destained in 2:1 MeOH and acetic acid solution for visualisation of bands.

4.2.5.3 CEP Western Analysis.

For Western analysis, the *in vitro* lipofuscin model preparations were extracted by boiling in SDS sample buffer containing 0.1 M DTT. The sample material (~20 µl) was applied to a PVDF membrane (Millipore, Bedford, MA) using a slot blot apparatus (Bethesda Research Laboratories HS-1878) and probed with mouse anti-2-(ω-carboxyethyl)pyrrole (CEP) mAb (Ebrahem *et al.*, 2006).

4.2.5.4 Analysis of A2E in samples

The samples were pelleted by centrifugation (10,000 *g*, 4°C, 10 mins) and the pellets extracted with 2 ml chloroform/methanol (2:1). 2 ml of water was added to the extracts, vigorously mixed and centrifuged for phase separation. The organic phase was collected, the watery phase re-extracted with 2 ml $CHCl_3$/MeOH (2:1). The organic extracts were combined and applied to a SepPak-C18-cartridge. The cartridge was then washed with 5 ml $CHCl_3$/MeOH (1:1) and eluted with MeOH + 0.1% TFA. The eluents were dried under a stream of nitrogen. The samples were re-dissolved in 100 µl MeOH and injected onto a reversed phase C18-column (Nucleosil 5C18, Phenomenex, 150 mm x 4.6 mm) and eluted with a gradient of methanol in water (85-96% + 0.1% TFA, 1ml/min). Elution was recorded fluorimetrically (excitation wavelength 430 nm, emission wavelength 632 nm).

4.2.5.5 Measurement of singlet oxygen production

4.2.5.5.1 Preparation of in vitro lipofuscin formation samples for laser flash photolysis work

Samples were prepared initially using a modification of Folch's lipid extraction technique; (Folch *et al.*, 1957) using 8 ml of chloroform/methanol (2:1) mixture that was added to 5 ml of each *in vitro* lipofuscin formation model. After vortexing, the solutions were centrifuged before the chloroform layer was removed. The chloroform layer was dried under vacuum and re-solubilised in benzene ready for further experiments.

4.2.5.5.2 Measurement of singlet oxygen production by the *in vitro* lipofuscin formation models

Measurement of singlet oxygen emission was conducted using an adaptation of the method described previously (Rozanowska *et al.*, 1998). This involved monitoring singlet oxygen emission at 1270 nm using a liquid nitrogen cooled germanium detector (Applied Detector Company, Fresco, CA, USA) coupled with an Agilent digitising scope (Infiniium 54830B DSO, Agilent, Santa Clara, USA) interfaced with a Risc computer (Acorn, Swadlincote, UK). Samples were photoexcited using a 5 ns laser pulse at 420 nm from a Q-switched Nd:YAG laser (Continuum Surelite II; Santa Clara, USA) equipped with an optical parametric oscillator (Panther OPO; Continiuum, Santa Clara, USA). The laser energy reaching the sample was regulated using neutral density filters, with the addition of each neutral density filter resulting in lower laser energy reaching the sample (see Figure 4.1).

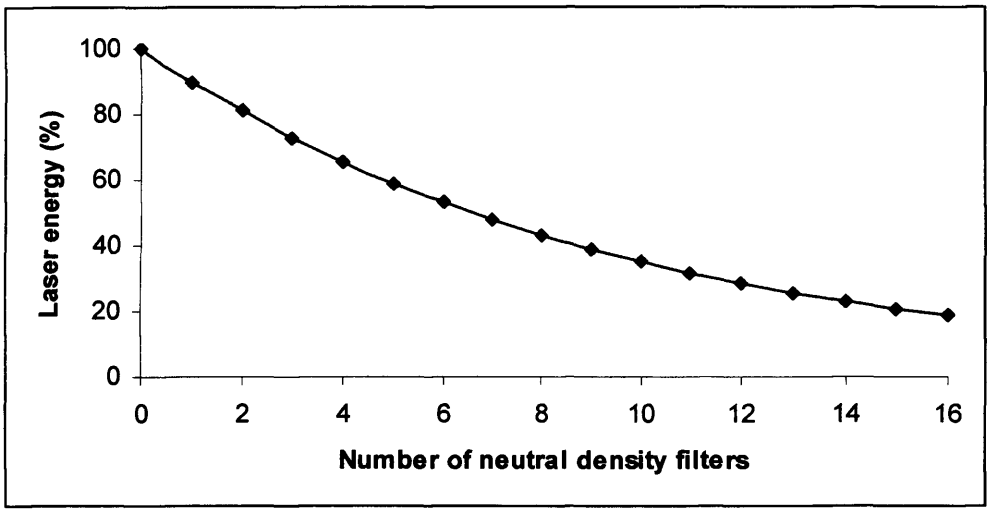

Figure 4.1. Graph displaying the reduction in laser energy with increasing number of neutral density filters.

Rose Bengal and all-trans-retinal were used as the standard singlet oxygen sensitisers. The quantum yield of singlet oxygen generation by all-trans-retinal (ATR) in benzene has been measured as 0.30 $\pm$ 0.04 (Rozanowska *et al.*, 1998). The difference in optical density of each of the samples did not allow for matching at the excitation wavelength of 420 nm, so a calibration curve of ATR absorbance against singlet oxygen yield was created to normalise for the difference in sample concentration when calculating quantum yields. A sample of Rose Bengal of equal concentration

(according to absorbance as measured at 420 nm) was used with each experiment as a standard to allow for normalisation of the variability of the geometry of the exposure between experiments. Initial emission intensity extrapolated from the experimental points was measured as a linear function of laser energy. The slopes of graphs generated with this data gave a value for singlet oxygen quantum yield generated by the *in vitro* lipofuscin model samples.

4.3 Results

4.3.1 Preparative results

4.3.1.1 Identification of the lysosomal enriched fraction using lysosomal enzyme assays.

Lysosomes were isolated from bovine liver pieces and four samples collected during the isolation procedure were analysed for enzyme activity for three lysosomal marker enzymes. Fractions were collected after successive centrifugation steps, Fraction 1 is the pellet collected after a 700 *g* spin, Fraction 2 collected after a 11,300 *g* spin, Fraction 3 collected after a 27,200 *g* spin and Fraction 4 after a 141,500 *g* spin. Results obtained using the three lysosomal marker enzymes suggest that fraction 4 was most enriched with lysosomes as this fraction showed the greatest activity with acid phosphatase, N-acetyl β-glucosaminase and Cathepsin D (Figure 4.2 a-c). Thus, fraction 4 was used to yield the lysosomal enzyme cocktail for the *in vitro* lipofuscin formation model as it would best mimic the lysosomal conditions under which lipofuscin forms within the RPE.

a) Acid phosphatase activity

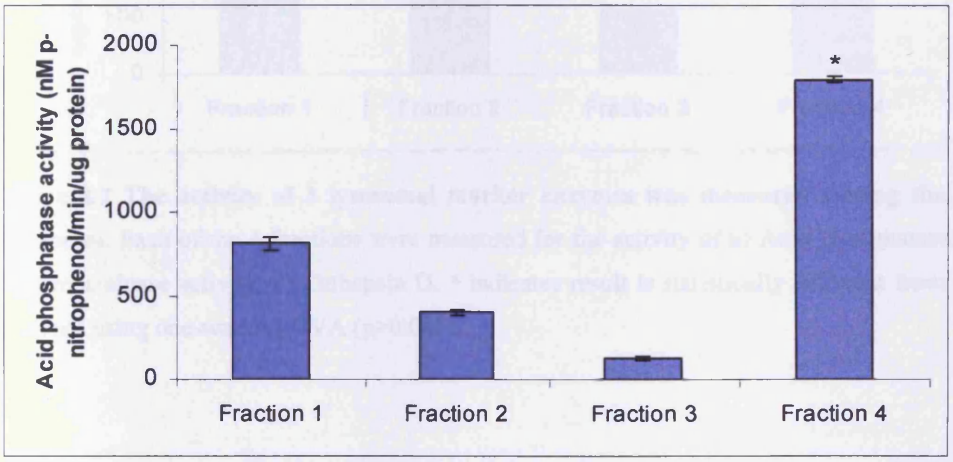

b) N-acetyl β-glucosaminase activity

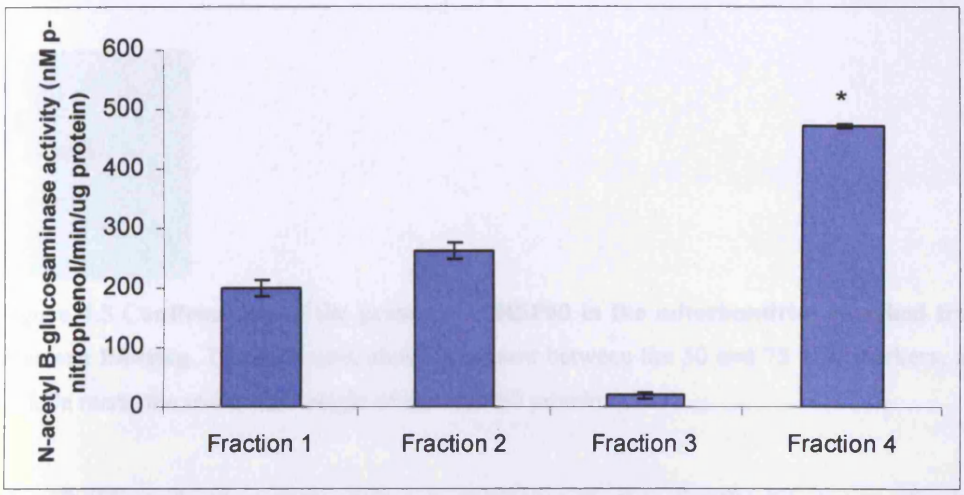

c) Cathepsin D activity

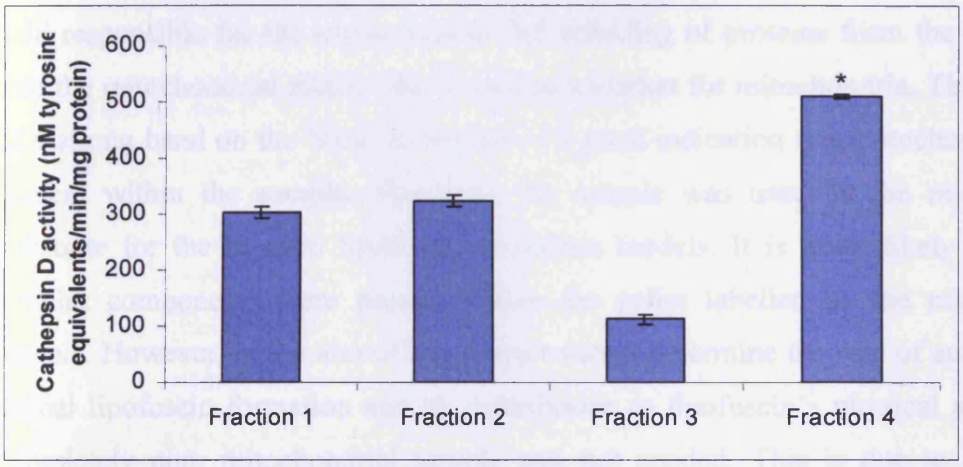

Figure 4.2 The activity of 3 lysosomal marker enzymes was measured during the isolation of lysosomes. Each of the 4 fractions were measured for the activity of a) Acid phosphatase, b) N-acetyl β-glucosaminase activity, c) Cathepsin D. * indicates result is statistically different from others when analysed using one-way ANOVA ($p>0.005$).

4.3.1.2 Identification of Heat Shock Protein (HSP) 60 as a marker of mitochondria presence.

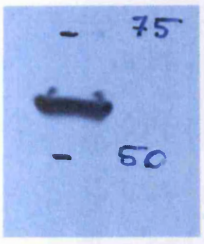

Figure 4.3 Confirmation of the presence of HSP60 in the mitochondrial enriched fraction using Western Blotting. The band seen above is present between the 50 and 75 kDa markers, at around the 60 kDa mark, the molecular weight of the HSP 60 protein.

Hsp60 (Heat shock protein 60) was used as a marker for the presence of mitochondria in the fraction expected to be enriched in mitochondria using the Western blotting technique (Figure 4.3). Hsp60 is a mitochondrial chaperone protein that is typically held responsible for the transportation and refolding of proteins from the cytoplasm into the mitochondrial matrix and is used as a marker for mitochondria. The presence of a strong band on the Western blot gel is a good indication that mitochondria were present within the sample. Therefore, the sample was used as the mitochondria substrate for the *in vitro* lipofuscin formation models. It is quite likely that other cellular components were present within the pellet labelled as the mitochondria sample. However, as the aim of this project was to determine the role of autophagy in retinal lipofuscin formation and its contribution to lipofuscin's physical attributes a completely pure mitochondrial sample was not needed. This is due to other sub-cellular components most likely also being involved in autophagy and the development of retinal lipofuscin.

4.3.1.3 Characterisation of rhodopsin levels in dark isolated POS compared to light isolated POS.

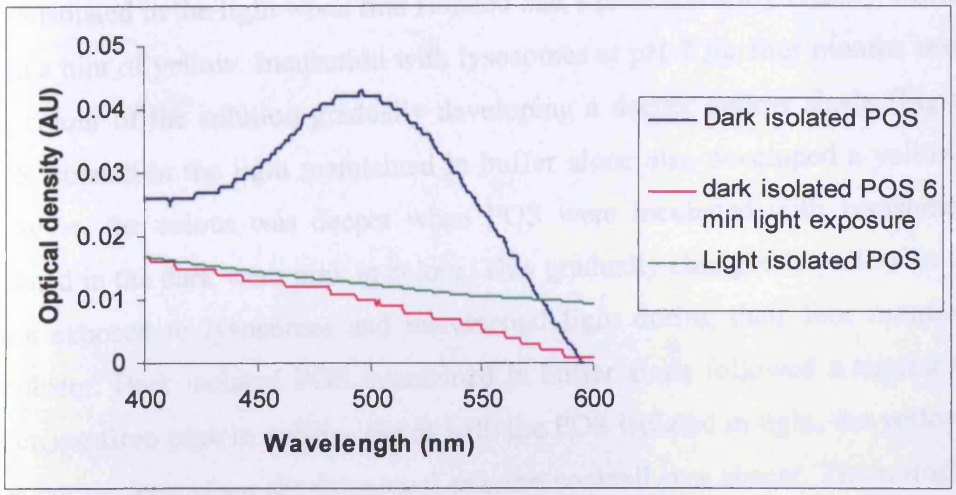

Figure 4.4. Optical density spectra of dark isolated POS (blue), dark isolated POS after 6 mins irradiation with light (pink) and light isolated POS (green).

The optical density spectra seen in Figure 4.4 show POS isolated under dim-red light (dark) have absorbance maxima at ~500 nm characteristic of the presence of rhodopsin. After irradiating the sample with light for six minutes the optical density spectra changed and the rhodopsin characteristic peak was lost, indicating rhodopsin was photodegraded during light exposure. The optical density spectra of POS isolated under light conditions did not have the peak characteristic of rhodopsin indicating that rhodopsin was bleached during the isolation procedure. Therefore, these samples were used as the dark and light isolated samples to determine if the presence of rhodopsin affected the formation of retinal lipofuscin and the characteristics of anything that forms within the models.

4.3.2 Physical characteristics of the *in vitro* lipofuscin models

POS isolated in the light when first isolated had a predominantly creamy-white colour with a hint of yellow. Incubation with lysosomes at pH 7 for four months resulted in the colour of the solution gradually developing a deeper yellow shade (Figure 4.5). POS isolated in the light maintained in buffer alone also developed a yellow shade; however, the colour was deeper when POS were incubated with lysosomes. POS isolated in the dark were pink in colour. This gradually changed to yellow as the POS were exposed to lysosomes and incremental light during their four months in the incubator. Dark isolated POS maintained in buffer alone followed a similar trend of changing from pink to yellow, but as with the POS isolated in light, the yellow colour was not as deep when the lysosomal enzyme cocktail was absent. The mitochondrial enriched fraction developed a browny-yellow colour over the 4 month period that was a lot denser than that seen in any of the POS samples. This was true of mitochondrial samples maintained with or without the presence of lysosomes.

The *in vitro* lipofuscin models that were maintained at pH 4.5 followed similar trends to those seen in the models maintained at pH 7 (Figure 4.6). Light and dark isolated POS developed a yellow colouring that was lipofuscin-like. This colouring was more prominent in the models containing lysosomes than the controls that contained POS alone. The sample containing mitochondria and lysosomes was more yellow than the control of mitochondria alone that had a dark yellow /brown appearance.

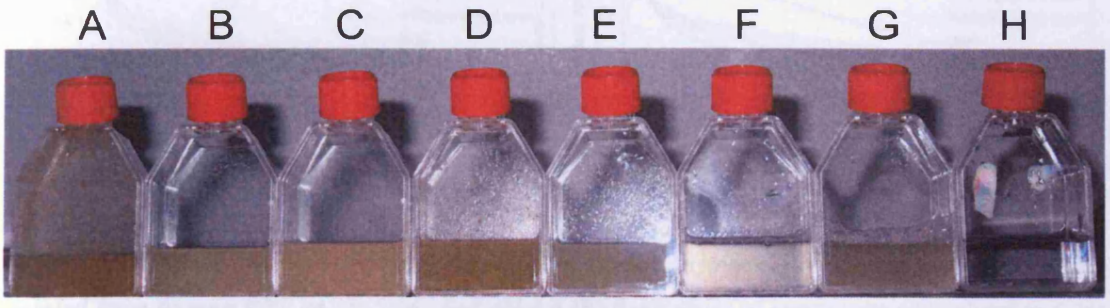

Figure 4.5. Line up of the *in vitro* lipofuscin models and their constituent parts separately at pH 7 after 4 months. From right to left; A = Mitochondria and lysosomes, B = POS (light) and lysosomes, C = POS (dark) and lysosomes, D = mitochondria alone, E = POS (dark) alone, F = Lysosomes alone, G =POS (light) alone, H = buffer solution alone.

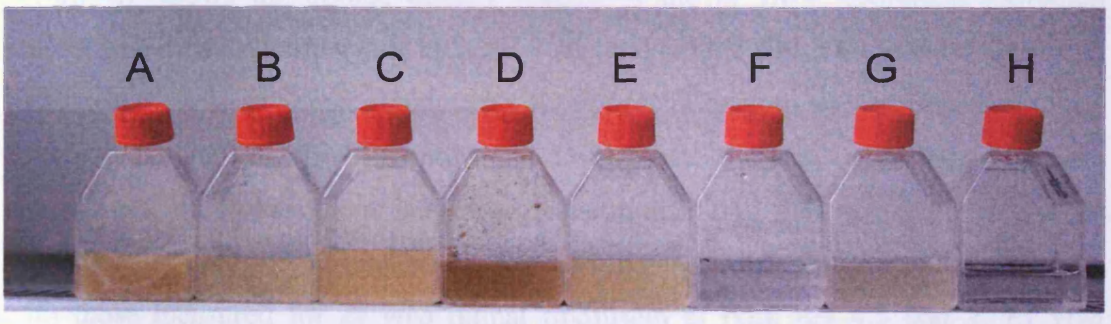

Figure 4.6. Line up of the *in vitro* lipofuscin models and their constituent parts separately at pH 4.5. after 4 months From right to left; A = Mitochondria and lysosomes, B = POS (light) and lysosomes, C = POS (dark) and lysosomes, D = mitochondria alone, E = POS (dark) alone, F= Lysosomes alone, G = POS (light) alone, H = buffer solution alone.

4.3.2.1 Spectra of in vitro lipofuscin models and components and ex vivo lipofuscin

a) Optical density spectra of *in vitro* lipofuscin models and components, and, *ex vivo* lipofuscin pH 7 and pH 4.5

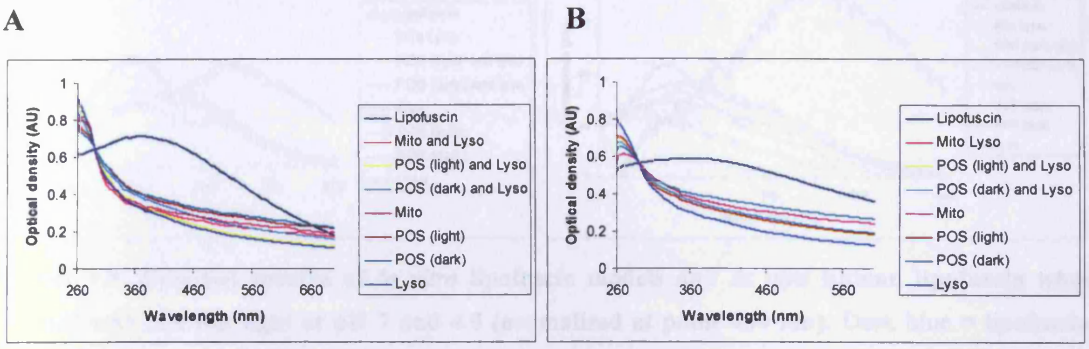

Figure. 4.7 Optical density spectra of the *in vitro* lipofuscin models as compared to lipofuscin isolated from human RPE at pH 7 (A) and pH 4.5 (B) (both series of spectra are normalised to point 290 nm). Dark blue = lipofuscin, Pink = Mito and Lyso, Yellow = POS (dark) and Lyso, Turquoise = POS (light) and Lyso, Mauve = Mito, Brown = POS (light), Green = POS (dark), light blue= Lyso. The in vitro models show emission maxima at approx. 260 nm at both pH 7 and 4.5. Lipofuscin from human donors shows a broader emission pattern with a maxima at a longer wavelength.

Figure 4.7 shows the optical density spectra of the *in vitro* lipofuscin formation models and *ex vivo* lipofuscin at both pH 7 (A) and pH 4.5 (B). The *in vitro* lipofuscin formation models and their constituents show optical density spectra that have little optical density at longer wavelengths that develop into a distinct absorbance maxima at ~260 nm. This phenomena is seen with the models and their constituents that are maintained at both pH 4.5 and pH 7. The absorbance profiles of the models contrast with those measured for *ex vivo* retinal lipofuscin at both pH 4.5 and 7. *Ex vivo* lipofuscin displays a broad-band optical density spectra with emission maxima at longer wavelengths than the *in vitro* lipofuscin formation models.

b) Fluorescence spectra of *in vitro* lipofuscin models and components, and, *ex vivo* lipofuscin pH7 and pH 4.5

A pH 7 B pH 4.5

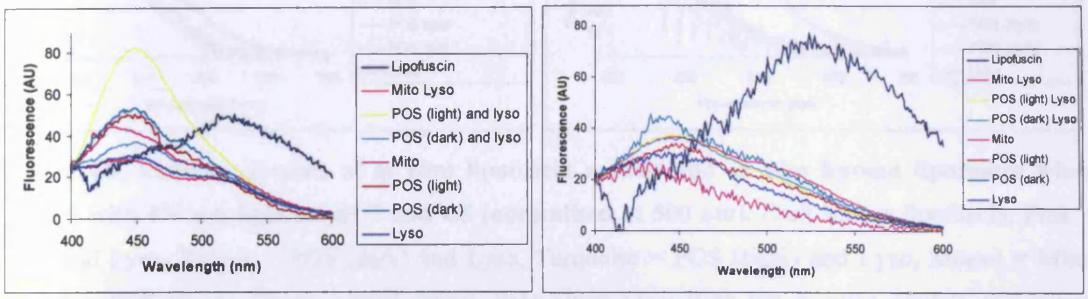

Figure 4.8. Emission spectra of *in vitro* lipofuscin models and *ex vivo* human lipofuscin when excited with 364 nm light at pH 7 and 4.5 (normalised at point 400 nm). Dark blue = lipofuscin, Pink = Mito and Lyso, Yellow = POS (dark) and Lyso, Turquoise = POS (light) and Lyso, Mauve = Mito, Brown = POS (light), Green = POS (dark), light blue= Lyso. The *in vitro* lipofuscin models and retinal lipofuscin isolated from human donors show similar emission patterns with that of lipofuscin red shifted.

When excited with light of wavelength 364 nm the lipofuscin *in vitro* models produce spectra that have emission maxima at shorter wavelengths than those produced by *ex vivo* lipofuscin at both pH 7 and 4.5 (Figure 4.8 A and B). Each of the retinal lipofuscin models display emission maxima at ~450 nm. Those maintained at pH 7 also have a shoulder or secondary peak at ~525 nm. This peak is also present in some of the samples maintained at pH 4.5. These samples include: POS (dark) and lyso, POS (dark) and mito and lyso. The emission maxima of *ex vivo* retinal lipofuscin is found at the longer wavelength of ~525 nm at both pH 4.5 and 7.

A pH 7 B pH 4.5

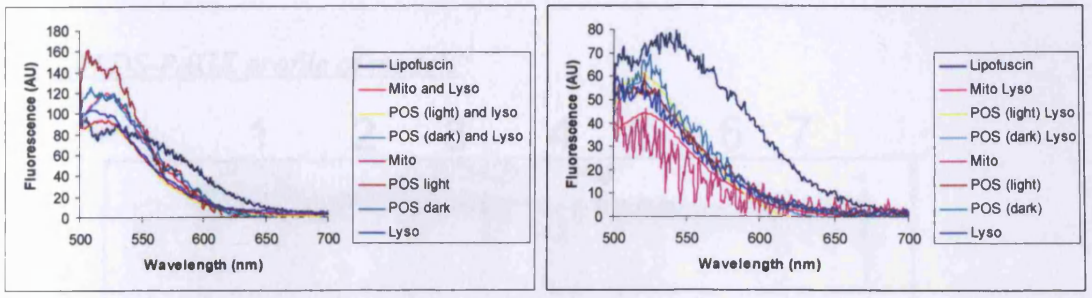

Figure 4.9. Emission spectra of *in vitro* lipofuscin models and *ex vivo* human lipofuscin when excited with 470 nm light at pH 7 and 4.5 (normalised at 500 nm). Dark blue = lipofuscin, Pink = Mito and Lyso, Yellow = POS (dark) and Lyso, Turquoise = POS (light) and Lyso, Mauve = Mito, Brown = POS (light), Green = POS (dark), light blue= Lyso Both the *in vitro* models and retinal lipofuscin isolated from human donors exhibit emission maxima in the blue region with lipofuscin red shifted approximately 20 nm.

Excitation of samples that have been maintained at pH 7 with light of wavelength 470 nm results in spectra that have emission maxima between 500 and 550 nm for the *in vitro* lipofuscin models and their constituents (Figure 4.9 A). POS from dark and light isolated sources both have emission maxima at ~510 nm with a secondary peak at ~540 nm. The mito sample and lyso sample incubated separately have emission maxima at ~ 525 nm with broad peaks. The samples incubated with lyso including: POS (dark), POS (light) and mito, each had a peak at ~ 525 nm which was sharper than when the constituents were incubated alone. The *ex vivo* retinal lipofuscin has a slightly red-shifted emission maxima, occurring at approximately 530 nm, with the spectra being broader than that seen with the *in vitro* models or their constituents. The lipofuscin formation models maintained at pH 4.5 (Figure 4.9 B) show similar emission spectra to those maintained at pH 7. The emission spectra of *ex vivo* lipofuscin measured in buffer at pH 4.5 was broader than the spectra seen with the *in vitro* models and had an emission maxima at ~540 nm.

4.3.3 Components of the *in vitro* lipofuscin models

4.3.3.1 SDS-PAGE profile of models

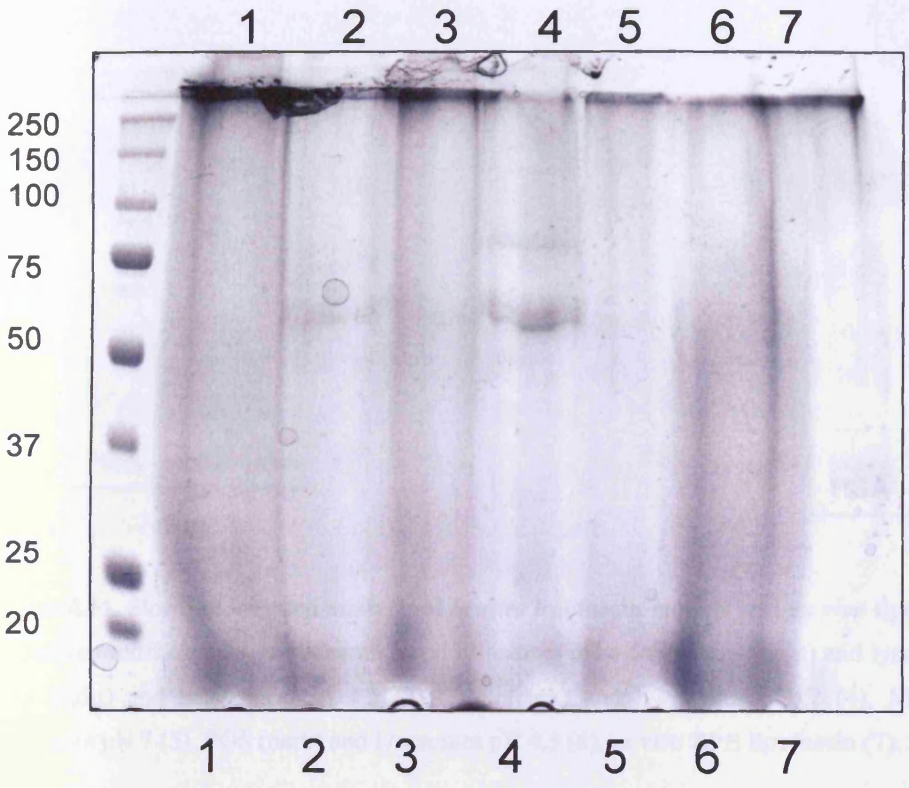

Figure 4.10. Protein profile of *in vitro* lipofuscin models and *ex vivo* lipofuscin by Coomassie blue staining of a 10% SDS-PAGE gel. Mitochondria and lysosomes pH 4.5 (1), POS (light) and lysosomes pH 7 (2), POS (light) and lysosomes pH 4.5 (3), POS (dark) and lysosomes pH 7 (4), Mitochondria and lysosomes pH 7 (5), POS (dark) and lysosomes pH 4.5 (6), ex vivo RPE lipofuscin (7).

SDS-PAGE analysis of the *in vitro* lipofuscin models show a similar smear pattern to that seen with SDS-PAGE analysis of *ex vivo* lipofuscin (Figure 4.10). Very few if any distinct protein bands are present, with samples leaving a lane long smear. This is indicative of the models containing proteins that have undergone modification.

4.3.3.2 Carboxyethylpyrrole (CEP)-modifications of models

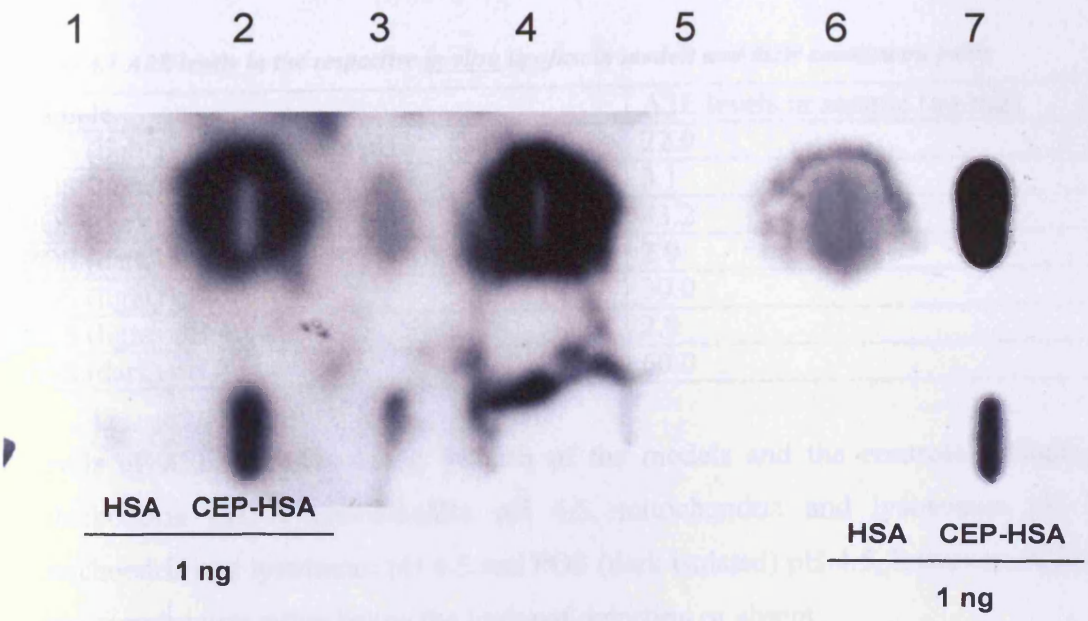

Figure 4.11. Slot-blot western analysis of *in vitro* lipofuscin models and *ex vivo* lipofuscin for CEP oxidative modifications. Mitochondria and lysosomes pH 4.5 (1), POS (light) and lysosomes pH 7 (2), POS (light) and lysosomes pH 4.5 (3), POS (dark) and lysosomes pH 7 (4), Mitochondria and lysosomes pH 7 (5), POS (dark) and lysosomes pH 4.5 (6), *ex vivo* RPE lipofuscin (7).

Using the slot-blot technique we were able to demonstrate that some of the *in vitro* lipofuscin models contained species that had under gone CEP-adduction in a manner similar to that seen in *ex vivo* lipofuscin (Figure 4.11). CEP-adduction was only seen in models that contained POS, and was not present in the models mimicking lipofuscin formed as a result of autophagy, i.e. those that contain the mitochondrial enriched sample. It is thought that the staining seen in lane 1 is due to background staining. That *in vitro* lipofuscin models consisting of POS have products that have undergone modification by CEP-adducts is to be expected as CEP is a downstream product of the peroxidation of DHA, a fatty acid that is present in high levels within the POS.

4.3.3.3 Measurement of A2E content of models.

Table 4.1 A2E levels in the respective in vitro lipofuscin models and their constituent parts

Sample	A2E levels in sample (ng/mg)
POS (light) and lysosomes pH 7	22.9
POS (light) and lysosomes pH 4.5	3.1
POS (dark) and lysosomes pH 7	43.2
POS (dark) and lysosomes pH 4.5	2.9
POS (light) pH 7	30.0
POS (light) pH 4.5	2.9
POS (dark) pH 7	60.0

Levels of A2E were measured in each of the models and the controls including: mitochondria pH 7, mitochondria pH 4.5, mitochondria and lysosomes pH 7, mitochondria and lysosomes pH 4.5 and POS (dark isolated) pH 4.5, however, A2E in these samples was either below the limits of detection or absent.

A2E has been proposed to be a major component of retinal lipofuscin by numerous authors (Sparrow *et al.*, 1999; Schutt *et al.*, 2001; Sparrow *et al.*, 2003a). So to determine if our *in vitro* models of retinal lipofuscin were valid A2E levels were measured in each of the models, together with the model constituents as controls. A2E was recorded in each of the models containing POS and controls with POS with the exception of dark isolated POS maintained at pH 4.5. A2E levels were higher in models maintained at pH 7 than those maintained at pH 4.5. However, levels of A2E seen in each of the models were quite low. No amount of A2E was recorded in the models containing mitochondria and lysosomes either together or alone.

4.3.4 Photoreactivity of *in vitro* lipofuscin models

4.3.4.1 Comparison of singlet oxygen production by photoexcited in vitro lipofuscin models, their constituents and ATR.

The absorbance spectra of ATR samples of increasing concentration were measured (Figure 4.12 A). The absorbance value of these samples at 420 nm was used to generate a calibration curve of singlet oxygen yield versus standard absorbance (Figure 4.12 B) that covered the range of *in vitro* lipofuscin formation model concentrations.

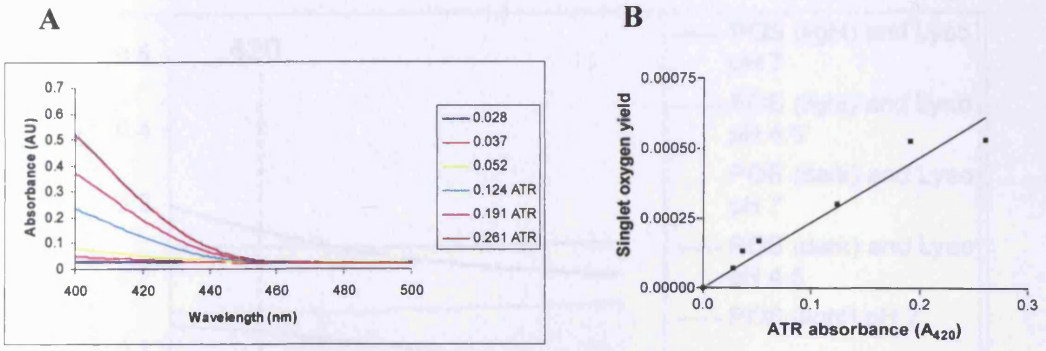

Figure 4.12. Absorbance spectra of ATR samples and calibration curve demonstrating the change in singlet oxygen yield when the concentration of ATR is changed. The absorbance spectra of the samples seen in A were used to generate B, which shows that an increase in ATR

Figure 4.13 A and B show the optical density spectra of the *in vitro* lipofuscin formation models and their constituents that were used to measure singlet oxygen production when excited with 420 nm light. As the optical density of the *in vitro* lipofuscin models were not concentration matched at 420 nm, the ATR standard calibration curve was used to normalise for the differences. Light scattering contributed to the optical density spectra of some of the *in vitro* lipofuscin models and as such generation of singlet oxygen by the models is measured as a lower limit of the quantum yield.

A

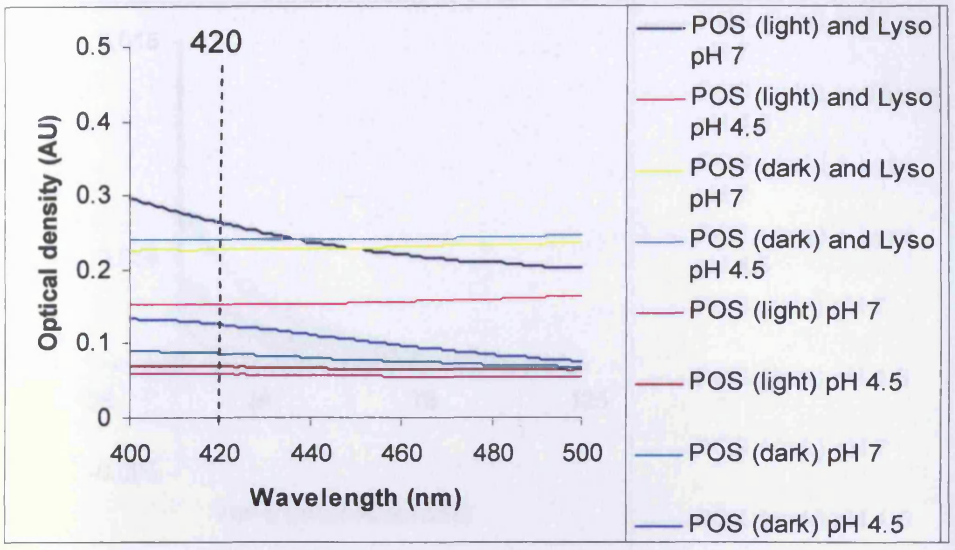

B

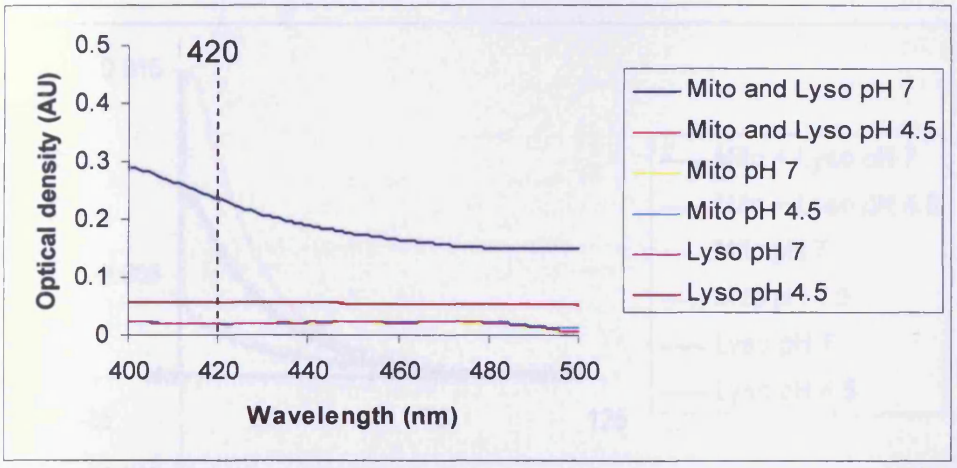

Figure 4.13. Optical density spectra of the samples used for the measurement of singlet oxygen production by the models and the controls. The spectra seen in A represent the *in vitro* lipofuscin formation models involving POS and the POS controls. Those seen in B represent the models containing mitochondria together with mitochondria and lysosomal enzyme cocktail controls.

Figure 4.14 A and B show representative singlet oxygen traces generated by the *in vitro* lipofuscin models and their constituent controls. Such data was collected for each sample using gradually increasing laser energy. The data collected was normalised for variations in laser output and used to generate the linear regression of the initial intensity value plots seen in Figure 4.15.

A

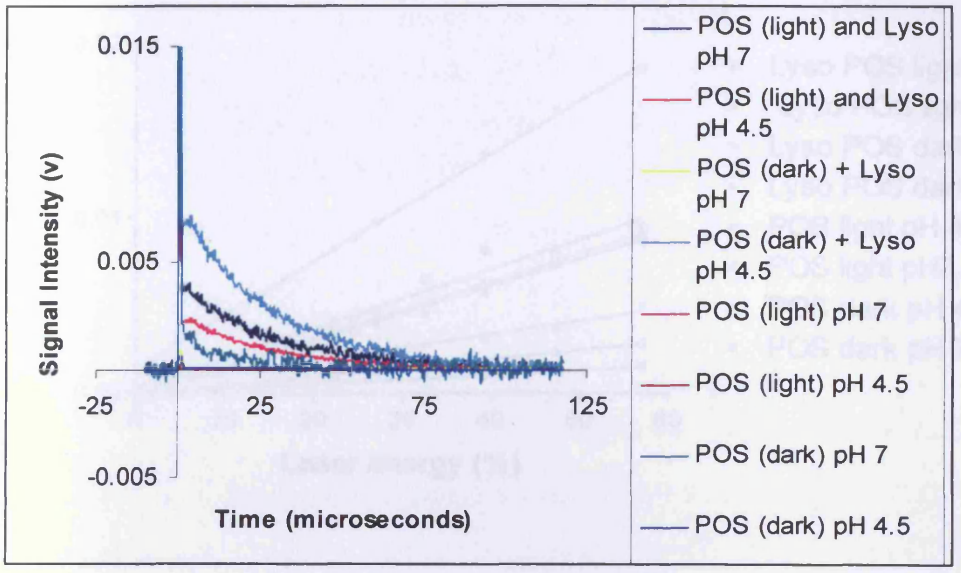

B

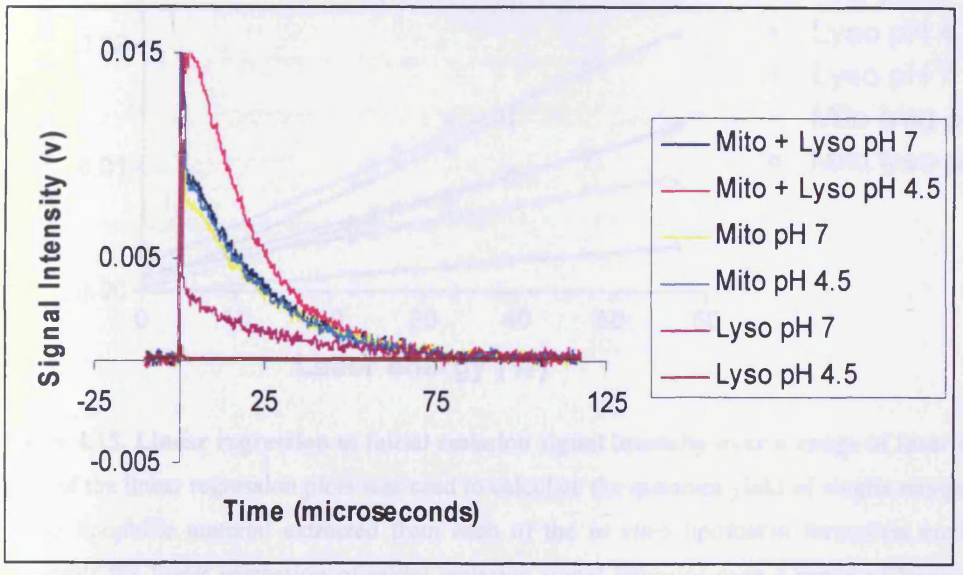

Figure 4.14. Singlet oxygen production by the lipofuscin formation models and the controls. The singlet oxygen phosphorescence kinetics for the *in vitro* models containing POS and the POS controls are shown in A, those for mitochondria models and mitochondria and lysosomal enzyme cocktail controls are displayed in B.

A

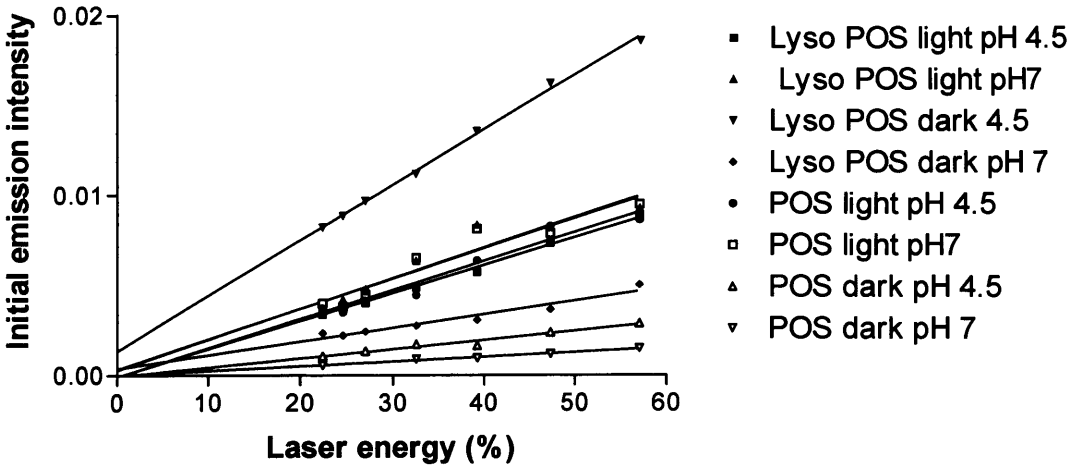

B

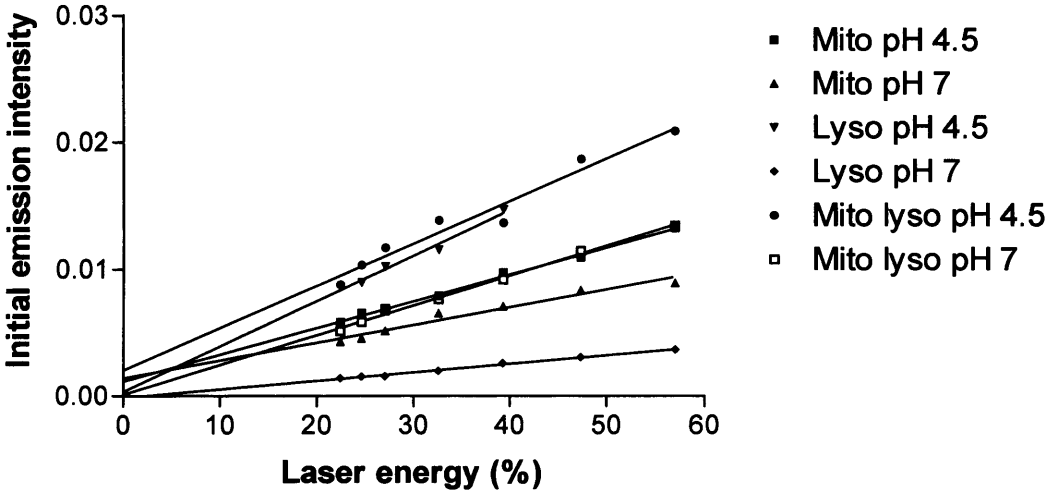

Figure 4.15. Linear regression of initial emission signal intensity over a range of laser energy. The slope of the linear regression plots was used to calculate the quantum yield of singlet oxygen generated by the lipophilic material extracted from each of the *in vitro* lipofuscin formation models. Plot A represents the linear regression of initial emission signal intensity over a range of laser energies for models and controls containing POS, B contains data for the models involving mitochondria and the mitochondria and lysosomal controls.

The slope created when the initial emission intensity measurement is plotted against laser energy gives an indication of the singlet oxygen produced by each of the samples and can be used to calculate the quantum yield of singlet oxygen formation for each of the samples (Figure 4.15 A and B). The slopes of absorbance matched samples can be used to compare their photoreactivity, as can the quantum yield,

however, the samples used in this study were not absorbance matched at 420 nm. To compare the relative photoreactivity the difference in concentration of each of the samples needs to be taken into consideration and the final outcome for each sample is termed the singlet oxygen yield. The singlet oxygen yield for each of the *in vitro* lipofuscin models is presented in Table 4.2 below. The sample with the greatest singlet oxygen yield was that which contained POS isolated in the light and incubated with the lysosomal enzyme cocktail at pH 4.5, similarly POS maintained at pH 4.5 alone showed high relative singlet oxygen production. The *in vitro* lipofuscin formation model consisting of mitochondria incubated at pH 4.5 with the lysosomal enzyme cocktail displayed the second highest relative singlet oxygen production of all the samples tested with a singlet oxygen yield greater than the equivalent model maintained at pH 7. Equally, mitochondria maintained alone at pH 4.5 had a greater singlet oxygen yield value than those maintained at pH 7. The singlet oxygen yields of the mitochondria samples were similar to those obtained for POS isolated in the dark and incubated with the lysosomal enzyme cocktail at both pH 4.5 and 7, suggesting that lipofuscin products formed from autophagy may play a role in the phototoxicity of retinal lipofuscin. The samples containing the lysosomal enzyme cocktail alone had very low relative singlet oxygen yields.

Table 4.2 Summary of the quantum yield of each of the lipofuscin formation models and the controls for comparison with ATR and also the Yield of singlet oxygen that has been normalised to account for differences in concentration of samples.

Sample	Lower limit of singlet oxygen quantum yield	Lower limit of singlet oxygen yield
ATR	0.3 ± 0.04	
Mito and Lyso pH 7	0.04 ± 0.013	0.020
Mito and Lyso pH 4.5	0.05 ± 0.014	0.033
POS (light) and Lyso pH 7	0.11 ± 0.150	0.024
POS (light) and Lyso pH 4.5	0.11 ± 0.015	0.036
POS (dark) and Lyso pH 7	0.06 ± 0.010	0.018
POS (dark) and Lyso pH 4.5	0.03 ± 0.020	0.015
Mito pH 7	0.02 ± 0.009	0.015
Mito pH 4.5	0.03 ± 0.009	0.019
POS (light) pH 7	0.05 ± 0.040	0.008
POS (light) pH 4.5	0.10 ± 0.021	0.031
POS (dark) pH 7	0.11 ± 0.005	0.022
POS (dark) pH 4.5	0.11 ± 0.007	0.030
Lyso pH 7	0.03 ± 0.009	0.008
Lyso pH 4.5	0.01 ± 0.020	0.005

4.4 Discussion

The aim of this study was to develop *in vitro* models of retinal lipofuscin formation that mimicked the processes of autophagy and phagocytosis to gauge how each of these mechanisms contributed to lipofuscin granule accumulation and how they affected the physical and chemical characteristics of the granules formed. To do this we identified the key components of retinal lipofuscin formation as being lysosomal enzymes, POS as substrates of phagocytosis and mitochondria to represent the contribution of autophagy in retinal lipofuscin formation.

The results of the lysosomal enzyme assays show that we have achieved an enriched lysosomal fraction from which to extract a lysosomal enzyme cocktail. This together with the Western blot results identifying the presence of the mitochondrial marker, HSP60, in the mitochondrial enriched fraction indicates that two of the components of the *in vitro* lipofuscin models have been obtained. Using spectrophotometry we have shown that two separate samples of POS have been isolated, one that contains intact rhodopsin (dark) and another in which the rhodopsin has been dissociated due to light exposure (light), thus, providing two separate models of the formation of retinal lipofuscin as a result of phagocytosis. These models could provide some insight into the role of intact rhodopsin in lipofuscin formation and any effect it may have on the physical characteristics of the granules.

Incubation of each of the retinal lipofuscin model components lead to the development of a yellow colour in the sample mixture over a four month period. This colour change is likely due to the peroxidation of lipid and protein constituents present within the models and controls (Yin, 1996; Nilsson and Yin, 1997). It is believed that oxidative modification of cellular components leads to the accumulation of lipofuscins, indeed, in this study adduction of cellular components to lipid peroxidation products were observed in some of the models.

The optical density and fluorescence spectra of the models show maxima at shorter wavelengths than those seen with retinal lipofuscin measured in this project and those published previously (Boulton *et al.*, 1990). The spectra seen with the lipofuscin

models resemble that of lipid peroxidation products that have been shown to emit in the far blue-region (Eldred and Katz, 1989,1991). The lipid peroxidation products may be responsible for the absorbance patterns of retinal lipofuscin at this wavelength, however, retinal lipofuscin contains a number of chromophores that may contribute to its absorbance spectra, some of which were not present in the *in vitro* lipofuscin models (Katz and Robison, 2002; Fishkin *et al.*, 2005).

The emission spectra of the lipofuscin models showed that they contained species that fluoresced at approximately 450 nm when excited with light of 364 nm. These results are similar to those recorded in other *in vitro* lipofuscin models based largely upon autophagy (Yin, 1992; Yin *et al.*, 1995). It is possible that these fluorophores are Schiff bases that have arisen as the result of Maillard reactions between the models constituents. Some of the models including: Mito and Lyso, Mito, Lyso, POS (dark) and Lyso and POS (dark) when incubated at pH 7 exhibited a shoulder at ~525 nm, this is also where the emission maxima of *ex vivo* retinal lipofuscin occurred. The shoulder at ~525 nm was only seen in the Mito and Lyso model when incubated at pH 4.5. The presence of the shoulder indicates that there could be fluorescent species present within the models that are similar to those present in *ex vivo* lipofuscin.

Previously published *in vitro* models of lipofuscin formation have displayed fluorescence spectra that resembled those obtained in this study. However, some of these models were developed using cellular organelles that had been damaged by UV-radiation (Nilsson and Yin, 1997). This study avoided inducing oxidative damage using UV light despite it apparently being a quick and easy method, as it has questionable physiological relevance to lipofuscin formation in the retina. The retina is well protected from UV-C light as the cornea does not transmit light of wavelength 286 – 300 nm (Dillon *et al.*, 2004). It is possible that longer wavelength UV-light would reach the retinas of children and aphakic individuals, however, lipofuscin continues to form in the eyes of older individuals whose crystalline lens no longer transmit light below ~ 400 nm and therefore the impact of UV in lipofuscin formation is likely to be minimal (Boettner and Wolter, 1962; Delori *et al.*, 2001; Ernest, 2004).

The SDS-PAGE analysis of the protein profile of the lipofuscin models showed similar patterns to that seen with *ex vivo* lipofuscin. The smear of protein along the

lane with very few if any distinct bands is indicative of the presence of numerous post-translational modifications. This phenomenon has previously been described in *ex vivo* lipofuscin (Warburton *et al.*, 2005; Ng *et al.*, 2008), and is seen again in this study. *In vitro* lipofuscin models and *ex vivo* lipofuscin also showed protein smearing with no distinct bands at the low molecular weight end of the gel, this would likely indicate that both samples contain partially digested or degraded proteins.

Of the numerous post-translational modifications that have been identified in retinal lipofuscin, one that has generated a lot of interest in the literature is CEP-adduction. CEP-adducts have been shown to be elevated in the blood plasma of AMD patients and to accumulate in drusen on Bruchs membrane (Crabb *et al.*, 2002; Gu *et al.*, 2003; Hollyfield *et al.*, 2008) Equally, CEP has been shown to induce neovascularisation *in vivo* upon administration to a chick model (Ebrahem *et al.*, 2006; Hollyfield *et al.*, 2008). The presence of CEP-adducts in the lipofuscin formation models adds credence to the theory of lipid peroxidation products playing an important role in the formation and accumulation of lipofuscin (Schutt *et al.*, 2003a; Kopitz *et al.*, 2004b). However, as seen in Figure 4.10 CEP-adducts were not present in all the models, being absent from those modelling lipofuscin formation as a result of autophagy. That CEP modifications were present in the models that contained POS is most probably due to the presence of large quantities of DHA, the unique precursor for CEP formation, which is present in high quantities within the POS (Bazan *et al.*, 1990).

No A2E was detectable in the models that contained only mitochondria or mitochondria and lysosomes. Previous studies have noted that A2E can accumulate in mitochondria, however, it was postulated that the A2E present was not formed within the mitochondria but had accumulated to a critical level within lysosomes and was released from there. The A2E then targeted the outer membranes of mitochondria and accumulated (Schutt *et al.*, 2007a).

It has been proposed that the precursors of A2E are formed within the POS before the final hydrolysis reaction that forms A2E occurs in the lysosomes (Liu *et al.*, 2000; Ben-Shabat *et al.*, 2002b). However, the presence of A2E in models containing only POS supports the findings of the Sparrow group, who have noted that A2E can form

in photoreceptors before they are phagocytosed to the RPE (Sparrow and Boulton, 2005). Measurement of A2E levels in the lipofuscin models also show a pattern of pH dependence, A2E levels were highest in the models maintained at pH 7, with the three lowest values each being at pH 4.5. This pattern of A2E formation may be linked to lysosomal enzyme activity, with activity decreasing at higher pH levels leading to less digestion of A2E precursors. Equally, phospholipase D is postulated as being one of the enzymes responsible for the hydrolysis reaction that converts the A2E precursor, A2PE, into A2E (Ben-Shabat *et al.*, 2002b). This is a plasma membrane associated enzyme that works optimally at neutral pH and so formation of A2E in the models at pH 7 could possibly occur more optimally than at pH 4.5. There was no obvious pattern as to what effect intact rhodopsin had on the generation of A2E. Models and controls that contained dark isolated POS were measured as having the highest (POS (dark) pH 7, 60 ng A2E/ mg sample) and the lowest (POS (dark) and Lyso pH 4.5, 2.9 ng A2E/ mg sample) A2E levels.

The singlet oxygen yield of the lysosomal enzyme cocktail incubated alone at pH 4.5 and 7 was lower than all others, with the exception of the light isolated POS sample at pH 7. However, when mitochondria and light isolated POS are incubated with the lysosomes the singlet oxygen yield of the model is greater than, or, equal to the sum of its parts. This may suggest that the mitochondria and light isolated POS undergo further modification when exposed to the lysosomal enzyme cocktail generating photoreactive species. The dark isolated POS did not follow this trend. Dark isolated POS had a lower singlet oxygen yield than those incubated alone.

A comparison of the quantum yield of singlet oxygen of A2E as calculated by Pawlak *et al* (0.0003) and the lower limits of singlet oxygen quantum yield obtained in this study for the *in vitro* lipofuscin formation models, suggests that each of the models generates more singlet oxygen when excited with blue-light than A2E (Pawlak *et al.*, 2003). As the models were composed of what are thought to be the principle substrates of retinal lipofuscin, it can be postulated that the models contain photoreactive species that would also be present in retinal lipofuscin and that these species are more potent than A2E.

Results obtained during this study imply that it is possible two species of RPE lipofuscin exist, one that originates from the incomplete degradation of old or damaged organelles and the other from the phagocytosis of POS. Equally, these two distinct origins could provide a source of material for the formation of a single type of lipofuscin granule that is a composite of both. Indeed, this may partially explain the heterogeneity of individual lipofuscin granules that has been noted (H aralampus-Grynaviski *et al.*, 2003).

The study has succeeded in developing three *in vitro* models of retinal lipofuscin formation, each at pH 4.5 and 7, simulating the processes of autophagy and phagocytosis. Results obtained in this study suggest that both processes contribute to retinal lipofuscin formation. Analysis of the models indicates that there are a number of similarities between the *in vitro* and *in vivo* lipofuscin samples, however, there are also some distinct differences that are symptomatic of more complex mechanisms being involved in lipofuscin formation than simply exposing cell components thought to be the main substrates to lysosomal enzymes.

Chapter 5

Can Yellow Tinted Filters Protect Against the Blue-Light Phototoxicity of Retinal Lipofuscin?

5.1 Introduction

The human eye is exposed to high energy non-ionizing radiation throughout life. However, irradiation below approximately 390 nm is prevented from reaching the retina by the cornea and lens allowing only the passage of light above this wavelength (Boettner and Wolter, 1962; van den Berg and Spekreijse, 1997). With age and increasing yellowing of the lens, likely due to the accumulation of tryptophan oxidation products and glycation of lens proteins, the quantity of short wavelength visible light in the blue region of the spectrum transmitted to the retina decreases (Weale, 1988; Dillon *et al.*, 2004). This affords protection to the retina from potentially harmful, high energy light in this region. However, this protective effect is negated by the age-related increase in the photoreactive pigment lipofuscin present in the RPE (Feeney-Burns *et al.*, 1984; Delori *et al.*, 2001).

As described previously, retinal lipofuscin has been shown to be photoreactive and damaging to RPE cells *in vitro* when excited with blue-light through multifaceted mechanisms including: damage to proteins, lipids and DNA (Boulton *et al.*, 1993; Rozanowska *et al.*, 1995; Rozanowska *et al.*, 1998; Davies *et al.*, 2001; Boulton *et al.*, 2004; Godley *et al.*, 2005). Such experimental work has resulted in retinal lipofuscin being theoretically linked to RPE cell damage and, as a consequence, a number of diseases relating to macular dysfunction, in particular AMD (Margrain *et al.*, 2004; Nowak, 2006b).

Intra-ocular lenses (IOLs) are artificial lenses that are used to replace opacified natural crystalline lenses during cataract surgery. Early IOLs were colourless and allowed transmission of UV irradiation as well as visible light. During the 1980s lenses were developed that prevented transmission of UV-light but still allowed the passage of harmful blue-light (Mainster, 1986). Replacement of a naturally yellowed lens with a clear one after cataract surgery exposes the aged retina to high energy blue-light when it is at its most vulnerable. Indeed, it has been reported that patients who have under gone cataract surgery and been implanted with a clear IOL are at increased risk of developing disciform ARM as compared to age matched controls (van der Schaft *et al.*, 1994; Pollack *et al.*, 1996). The association of blue light and lipofuscin with macular degeneration and the theoretical protective properties of

yellow compared to clear or UV-blocking only lenses has led to the development of a new series of IOLs that have the ability to block blue-light, but have yet to be universally accepted (Meyers *et al.*, 2004; Mainster, 2005,2006).

There are a number of arguments against the use of blue-blocking lenses. One is that reducing the amount of blue-light reaching the back of the eye could adversely affect the patients colour sensitivity and also theoretically lead to a loss in scotopic vision (Pons *et al.*, 2007). However, the amount of blue light blocked by an IOL is less than that of a natural 70 year old lens (van de Kraats and van Norren, 2007). Indeed, several clinical trials have failed to find any significant difference in scotopic vision, visual acuity, contrast sensitivity or colour vision between patients with blue-blocking and clear IOLs (Marshall *et al.*, 2005; Hayashi and Hayashi, 2006; Greenstein *et al.*, 2007; Landers *et al.*, 2007; Muftuoglu *et al.*, 2007). Another cause for concern is based around the suggestion that the use of blue-blocking lenses may interrupt the excitation of melanopsin, a molecule found in blue-light sensitive retinal ganglion cells, believed to modulate circadian rhythms and pupillary function (Berson *et al.*, 2002; Dacey *et al.*, 2005; Kawasaki and Kardon, 2007; Zaidi *et al.*, 2007). A solution to this theoretical problem is the use of sharp cut-off filters that would block shorter wavelength visible light (the blue-light hazard peaks between 430-440 nm) but allow transmission at 480 nm which is the peak spectral sensitivity of melanopsin (Algvere *et al.*, 2006; van de Kraats and van Norren, 2007). These problems highlight the importance of design when considering the manufacture of blue-blocking lenses where a balance needs to be struck between photoprotection and photoreception.

Previous studies demonstrated that blue-light blocking lenses had a protective capacity towards RPE cells exposed to high intensity light for short periods and inhibit the light induced production of VEGF by RPE cells (Sparrow *et al.*, 2004; Yanagi *et al.*, 2006). Both studies used a single model of IOL that was a gradual blue-light blocker.

The aims of this study were to investigate the photoprotection offered by different IOLs, or equivalent filters, on the phototoxicity of retinal lipofuscin and associated RPE cell death. The relationship between lipofuscin granule number per cell and cell viability after light exposure was also explored. The effectiveness of optical filters

was quantified using the MTT assay and visualised with the Live-Dead cell assay using a fluorescence microscope. This study sought to determine if there was a difference between the photoprotection afforded by a sharp-cut off filter and a gradual blue-blocking filter.

5.2 Materials and Methods

5.2.1 Measurement of transmittance of light through blue-light transmitting filters

Transmission of light (290-1000 nm) through filters was measured using a spectrophotometer (U2800, Hitachi Digilab). The data was transferred from the UV solutions 2.0 software to Excel for graphing.

5.2.2 Optimisation of choice of blue-light transmitting filter to be used in this study

In order to identify a blue light filter with the appropriate spectral range and sufficient irradiance the transmission of a number of "blue-light" filters was measured. Initially the transmission of sharp cut-off filters (provided by AMO Inc, Santa Ana, CA), that allowed the passage of light between 400-440 and 440-500 nm, was recorded. These proved interesting as light of very specific wavelengths could be used. However, whilst an irradiance of 2.8 mW/cm^2 could be achieved with the 440-500 nm filter, light levels attainable with the 400-440 nm filter were lower than those used in the validation studies. Increases in irradiation intensity can be achieved by moving the light source closer to the cells, however, this results in the temperature of the cells increasing. Using the 400-440 nm light transmitting filter it was not possible to achieve the required light level and maintain the temperature at a level that would not affect cell viability. For this reason work with these filters did not proceed.

Next, the transmission profile of blue-light creating filters purchased from Lee filters (Hampshire, UK) were measured, using single and combinations of filters. Both the Zenith blue (# 195) (Fig. 5.1.A) and the Special Medium Blue (#363) (Fig. 5.1.C) filters transmitted light of wavelength and irradiance suitable for future investigations. The addition of a Mauve filter (# 126) (Fig. 5.1B & D) to reduce the amount of red light passing through the filter reduced the irradiance of light effectively creating the same problem that was encountered with the sharp cut-off filters. Therefore, the Special Medium Blue filter was chosen as this filter suited our needs and had been

used in previous work on RPE phototoxicity studies found in the literature (Godley *et al.*, 2005).

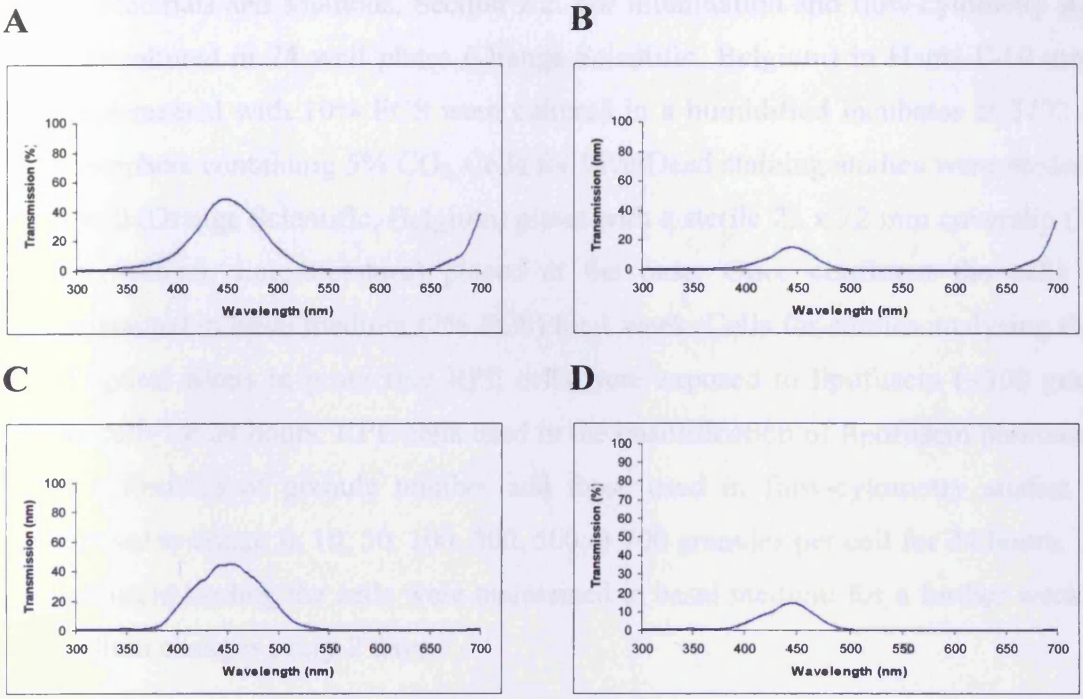

Figure 5.1. Transmission spectra of blue light transmitting filters for 400-500 nm. The transmission of light through the filter was measured between 300 and 700 nm using a spectrophotometer (U2800 Hitachi digilab) as described in 5.2.1. Transmission spectra through zenith blue (A), zenith blue and mauve (B), special medium blue (C) and special medium blue and mauve (D) filters were measured.

5.2.3 Isolation of lipofuscin

Lipofuscin was isolated as described in the Materials and Methods, Section 2.1. Briefly, RPE cells were isolated from human donor eyes obtained from Bristol Eye Bank with Human Tissue License (average age of donor 68 years, donors within the age range 58-92 years old). RPE cells were disrupted and the lipofuscin isolated using a series of discontinuous sucrose density gradients. Once isolated lipofuscin was quantified by counting on a haemocytometer (Bürker, Germany) and stored at -80°C until required.

5.2.4 Cell culture

Prior to experimentation ARPE-19 cells were stored and maintained as described in the Materials and Methods, Section 2.2. For illumination and flow-cytometry studies cells cultured in 24 well plates (Orange Scientific, Belgium) in Hams F-10 medium supplemented with 10% FCS were cultured in a humidified incubator at 37°C in an atmosphere containing 5% CO_2. Cells for Live/Dead staining studies were seeded into 6-well (Orange Scientific, Belgium) plates with a sterile 22 x 22 mm coverslip (VWR International, Leicestershire) placed at the base. Once confluent the cells were maintained in basal medium (2% FCS) for 1 week. Cells for studies analysing the use of optical filters in protecting RPE cells were exposed to lipofuscin (~300 granules per cell) for 24 hours. RPE cells used in the quantification of lipofuscin phototoxicity as a function of granule number and those used in flow-cytometry studies were exposed to either: 0, 10, 50, 100, 300, 500 or 700 granules per cell for 24 hours. After lipofuscin loading the cells were maintained in basal medium for a further week with medium changes every 2 days.

5.2.5 Experimental set-up for illumination

For illumination studies light was generated using a Sunlight simulator (SOL 120, Honle technology, Munich, Germany). Cells with and without lipofuscin were placed above the optical filter being tested. Light exposed control cells were irradiated directly by the light. Dark control cells were wrapped in black foil and placed atop the light source. Aluminium foil was positioned between the dark control cells and lamp to prevent over heating. The distance cells were kept from the lamp and the use of heat shields ensured that cells were exposed to light at the intensity required and also maintained at a constant temperature of 37°C (Fig. 5.2). Spectral range of light was controlled by using a Special Medium Blue filter for blue-light exposures and a clear glass sheet for white light (390-720 nm).

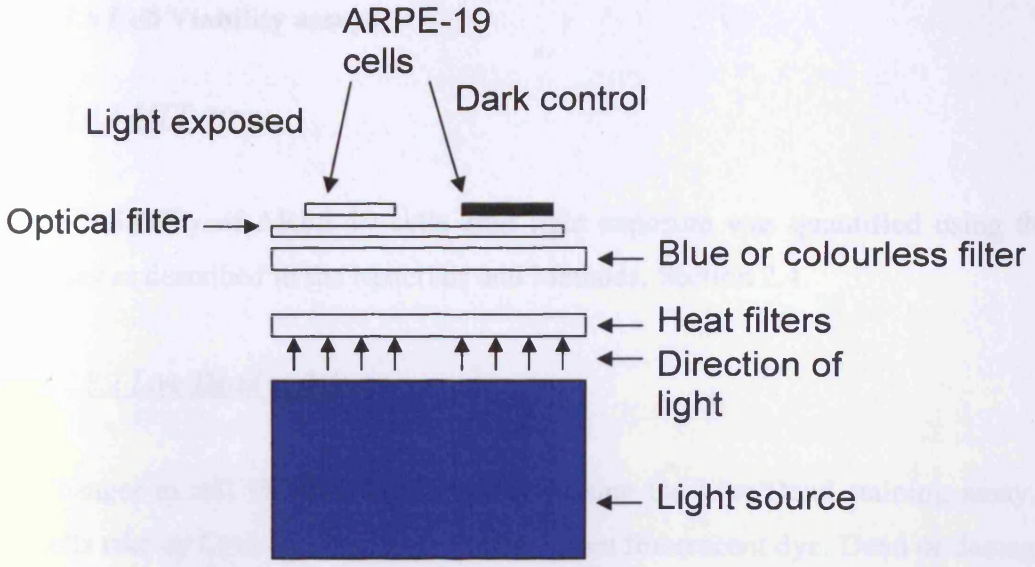

Figure 5.2. Experimental set-up used for determining the potential of blue-light blocking lenses in reducing the blue-light hazard of retinal lipofuscin

5.2.6 Illumination of RPE Cells

Prior to light exposure, the basal medium was replaced with SF10PF (Gibco, UK) medium, which lacks the photosensitisers phenol red, tryptophan, tyrosine, riboflavin and folic acid.

Light conditions used were;

(a) blue-light, 400-500 nm, 2.8 mW/cm^2, 37 °C.

(b) white-light, 380-720 nm, 19.0 mW/cm^2, 13.0 mW/cm^2 or 2.8 mW/cm^2, 37 °C.

5.2.7 Measurement of spectral irradiance of light emitted from the sunlight simulator

Spectral irradiances were measured using a spectroradiometer (Specbos 121, HORIBA Jobin Yves, UK) held over the light source in the position of the cell culture plate. Data was transferred from the JetLi software to Excel for graphing.

5.2.8 Cell Viability assays

5.2.8.1 MTT assay

Cell viability of ARPE-19 cells after light exposure was quantified using the MTT assay as described in the Materials and Methods, Section 2.4.

5.2.8.2 Live/Dead staining

Changes in cell viability were visualised using the Live/Dead staining assay. Viable cells take up Cyto-dye, a cell-permeable green fluorescent dye. Dead or damaged cells take up propidium iodide, a non-permeable red fluorescent dye that can only enter the cell when there has been membrane damage that results in permeabilisation (Frey, 1995).

Cells with and without lipofuscin were prepared as described above and either exposed to blue-light (400-500 nm) at an intensity of 2.8 mW/cm^2 in the presence or absence of Filters 1 or 2 supplied by AMO (Santa Ana, CA, USA) or maintained in the dark for 48 hours.
After a 48 hour exposure to light or maintenance in the dark, cells were treated with 1 ml of Live/Dead staining solution (Calbiochem, UK) for 15 mins at 37°C as recommended by the manufacturer. The coverslips were removed from the wells of 24-well plates and inverted onto glass microscope slides with a small drop of PBS to prevent cells drying out during microscopy. The cells were viewed immediately using a fluorescence microscope (Leica CTR 6000, Leica, Milton Keynes) equipped with band-pass filters that detect FITC and rhodamine and a DFC359 FX camera (Leica, Milton Keynes). Images were analysed using Microsoft Picture Manager (Microsoft, USA).

5.2.9 Measurement of lipofuscin-like fluorescence of cells using flow cytometery

Cells were prepared for analysis by flow cytometry as described in Chapter 2 Section 2.5. However, one week before experimentation cells were exposed to a graduated series of lipofuscin granule concentrations that ranged from 0 – 700 granules/cell for

24 hours. The range was as follows: 0, 10, 50, 100, 300 and 700 granules/cell. Cells were then maintained in basal medium containing 2% FCS and a full complement of antibiotics and fungizone for 7 days.

5.2.10 Statistical analysis

All tests of optical filters were carried out at least three times and in triplicate. Analysis of variance (ANOVA) was used to determine the significance of differences in cell viabilities of populations treated with different filters or loaded with differing numbers of lipofuscin granules using Minitab software (Minitab 14, Minitab Ltd, Coventry, UK). Students' *t*-test was used to determine the significance of results gathered in the validation of methodology section, when only two values were compared (Excel, Microsoft). $p < 0.05$ was regarded as statistically significant.

5.3 Results

5.3.1 Optimisation of Experimental Conditions

5.3.1.1 (Photo)toxic effect of lipofuscin on ARPE-19 cells

This experiment was undertaken to investigate whether retinal lipofuscin was phototoxic to RPE cells under standard experimental conditions used in the laboratory and to optimise an exposure time for the IOL trials. The results in Figure 5.3 show that lipofuscin was phototoxic towards ARPE-19 cells when exposed to blue light (400-500 nm, created using Special Medium Blue filter, 2.8mW/cm^2). This resulted in a significant ($p<0.05$) loss of RPE cell viability (60% cell viability) over a 24 hour period when compared to cells maintained in the dark (100% cell viability) or not exposed to lipofuscin (90% cell viability). To determine if cell viability was dependant on irradiance time, the length of exposure was increased from 24 to 48 hours. Figure 5.4 shows that there was a greater loss in cell viability between RPE cells loaded with lipofuscin and those not after a 48 hour period (43 and 84%, respectively) compared with 24 hours. 48 hours was, therefore, chosen as the appropriate time duration for future experiments. This series of experiments also verified that the experimental set-up was suitable for analysing the effect of blue-light and optical filters on cell viability of light irradiated cells.

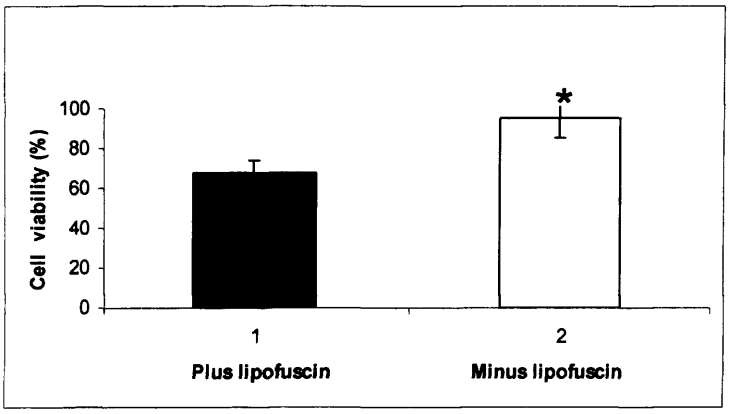

Figure 5.3. Cell viability of ARPE-19 cells after a 24 hour exposure to 400-500 nm light.
A comparison of the viability of cells that have been exposed to ~300 lipofuscin granules per cell and those that have not been exposed to lipofuscin after irradiation with blue-light (400-500 nm, 2.8 mW/cm^2) for 24 hours. Results are the average of three exposures, each performed in triplicate. Error bars indicate standard deviation. Values significantly different to those of cells loaded with lipofuscin and irradiated with blue-light: *$p< 0.05$.

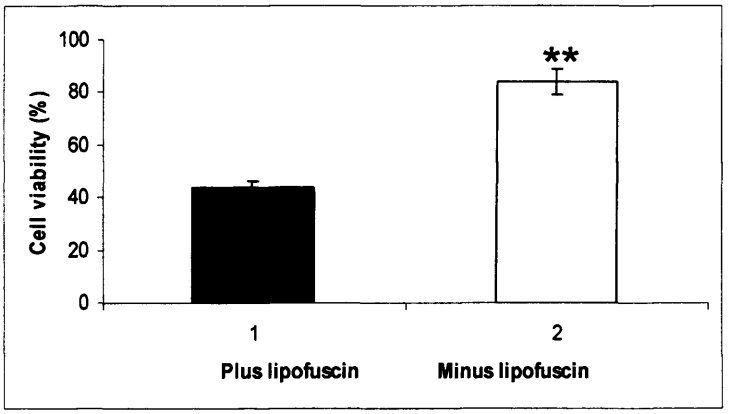

Figure 5.4. Cell viability of ARPE-19 cells after a 48 hour exposure to 400-500 nm light.
A comparison of the viability of cells that have been exposed to ~300 lipofuscin granules per cell and those that have not after irradiation with blue-light (400-500 nm, 2.8 mW/cm^2) for 48 hours. Results are the average of three exposures each performed in triplicate. Error bars indicate standard deviation. Values significantly different to those of cells loaded with lipofuscin and irradiated with blue-light: **$p< 0.01$.

5.3.2 Determination of the phototoxicity of lipofuscin as a function of the number of granules taken up by RPE cells

The results seen in Figure 5.5 indicate there is a relationship between increasing number of lipofuscin granules per cell and decreasing cell viability within the population. The trend is reproduced with each of the light conditions; higher and lower intensity white light and blue-light. However, the loss in cell viability when using the lower intensity white light (2.8 mW/cm^2) did not become significantly different from 0 lipofuscin granules until cells were exposed to 500 granules per cell ($P< 0.01$), with a further significant decrease when cells were exposed to 700 granules per cell ($P<0.005$)

When exposed to higher intensity white light (13 mW/cm^2) or blue-light (2.8 mW/cm^2), the loss in cell viability compared to cells loaded with 0 lipofuscin granules becomes significantly different when cells have been exposed to 50 lipofuscin granules per cell ($P< 0.005$). The effect of increasing numbers of lipofuscin granules showed a dose-dependent loss of cell viability up to the accumulation of 300 granules per cell with blue-light and 100 granules with white-light. At this point there continues to be an increase in cell death with increasing granule number, however, the difference in cell viability measured by the MTT assay is not as great as at lower lipofuscin granule levels. This is possibly due to the limitations in sensitivity in the MTT assay at low cell numbers. By 700 lipofuscin granules per cell, viability was less than 10%. This work indicates that the effect of lipofuscin upon cells is both concentration and light intensity dependant (Fig. 5.5D).

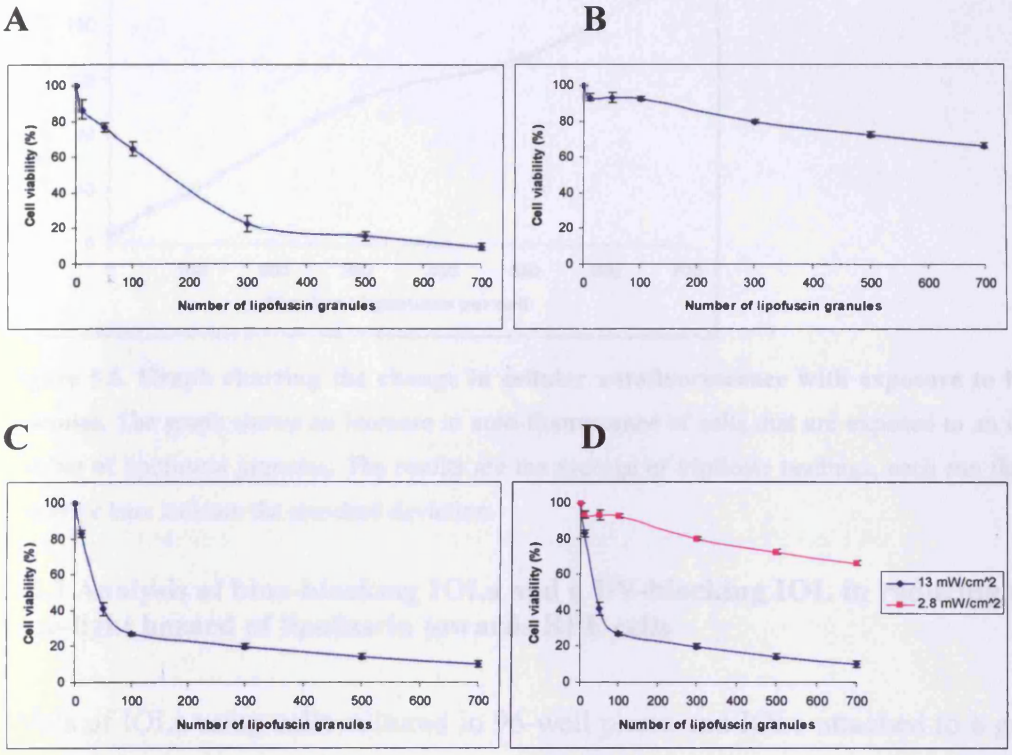

Figure 5.5. Quantification of lipofuscin phototoxicity as a function of granule number. Cells were exposed to an increasing number of lipofuscin granules and irradiated with **A**, blue light (400-500 nm, 2.8 mW/cm^2), **B**, lower intensity white light (380-720 nm, 2.8 mW/cm^2) or **C** higher intensity white light (380-720 nm, 13 mW/cm^2) for 48 hours. **D** is a comparison of figures 5 **B** and **C**. Control cells were maintained in the dark by wrapping in black foil. Data are the average of 3 exposures each carried out in triplicate. Error bars represent standard deviation.

To determine if uptake of lipofuscin granules by RPE cells increased with exposure to increasing number of granules cells were exposed to a range of lipofuscin granule concentrations from 0 to 700 per cell. The lipofuscin-like autofluorescence within the cells was then semi-quantitatively measured by flow cytometery. The results indicate that increasing the number of lipofuscin granules that RPE cells are exposed to causes an increase in the number of lipofuscin granules phagocytosed by the cells (Fig. 5.6).

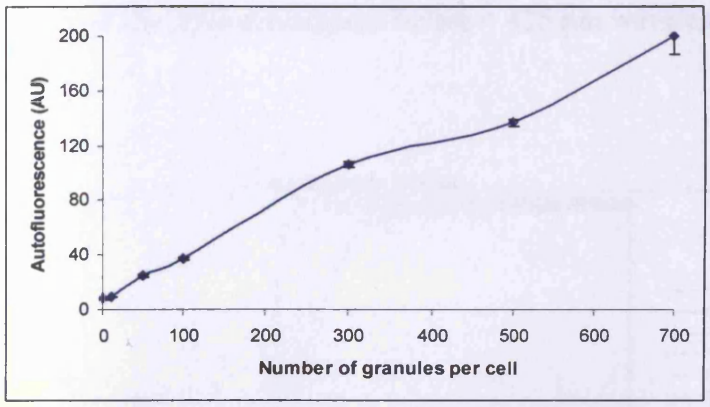

Figure 5.6. Graph charting the change in cellular autofluorescence with exposure to lipofuscin granules. The graph shows an increase in auto-fluorescence of cells that are exposed to an increasing number of lipofuscin granules. The results are the average of triplicate readings, each run three times. The error bars indicate the standard deviation.

5.3.3 Analysis of blue-blocking IOLs and a UV-blocking IOL in reducing the blue-light hazard of lipofuscin towards RPE cells

Trials of IOLs using cells cultured in 96-well plates and IOLs attached to a grid gave results that showed inconsistencies between wells under the same conditions and repeats of trials. It was suggested that the irregularities arose because of a lack of sensitivity of the MTT assay with cells cultured in 96-well plates and focusing issues of the IOLs. To overcome the problem of sensitivity and to increase the irradiance area new filters which exhibited the transmission characteristics of the yellow IOLs and a UV-blocking control were manufactured.

5.3.4 Testing of AMO filters

5.3.4.1 Transmission spectra of optical filters received from AMO

The filters used in this study were labelled as: Control 1a and 1b, Filter 1a and 1b and Filter 2a and 2b so that trials would be carried out in a 'blind' manner. The transmission of light through each filter can be seen in Figure 5.7. The transmission spectra show that the control filters used in these trials are UV-blocking filters that prevent the passage of nearly 100% of light below 400 nm in wavelength, but transmit light of longer wavelength. Filter 1 is a blue-light blocking filter that allows the passage of minimal light below 400 nm but gradually allows the transmittance of light up to 500 nm, and all greater than this. Filter 2 is a sharp cut-off blue-light blocking

filter that has 0% transmission below ~ 425 nm wavelength but almost 100% at ~ 450 nm.

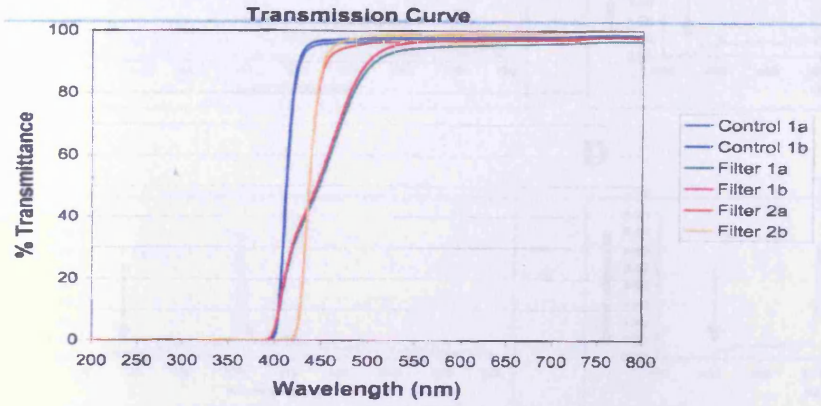

Figure 5.7.Transmission spectra of optical filters (AMO, Inc., Santa Ana, CA)

5.3.4.2 Transmission of light from the sunlight simulator through the optical filters

Figures 5.8 and 5.9 show the spectral irradiance that cells are exposed to during white-light and blue-light exposures, respectively, and the effect each of the filters has on the spectrum of light reaching the cells. Figures 5.8 A and 5.9 A show the full spectrum as would be transmitted with no filter. Figures 5.8 B and 5.9 B are the full spectrum via the control filter. It can be seen that light below ~400 nm is blocked by the control filter, but light of longer wavelengths is not obstructed. Figures 5.8 C and 5.9 C show the light that would reach cells via filter 1. Filter 1 also blocks light below 400 nm, plus causes a decrease in the intensity of blue-light up to approximately 480 nm. Figures 5.8 D and 5.9 D represent light that would reach cells via filter 2. It can be seen that there is a sharp cut off point at approximately 430 nm. Light below that wavelength is blocked but light above is transmitted.

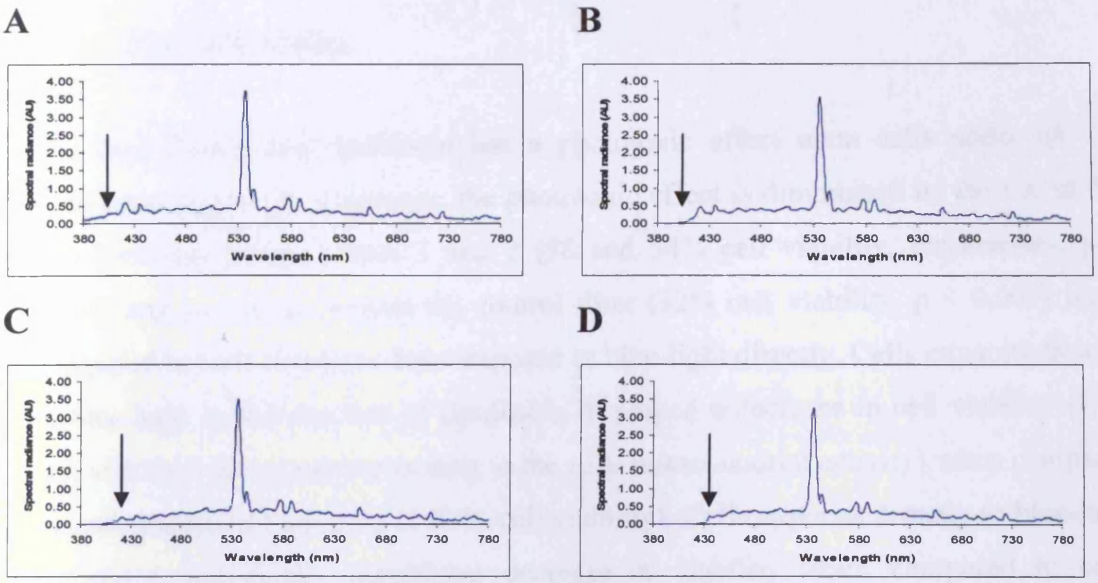

Figure 5.8. Irradiance spectra measured at the level of cells from the sunlight simulator equipped with a combination of heat shield and white light-transmitting filters with and without tested filters. A is with no filter, **B** through control filter, **C** is through filter 1 and **D** through filter 2. Arrows high-light the differences in spectra caused by the filters at the shorter wavelength end of the spectrum.

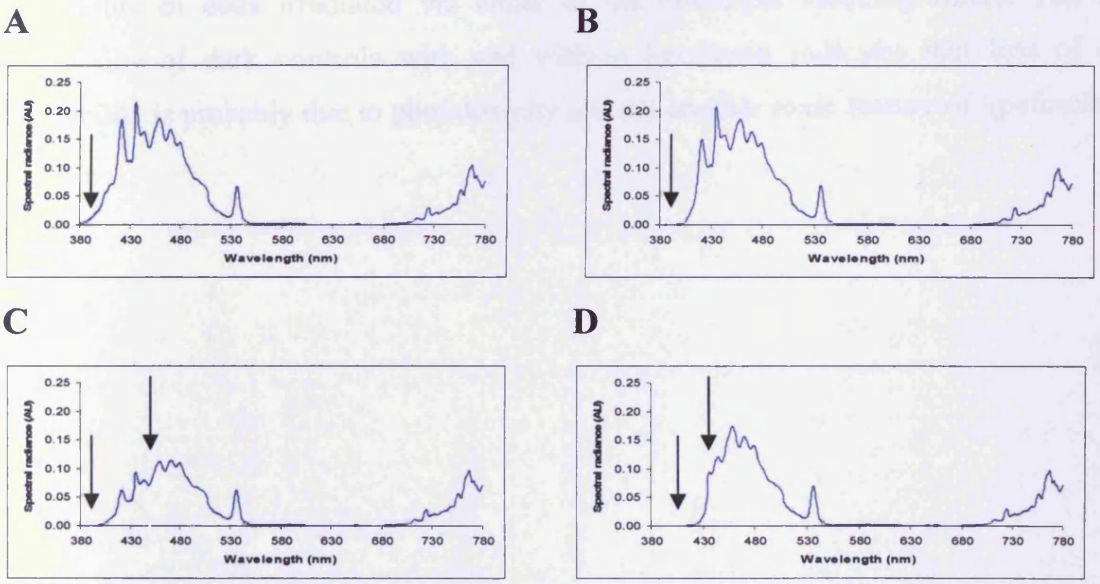

Figure 5.9 Irradiance spectra measured at the level of cells from the sunlight simulator equipped with a combination of heat shield and blue light-transmitting filters with and without tested filters. A is with no filter, **B** through control filter, **C** is through filter 1 and **D** through filter 2. Arrows high-light the differences in spectra caused by the filters at the shorter wavelength end of the spectrum.

5.3.5 Assessment of filters in reducing the lipofuscin phototoxicity to RPE cells

5.3.5.1 Blue-light studies

The data shows that lipofuscin has a phototoxic effect upon cells under all test conditions (Fig 5.10). However, the phototoxic effect is diminished by the use of the blue-blocking filters, Filters 1 and 2 (56 and 54% cell viability, respectively, $p < 0.001$) and to a lesser extent the control filter (32% cell viability, $p < 0.005$) when compared to cells that have been exposed to blue-light directly. Cells exposed directly to blue-light in the absence of lipofuscin displayed a decrease in cell viability (73% cell viability) (measured according to the cells mitochondrial activity) when compared to dark maintained controls (100 % cell viability). Cells exposed directly to blue-light showed a statistically significant decrease in viability when compared to cells irradiated via the blue-light blocking filters, Filters 1 and 2 (89 and 98% cell viability, respectively, $p < 0.005$). There was no statistical difference between cells that were irradiated via either the control filter or no filter in the absence of lipofuscin. The data collected in this study also determined that there was no statistical difference in the viability of cells irradiated via either of the blue-light blocking filters. The cell viability of dark controls with and without lipofuscin indicates that loss of cell viability is probably due to phototoxicity and not another toxic feature of lipofuscin.

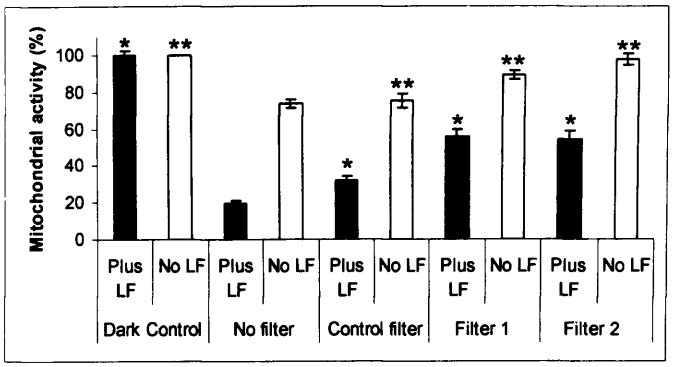

Figure 5.10. The effect of blue-light irradiation and lipofuscin loading on ARPE-19 cells. Cells were irradiated with blue-light (400-500 nm 2.8 mW/cm^2) for 48 hours. Cells were either wrapped in black foil as a dark control, exposed directly to blue light or blue light through an optical filter. For each condition cells were present with or without lipofuscin (exposed to ~300 granules per cell). Results are the average of 3 exposures each carried out in triplicate. Error bars represent standard deviation. Statistically significant difference to cells loaded with lipofuscin and irradiated directly with blue-light: *p< 0.05. Statistically significant difference to cells not loaded with lipofuscin and irradiated directly with blue-light: **p< 0.05.

5.3.5.2 White light studies

As was found in the blue-light studies, studies using white light showed no statistical difference in cell viability of cells maintained in the dark regardless of whether they had been loaded with lipofuscin or not. This would indicate that any loss in cell viability seen during these tests can be attributed to a phototoxic effect.

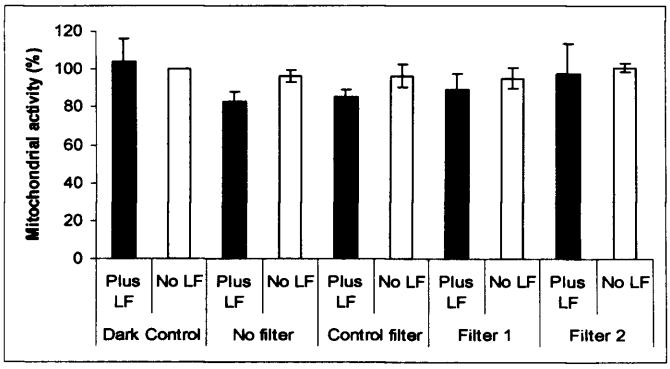

Figure 5.11. The effect of white-light irradiation and lipofuscin loading on ARPE-19 cells. Cells were irradiated with white-light (380-720 nm 2.8 mW/cm^2) for 48 hours. Cells were either wrapped in black foil as a dark control, exposed directly to white light or white light through an optical filter. For each condition cells were present with or without lipofuscin (exposed to ~300 granules per cell). Results are the average of 3 exposures carried out in triplicate. Error bars represent standard deviation.

Under the test conditions described in the experimental design section (section 5.2.5/6) it was found that cells loaded with lipofuscin and irradiated with white light (390 – 720 nm) at an intensity of 2.8 mW/cm^2 (Fig. 5.11) showed a consistent decrease in viability. Cells maintained in equivalent conditions but without lipofuscin showed no decrease in viability, however, this difference was found to be statistically insignificant. The study found that at this intensity there was no statistical difference between cells irradiated with the test filters, control filter or no filter.

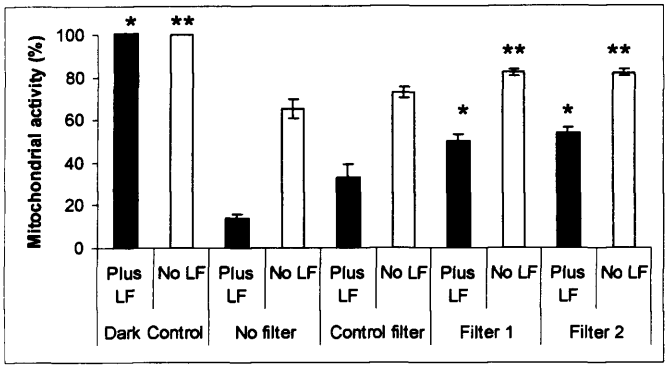

Figure 5.12. The effect of white-light irradiation and lipofuscin loading on ARPE-19 cells. Cells were irradiated with white-light (390-720 nm 13 mW/cm^2) for 48 hours. Cells were either wrapped in black foil as a dark control, exposed directly to white light or white light through an optical filter. For each condition cells were present with or without lipofuscin (exposed to ~300 granules per cell). Results are the average of 3 exposures carried out in triplicate. Error bars represent standard deviation. Statistically significant difference to cells loaded with lipofuscin and irradiated directly with white-light: *$p< 0.05$. Statistically significant difference to cells not loaded with lipofuscin and irradiated directly with white-light: **$p< 0.05$.

Increasing the intensity of light to 13 mW/cm^2 (providing 2.8 mW/cm^2 in the range 400-500 nm) resulted in a decrease in cell viability of cells under all conditions when compared to the dark maintained controls (Fig. 5.12). Cells exposed directly to high intensity white light recorded the lowest cell viability (65%), followed by cells above the control filter (72%). Cells placed above filters 1 and 2 showed identical cell viability, both recording averages of 82%. Cells loaded with lipofuscin showed the greatest decrease in viability. This effect was reduced by the presence of the yellow-tinted, blue-light blocking filters (Filter 1 and 2, 50 and 54% cell viability, respectively) compared with the effect of the control (33% cell viability) or no filter (14% cell viability) ($P < 0.005$). However, there was no significant difference between the viabilities of cells protected by either of the blue-light blocking filters. The blue-

blocking filters also conferred more protection from white light to cells not loaded with lipofuscin than either the control or no filter ($P < 0.001$).

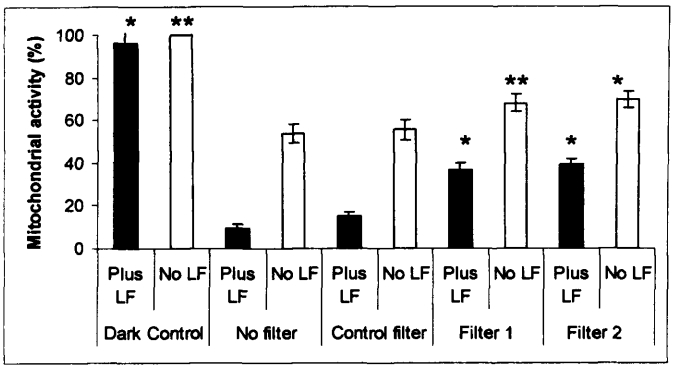

Figure 5.13. The effect of white-light irradiation and lipofuscin loading on ARPE-19 cells. Cells were irradiated with white-light (390-720 nm 19 mW/cm^2) for 48 hours. Cells were either wrapped in black foil as a dark control, exposed directly to white light or white light through an optical filter. For each condition cells were present with or without lipofuscin (exposed to ~300 granules per cell). Results are the average of 3 exposures carried out in triplicate. Error bars represent standard deviation. Statistically significant difference to cells loaded with lipofuscin and irradiated directly with white-light: *$p < 0.05$. Statistically significant difference to cells not loaded with lipofuscin and irradiated directly with white-light: **$p < 0.05$.

A further increase in white light intensity (19 mW/cm^2) resulted in more drastic decreases in viability (Fig. 5.13). Lipofuscin loaded cells showed greater loss in viability than cells not loaded with lipofuscin and maintained under equivalent conditions. Cells loaded with lipofuscin and exposed to high intensity light via the control or no filter had viabilities of 9 and 15% of the dark control, respectively.

When Filters 1 and 2 were used the loss in cell viability was significantly decreased when compared to the clear or control filters ($P < 0.05$), displaying cell viabilities of 36% and 39%, respectively. There was, however, no statistically significant difference between cells irradiated via either of the blue-light blocking filters.

Tests using cells that had not been loaded with lipofuscin showed that there was no significant protection afforded by the control filter when compared to no filter. However, both Filter 1 and 2 showed significant protection ($P < 0.05$) when compared to the control or no filter. No significant difference between the two blue-light blocking filters was seen.

5.3.6 Live/Dead staining

Control cells, with or without lipofuscin, maintained in the dark showed an uptake of the cell-permeable green fluorescent dye but none of the cells stained with propidium iodide (Fig. 5.14 A, B). Red autofluorescent lipofuscin granules could be observed in the cells fed lipofuscin (Fig. 5.14 B). The staining patterns confirmed that the ARPE-19 cells remained viable throughout the 48 hour period. Cells exposed to light without lipofuscin also showed uptake of Cyto-dye with minimal co-staining for propidium iodide thus indicating their viability (Fig. 5.14 C). However, a large number of lipofuscin-fed cells exposed to blue-light became co-stained with Cyto-dye and propidium iodide which suggested cell damage (Fig. 5.14 D). In addition, it was apparent that some cells that had become detached from the coverslip surface. However, experiments using cells loaded with lipofuscin using the blue blocking filters, Filter 1 or Filter 2, in the presence of blue light exhibited minimal cell death (Figs. 5.14 F, H).

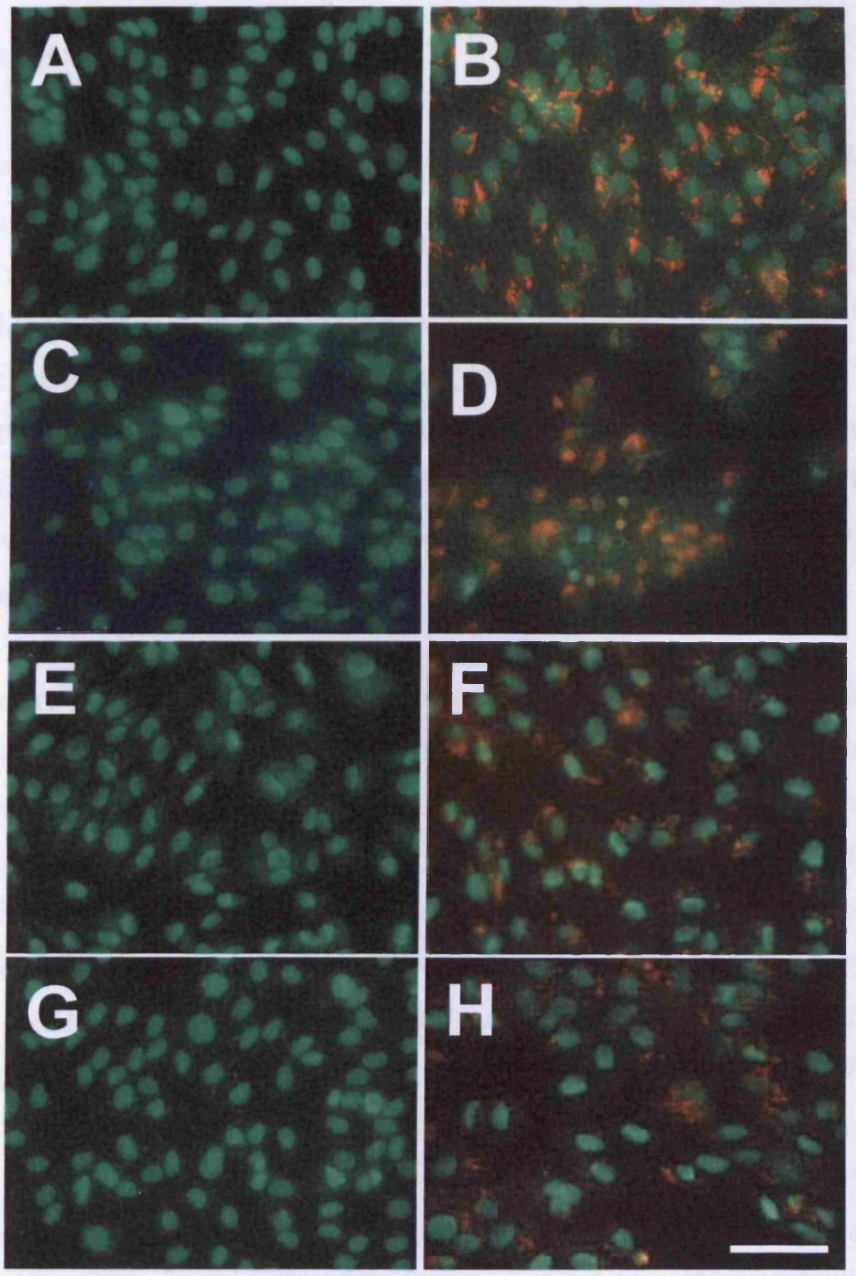

Figure 5.14. The effect of blue-light exposure with/without lipofuscin loading on the viability of ARPE-19 cells visualised with Live/Dead staining. ARPE-19 cells with (B, D, F, H) or without (A, C, E, G) lipofuscin either maintained in the dark (A, B), exposed to blue light (C, D) or using the blue blocking filters (Filter 1 (E,F), Filter 2 (G,H) together with blue light exposure for 48 hours. Scale bar represents 75 μm.

5.4 Discussion

This study has demonstrated that the phototoxicity of lipofuscin towards RPE cells is dependent on the number of granules present, with increasing granule number per cell leading to a decrease in the viability of a cell population. This effect has been verified using blue and white-light. When tested with full visible spectrum light (390-720 nm) lipofuscin phototoxicity was shown to be light intensity dependent, where an increase in light intensity led to an increase in cell death when equal concentrations of lipofuscin granules were used. These findings correlate with the work of Boulton *et al* (1993) who noted that lipofuscin granules in suspension generated free radicals in a light intensity dependant manner.

This project has also led to the development of an experimental design that is capable of allowing fair comparison between optical filters and the appropriate controls. Trials involving lower intensity full visible spectrum light showed no significant difference in viability between the dark maintained controls and experimental cells. It is possible that light at this intensity and for the relatively short period of time was not sufficient to cause measurable damage to the cells and that any ROI generated by lipofuscin present could be dealt with by anti-oxidants and other protective mechanisms present within the cells (Snodderly, 1995; Cai *et al.*, 2000; Jarrett and Boulton, 2005).

Using blue-light (400-500 nm) and higher intensity full spectrum light (390-720 nm), we were able to demonstrate that the control filter had a positive protective effect when compared to no filter. It is possible to explain this effect using the spectra of light reaching the cells via the filters as measured with a spectroradiometer. The spectra show that the control filter blocks light up to about 400 nm, preventing the passage of light between 390 and 400 nm that would still reach the cells that are irradiated directly. As this would be high energy light, preventing it reaching the cells above the control filter could have caused the decrease in loss of cell viability. Equally, there may be a number of chromophores present in the lipiofuscin granules or RPE cells that absorb light in this region and exhibit photosensitiser properties. Preventing the excitation of such chromophores by blocking light of short wavelength

would reduce the number of photoactivated molecules present within the cell that could generate ROI. This again would provide a protective effect towards the cells.

We have also demonstrated that yellow tinted blue-light blocking optical filters (Filters 1 and 2) have a significant protective effect towards the RPE by reducing the blue-light hazard when compared with the presence of a UV-blocking (control) optical filter or no filter. Results obtained using the Live/dead staining technique support our observations with the MTT assay. These data correlate with previous studies that examined the protective effect of a single blue-light blocking lens towards A2E-laden RPE cells (Sparrow *et al.*, 2004; Yanagi *et al.*, 2006) The protective effect was seen in both cells loaded with lipofuscin and those not. RPE cells, even in the absence of lipofuscin, have been shown to generate free radicals and undergo mitochondrial DNA damage when exposed to blue-light (Dorey *et al.*, 1990; Godley *et al.*, 2005). Lipofuscin has been shown to have a multi-faceted phototoxic effect on cells that have been exposed to blue-light or high intensity white light (Davies *et al.*, 2001). Thus, the protective effect of both the blue-light blocking optical filters can probably be explained as a reduction in these processes. A greater relative protective effect was seen when cells had been loaded with lipofuscin. This is most likely due to the reduction in photoexcitation of the photosensitisers present in the granules (Rozanowska *et al.*, 1998; Schutt *et al.*, 2000; Sparrow *et al.*, 2000; Sparrow *et al.*, 2002).

The fact that there was not a total reduction in cell death is probably attributable to not all blue-light being blocked by the lenses, therefore, some high energy light was still able to reach the RPE cells. As blue-light is critical for a number of ocular functions and also in maintenance of a regular circadian rhythm, the detrimental effects of completely blocking blue-light would probably outweigh the benefits (Brainard *et al.*, 2001; Berson *et al.*, 2002; Hanifin and Brainard, 2007; Hankins *et al.*, 2008). As such, a sharp cut-off blue-light blocking filter would possibly be of greatest benefit to a patient who would require such an optical filter. The rational behind this lies in the fact that as there was no statistical difference in protection afforded by either of the blue-light blocking filters, preference must be drawn from other properties of the filters. Filter 2 is less likely to affect circadian rhythm as it blocks less of the light involved in stimulating melanopsin, which peaks at 480 nm, whereas Filter 1

continues to block light of 480 nm wavelength. If yellow tinted lenses were to have an effect on scotopic vision, which peaks at 506 nm, it is likely that Filter 1 would again have the greatest unfavourable effect.

If no adverse effects of the insertion of yellow lenses are proven and the positive effects such as reduced susceptibility to the blue-light hazard are real, with the development of sharp-cut off filters that would reduce any impact on circadian rhythm the widespread use of blue-light blocking filters in cataract surgery should have a beneficial impact for the patient.

Chapter 6

The Use of Nanomedicines in Degrading or Preventing the Formation of Retinal Lipofuscin.

6.1 Introduction

Nanotechnology is a term that has begun to appear in the media and scientific journals with increasing regularity as people strive to design and create products that are smaller and more efficient. The ability to produce designs on such a minute scale has captivated both the scientific and medical communities and has led to the advent of nanomedicines. Like other nanotechnologies, nanomedicines are compounds that are defined by their scale (usually between 1 and 1000 nm) and the term is most widely used when describing molecules that have potential therapeutic capabilities and are sized within this range. However, unlike other nanotechnologies which have small workings for the sake of convenience or style, the tiny scale of nanomedicines has a functional role. Nanomedicines often consist of a carrier molecule such as a polymer, dendrimer, micelle or liposome that is conjugated to, or, encapsulates an active component. Active components are most often a drug or an enzyme, yet in certain instances the carrier molecule itself can fulfil this role.

Carrier molecules are often designed to combine a helpful blend of lipophilicity and hydrophilicity to ensure quick and efficient delivery. The hydrophilicity allows the molecules to be transported through the aqueous phases of the circulatory system and the lipophilic nature of the molecule assists its passage across cell membranes. Carrier molecules exist to encase the active component of the medicine until the conjugated molecules reach their target area; thus, performing a dual function of assisting passage of the active component through the delivery pathway and preventing its degradation or non-specific activity until reaching the target cells. The use of carrier molecules in this way aids the localised accumulation of active molecules at the required site without the side effects of the drugs or enzymes effecting other cells or tissues that are not its targets, particularly in areas prone to toxicity such as the heart and bone marrow (Duncan *et al.*, 2005) This results in higher drug levels at the target site without concomitant side effects that would be seen with a non-specific drug delivery system.

Unfortunately, the problem with many of the polymers that have been trialled previously, whether synthetic or natural, is that they are non-biodegradable (Garnett

and Kallinteri, 2006). Synthetic polymers such as poly(ethyleneglycol) (PEG) and N-(2-hydroxypropyl)methacrylamide (HPMA) are non-biodegradable. Some natural polymers such as dextran, which in its natural state is biodegradable, became considerably less so when modified, for example, by the attachment of an active component (Etienne Schacht, 1985; Schacht *et al.*, 1985). The reduction in biodegradability means that prolonged administration of the conjugate holds the possibility of high levels of polymer accumulation within the target cells.

One polymer that has proven therapeutic potential for drug delivery is dextrin (Hardwicke *et al.*, 2008). Dextrins are low molecular-weight carbohydrates that are analogues of glucose and are used routinely as thickeners in food products due to the low cost and ease of their production, they are also used in peritoneal dialysis solution due to their non-toxic properties (Duncan *et al.*, 2008). Dextrin is degraded by amylase; meaning that it is a biodegradable product that is unlikely to accumulate within cells or tissues. The rate at which dextrin is degraded can be determined by the level of succinoylation, with increasing succinoylation leading to an increase in degradation time (Hreczuk-Hirst *et al.*, 2001). Dextrins contain less than 5% α-1,4 links and therefore do not demonstrate much branching. This allows their molecular weight to be kept below 40,000 daltons, which is an important size as this means the molecules can undergo renal elimination.

As stated previously, non-specific activity of the drug whist in circulation would be undesirable. Previous studies have shown that conjugating dextrin to a protein can considerably reduce its activity. Addition of dextrin to trypsin reduced its activity by up to 66% when polymer bound, with activity being restored to approximately 100% when the polymer was degraded (Duncan, 2007; Duncan *et al.*, 2008).

An enzyme of potential therapeutic application in detoxification and removal of lipid peroxidation products is Glutathione s transferase (GST). GSTs exist as a family of isoenzymes that catalyse the conjugation of glutathione (GSH) to the electrophilic centres of other compounds. GSTs have two active sites, one of which is highly specific towards the binding of GSH, the other which binds substrates, is less specific and thus assists catalysis of the conjugation of GSH to a variety of substrates (Ketterer and Meyer, 1989; Ketterer, 1998; Salinas and Wong, 1999). Conjugation of molecules

that are potentially harmful to the cell to GSH renders them less reactive and more water soluble, thus they are more easily eliminated from the cell. Substances that act as substrates to GST include environmental pollutants and other xenobiotics, but also importantly and pertinent to this study, metabolic waste products and the products of biological oxidative stress including; epoxides, aldehydes and hydroperoxides (Alin *et al.*, 1985). As lipofuscin has been shown to be composed of a number of species that have been modified due to oxidative stress an increase in the GST composition of the RPE cell could theoretically assist the cell in degrading or removing potentially harmful substances and reduce the accumulation of lipofuscin. Equally, the action of GST and GSH may assist in the degradation of lipofuscin that has already accumulated within the cell, as well as reducing secondary accumulation that occurs when photo-excited lipofuscin reacts with the lipid membrane of the lysosomes in which it is housed.

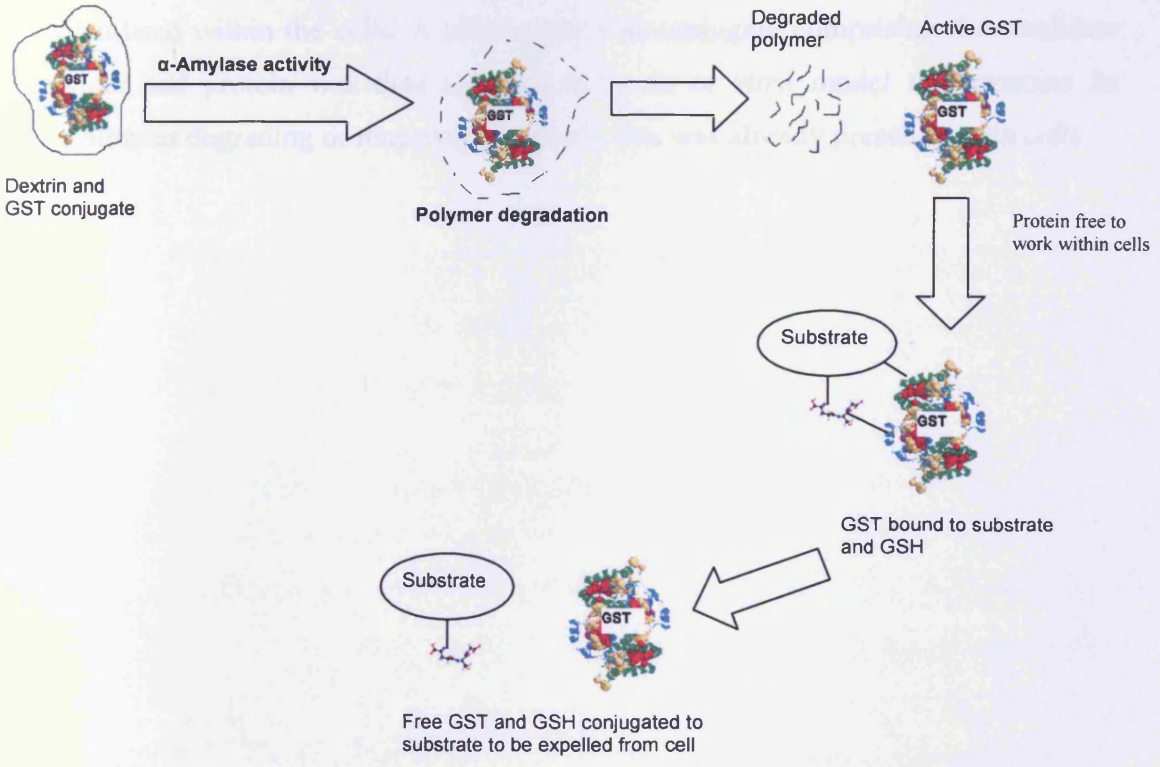

Figure 6.1. Schematic showing the theoretical stages of drug delivery. The protein is delivered masked by the polymer. The polymer is degraded by the activating enzyme releasing the active protein. The protein is then free to catalyse a reaction between the substrate and acceptor molecule. GST = Glutathione s transferase. GSH = Glutathione.

A theoretical mode of action of the proposed nanomedicine is outlined in Figure 6.1. The polymer-protein is delivered to the target cell where the polymer is degraded. This leaves the unbound polymer free within the cell to undertake the task for which it was chosen (Duncan *et al.*, 2008). In this instance it is proposed that GST would conjugate to GSH and reactive molecules within the cell. GST would next catalyse the conjugation of GSH and the reactive molecule, thus rendering it less reactive and assisting it removal from the cell.

The aims of this study were to identify a drug delivery system that was non-toxic to RPE cells even after prolonged exposures and could be specifically targeted to the lysosomes of RPE cells when conjugated to a protein. The study also sought to identify a protein that has the potential to assist RPE cells in the degradation or removal of the substrates of lipofuscin or remove lipofuscin that had already accumulated within the cells. A polymer-protein conjugate comprising the candidate polymer and protein was then assessed using an *in vitro* model to determine its capability in degrading or removing lipofuscin that was already present within cells.

6.2 Experimental Design

6.2.1 Synthesis and characterisation of dex-GST conjugate

6.2.1.1 Succinoylation of dextrin

Chemical modification of dextrin and the synthesis of dex-GST conjugate, together with the characterisation and measurement of dex-GST enzyme activity was undertaken at the Cardiff School of Chemistry, Cardiff University in the laboratory of Dr Alison Paul. Succinoylation of dextrin (51 000 g mol^{-1}) was performed according to methods described previously (Hreczuk-Hirst *et al.*, 2001). Briefly, Dextrin and Succinic anhydride were stirred in a 1:1 ratio in anhydrous *N,N'*-dimethyl formamide (DMF), under nitrogen. 4-Dimethylaminopropanol (DMAP) was dissolved in DMF and added under nitrogen. The reaction was heated to 60°C and stirred overnight. After 15 hours the reaction mixture was cooled to room temperature before precipitation of the polymer with the addition of diethyl ether. The crude product was obtained by filtration and washing. The modified polymer was purified by dialysis and freeze dried. Succinoylation was confirmed by Fourier transform infrared spectroscopy (FTIR) (absorbance band 1716cm^{-1} from ester group). The degree of modification was calculated by titration of carboxylic acid groups with sodium hydroxide using bromophenol blue indicator.

6.2.1.2 Conjugation of succinoylated dextrin and GST

Succinoylated dextrin and *N*-ethyl-*N'*-(3-dimethylaminopropyl)carbodiimide (EDC) in a 2:1 ratio were dissolved in PBS at pH 7.4 and stirred at room temperature for 10 minutes. Two equivalents of *N*-hydroxysulfosuccinimide (Na-NHS) were added as a solution in PBS. The GST protein was added after 30 minutes as a solution in PBS to create a 2:1 polymer:protein ratio. After stirring overnight the crude reaction mixture was purified by fast-protein liquid chromatography (FPLC) to remove free protein and unreacted EDC/Na-NHS, using a Superdex 75HR 10/30 column connected to an Akta FPLC set-up (P-920 pump, UPC-900 monitor) with UV detector. The pooled fractions were concentrated by centrifugation using a Centriprep (30 000 MW cut-off)

membrane, and desalted by washing with water before freeze drying to obtain the conjugate.

6.2.1.3 Results of succinoylation and conjugation

Results of the succinoylated dextrin and dextrin-GST conjugate analysis are given in Table 6.1 and Figure 6.2. Succinoylation of dextrin was confirmed by an increase in the FTIR absorbance band at 1716 cm^{-1} and quantified by titration giving consistently 18 (±3) mol% succinoylation typically. Dextrin-GST conjugates were purified by size exclusion chromatography (Figure 6.2). A clear shift of the observed peak towards shorter retention times indicates a significant increase in size of the conjugate compared to the free protein, consistent with conjugation to the polymer. Fractionation at the slight shoulder of the peak (shown by the dotted lines in figure 6.2) ensures removal of free protein as indicated by an analytical FPLC trace of purified conjugate shown over the same x-axis in the figure. Total protein content was obtained by BCA assay, with results shown in Table 1.

Table 6.1 Characterisation of synthesised succinoylated dextrin, conjugates and fluorescent probe labelled materials.

Sample	Mol% Succinoylation	Oregon-green loading/ wt% (free)	Protein content/ wt%	Overall wt% yield (wt% wrt protein)
Succinoylated dextrin	18	n/a	n/a	75
Succinoylated dextrin	16	n/a	n/a	90
Succinoylated dextrin	13	n/a	n/a	90
Succinoylated dextrin	18	n/a	n/a	90
Dex-OG	18	0.85	n/a	92
Dex-GST	16	n/a	15.5	37(34)
Dex-GST	16	n/a	13	42
Dex-GST-OG	16	n/a	13	Not determined

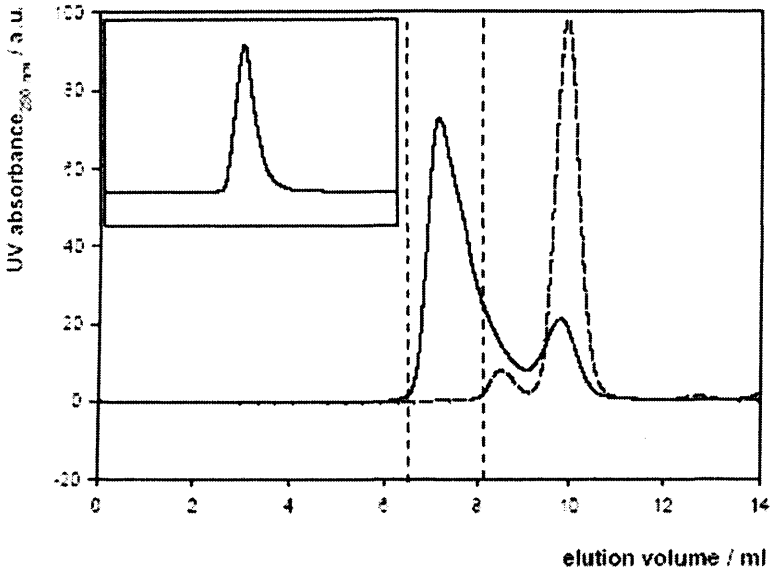

Figure 6.2 Preparative FPLC trace showing volume collected (vertical dashed lines) for dex-GST conjugate (solid line). Also shown, FPLC trace for free GST protein (dashed line). Inset, analytical trace for purified conjugate.

6.2.1.4 Characterisation of the dex-GST conjugate

Conjugate characterisation was by assay of total protein using a BCA assay (see section 4.2.1.2.1, Chapter 4) with GST standards and SDS-PAGE. A separating gel was prepared using water, running gel buffer, SDS (10% w/v), 40% acrylamide/bis, APS (10% w/v) and TEMED. Stacking gel (0.125 M Trizma base, pH 6.8) was prepared from water, stacking buffer ((100 ml prepared in water using Trizma base (6g), adjusted to pH 6.8 with 1 M HCl), 2.5ml), SDS (10% w/v), 40% acrylamide/bis, ammonium persulphate (10% w/v) and TEMED (1%). Conjugate or protein samples (approx. 1 mg ml^{-1}, 20µl) were prepared in PBS and mixed with an equal volume of denaturing solution consisting of water, Tris HCl solution (0.05 M, pH6.8), Glycerol and SDS (10%w/v solution (aq.)), mercaptoethanol and bromophenol blue (1% w/v). Samples were heated for 5 mins at 100°C and loaded onto the gel (20 µl per well). The electrophoresis experiment was run for approx. 40 minutes at 140 V (constant voltage), 400 mA. Gels were developed with Coomassie blue solution and air dried.

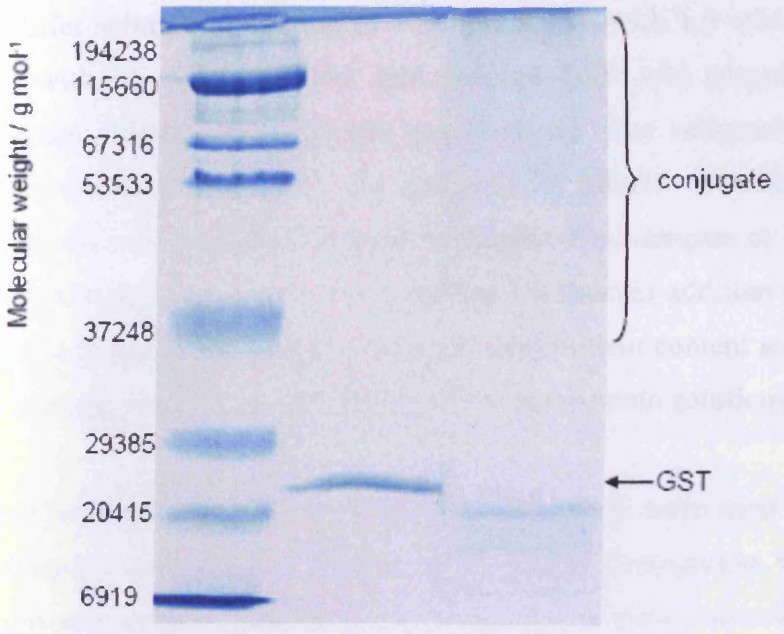

Figure 6.3 SDS-PAGE gels showing molecular weight standards, dex-GST conjugate and free GST.

SDS-PAGE analysis (Figure 6.3) shows a high running band (high MW) for the conjugate and a feint band for residual GST at 27 000 kDa. The free GST was not noted with the FPLC trace implicating that dimerised GST is released after denaturation with SDS. This suggests that in some species the polymer may only be bound to one half of the dimer.

6.2.1.5 Labelling of succinoylated dextrin with a fluorescent probe

Succinoylated dextrin, EDC and Na-NHS were dissolved in a solution of PBS in the ratio; 1:2:2.2. After stirring, Oregon Green 488 cadaverine *5-isomer was added and the pH increased to 9 by addition of sodium hydroxide. The reaction was stirred in the dark for 2-4 hours, monitored by TLC in methanol, viewed under UV light. The crude reaction mixture was purified by dialysis in the dark and free Oregon green removed before freeze drying.

6.2.1.6 Measurement of enzyme activity of free GST and dex-GST conjugate

The enzyme activity of GST was determined with respect to 1-chloro-2,4-dinitrobenzene according to the method of Habig *et al* (1974). GST was dissolved in

a buffer solution consisting of 100 mM K_2PO_4 with 1.0 mM EDTA, adjusted to pH 6.5 with 1.0 M KOH. 100 mM reduced GSH was prepared in the same buffer solution. These solutions were stored on ice. The substrate solution, 1-chloro-2,4-dinitrobenzene (100mM) was prepared in EtOH. Protein, substrate and buffer solutions were mixed as required to provide 1 ml samples at 1 mM GSH and CDNB. Absorbance at 340 nm was recorded for 3 mins after addition of the enzyme. Samples with conjugate were prepared at equivalent protein content and the activity compared to a calibration plot constructed from the free protein solutions.

Free protein controls at equivalent protein activity were used in all conjugate activity evaluation experiments. Protein activity after conjugation was measured using an equivalent protein concentration to the free protein controls, based on the protein content of the conjugate from BCA assay. It was found that the protein retains activity on conjugation to the polymer. This suggests that the active site is not occluded by the polymer which may reflect the location of polymer conjugation to the polymer, the conformation of the polymer around the protein or the amount of polymer bound.

6.2.2 Analysis of dextrin as a potential carrier polymer

6.2.2.1 Safety of dextrin loaded into RPE cells

Cells were maintained in a humidified incubator at 37°C, in an atmosphere of 95% air and 5% CO_2 (Galaxy S, Wolf Laboratories). Cultures were grown in 24-well plates (Orange Scientific) in Hams F-10 nutrient mix (Gibco, UK) containing 10% FCS (Bio-West, UK), antibiotics - streptomycin, kanamycin and penicillin (100, 100 and 60 μg/mL, respectively, all from Sigma) and fungizone (1.25 μg/mL, ampotericin, Gibco) until confluent. When confluent, the amount of FCS in the medium was reduced to 2% and cells were stabilised in this for a further week. At this point cells were either maintained in basal medium or in basal medium supplemented with succinoylated dextrin (1 μg/ml succinoylated dextrin) with medium changes every two days. The viability of cells was measured after 7, 14 and 21 days using the MTT (Sigma, UK) assay, as described in the General Material and Methods Section 2.4.

6.2.2.2 Uptake of dextrin tagged with Oregon-green into RPE cells

6.2.2.2.1 Flow cytometry

Analysis of uptake of OG into ARPE-19 cells as measured by flow cytometry was undertaken as described in the General Materials and Methods chapter, Section 2.5. However, some alterations in the experimental design were made and these are described below. Cells were seeded at a density of 1 x 10^6 per well into wells of a six-well plate (Orange Scientific). Cells were maintained in Hams F-10 nutrient mix (Gibco, UK) containing 10% FCS (Bio-West, UK), antibiotics - streptomycin, kanamycin and penicillin (100, 100 and 60 µg/mL, respectively, all from Sigma) and fungizone (1.25 µg/mL, ampotericin, Gibco) in a humidified incubator at 37°C (Galaxy S, Wolf Laboratories, UK) in an atmosphere of 5% CO_2 for 24 hours.

Hams F-10 nutrient mix containing 10% FCS medium was removed from wells and replaced with Hams F-10 nutrient mix containing 2% FCS and dextrin-Oregon green (OG)(1.5 µg/ml with respect to OG), initially for the 180 mins time point. This was repeated for each of the time points, 120 mins, 90 mins, 60 mins, 30 mins and 0 mins in this study. The cells were maintained in the incubator and wrapped loosely in black foil (Lee filters, UK) to allow air circulation. When cells had been exposed to dextrin-OG for the required time, the medium was removed and immediately replaced with ice-cold PBS (PBS tablets, Sigma, UK). For 0 mins, Hams F-10 nutrient mix containing 10% FCS medium was removed and replaced with Hams F-10 nutrient mix containing 2% FCS and dextrin-OG, this was immediately removed and replaced with ice cold PBS.

Cells were washed three times by the gentle addition of PBS. After the third PBS wash cells were detached from the wells by exposure to a 0.25% (w/v) trypsin solution (Sigma, UK) containing 0.02% EDTA (w/V) made up in PBS and incubated for 2 mins (37°C, 95% air, 5% CO_2). Trypsin was inactivated by the addition 1 ml of Hams-F10 medium containing 10% FCS. Cell suspensions were removed from their wells and centrifuged at 340 *g*, 4°C for 5 mins (U-32R, Boeco, UK) to create a pellet. The medium was gently aspirated from the centrifuge tube and replaced with 1 ml of PBS. The pellet of cells was then washed twice in PBS by centrifugation at 340 *g*, 4°C

for 5 mins. After the final wash cells were re-suspended in 300 µl of PBS and transferred to a FACs tube (Falcon, UK). FACs tubes containing cell suspensions were taken on ice to the flow cytometer (FACSCaliber, BD Life Sciences, UK) for analysis. The levels of OG fluorescence were measured using the flow cytometry, with an increase in Oregon green specific fluorescence being interpreted as an increase in the up take of the dextrin-OG conjugate into ARPE-19 cells.

6.2.2.2.1.1 Flow Cytometry Data Analysis

Data collected from the FACSCaliber was analysed using WinMDI 2.8 Software (Purdue University, USA) and Excel software (Microsoft, USA) as described in the General Materials and Methods chapter, Section 2.5.1.

6.2.2.2.2 Confocal Microscopy Analysis

6.2.2.2.2.1 Cell preparation

Cells were prepared as for the flow cytometry work, with the exception that the 6-well plates had a glass cover slip placed at the bottom of the well. Hams F-10 medium containing 10% FCS and a full compliment of antibiotics and fungizone was replaced with medium containing 2% FCS and dextrin-OG (1.5 µg/ml with respect to OG) for 0, 5, 10, 30, 60 and 180 mins. At the respective time point, cells were washed thrice with sterile PBS then fixed.

6.2.2.2.2.2 Fixation of cells

Cells were fixed in 2% paraformaldehyde (20 mins at 25°C) made in PBS, fresh on the day of use. Samples were mounted using Vectashield (Vector Labs, USA) mounting medium (30 µl) to prevent sample photobleaching during microscopic examination.

6.2.2.2.2.3 Microscopy

Confocal microscopy was performed using a Leica SP5 system (Leica, UK). Data was collected using dedicated software supplied by the manufacturers and exported as tagged image files (TIF). At least three representative images were obtained from each sample. Standard procedures were used to minimise bleed from channel to channel and sample photobleaching. All images were collected using monochromatic CCD cameras.

6.2.2.3 Determination of the ratio of dex-OG to free OG

Free and dextrin bound OG were separated using a PD-10 column (Amersham Biosciences, UK). The column was equilibrated using 25 ml of elution buffer with the through flow being discarded once collected. The sample was layered onto the column in 2.5 ml of buffer and the eluent discarded. A further 25 ml of buffer was added to the column with the eluent being collected in 0.5 ml fractions. The fluorescence of each fraction was measured at 494 nm using a Fluostar Optima plate reader (BMG Lab Technologies, Offenburg, Germany).

6.2.2.4 Localisation of dextrin tagged with Oregon-green in RPE cells

6.2.2.4.1 Preparation of cells

Cells were cultured as for the uptake of dextrin-OG studies using confocal microscopy. After 24 hours the medium was replaced with basal medium containing Texas-red bovine serum albumin (TxR-BSA, 10 mg/ml) or TxR-BSA and dextrin-OG or TxR-BSA and dextrin-GST-OG. Cells were exposed to this medium for four hours then washed three times with PBS, followed by 16 hours incubation in basal medium at 37°C, 95% air 5% CO_2.

6.2.2.4.2 Fixation

Cells were immuno-stained using EEA1 (an early endosomal marker) and anti-LAMP1 (a late endosome/ lysosomal marker) markers. Cells were fixed in cold

methanol (pre-chilled at -20°C) and incubated for 5 mins at -20°C. Cells were then fixed using 2% paraformaldehyde (20 mins at 25°C) made in PBS, fresh on the day of use.

6.2.2.4.3 Immuno-labelling

Cells to be immuno-labelled were first incubated in 2% (v/v) goat serum (in PBS) for 60 mins at 25°C. Primary antibody incubations were then conducted over 60 mins at 25°C in the dark. The following antibody dilutions were used; anti-EEA1 (1:300) and anti-LAMP-1 (1:10). Secondary incubations were performed using either anti-mouse or rabbit specific antibodies labelled with Alexa Fluor 488, Cy5 or FITC. An incubation period of 60 mins at 25°C after dilution (1:200 using 1% (v/v) goat serum in PBS) was conducted in the dark. All samples were mounted using Vectashield mounting medium (30 µl) to prevent sample photobleaching during microscopic examination.

6.2.2.4.4 Microscopy

Microscopy was carried out as described in section 6.2.2.2.2.

6.2.3 Analysis of GST as the active component in the nanomedicine

6.2.3.1 Analysis of free GST in preventing the accumulation of lipofuscin-like fluorescent inclusions in RPE cells loaded with POS?

6.2.3.1.1 Isolation of POS

POS were isolated as described in the General Materials and Methods chapter, Section 2.3.

6.2.3.1.2 Cell Culture.

Cells were cultured in 24-well plates as described previously (General Materials and Methods, Section 2.2) Once confluent, cells were maintained in basal medium for a further 7 days. After 7 days cells were maintained in 1 ml of basal medium containing 1 x 10^7 POS and 'free' GST protein (not conjugated to dextrin, equivalent to 1, 4 or

10 units GST activity, plus GSH 0.5 mM and N-acetyl cysteine (NAC) 0.5 mM). Medium was replaced every two days for 21 days. Control cells were each maintained in either basal medium alone, basal medium supplemented with free GST protein (equivalent to 1, 4 or 10 units GST activity, 0.014, 0.056 and 0.14 mg GST respectively), plus GSH (0.5 mM) and NAC (0.5 mM)), or 1 x 10^7 POS for 21 days. After 21 days the lipofuscin-like fluorescence of cells maintained under each of the conditions was measured using flow cytometry.

6.2.3.1.3 Measurement of lipofuscin-like fluorescence in ARPE-19 cells using flow cytometry

For analysis using flow cytometry cells were treated as described in the General Materials and Methods chapter (Section 2.5).

6.2.3.1.4 Data analysis

Data collected from the FACSCaliber was analysed using WinMDI 2.8 Software (Perdue University, USA) and represented graphically using Excel software (Microsoft, USA)

6.2.3.2 Can free GST degrade or remove lipofuscin that has accumulated in ARPE-19 cells?

6.2.3.2.1 Isolation of lipofuscin

Lipofuscin was isolated as described in the Materials and Methods chapter, Section 2.1.

6.2.3.2.2 Cell Culture

For analysis of the ability of free GST to degrade retinal lipofuscin in cells, cells were cultured as described in General Materials and Methods, Section 2.2. After 7 days in basal medium cells were exposed to ~ 300 lipofuscin granules per cell for 24 hours. After 24 hours medium was changed to basal medium not containing lipofuscin. Cells were then allowed to stabilise for a further 7 days in basal medium. After this period, medium was changed to basal medium supplemented with 'free' GST protein

(equivalent to 4 units GST activity). Cells were maintained in the GST supplemented medium for 7 days, with changes of medium every two days. Control cells included; cells that had not been loaded with lipofuscin but maintained in basal medium alone, basal medium supplemented with free GST protein (equivalent to 4 units GST activity) or cells that had been loaded with lipofuscin (exposed to ~ 300 granules per cell) and maintained in basal medium alone. After treatment the lipofuscin-like autofluorescence of cells was measured using flow cytometry.

6.2.3.2.3 Flow cytometry

For analysis using flow cytometry cells were treated as described in the General Materials and Methods chapter (Section 2.5) with the lipofuscin-like autofluorescence of cells being measured using the flow cytometer (FACSCaliber, BD Life Sciences, UK).

6.2.3.2.4 Data analysis

Data collected from the FACSCaliber was analysed using WinMDI 2.8 Software (Perdue University, USA) and represented graphically using Excel software (Microsoft, USA).

6.2.4 Can the dextrin-GST nanomedicine degrade or remove lipofuscin that has accumulated in ARPE-19 cells?

6.2.4.1 Isolation of lipofuscin

Lipofuscin was isolated as described in the General Materials and Methods chapter, Section 2.1.

6.2.4.2 Cell Culture

For analysis of the ability of dextrin-GST conjugate to degrade retinal lipofuscin in cells, cells were prepared as described in section 6.2.3.2.2. After the second 7 day period, medium was changed to basal medium supplemented with dextrin-GST conjugate (equivalent to 4 units GST activity). Cells were maintained in the GST

supplemented medium for 7 days, with changes of medium every two days. Control cells included; cells that had not been loaded with lipofuscin but maintained in basal medium alone, basal medium supplemented with dextrin-GST conjugate (equivalent to 4 units GST activity) or cells that had been loaded with lipofuscin (exposed to ~ 300 granules per cell) and maintained in basal medium alone. After treatment the lipofuscin-like autofluorescence of cells was measured using flow cytometry and cells were analysed using TEM analysis.

6.2.4.3 Flow cytometry

For analysis using flow cytometry cells were treated as described in the General Material and Methods, Chapter 2, Section 2.5

6.2.4.4 TEM analysis of cells

TEM analysis of the cells was conducted as described in the General Materials and Methods chapter, Section 2.6. Images collected to determine if dex-GST could assist in the degradation or removal of retinal lipofuscin were analysed using Image J software (NIH, USA) and Excel (Microsoft, USA). This allowed for calculation of the average size of retinal lipofuscin granules in the cell populations and the percentage cell area occupied by the granules.

6.2.5 Statistical analysis

The statistical significance of the difference between the means of results obtained in determining the safety of dextrin and the ability of GST in preventing the accumulation of lipofuscin were determined using one-way ANOVA and separately Tukey Post-Hoc test (SPSS 12.0 for Windows, SPSS Inc, USA). The significance of results obtained in lipofuscin degradation studies, lipofuscin granule size and cellular occupation were determined using Students t-test (Excel, Microsoft USA).

6.3 Results

6.3.1 Cell viability of cultures maintained in medium supplemented with succinoylated dextrin

The initial series of experiments conducted in this study sought to determine the safety of the chosen carrier molecule towards ARPE-19 cells. The carrier polymer of choice in this study was dextrin, a D-glucose polymer that is used in a variety of roles including: food products and dialysis fluid. Consequently it has been shown to be non-toxic to most cells and tissues within the body. However, as the dextrin based nanomedicine under investigation in this study is targeted directly to the RPE, levels of dextrin may exceed those experienced under normal circumstances. Therefore, it was pertinent that the initial stage of this trial determined whether dextrin displayed any toxicity towards RPE cells over prolonged exposures. The mitochondrial activity (used as a measure of cell viability) of cells maintained in medium with or without succinoylated dextrin was compared every 7 days over a 21 day time course (Figure 6.4). No statistically significant difference in mitochondrial activity was observed between the two populations of cells indicating that dextrin modified by succinoylation does not display toxicity towards RPE cells even after prolonged exposure.

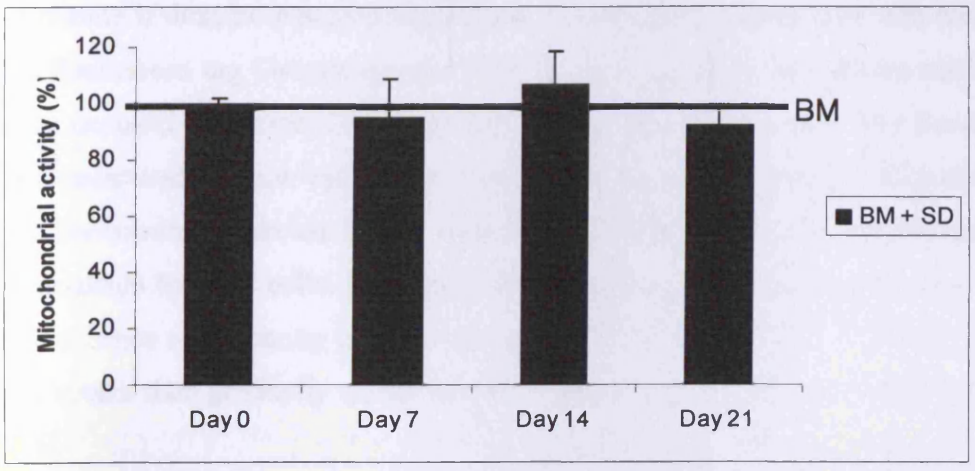

Figure 6.4 Comparison of mitochondrial activity of cells maintained in basal medium or basal medium supplemented with succinoylated dextrin. Cells were maintained in basal medium (BM) with/without succinoylated dextrin (SD) for up to 21 days with the cell viability being measured every 7 days using the MTT assay. Control cells were considered to be those maintained in basal medium without SD. Data are the mean of three experiments each conducted in triplicate. Error bars represent SEM.

6.3.2 Uptake of succinoylated dextrin into RPE cells as measured by flow cytometry and confocal microscopy

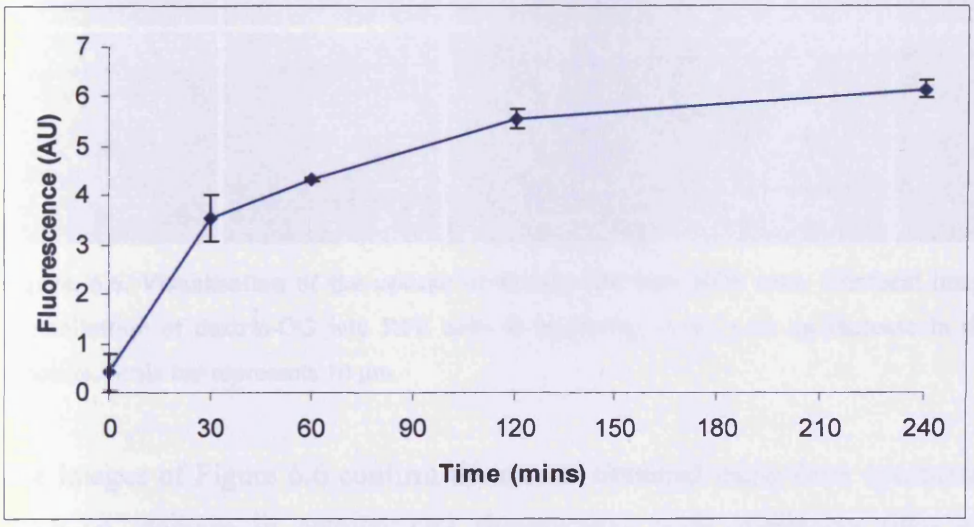

Figure. 6.5. Uptake of dextrin-OG by ARPE-19 cells as measured by flow cytometry. The uptake of dextrin-OG into RPE cells over a 4 hour period was determined using flow-cytometry by measuring the increase in fluorescence of the cells. Controls included cells that were not exposed to OG, the autofluorescence of these cells was normalised to 0.

For drug delivery to be successful the polymer conjugated to the active component must be able to traverse the cell membrane and be internalised by the cell. To

determine if dextrin was able to perform this function the polymer was conjugated to the fluorescent tag Oregon-green (OG) and solubilised in the culture medium. Cells were exposed to dextrin-OG for increasing lengths of time, then OG fluorescence of cells measured by flow cytometry (Figure 6.5). Increasing length of exposure resulted in a concomitant increase in OG related fluorescence indicating that dextrin-OG was internalised by RPE cells. The graph shows an initial burst in the increase in cellular fluorescence representing polymer-OG endocytosis by the RPE. The rate of polymer-OG uptake then gradually slows, however, polymer continues to be internalised by the RPE.

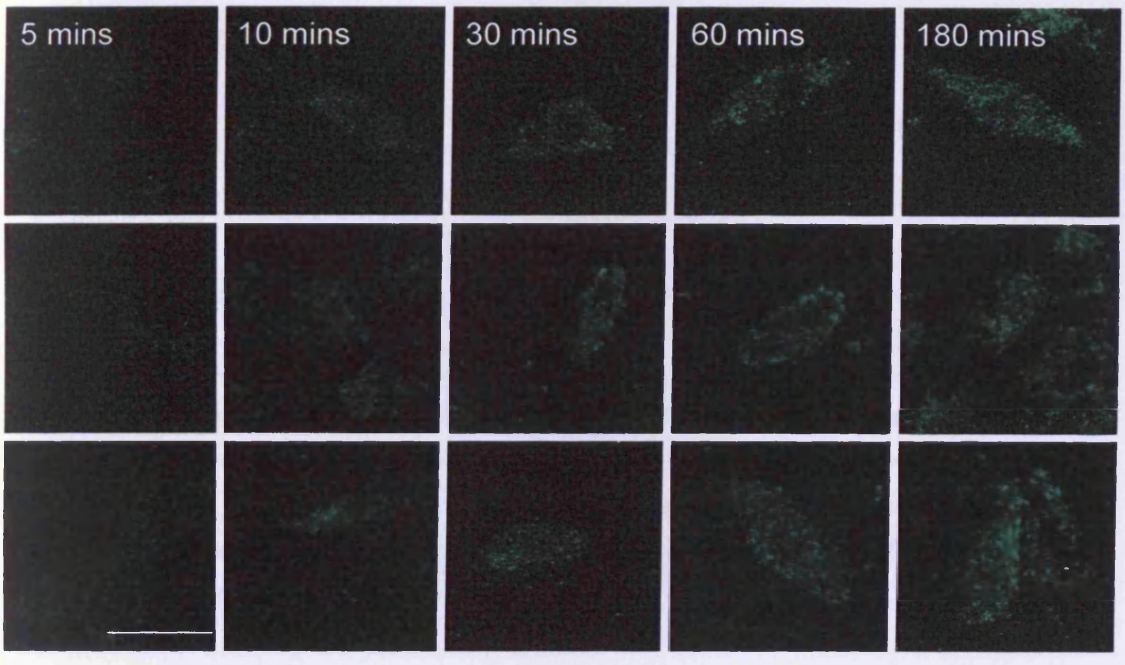

Figure. 6.6. Visualisation of the uptake of dextrin-OG into RPE cells. Confocal images showing internalisation of dextrin-OG into RPE cells at increasing levels with an increase in the length of exposure. Scale bar represents 10 μm.

The images of Figure 6.6 confirm the results obtained using flow cytometry. Images show an increase in cellular OG fluorescence with increasing time of dex-OG exposure enabling the visualisation of dex-OG uptake. The fluorescent granules are present in distinct punctuate moieties indicating that the polymer conjugate has been internalised into the RPE cells and is not cell membrane bound.

6.3.3 Determination of the quantity of free and dextrin bound OG used in experiments

The proportion of unconjugated OG present in the dextrin-OG mixture was measured before, and after 4 hours of exposure to RPE cells (Figure 6.7). Initial levels of free OG were 0.11% but rose to just under 4% after 4 hours of incubation. Such low levels of free OG mean that results seen are representative of the uptake of dextrin-OG and not biased by the action of free-OG. The increase in free-OG present in the basal medium after 4 hours of exposure to RPE cells could represent OG formerly bound to polymer that has been internalised, degraded and exocytosed by RPE cells.

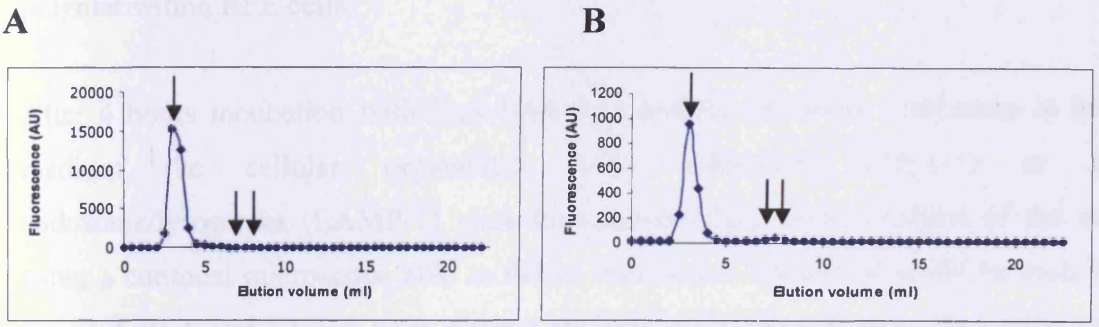

Figure. 6.7. Evaluation of the proportion of free and dextrin-bound OG present in the dextrin-OG mixture, before (A) and after (B) incubation with RPE cells. Free and conjugated OG was separated according to size using a PD-10 column. The fluorescence of fractions eluting from the column were then assessed using a fluorescence plate reader. Single arrow identifies bound dex-GST, double arrow represents free OG.

Table. 6.2 Levels of free and conjugated Oregon green (OG) before and after incubation with ARPE-19 cells

Before incubation		**After 4 hr incubation**	
Total fluorescence (AU)	33647 (100%)	Total fluorescence (AU)	2579 (100%)
Fluorescence attributable to conjugated OG (AU)	33611 (99.89%)	Fluorescence attributable to conjugated OG (AU)	1809 (96.07%)
Fluorescence attributable to 'free' OG	36 (0.11%)	Fluorescence attributable to 'free' OG	770 (4%)

The percentage of free OG present with dextrin-OG that RPE cells were exposed to was calculated by separating free OG from dextrin bound using a PD-10 column. The

free and bound OG was separated according to size and the fluorescence of each fraction eluting from the column measured using a fluorescence plate reader (Figure 6.7 A and B). The amount of free OG present increased after exposure to RPE cells. Total fluorescence levels dropped in the sample that had been exposed to cells as the dex-OG had been diluted by the cell culture medium.

6.3.4. Endocytic fate of dextrin-OG in RPE cells

To determine the endocytic fate of the dex-OG polymer an immunocytochemistry technique for identifying cellular organelles, optimised by members of the group (Richardson *et al.*, 2008) was used to establish the intracellular localisation of the polymer within RPE cells.

After 4 hours incubation with TxR-BSA followed by 16 hours incubation in basal medium the cellular organelles: early endosomes (EEA-1) or late endosome/lysosomes (LAMP-1) were immuno-labelled. Upon analysis of the cells using a confocal microscope able to detect fluorescent markers it could be seen that the TxR-BSA and EEA-1 were distinct structures (Figure 6.8 a-c). Secondly, cells were immuno-labelled with LAMP-1 antibody. Images showed labelling of cellular components that were visible as doughnut-like structures (Figure 6.9). Merged images highlight the TxR-BSA molecules occupying the 'ring' of the lysosomal doughnut, indicating that at this time the BSA was localised within the late endosomal or lysosomal compartments of the cell.

Therefore, if another molecule was to co-localise with the BSA-TxR under the same conditions, it could be assumed that both molecules were present within the late endosomal/ lysosomal compartments of the cell. Merged images in Figure 6.10 show BSA-TxR and dex-OG co-localising within RPE cells, indicating that the dex-OG is present within the cells lysosomal machinery at this time. Conjugation of GST to dextrin in the presence of OG did not affect the movement of dextrin through the cells endocytic pathway. Cells co-loaded with dex-GST-OG and BSA-TxR showed that the two fluorophores accumulated in the same cellular compartments (Figure 6.11), previously shown to be the cells late endosomes/ lysosomes.

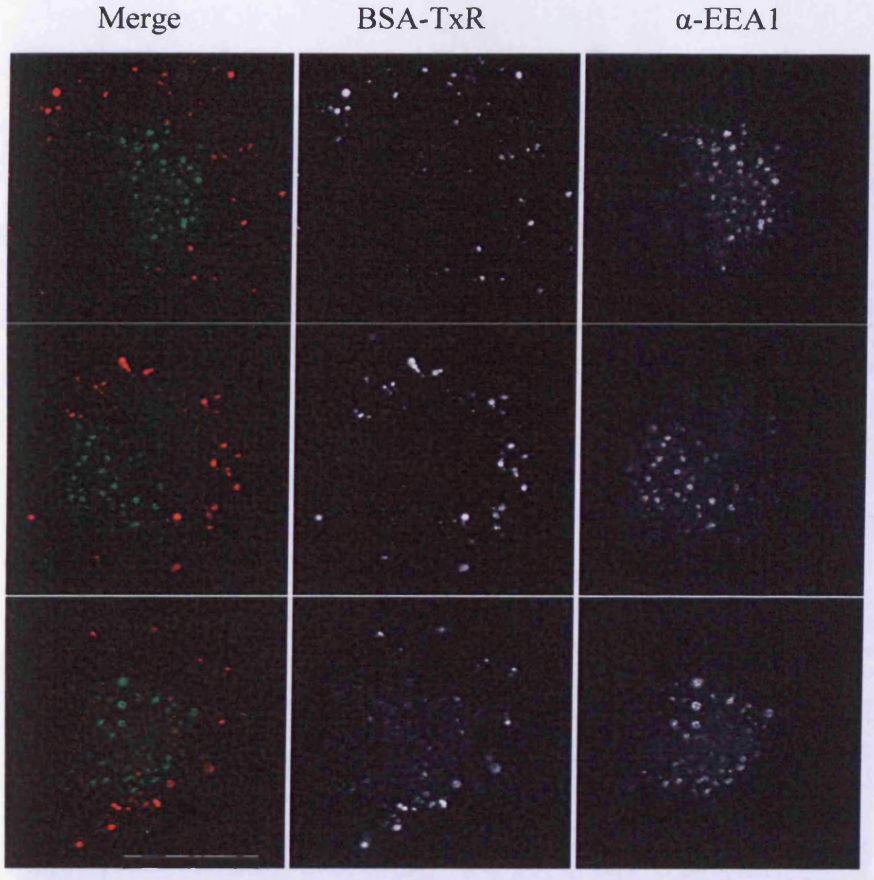

Figure. 6.8. Tracking the intra-cellular distribution of BSA-TxR in ARPE-19 cells. ARPE- 19 cells were incubated with BSA-TxR for 4 hours and then chased for 16 hours. Images were taken 20 hours after initial exposure to the fluorophore. The early endocytic compartments were immuno-stained with EEA1. The merged images show at this point the early endosomes (green) and BSA (red) are distinct moieties. Three representative images were recorded on a Leica SP5 system confocal microscope, images were collected using a monochromatic CCD camera. Scale bar represents 5μm.

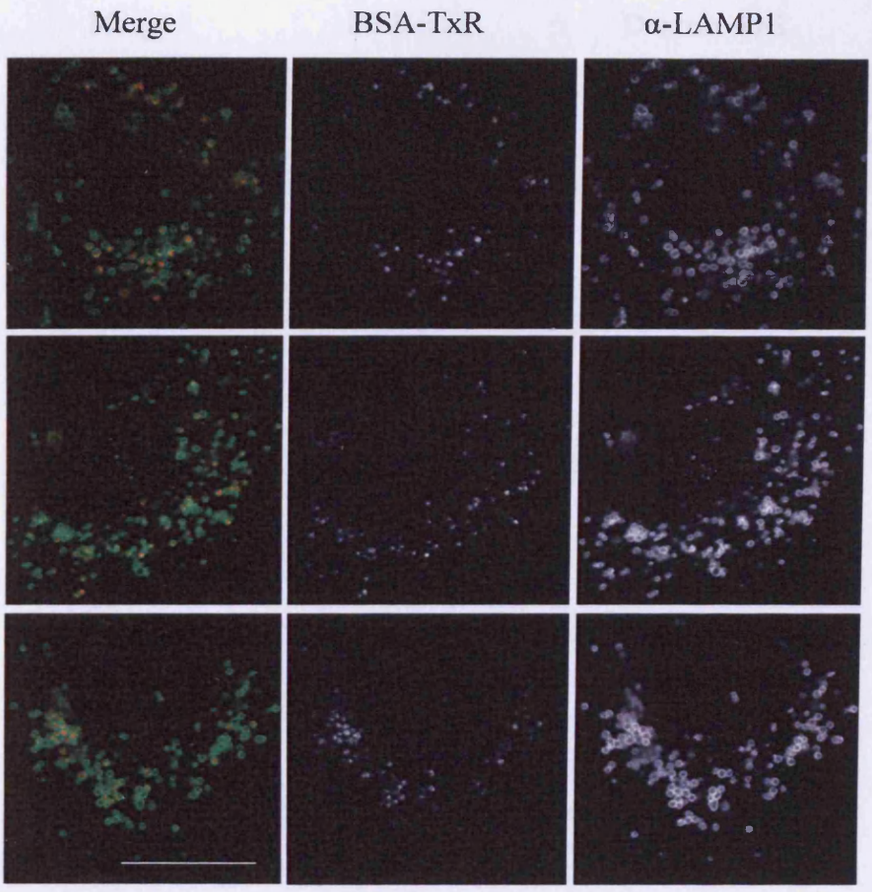

Figure. 6.9. Localisation of BSA-TxR (red) into lysosomal-associated membrane protein (LAMP-1, green) positive structures. Cells were loaded with TxR labelled BSA with a 4 hour pulse and 16 hour chase. Images were taken 20 hours after initial exposure to the fluorophore. Cells were then fixed and immuno-labelled with anti-LAMP-1 antibody. LAMP-1 positive structures appeared doughnut-like with the TxR-BSA located within the 'ring' on the merged cells. This indicates that the BSA-TxR has been taken up into lysosomes within the cell. Other experimental conditions as in Figure 6.6. Scale bar represents 5μm

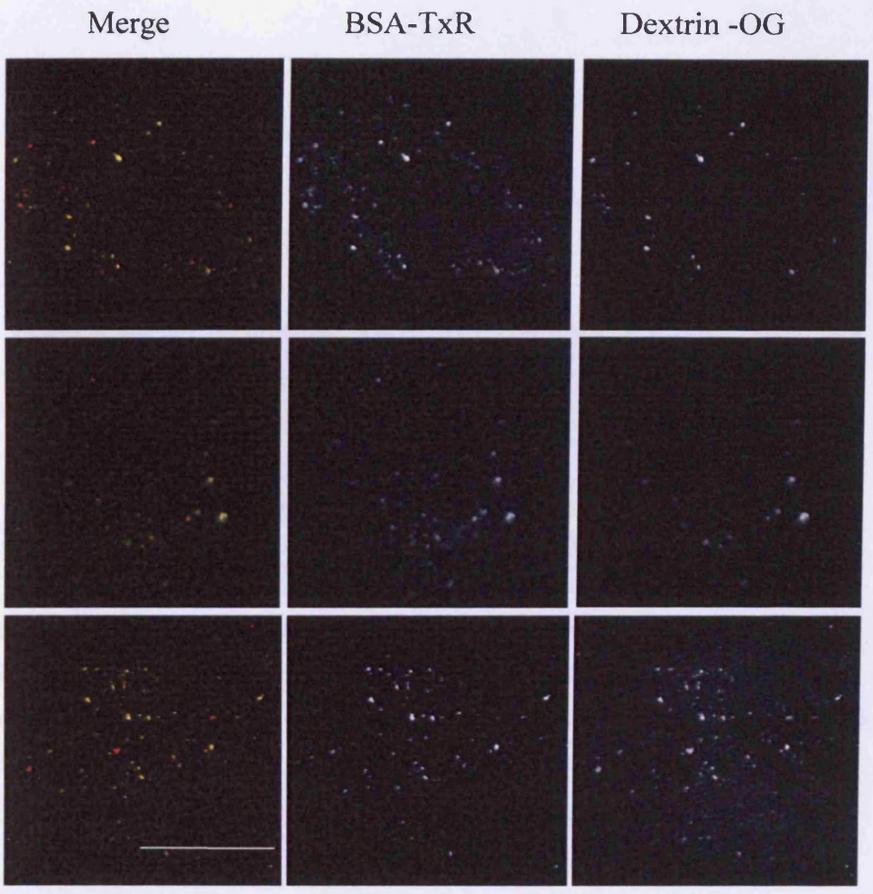

Figure. 6.10. Tracking the intra-cellular distribution of dextrin-Oregon green and BSA-TxR in ARPE-19 cells. Cells were incubated with dextrin-OG and BSA-TxR for 4 hours and then chased for 16 hours. Images were taken 20 hour after initial exposure to the fluorophore. In the merge image the yellow areas indicate co-localisation between the dextrin-Oregon green molecules (green) and the BSA-TxR (red). Previous work demonstrated that BSA-TxR is located within LAMP-1 positive structures (lysosomal organelles) at this time, so co-localisation with dextrin-OG infers that both molecules are lysosomally located. Other experimental conditions as in Figure 6.6. Scale bar represents 5μm

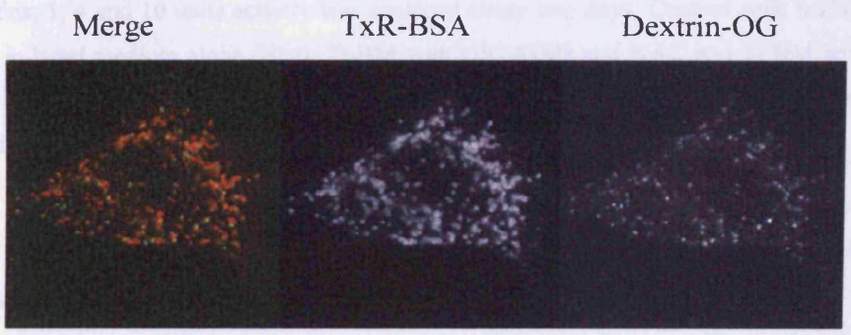

Figure. 6.11. Tracking the intra-cellular distribution of dextrin-Oregon green-GST and BSA-TxR in ARPE-19 cells. Dex-OG-GST localises with BSA-TxR indicating that GST does not disrupt the movement of dextrin within the cell. Other experimental conditions as in Figure 6.6. Scale bar represents 5μm

6.3.5 Prevention of the accumulation of lipofuscin-like inclusions in RPE cells

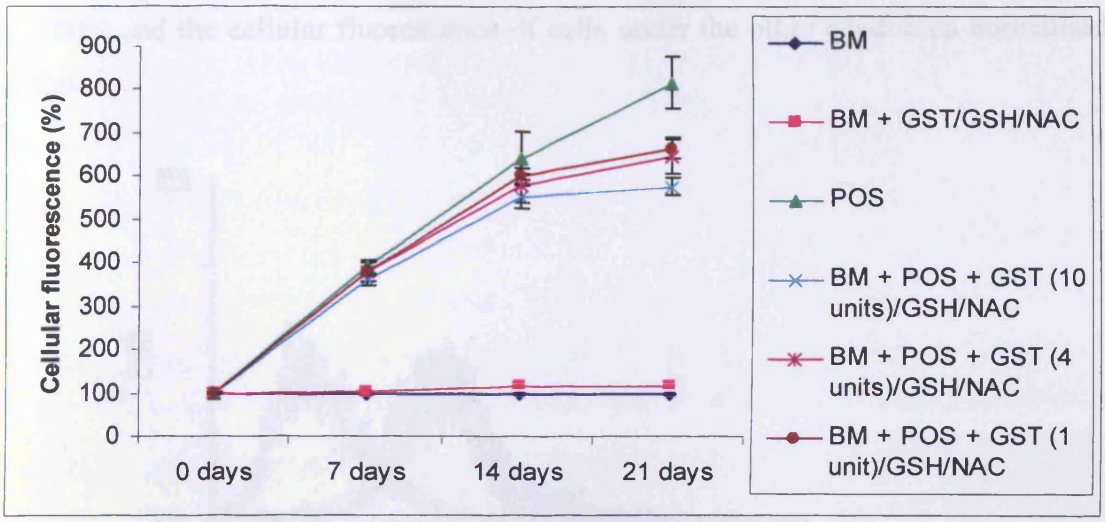

Figure. 6.12 Monitoring of changes in lipofuscin-like fluorescence of cells using flow cytometry over a 21 day period. Culture medium containing the POS, GSH, NAC and GST at three concentrations; 1, 4 and 10 units activity was replaced every two days. Control cells included 1) those maintained in basal medium alone (BM), 2) BM with GST/GSH and NAC and 3) BM with POS. The lipofuscin-like fluorescence of cells maintained in basal medium containing POS was taken as 100% for this study. Trials were carried out three times, each in triplicate.

Exposing RPE cells to POS in their medium has been shown to lead to the development of inclusion bodies that have lipofuscin-like fluorescence properties (Boulton *et al.*, 1989; Wihlmark *et al.*, 1996a). The ability of GST in preventing this accumulation was analysed by measuring the lipofuscin-like fluorescence of cells exposed to POS using flow cytometry. Figure 6.12 shows that cells loaded with POS developed lipofuscin-like fluorescence to levels approximately 8 times higher than cells maintained in basal medium alone. The weekly increase in cellular fluorescence slowed in the presence of GST, GSH and NAC, with a statistically significant difference in the lipofuscin-like fluorescence of cells fed POS in basal medium (825 $\pm$ 47.9 % cellular fluorescence) compared to those fed POS in the presence of 10 units GST activity (578 $\pm$ 16.4 % cellular fluorescence) and 4 units GST activity (624 $\pm$ 23.0 % cellular fluorescence) after 21 days ($p < 0.05$). No difference in cellular fluorescence between cells maintained in basal medium and cells maintained in basal medium supplemented with GST/GSH and NAC was observed. To generate Figure 6.12, the geometric mean of a cells' lipofuscin-like fluorescence was calculated using

histograms created using WinMDI software (Figure 6.13) from data collected by the flow cytometer. Cellular fluorescence of cells maintained in basal medium was taken as 100% and the cellular fluorescence of cells under the other conditions normalised to this.

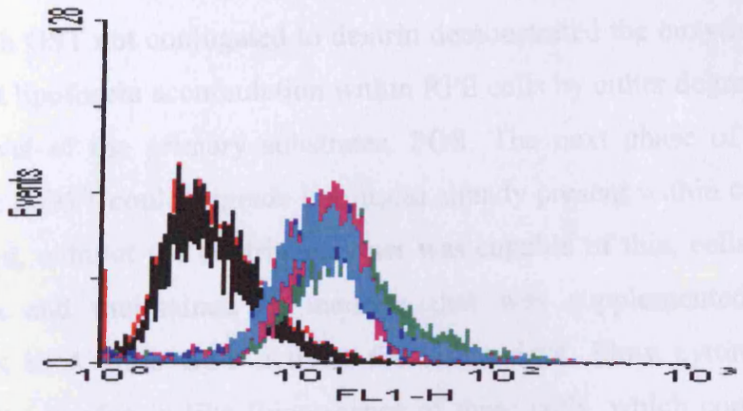

Figure 6.13 Histograms generated using data collected from flow cytometery. The mean fluorescence of the cells is calculated using the histograms and was used to create Figure 6.11. (BM-Red, BM + GST/GSH/NAC – Black, BM + POS – Green, BM + POS + GST (10 units)/GSH/NAC – Turquoise, BM + POS + GST (4 units)/GSH/NAC – Purple, BM + POS + GST (1 unit)/GSH/NAC – Blue).

Figure 6.13 shows a histogram representing the fluorescence distribution of cells after 21 days. FL1-H represents the lipofuscin-like fluorescence of cells on a log scale. The results show that cells not exposed to POS have a much lower fluorescence than those that were exposed to POS. Cells that have been exposed to POS without the presence of GST/GSH and NAC represented by the green plot have its maxima furthest to the right signifying these cells have the highest levels of cellular fluorescence. The rate at which the fluorescence of cells exposed to POS and GST/GSH/NAC increased was inversely proportional to the concentration of GST present in the culture medium, with fluorescence of cells being 10 units< 4 units< 1 unit (percentage fluorescence of 578, 624 and 676, respectively). After analysis of the results of this trial it was decided that future studies would be conducted using 4 units GST activity. The decision was based on results obtained thus far in the study including: medium containing 4 units GST resulted in significantly lower lipofuscin-like fluorescence in cells fed POS compared to those fed POS alone ($p < 0.05$). Another contributing factor was the expense of the GST and its limited availability at this time. Thus, using the

optimised level of GST activity ensured that the most work could be carried out within the constraints of this projects time and budget.

6.3.6. Assessment of the use of GST in degrading lipofuscin in RPE cells when in its free state or when conjugated to dextrin polymer

Work with GST not conjugated to dextrin demonstrated the enzyme had the potential to prevent lipofuscin accumulation within RPE cells by either degrading or facilitating the removal of the primary substrates, POS. The next phase of this study was to determine if GST could degrade lipofuscin already present within cells. To establish if GST alone, without the dextrin polymer was capable of this, cells were loaded with lipofuscin and maintained in medium that was supplemented with free GST, equivalent to 4 units GST activity for seven days. Flow cytometry was used to measure the lipofuscin-like fluorescence of these cells, which could be compared to control cells loaded with lipofuscin and maintained in basal medium alone. Figure 6.14 shows that cells loaded with lipofuscin had fluorescence levels approximately 12 times greater than cells not loaded with lipofuscin. Cells loaded with lipofuscin and maintained in either basal medium alone or basal medium supplemented with free GST showed no statistically significant difference in cellular fluorescence. This indicates that supplementing cells with free GST alone does not decrease the level of lipofuscin in cells or degrade the granules in anyway that would lead to a reduction in lipofuscin-like fluorescence levels.

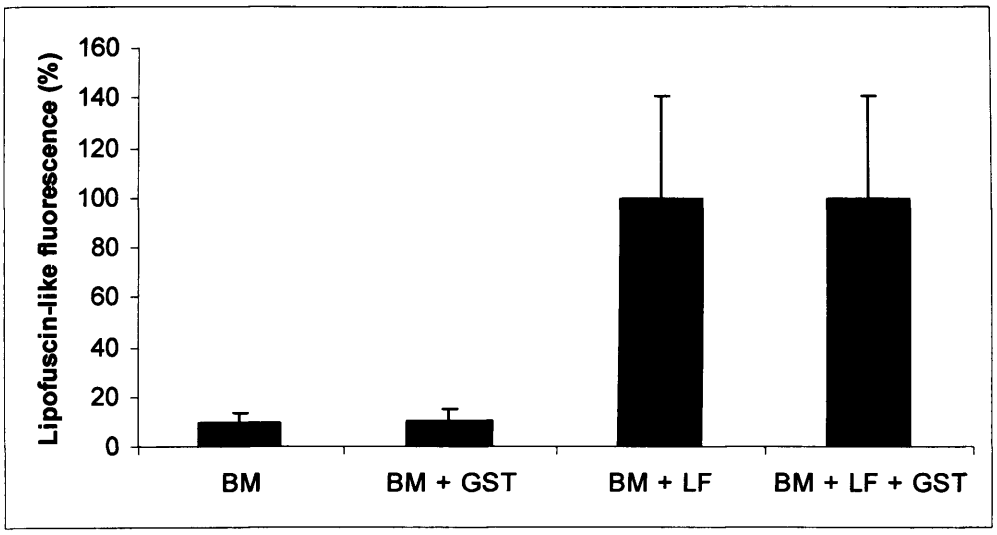

Figure 6.14. Lipofuscin-like fluorescence of cells with/without lipofuscin maintained with/without free GST. Cellular lipofuscin-like fluorescence was measured in cells using flow cytometry. Cells that were not loaded with lipofuscin were maintained in either basal medium (BM) alone or in BM supplemented with free GST. Cells loaded with lipofuscin (~ 300 granules per cell) were maintained in BM alone or BM supplemented with free GST. Cellular fluorescence of cells loaded with lipofuscin and maintained in BM was assumed as 100% and other results normalised to this. Data represents the results of three experiments each carried out in triplicate. Error bars represent ± SD.

Next, cells loaded with lipofuscin were maintained in medium that had been supplemented with the dextrin-GST conjugate at levels equivalent to 4 units GST activity. Again, cells loaded with lipofuscin displayed greater levels of fluorescence than those not exposed to lipofuscin. The level of lipofuscin-like autofluorescence was significantly lower in cells loaded with lipofuscin and maintained in basal medium supplemented with GST-dextrin conjugate (lipofuscin-like fluorescence 60.59%) than cells loaded with lipofuscin and maintained in basal medium alone (lipofuscin-like fluorescence 100%) ($p = <0.05$). This indicates that the conjugate, in which GST is protected and localised to the lysosome, has the capacity to degrade or alter lipofuscin granules in a way so as to lower their fluorescence.

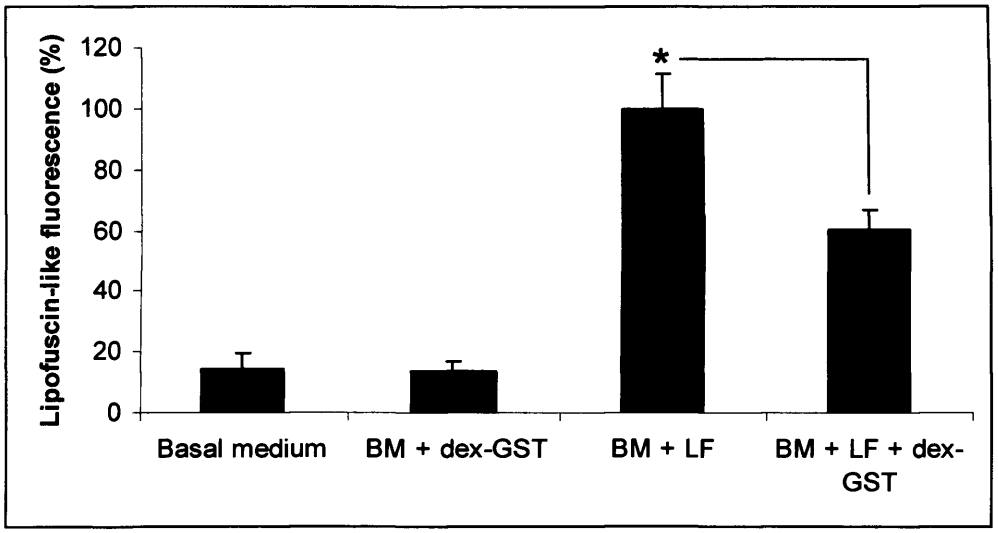

Figure 6.15. Lipofuscin-like fluorescence of cells with/without lipofuscin maintained with/without dex-GST. Cellular lipofuscin-like fluorescence was measured in cells using flow cytometry. Cells that were not loaded with lipofuscin were maintained in either basal medium (BM) alone or BM supplemented with the dextrin-GST conjugate (dex-GST). Cells loaded with lipofuscin (~ 300 granules per cell) were maintained in BM alone or BM supplemented with dex-GST. Cellular fluorescence of cells loaded with lipofuscin and maintained in BM was assumed as 100% and other results normalised according to this. Data represents the results of three experiments each carried out in triplicate. Error bars represent $\pm$ SD. * represents a statistically significant difference $p < 0.005$.

The reduction in lipofuscin-like fluorescence measured in cells treated with dex-GST could be the result of lipofuscin granules being degraded or removed from cells. However, it could be a consequence of the granules having been manipulated so as to reduce their fluorescence, perhaps by removal or alteration of the fluorophores present. To gain a greater understanding of the effect that dex-GST is having on lipofuscin granules, TEM images of cells with or without lipofuscin and then maintained either in basal medium with or without supplementation with dex-GST were analysed. Cells not exposed to lipofuscin showed characteristic organelles of functional cells including mitochondria, endoplasmic reticulum and a nucleus (Figure 6.16), as did those exposed to lipofuscin (Figure 6.17). In cells that were exposed to lipofuscin, the granules were obvious as electron dense bodies (Figure 6.17), the morphology, size and abundance of which could be compared between the test conditions (Table 6.3). Using image J software to calculate the percentage of the cell area occupied by lipofuscin it was found that on average less of the cells cytoplasmic space was taken up by lipofuscin in cells maintained in medium supplemented with dex-GST (6.02%) than cells maintained in basal medium alone (10.90%) ($p = <0.05$).

Analysis of the micrographs also revealed that lipofuscin granules were significantly smaller in cultures maintained in the dex-GST medium (0.53 μm^2) than basal medium (0.72 μm^2) ($p=<0.05$).

Table 6.3 Comparison of cytoplasmic area of cell occupied by lipofuscin and size of lipofuscin granules in RPE cells loaded with lipofuscin and maintained in medium with/without dex-GST.

	Cells exposed to lipofuscin and maintained in BM	Cell exposed to lipofuscin and maintained in BM supplemented with dex-GST
Average area of cell occupied by lipofuscin (%)	10.90 % ($\pm$4.70)	6.02 % ($\pm$5.40)
Average size of lipofuscin granules (μm^2)	0.72 ($\pm$0.48)	0.53 ($\pm$ 0.52)

Lipofuscin granules seen in TEM images of cells maintained in medium with or without dex-GST appear to have similar morphology and are consistent with images found in the literature (Boulton *et al.*, 1990). Some granules in cells treated with dex-GST conjugate appear to have undergone modification leaving a prominent endoskeleton surrounded by a less electron dense granule. These granules were present in a number of the images collected of cells maintained in medium containing dex-GST but in none of the images taken of cells loaded with lipofuscin and maintained in basal medium alone.

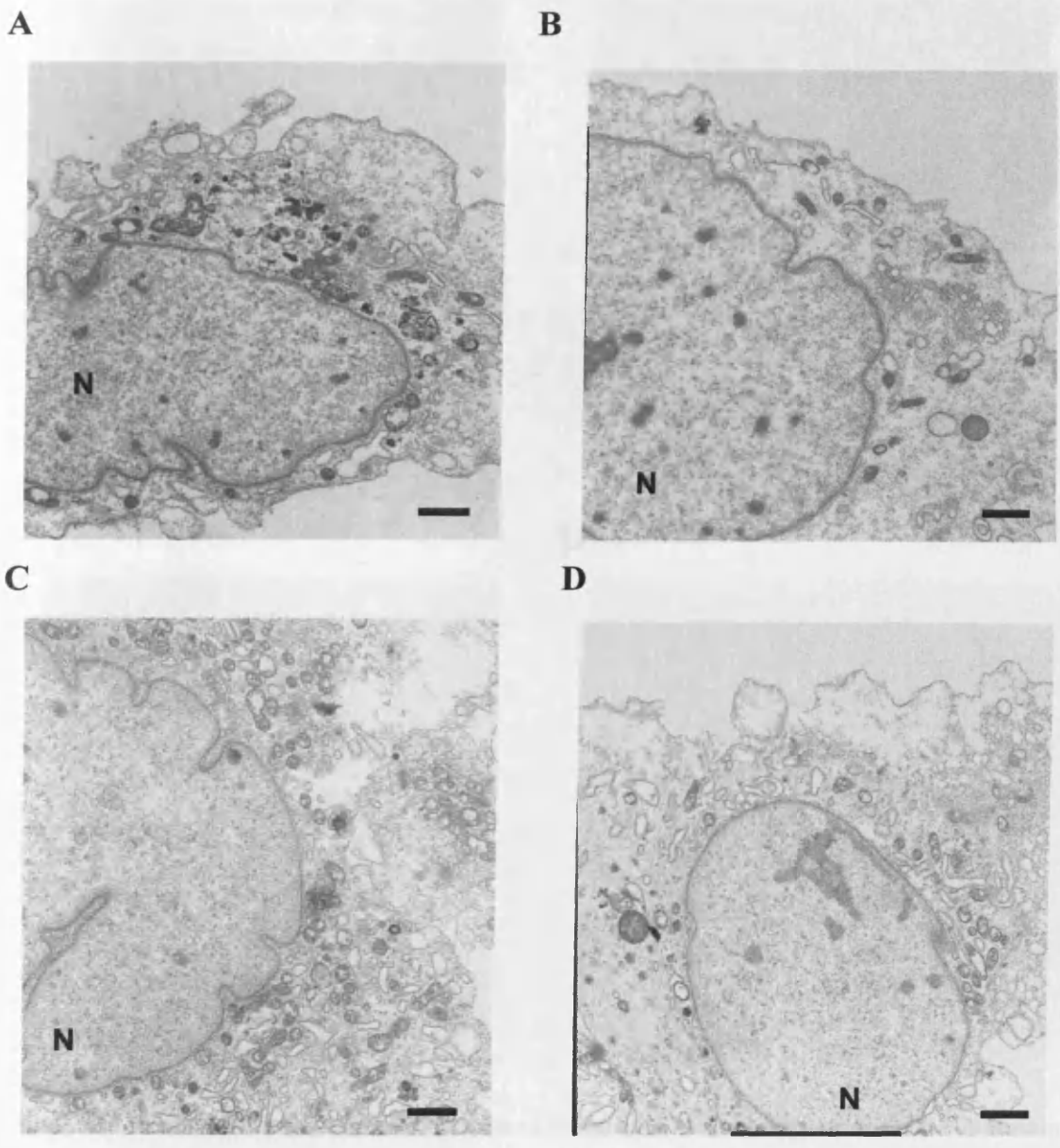

Figure 6.16. Representative TEM micrographs of cultured ARPE-19 cells maintained in (A, B) basal medium alone, (C, D) basal medium supplemented with dex-GST. N denotes the nucleus of each of the cells. All images were taken at the same magnification (8K magnification), the scale bar represents 1μm.

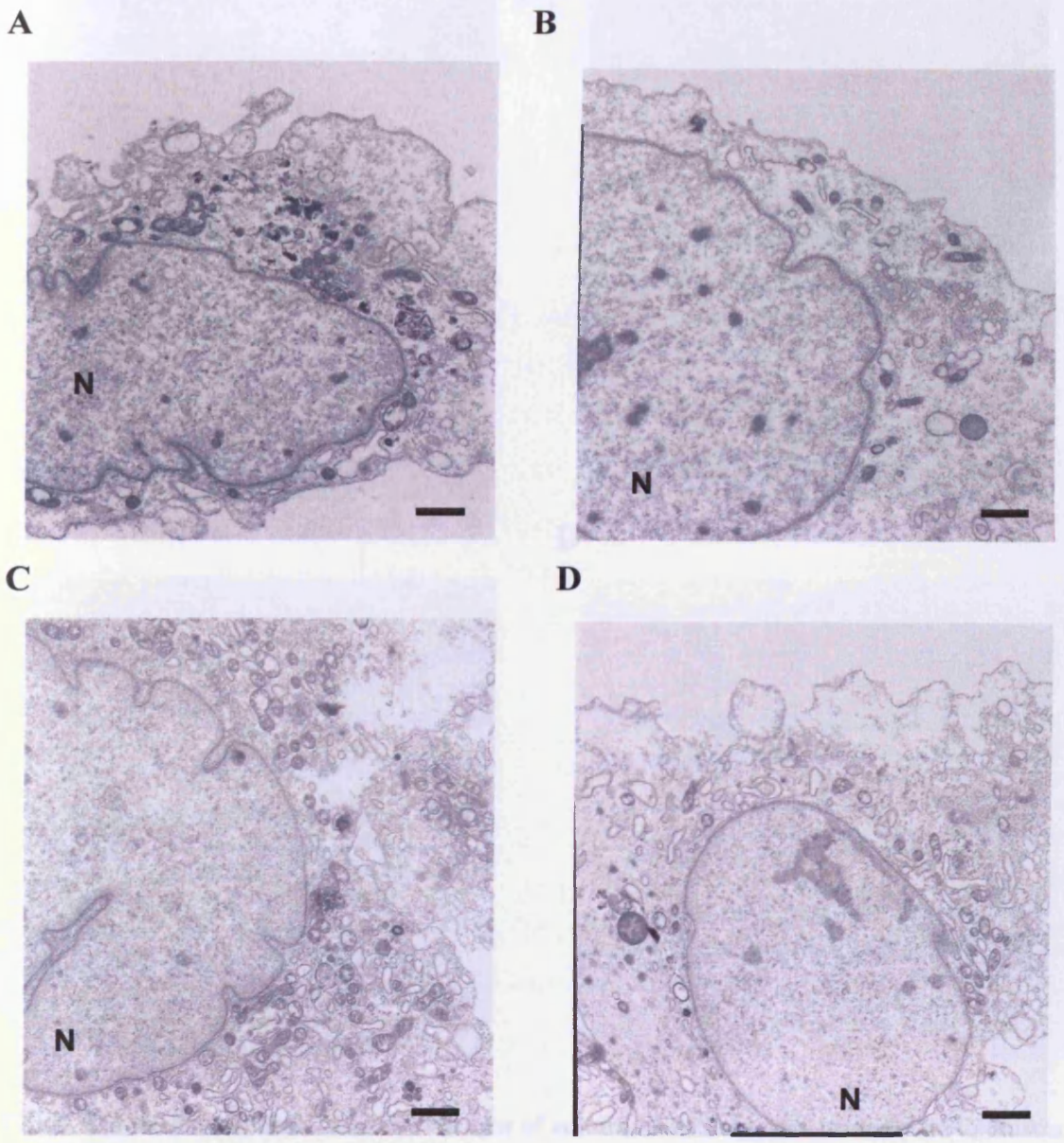

Figure 6.16. Representative TEM micrographs of cultured ARPE-19 cells maintained in (A, B) basal medium alone, (C, D) basal medium supplemented with dex-GST. N denotes the nucleus of each of the cells. All images were taken at the same magnification (8K magnification), the scale bar represents 1μm.

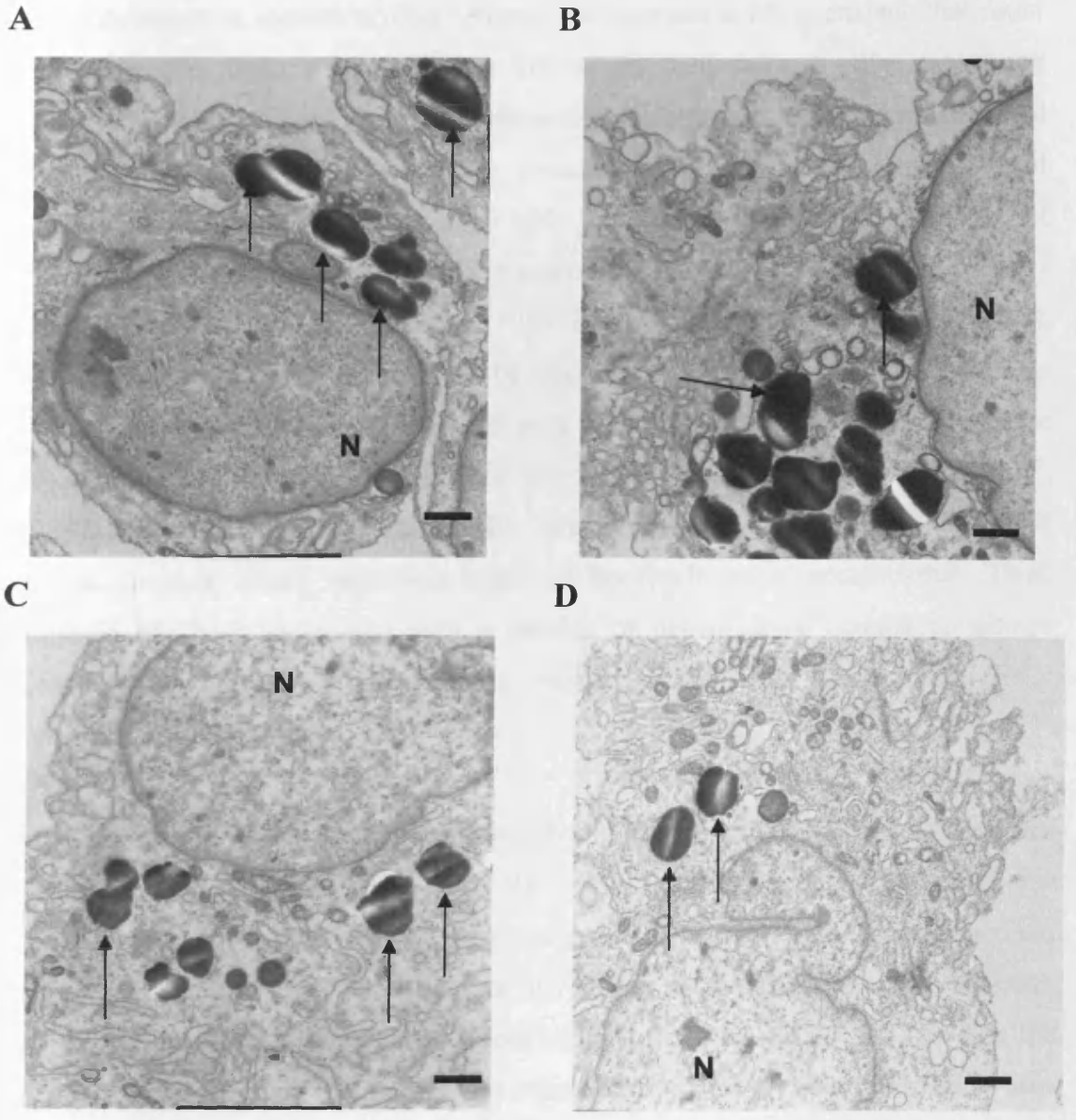

Figure 6.17. Representative TEM micrographs of cultured ARPE-19 cells loaded with lipofuscin and maintained in basal medium (A, B) and loaded with lipofuscin and maintained in basal medium supplemented with dex-GST (C, D). The electron dense bodies, highlighted with single arrows, seen in the images are lipofuscin granules. N denotes the nucleus of each of the cells. All images were taken at the same magnification (8K magnification), the scale bar represents 1μm.

6.4 Discussion

This study aimed to identify a drug delivery polymer and suitable enzyme that could be conjugated to form a nanomedicine that assists RPE cells in either preventing lipofuscin formation by the removal of lipofuscin substrates or in the degradation and removal of lipofuscin that is already present. As discussed previously, retinal lipofuscin accumulates in RPE cells with age and is composed primarily of oxidatively modified components of POS and other intra-cellular organelles (Feeney - Burns and Eldred, 1983; Boulton *et al.*, 1989; Brunk *et al.*, 1992; Brunk *et al.*, 1995). Lipofuscin has been demonstrated to be phototoxic to RPE cells *in vitro* and to generate free radicals when illuminated with blue-light with the potential to cause RPE dysfunction (Boulton *et al.*, 1993; Rozanowska *et al.*, 1997; Rozanowska *et al.*, 1998; Davies *et al.*, 2001). Loss of RPE function is a key feature in a number of macular diseases where increased levels of lipofuscin have accumulated. Thus, lipofuscin has been associated with a number of degenerative macula conditions including; AMD, Best's and Stargardt's diseases (Katz, 2002; Karan *et al.*, 2005; Gerth *et al.*, 2007; Kim *et al.*, 2007).

Initially, the safety of dextrin, the polymer chosen as a potential delivery vehicle, was measured by assaying the viability of RPE cells maintained in medium that was supplemented with it. The viability was compared to control cells in basal medium with no statistically significant difference in viability between the two. This indicates that dextrin, even in its succinoylated form, is non-toxic to RPE cells. This was the predicted outcome given that dextrin has been approved for a variety of clinical uses (Verco *et al.*, 2000). However, this study is the first to target dextrin specifically to the RPE and these results are important in showing that the polymer is compatible with our cell type. Therefore, proceeding with further studies using dextrin as our carrier molecule of choice was justified.

Having ensured that the polymer was non-toxic to RPE cells, next we demonstrated, using both flow cytometry and confocal microscopy, that dextrin-tagged with Oregon-green was internalised by RPE cells. Endocytosis of dextrin molecules into RPE cells is likely to be predominantly via phagocytosis with pinocytosis also involved (Geiser

et al., 2005). Most discussion of movement of nanomedicines across cell membranes has focused on receptor mediated mechanisms (van Deurs *et al.*, 1989). Dextrin is an analogue of mannose, thus it is probable that the mannose receptors that have been identified on the apical membrane of the RPE are largely responsible for the internalisation of the dextrin conjugates (Tarnowski *et al.*, 1988; Shepherd *et al.*, 1991).

Once intracellular, for nanomedicines to be clinically relevant it is essential to understand their endocytic fate by identifying the organelles they associate with (Duncan, 2007). In this instance the target organelles were the numerous lysosomes that are present within the RPE, where lipofuscin gradually accumulates. To determine the intracellular fate of dex-OG and later dex-GST-OG within the RPE cell, a novel immunocytochemical technique was developed to visualise the endocytic outcome of the polymer and polymer-protein conjugate. Previous studies have used sub-cellular fractionation to determine the localisation of polymeric drugs. This is a technique that has many draw-backs including the need for excellent levels of user skill, standardisation for each cell type used and the high risk for contamination between fractions, particularly when the organelles of interest are of similar density (Brunet *et al.*, 2003). The immunocytochemistry technique developed through this study allows for the accurate labelling of specific intracellular compartments in a way that is transferable to many cell types (Richardson *et al.*, 2008). The technique works by tagging essential components in the endocytic pathway (Figure 6.17) to see which are co-localised with the polymeric drug of choice. Using a combination of TxR-BSA, dex-OG and immuno-labelled organelles we showed for the first time in ARPE-19 cells the endocytosis and intracellular localisation of a polymeric carrier. The nanomedicine was found to be exclusively within late endocytic structures. Thus, we had succeeded in choosing a polymer that would localise to the area of our cells that was required.

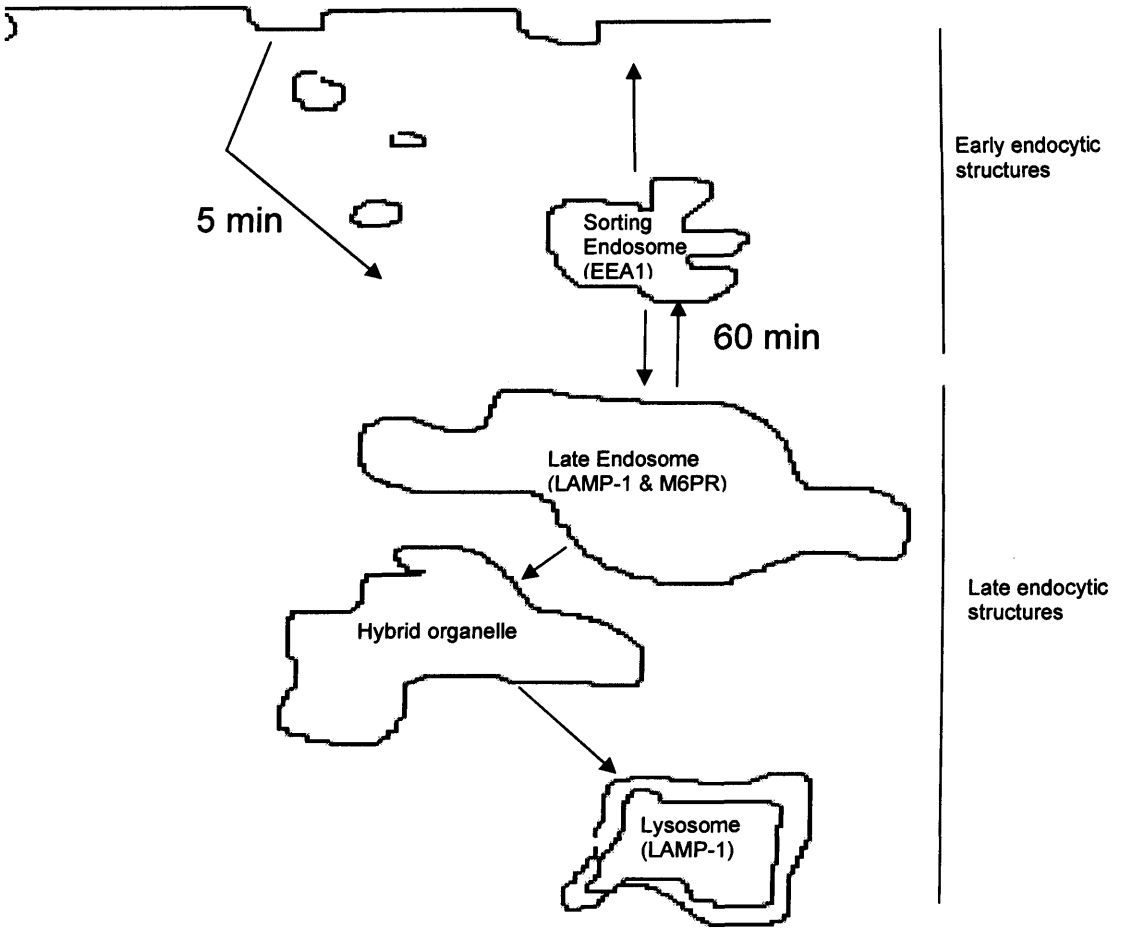

Figure 6.17. Simplified diagram of the endocytic pathway. The principle components together with markers used for definition are annotated. Times indicate approximate values taken by materials to reach the compartments. Adapted from Richardson et al (Richardson *et al.*, 2008).

Whilst characterising dextrin and its endocytic behaviour within RPE cells, the enzyme, GST, was being assessed with regard to its suitability as the active component in preventing lipofuscin accumulation. GST (at three concentrations, 1, 4 and 10 units activity), together with GSH and NAC, the precursor for GSH formation within the body, were supplemented in basal medium of RPE cells exposed to POS (Tirouvanziam *et al.*, 2006). The lipofuscin-like fluorescence of these cells was then compared to cells exposed to POS in basal medium alone. It was noted that the combination of GST, GSH and NAC resulted in a reduction in the rate at which the lipofuscin-like fluorescence of cells increased. The difference in lipofuscin-like fluorescence measured in cells exposed to POS alone and those exposed to POS, GSH, NAC and 1 unit GST could be the result of a combined response of GSH, NAC and GST to the POS challenge. Indeed, previous studies have shown that lysosomal

accumulation of lipofuscin-like products was reduced in RPE cells exposed to POS when the cells were also supplemented with NAC, whilst other studies have demonstrated that NAC can protect RPE cells against oxidative insult (Sternberg *et al.*, 1993; Schutt *et al.*, 2007b). Equally, GSH has been shown to detoxify reactive aldehydes generated from lipid peroxidation and to alter the redox potential of cells, determining the function of the ubiquitin proteasome pathway (Sternberg *et al.*, 1993; Jahngen-Hodge *et al.*, 1997). Changes in the ratio of reduced and oxidised glutathione that results in an increase in oxidised glutathione have been shown to down regulate proteasome activity in RPE cells resulting in increased levels of protein carbonyls (Shang and Taylor, 1995; Shang and Taylor, 2004). Both co-factors could be influential in reducing the level of accumulation of lipofuscin-like products within the RPE. However, the difference in lipofuscin-like fluorescence recorded between the cells cultured in medium supplemented with different levels of GST activity could only be the result of GST action as GSH and NAC were maintained at constant levels in each of the cultures. The results obtained in this study corroborate with work in the literature that have established that GSTs are key in protecting the RPE against oxidative stress, particularly against reactive aldehyde accumulation (Singhal *et al.*, 1999; Maeda *et al.*, 2005).

The statistically significant difference in lipofuscin-like fluorescence measured between cells exposed to POS with or without GST indicated that GST was indeed a potential candidate for the active component of a nanomedicine. Unfortunately, due to difficulties in the production of GST-dextrin conjugate, studies looking into whether the nanomedicine was capable of preventing the formation of lipofuscin-like material were not conducted. To determine whether GST was able to remove or degrade retinal lipofuscin, cells were pre-loaded with lipofuscin and maintained in medium supplemented with free GST. After 7 days of supplementing cells with free GST the lipofuscin-like fluorescence of these cells was compared to cells maintained in basal medium alone with no significant difference noted. These results contrasted with those seen with cells pre-loaded with lipofuscin and maintained in basal medium supplemented with dex-GST. Dex-GST treated RPE cells showed significantly lower lipofuscin-like fluorescence than those maintained in basal medium, with cells containing smaller lipofuscin granules that occupied less of the cytoplasmic area. This

is symptomatic that the polymer-protein conjugate was in some way degrading or removing lipofuscin granules, or components of the granules.

It is possible that free GST had little or no effect in reducing lipofuscin-like fluorescence in cells as it was itself metabolised before exerting any influence. GST conjugated to dextrin however, may have had sufficient protection from the polymer so as to be able to act upon the lipofuscin granules before being degraded. This mechanism of action for polymers has been previously described in the literature and given the acronym PUMPT, standing for polymer masked-unmasked protein therapy (Duncan *et al.*, 2008). By enveloping the protein, the polymer protects it from degradation until it is digested itself. It is predicted that by the time of degradation the polymer-protein conjugate has reached its intended destination and that the freed active component can have its desired effect. We have shown that the dex-GST conjugate is localised to the cells lysosomes where lipofuscin accumulates. It is, therefore, likely that the dextrin surrounding and protecting GST is degraded by one of numerous enzymes capable of degrading α-1,4-linkages in polysaccharides present in human lysosomes (Journet *et al.*, 2000; Journet *et al.*, 2002). Liberated GST would then have an opportunity to act on the lipofuscin present in the lysosomes, before being broken down.

Towards developing a nanomedicine that could be used to prevent lipofuscin accumulation within the RPE, we have succeeded in demonstrating dextrin is a polymer that is: non-toxic to RPE cells, is internalised by the cells and can be shown to associate with late endocytic structures using a novel technique for visualising the endocytic fate of polymeric drugs within cells. Thus, dextrin has been identified as an ideal candidate for the carrier molecule for this drug.

We have also conjugated the potential drug delivery polymer to an enzyme with the capacity to degrade the primary substrates of lipofuscin formation in its free state and degrade lipofuscin already present within RPE cells when supplemented as a conjugate. Together, the results obtained with the polymer and enzyme indicate that when conjugated they have the potential to be developed as a therapeutic agent against the onset of AMD if a causal link between lipofuscin and the disease can be proven. The advantage of a strategy such as this over drugs currently available in the

battle against AMD is that the nanomedicine could be used to prevent the onset of the disease and be used against the dry form of the disease, whereas current treatments attempt to prevent further progression once the late stage of the wet form of the disease has been reached.

As discussed in Chapter 1, lipofuscin accumulates in many post-mitotic cells with age. Lipofuscin accumulation has been associated with loss of function in these cells and subsequently the onset of age-related diseases. The results collected to date using the early-stage nanomedicine indicate that it has the potential as a therapeutic agent in a variety of lipofuscin-related afflictions of the aged.

The development of this nanomedicine would benefit from further research using the *in vitro* RPE model before moving onto an *in vivo* model. One necessary study would be to complete the analysis of preventing the formation of lipofuscin-like products in RPE cells when fed POS in conjunction with the dex-GST conjugate. Further to this, phototoxicity measurements need to be carried out on cells that have either been pre-loaded with lipofuscin or exposed to POS and administered the dex-GST conjugate. Viability levels would then be compared to cells laden with lipofuscin or fed POS and maintained in basal medium. As many of the deleterious effects of lipofuscin have been attributed to its phototoxic properties, the effect the conjugate has on this would be most important.

Results obtained during this study indicated that exposing lipofuscin-loaded cells to the dex-GST conjugate led to a decrease in the lipofuscin-like fluorescence of the cells compared to lipofuscin-loaded cells maintained in basal medium. However, the exact mechanism of how the conjugate works is not fully understood. Analysis of lipofuscin granule size suggests that granules in cells fed dex-GST were significantly smaller than those maintained in basal medium. This change could possibly account for the decrease in the lipofuscin-like fluorescence of cells; nevertheless, another possible mechanism that would reduce lipofuscin-like fluorescence would be the conjugate specifically targeting lipofuscin fluorophores. It would be interesting to chromatographically analyse cells that had been loaded with lipofuscin and treated with dex-GST or basal medium to see if any constituents of the lipofuscin granules had been specifically degraded or removed.

Upon completion of the *in vitro* work using the dex-GST conjugate, studies could proceed on *in vivo* work, with a mouse model of AMD being an ideal system. *In vivo* work would most probably mirror the studies conducted with the *in vitro* model. Initially, the drug would need to be targeted to the lysosomes of the RPE and the safety of the drug assessed. If the drug is safe within a living system and could be targeted to the required area, analysis of any changes in lipofuscin accumulation could start. Of interest would be the quantification of lipofuscin granules present, spectral changes of the retina and measurement of disease progression within the model.

Chapter 7

Discussion and Conclusions

7.1 General discussion

The formation of retinal lipofuscin has been shown to involve POS that have been phagocytosed into the RPE (Feeney -Burns and Eldred, 1983; Boulton *et al.*, 1989; Wihlmark *et al.*, 1996a,b). Equally, others have shown that old or damaged organelles, in particular mitochondria, that under go autophagy also play a role (Moore *et al.*, 2006; Terman *et al.*, 2006; Kurz *et al.*, 2007; Kurz *et al.*, 2008). However, some authors believe that one or other is the dominant process (Katz and Robison, 2002).

In vitro models of retinal lipofuscin based around the substrates that derive from phagocytosis and autophagy developed during this project (**Chapter 4**) indicate that both processes contribute to retinal lipofuscin formation. Lipofuscin-like products that were formed from both models displayed similar optical density and fluorescent spectra. They also present some characteristics that were reminiscent of *ex vivo* retinal lipofuscin including: protein smears when analysed using SDS-PAGE and the ability to photogenerate singlet oxygen. However, analysis also highlighted differences between the autophagy and phagocytosis models. The lipofuscin models that were formed using POS contained A2E and molecules adducted to CEP. These were absent from the autophagy model, indicating that retinal lipofuscin does indeed obtain unique components from the phagocytosed material that may not be present in lipofuscins found in other post-mitotic cells. We have demonstrated that retinal lipofuscin accumulates as a result of malfunctions in the processes of phagocytosis and autophagy, however, the products formed consequently are slightly different. It is, therefore, possible that there are two distinct forms of retinal lipofuscin that accumulate, or, that retinal lipofuscin is an amalgamation of material accrued from both sources.

RPE lysosomes contain over forty hydrolytic enzymes that are there to rid the cell of waste and degrade spent tips of photoreceptors (Kennedy *et al.*, 1993; Boulton *et al.*, 1994). Nonetheless, the degradation is an inefficient process as demonstrated by the accumulation of retinal lipofuscin. It is proposed that organelles of the RPE and the POS are subject to oxidative stress and thus, undergo oxidative modification leading

to products that are no longer recognised by the lysosomal enzymes (Schutt *et al.*, 2003a; Kopitz *et al.*, 2004a; Kaemmerer *et al.*, 2007). Indeed, in **Chapter 3** we demonstrated that lipofuscin granules, although almost devoid of protein, did indeed have a number of components present that had been adducted to: nitro-tyrosine, iso[4]LGE_2 or CEP, each of which are markers of oxidative stress (Ng *et al.*, 2008). These findings add credence to the theory that oxidative stress precedes retinal lipofuscin accumulation (Katz, 1985; Wihlmark *et al.*, 1996a,b; Holz *et al.*, 2004; Hoppe *et al.*, 2004).

The progressive accumulation of retinal lipofuscin with time means that by the age of 80 years it can occupy up to 20% of an RPE cells' cytoplasmic volume (Feeney-Burns *et al.*, 1984). Amassing such waste can have adverse consequences on the cells function. Some effects may simply arise through congestion within the cell, but also as demonstrated in **Chapter 5**, increasing the concentration of lipofuscin in a cell increases the phototoxic effect it exerts.

The phototoxic properties of retinal lipofuscin have been demonstrated to be wavelength dependant, with the production of reactive oxygen species being greater when lipofuscin is irradiated with light of shorter rather than longer wavelength (Rozanowska *et al.*, 1998; Davies *et al.*, 2001). In this study we have demonstrated that irradiance levels as well as the wavelength of light influence the impact that retinal lipofuscin has on RPE cell viability. These findings emphasise the importance of light irradiance levels when considering the design of *in vitro* experiments.

In vitro experimentation demonstrating the toxic effect of retinal lipofuscin towards RPE cells has led to its theoretical association with AMD (Davies *et al.*, 2001; Katz, 2002; Kopitz *et al.*, 2004a; Nowak, 2006b). It has also been noted that there is an increased incidence of AMD in patients who have under gone cataract surgery than in age matched controls (van der Schaft *et al.*, 1994; Pollack *et al.*, 1996). The cause of this has been speculated to be photic injury during surgery or inflammatory changes as a result of surgery. Another possible explanation is that during cataract surgery the naturally yellowed lens is often replaced with a UV-blocking only lens. This subjects the retina to increased levels of high-energy blue-light that can photoexcite lipofuscin, placing it under oxidative stress at a time when it is most vulnerable. Consequently,

artificial lenses that mimic the blue-light blocking properties of aged lenses are being developed (Ernest, 2004). **Chapter 5** describes a comparison of two blue-light blocking optical filters, one that gradually blocks blue-light between 400-500 nm and another sharp-cut off lens that blocks light below ~425 nm, with an optical filter with transmission properties similar to conventional UV-blocking IOLs. The data suggest that both the yellow-tinted filters provide significantly more protection against lipofuscin phototoxicity than the UV-blocking filter when irradiated with blue or white light. Thus, as blue-light blocking lenses have been shown to have no adverse effects on visual acuity, contrast sensitivity, colour vision or scotopic vision they could prove to be beneficial to the retinas of cataract patients (Marshall *et al.*, 2005; Hayashi and Hayashi, 2006; Greenstein *et al.*, 2007; Landers *et al.*, 2007; Muftuoglu *et al.*, 2007).

To date, therapeutic strategies aimed at combating AMD have targeted the wet form of the disease and have largely avoided treatment of the early stages of the disease. The wet form is the more aggressive and the cause of a larger number of cases of blindness than the dry form. However, around 80% of AMD sufferers have the dry form, for which there are currently no proven treatments. Retinal lipofuscin has been identified as a potential target in the treatment of early AMD due to its phototoxic properties that exert oxidative stress upon RPE cells (Nowak, 2006a,b; Birch and Liang, 2007).

Chapter 6 describes the development of a nanomedicine that has the potential for degrading retinal lipofuscin or preventing its formation within the RPE. It was demonstrated that the carrier molecule, dextrin, could be targeted to RPE lysosomes and that the active component of the drug, GST, could assist in the degradation or removal of POS in *in vitro* RPE cells. When conjugated, the nanomedicine had the ability to reduce the level of retinal lipofuscin that had been loaded into *in vitro* RPE cells. Results obtained during these studies prove there is potential for further development of a nanomedicine for the treatment of early AMD. The ability to target the drug to the RPE and to be activated within the lysosomes leads to the possibility of replenishing levels of lysosomal enzymes. Of particular interest would be increasing levels of the Cathepsin family of enzymes. These have been identified as important in the degradation of POS, which, as demonstrated in a previous chapter

(**Chapter 3**), are key substrates in the formation of retinal lipofuscin (Deguchi *et al.*, 1994; Rakoczy *et al.*, 1999; Rakoczy *et al.*, 2002; Sugano *et al.*, 2006). Equally, anti-oxidants, either enzymatic or not, could be specifically targeted to RPE lysosomes, possibly in combination with other treatments to maintain the health of the RPE.

7.2 Conclusions

The work contained within this thesis sought to gain important insight into the genesis, phototoxicity and means of degrading retinal lipofuscin. The aims of the project were broad in nature; however, they were all interconnected by the theme of retinal lipofuscin as detailed in Figure 7.1.

In summary the conclusions of this study are:

- Retinal lipofuscin contains a minimal amount of protein, but is comprised of a number of molecules adducted to lipid peroxidation products.
- Substrates for retinal lipofuscin are derived from material shuttled to RPE lysosomes during both phagocytosis and autophagy. The material that accumulates is that which cannot be degraded by the lysosomes.
- POS are the main source of A2E and CEP-adducts for retinal lipofuscin
- Yellow-tinted optical filters provide significantly more protection to *in vitro* lipofuscin-loaded RPE cells than UV-blocking optical filters when irradiated with high intensity blue or full spectrum visible light.
- The phototoxic effect of retinal lipofuscin towards RPE cells is retinal lipofuscin concentration and light intensity dependant.
- The nanomedicine carrier molecule, dextrin, can be specifically targeted to the lysosomal compartment of RPE cells.
- GST has been identified as an enzyme able to assist RPE cells *in vitro* to degrade phagocytosed POS.
- When conjugated, dex-GST can decrease the lipofuscin-like fluorescence of retinal lipofuscin loaded RPE cells and cause a reduction in granule size when treated *in vitro*.

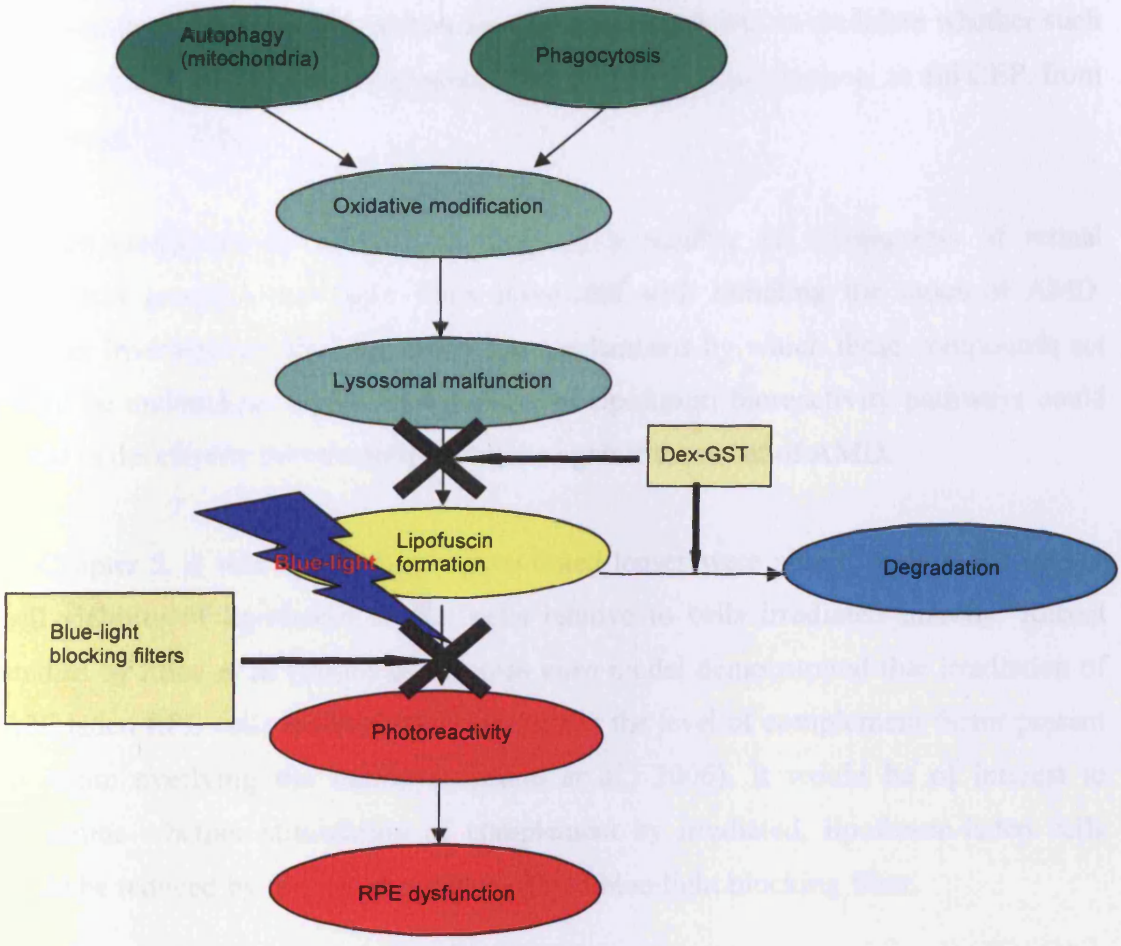

Figure 7.1 Flow diagram linking the broad interests of this project. Genesis of retinal lipofuscin via incomplete autophagy or phagocytosis may lead to possible deleterious consequences of lipofuscin accumulation and its photoreactivity. Additionally, key targets for preventing lipofuscin formation and diminishing its phototoxic effects are highlighted, together with the strategies investigated during the studies to facilitate that.

7.3 Future work

Results obtained in Chapter 4 using the *in vitro* lipofuscin formation models indicate that they are capable of producing singlet oxygen when excited with short wavelength visible light (420 nm). *Ex vivo* lipofuscin has been demonstrated to also produce other ROI including the super oxide anion (Boulton *et al.*, 1993). Analysis of the ability of our retinal lipofuscin models to generate such ROI may prove interesting. Also of interest would be to analyse whether other lipid peroxidation products such as nitrotyrosine and iso[4]LGE_2 that form adducts in *ex vivo* retinal lipofuscin were present in the *in vitro* lipofuscin models. This would help to validate the similarity

between the *in vitro* models and *ex vivo* lipofuscin and also to elucidate whether such lipid peroxidation products originated from the phagocytosis source, as did CEP, from autophagy, or, both.

Studies conducted in Chapter 3 identified a number of components of retinal lipofuscin granules that have been associated with initiating the onset of AMD. Further investigation into the molecular mechanisms by which these compounds act could be undertaken. Greater knowledge of lipofuscin bioreactivity pathways could assist in developing preventative measures against the onset of AMD.

In Chapter 5, it was shown that yellow-tinted lenses were able to reduce the loss in cell viability of lipofuscin loaded cells relative to cells irradiated directly. Recent studies by Zhou *et al* (2006) using an *in vitro* model demonstrated that irradiation of A2E laden RPE cells resulted in an increase in the level of complement factor present in serum overlying the cell-layer (Zhou *et al.*, 2006). It would be of interest to determine whether stimulation of complement by irradiated, lipofuscin-laden cells could be reduced by the use of a yellow-tinted blue-light blocking filter.

The work conducted in Chapter 6 was part of a preliminary study that yielded some very interesting results. As such, further research could stem from these introductory experiments forming future projects. Work that could develop from the preliminary findings is discussed in Chapter 6, Section 6.4.

Bibliography

Adithi M, Nalini V, Krishnakumar S (2005) The role of nitric oxide synthases and nitrotyrosine in retinoblastoma. *Cancer.* 103:1701-1711.

Ahn J, Wong JT, Molday RS (2000) The effect of lipid environment and retinoids on the ATPase activity of ABCR, the photoreceptor ABC transporter responsible for Stargardt macular dystrophy. *Journal of Biological Chemistry.* 275:20399-20405.

Algvere PV, Marshall J, Seregard S (2006) Age-related maculopathy and the impact of blue light hazard. *Acta Ophthalmologica Scandinavica.* 84:4-15.

Alin P, Danielson UH, Mannervik B (1985) 4-Hydroxyalk-2-enals are substrates for glutathione transferase. *FEBS Letters.* 179:267-270.

Allikmets R (1997) A photoreceptor cell-specific ATP-binding transporter gene (ABCR) is mutated in recessive Stargardt macular dystrophy. *Nature Genetics.* 17:122.

Allikmets R, Seddon J, Bernstein P, Hutchinson A, Atkinson A, Sharma S, Gerrard B, Li W, Metzker M, Wadelius C, Caskey C, Dean M, Petrukhin K (1999) Evaluation of the Best disease gene in patients with age-related macular degeneration and other maculopathies. *Human Genetics.* 104:449-453.

Aslan M, Yücel G, Ciftçiolu MA, Yücel I, Akar Y, Sanlioglu S (2006) Nitrotyrosine formation and apoptosis in rat models of ocular injury. *Free Radical Research Communications.* 40:147-153.

Bakall B, McKay BS, Travis GH, Burke JM, Mullins RF, Radu RA, Stanton JB, Wadelius C, Stone EM (2007) Enhanced accumulation of A2E in individuals homozygous or heterozygous for mutations in BEST1 (VMD2). *Experimental Eye Research.* 85:34-43.

Bakall B, Zhang Y, Marmorstein AD, Hartzell HC, McLaughlin P, Stanton JB, Marmorstein LY (2008) Bestrophin-2 is involved in the generation of intraocular pressure. *Investigative Ophthalmology and Visual Science.* 49:1563-1570.

Ban Y, Rizzolo LJ (2000) Regulation of glucose transporters during development of the retinal pigment epithelium. *Developmental Brain Research.* 121:89-95.

Basinger S, Hoffman R, Matthes M (1976) Photoreceptor shedding is initiated by light in the frog retina. *Science.* 194:1074-1076.

Batten ML, Moise AR, Baehr W, Tu DC, Possin D, Imanishi Y, Maeda T, Bronson D, Van Gelder RN (2004) Lecithin-retinol acyltransferase is essential for

accumulation of all-trans-retinyl esters in the eye and in the liver. *Journal of Biological Chemistry.* 279:10422-10432.

Bazan HEP, Bazan NG, Feeneyburns L, Berman ER (1990) Lipids in human lipofuscin-enriched subcellular-fractions of 2 age ppulations - comparison with rod outer segments and neural retina. *Investigative Ophthalmology & Visual Science.* 31:1433-1443.

Bazan NG, Gordon WC, Rodriguez de Turco EB (1992) Docosahexaenoic acid uptake and metabolism in photoreceptors: retinal conservation by an efficient retinal pigment epithelial cell-mediated recycling process. *Advances in Experimental and Medical Biology.* 318:295-306.

Beatty S, Henson D, Boulton M, Koh H, Phil M The role of oxidative stress in the pathogenesis of age-related macular degeneration. *Surv Ophthalmol.* 45:115-134.

Beatty S, Henson D, Boulton M, Koh H, Phil M (2000) The role of oxidative stress in the pathogenesis of age-related macular degeneration. *Survey of Ophthalmology.* 45:115-134.

Ben-Shabat S, Itagaki Y, Jockusch S, Sparrow JR, Turro NJ, Nakanishi K (2002a) Formation of a nonaoxirane from A2E, a lipofuscin fluorophore related to macular degeneration, and evidence of singlet oxygen involvement. *Angewandte Chemie-International Edition.* 41:814-817.

Ben-Shabat S, Parish CA, Vollmer HR, Itagaki Y, Fishkin N, Nakanishi K, Sparrow JR (2002b) Biosynthetic studies of A2E, a major fluorophore of retinal pigment epithelial lipofuscin. *Journal of Biological Chemistry.* 277:7183-7190.

Bergmann M, Schutt F, Holz FG, Kopitz J (2004) Inhibition of the ATP-driven proton pump in RPE lysosomes by the major lipofuscin fluorophore A2-E may contribute to the pathogenesis of age-related macular degeneration. *Faseb Journal.* 18:562-564.

Berson DM, Dunn FA, Takao M (2002) Phototransduction by retinal ganglion cells that set the circadian clock. *Science.* 295:1070-1073.

Bibb C, Young RW (1974) Renewal of fatty-acids in membranes of visual cell outer segments. *Journal of Cell Biology.* 61:327-343.

Birch DG, Liang FQ (2007) Age-related macular degeneration: a target for nanotechnology derived medicines. *International Journal of Nanomedicine.* 2:65-77.

Birnbach C, Jarvelainen M, Possin D, Milam A (1994) Histopathology and immunocytochemistry of the neurosensory retina in fundus flavimaculatus. *Ophthalmology.* 101:1211-1219.

Boettner E, Wolter J (1962) Transmission of the ocular media. *Investigative Ophthalmology and Visual Science.* 1:776-783.

Bok D (1993) The retinal pigment epithelium: a versatile partner in vision. *Journal of Cell Science - Supplement.* 17:189-195.

Boulton M, Marshall J (1985) Repigmentation of human retinal pigment epithelial cells in vitro. *Experimental Eye Research.* 41:209-218.

Boulton M, Marshall J (1986) Effects of increasing numbers of phagocytic inclusions on human retinal pigment epithelial cells in culture: a model for aging. *British Journal of Ophthalmology.* 70:808-815.

Boulton M, McKechnie NM, Breda J, Bayly M, Marshall J (1989) The formation of autofluorescent granules in cultured human RPE. *Investigative Ophthalmology and Visual Science.* 30:82-89.

Boulton M, Docchio F, Dayhaw-Barker P, Ramponi R, Cubeddu R (1990) Age-related changes in the morphology, absorption and fluorescence of melanosomes and lipofuscin granules of the retinal pigment epithelium. *Vision Research.* 30:1291-1303.

Boulton M, Dontsov A, Jarvis-Evans J, Ostrovsky M, Svistunenko D (1993) Lipofuscin is a photoinducible free radical generator. *Journal of Photochemistry and Photobiology B.* 19:201-204.

Boulton M, Marcyniuk B, Moriarty P, Jarvis-Evans J (1994) Regional variation and age-related changes of lysosomal enzymes in the human retinal pigment epithelium. *British Journal of Ophthalmology.* 78:125-129.

Boulton M, Rozanowska M, Rozanowski B (2001) Retinal photodamage. *Journal of Photochemistry and Photobiology B-Biology.* 64:144-161.

Boulton M, Rozanowska M, Rozanowski B, Wess T (2004) The photoreactivity of ocular lipofuscin. *Photochemical & Photobiological Sciences.* 3:759-764.

Brainard GC, Byrne B, Rollag MD, Glickman G, Hanifin JP, Greeson JM, Gerner E (2001) Action spectrum for melatonin regulation in humans: evidence for a novel circadian photoreceptor. *Journal of Neuroscience.* 21:6405-6412.

Brunet S, Kearney P, Bergeron JJM, Thibault P, Gagnon E, Desjardins M (2003) Organelle proteomics: looking at less to see more. *Trends in Cell Biology.* 13:629-638.

Brunk UT, Jones CB, Sohal RS (1992) A novel hypothesis of lipofuscinogenesis and cellular aging based on interactions between oxidative stress and autophagocytosis. *Mutatation Research.* 275:395-403.

Brunk UT, Wihlmark U, Wrigstad A, Roberg K, Nilsson SE (1995) Accumulation of lipofuscin within retinal pigment epithelial cells results in enhanced sensitivity to photooxidation. *Gerontology.* 41:201-211.

Brunk UT, Terman A (2002) Lipofuscin: Mechanisms of age-related accumulation and influence on cell function. *Free Radical Biology and Medicine.* 33:611-619.

Burcham PC, Kuhan YT (1997) Diminished susceptibility to proteolysis after protein modification by the lipid peroxidation product malondialdehyde: Inhibitory role for crosslinked and noncrosslinked adducted proteins. *Archives of Biochemistry and Biophysics.* 340:331-337.

Burke JM, Skumatz CM (1998) Autofluorescent inclusions in long-term postconfluent cultures of retinal pigment epithelium. *Investigative Ophthalmology and Visual Science.* 39:1478-1486.

Cabral L, Unger W, Boulton M, Lightfoot R, McKechnie N, Grierson I, Marshall J (1990) Regional distribution of lysosomal-enzymes in the canine retinal-pigment epithelium. *Investigative Ophthalmology & Visual Science.* 31:670-676.

Cai JY, Nelson KC, Wu M, Sternberg P, Jones DP (2000) Oxidative damage and protection of the RPE. *Progress in Retinal and Eye Research.* 19:205-221.

Cangemi FE (2007) TOZAL Study: an open case control study of an oral antioxidant and omega-3 supplement for dry AMD. *BMC Ophthalmology.* 7:3.

Cantrell A, McGarvey DJ, Roberts J, Sarna T, Truscott TG (2001) Photochemical studies of A2-E. *Journal of Photochemistry and Photobiology B-Biology.* 64:162-165.

Cantrell A, Rancan F, Böhm F, McGarvey DJ, Truscott TG (2003) Singlet oxygen quenching by dietary carotenoids in a model membrane environment. *Archives of Biochemistry and Biophysics.* 412:47-54.

Chen H, Yang X, Ma X, Hau V, Yang Z, Gibbs D, Luo L, Zhao P, Zeng J (2008) Association of HTRA1 polymorphism and bilaterality in advanced age-related macular degeneration. *Vision Research.* 48:690-694.

Choudhary S, Chan LL, Zhang W, Van Kuijk FJGM, Xiao T, Srivastava S, Vergara LA, Ansari NH (2005) Toxicity and detoxification of lipid-derived aldehydes in cultured retinal pigmented epithelial cells. *Toxicology and Applied Pharmacology.* 204:122-134.

Christen WG, Ajani UA, Buring JE, Glynn RJ, Manson JE (1996) A prospective study of cigarette smoking and risk of age-related macular degeneration in men. *JAMA.* 276:1147-1151.

Combadiere C, Feumi C, Raoul W, Keller N, Rodero M, Pezard A, Lavalette S, Houssier M, Jonet L, Picard E, Debre P, Sirinyan M, Deterre P, Ferroukhi T, Cohen SY, Chauvaud D, Jeanny JC, Chemtob S, Behar-Cohen F, Sennlaub F (2007) CX3CR1-dependent subretinal microglia cell accumulation is associated with cardinal features of age-related macular degeneration. *Journal of Clinical Investigation.* 117:2920-2928.

Crabb JW, Miyagi M, Gu XR, Shadrach K, West KA, Sakaguchi H, Kamei M, Hasan A, Yan L, Rayborn ME, Salomon RG, Hollyfield JG (2002) Drusen proteome analysis: An approach to the etiology of age-related macular degeneration. *Proceedings of the National Academy of Sciences of the USA.* 99:14682-14687.

Cruickshanks KJ, Klein R, Klein BE (1993) Sunlight and AMD: The Beaver Dam Study. *Archives of Ophthalmology.* 111:514-518.

Cruickshanks KJ, Nondahl DM, Shetterly SM, Hamman RF, Klein R (1997) The prevalence of age-related maculopathy by geographic region and ethnicity. The Colorado-Wisconsin Study of Age-Related Maculopathy. *Archives of Ophthalmology.* 115:242-250.

Curcio CA, Medeiros NE, Millican CL (1996) Photoreceptor loss in age-related macular degeneration. *Investigative Ophthalmology and Visual Science.* 37:1236-1249.

Dacey DM, Robinson FR, Yau K-W, Smith VC, Liao H-W, Peterson BB, Pokorny J, Gamlin PD (2005) Melanopsin-expressing ganglion cells in primate retina signal colour and irradiance and project to the LGN. *Nature.* 433:749-754.

Dalen H, Saetersdal T, Odegarden S (1987) Some ultrastructural features of the myocardial cells in the hypertrophied human papillary muscle. *Virchows Archievew A Pathology Anatomy & Histopathology.* 410:281-294.

Davies S, Elliott MH, Floor E, Truscot TG, Zareba M, Sarna T, Shamsi FA, Boulton ME (2001) Photocytotoxicity of lipofuscin in human retinal pigment epithelial cells. *Free Radical Biology and Medicine.* 31:256-265.

Defoe DM, Hughes BA, Ahmad A, Chen W (1994) Membrane polarity of the Na(+)-K+ pump in primary cultures of Xenopus retinal pigment epithelium. *Experimental Eye Research.* 59:587-596.

Deguchi J, Moriyama Y, Uyama M, Sugasawa K, Suzuki T, Yamamoto A, Yoshimori T, Futai M, Kato K (1994) Acidification of phagosomes and degradation of rod outer segments in rat retinal pigment epithelium. *Investigative Ophthalmology and Visual Science.* 35:568-579.

Dei R, Nakagomi Y, Yasuda Y, Li M, Inagaki T, Takeda A, Niwa H, Watanabe M, Washimi Y (2002) Lipid peroxidation and advanced glycation end products in the brain in normal aging and in Alzheimer's disease. *Acta Neuropathology.* 104:113-122.

Delori FC, Dorey CK, Staurenghi G, Arend O, Goger DG, Weiter JJ (1995a) In-vivo fluorescence of the ocular fundus exhibits retinal-pigment epithelium lipofuscin characteristics. *Investigative Ophthalmology & Visual Science.* 36:718-729.

Delori FC, Staurenghi G, Arend O, Dorey CK, Goger DG, Weiter JJ (1995b) In-vivo measurement of lipofuscin in Stargardts-disease - Fundus Flavimaculatus. *Investigative Ophthalmology & Visual Science.* 36:2327-2331.

Delori FC, Goger DG, Dorey CK (2001) Age-related accumulation and spatial distribution of lipofuscin in RPE of normal subjects. *Investigative Ophthalmology & Visual Science.* 42:1855-1866.

Dewan A, Liu DTL, Lam DSC, Zhang SS-M, Tam POS, Liu M, Hartman S, Zhao C, Chan WM (2006) HTRA1 promoter polymorphism in wet age-related macular degeneration. *Science.* 314:989-992.

Dillon J, Zheng L, Merriam JC, Gaillard ER (2004) Transmission of light to the aging human retina: possible implications for age related macular degeneration. *Experimental Eye Research.* 79:753-759.

Dingle JT, Lucy JA (1965) Membrane phenomenons in relation to vitamin A. *Proceedings of the Nutrition Society.* 24:170-172.

Docchio F, Boulton M, Cubeddu R, Ramponi R, Barker PD (1991) Age-related changes in the fluorescence of melanin and lipofuscin granules of the retinal pigment epithelium: a time-resolved fluorescence spectroscopy study. *Photochemistry Photobiology.* 54:247-253.

Dolara A, Santoro G, Gori F (1996) Myocardial lipofuscinosis of unknown etiology in a young asymptomatic woman. *Cardiologia.* 41:275-277.

Dorey CK, Garsd A, Weiter JJ, Wu G, Ebenstein D (1989) Cell loss in the aging retina. Relationship to lipofuscin accumulation and macular degeneration. *Investigative Ophthalmology and Visual Science.* 30:1691-1699.

Dorey CK, Delori FC, Akeo K (1990) Growth of cultured RPE and endothelial cells is inhibited by blue light but not green or red light. *Current Eye Research.* 9:549-559.

Dowling JE, Sidman RL (1962) Inherited retinal dystrophy in the rat. *Journal of Cell Biology.* 14:73-109.

Duncan R, Nicholson RI, Vicent MJ, Greco F (2005) Polymer-drug conjugates: towards a novel approach for the treatment of endrocine-related cancer. *Endocrine Related Cancer.* 12Suppl1:S189-199.

Duncan R (2007) Designing polymer conjugates as lysosomotropic nanomedicines. *Biochemical Society Transactions.* 35:56-60.

Duncan R, Vicent MJ, Gilbert HRP, Carbajo RJ (2008) Polymer masked-unmasked protein therapy. 1. Bioresponsive dextrin-trypsin and -melanocyte stimulating hormone conjugates designed for alpha-amylase activation. *Biomacromolecules.* 9:1146-1154.

Dunn KC, Hjelmeland LM, Aotaki-Keen AE, Putkey FR (1996) ARPE-19, a human retinal pigment epithelial cell line with differentiated properties. *Experimental Eye Research.* 62:155-169.

Ebrahem Q, Gu X, Anand-Apte B, Vasanji A, Salomon RG, Renganathan K, Sears J, Lu L, Crabb JW (2006) Carboxyethylpyrrole oxidative protein modifications stimulate neovascularization: Implications for age-related macular degeneration. *Proceedings of the National Acadamy of Sciences of the U S A.* 103:13480-13484.

Edge R, McGarvey DJ, Truscott TG (1997) The carotenoids as anti-oxidants--a review. *Journal of Photochemistry and Photobiology B.* 41:189-200.

Edwards AO, Panhuysen C, Manning A, Ritter R, Abel KJ, Farrer LA (2005) Complement factor H polymorphism and age-related macular degeneration. *Science.* 308:421-424.

El-Remessy AB, Caldwell RW, Franklin T, Behzadian MA, Abou-Mohamed G, Caldwell RB (2003) Experimental diabetes causes breakdown of the blood-retina barrier by a mechanism involving tyrosine nitration and increases in expression of vascular endothelial growth factor and urokinase plasminogen activator receptor. *American Journal of Pathology.* 162:1995-2004.

Eldred G, Katz ML (1988) Fluorophores of the human retinal pigment epithelium: separation and spectral characterization. *Experimental Eye Research.* 47:71-86.

Eldred GE, Katz ML (1989) The Auto-Fluorescent Products of Lipid-Peroxidation May Not Be Lipofuscin-Like. *Free Radical Biology and Medicine.* 7:157-163.

Eldred GE, Katz ML (1991) The lipid peroxidation theory of lipofuscinogenesis cannot yet be confirmed. *Free Radicals Biology and Medicine.* 10:445-447.

Eldred GE, Lasky MR (1993) Retinal age pigments generated by self-assembling lysosomotropic detergents. *Nature.* 361:724-726.

Eldred GE (1998) Lipofuscin and other lysosomal storage deposits in the retinal pigment epithelium. In: *The retinal pigment epithelium* (Marmor MF, Wolfensberger T, eds), pp 651-668: Oxford City Press.

Ernest PH (2004) Light-transmission-spectrum comparison of foldable intraocular lenses. *Journal of Cataract and Refractive Surgery.* 30:1755-1758.

Etienne Schacht LRJVJPRRD (1985) Dextran and Inulin Derivatives of Procainamide. *Annals of the New York Academy of Sciences.* 446:199-212.

Evans JR (2001) Risk Factors for AMD. *Progress in Retinal and Eye Research.*227-253.

Evans JR, Henshaw K (2008) Antioxidant vitamin and mineral supplements for preventing age-related macular degeneration. *Cochrane Database of Systematic Reviews.* 11:CD000253.

Feeney-Burns L, Berman ER, Rothman H (1980) Lipofuscin of human retinal pigment epithelium. *American Journal of Ophthalmology.* 90:783-791.

Feeney-Burns L, Hilderbrand ES, Eldridge S (1984) Aging human RPE: morphometric analysis of macular, equatorial, and peripheral cells. *Investigative Ophthalmology and Visual Science.* 25:195-200.

Feeney -Burns L, Eldred G (1983) The fate of the phagosome: conversion to 'age pigment' and impact in human retinal pigment epithelium. *Transactions of the Ophthalmological Societies of the U K.* 103 416-421. .

Feng W, LaVail M, Vollrath D (2002a) Mertk is directly involved in ingestion of photoreceptor outer segments during RPE phagocytosis. *Investigative Ophthalmology & Visual Science.* 43:U1301-U1301.

Feng W, Yasumura D, Matthes MT, LaVail MM, Vollrath D (2002b) Mertk triggers uptake of photoreceptor outer segments during phagocytosis by cultured retinal pigment epithelial cells. *Journal of Biological Chemistry.* 277:17016-17022.

Finnemann SC, Rodriguez-Boulan E, Bonilha VL, Marmorstein AD (1997) Phagocytosis of rod outer segments by retinal pigment epithelial cells requires alpha(v)beta5 integrin for binding but not for internalization. *Proceedings of the National Acadamy of Sciences of the U S A.* 94:12932-12937.

Finnemann SC (2001) Focal adhesion kinase controls alpha v beta 5 integrin dependent photoreceptor phagocytosis by retinal pigment epithelial cells. *Molecular Biology of the Cell.* 12:458A-458A.

Finnemann SC, Kim YA, Nandrot EF (2003) Effects of beta 5 knockout on mouse RPE function in vivo and in vitro reveal an important role of alpha v beta 5 integrin rectors in phagocytosis by the retinal pigment epithelium. *Investigative Ophthalmology & Visual Science.* 44:U73-U73.

Fisher SK, Pfeffer BA, Anderson DH (1983) Both rod and cone disc shedding are related to light onset in the cat. *Investigative Ophthalmology and Visual Science.* 24:844-856.

Fishkin N, Sparrow JR, Nakanishi K, Jang Y-P, Itagaki Y (2003) A2-rhodopsin: a new fluorophore isolated from photoreceptor outer segments. *Organic Biomolecular Chemistry.* 1:1101-1105.

Fishkin N, Nakanishi K, Berova N, Pescitelli G, Sparrow JR (2004) Absolute configurational determination of an all-trans-retinal dimer isolated from photoreceptor outer segments. *Chirality.* 16:637-641.

Fishkin NE, Nakanishi K, Sparrow JR, Allikmets R (2005) Isolation and characterization of a retinal pigment epithelial cell fluorophore: an all-trans-retinal dimer conjugate. *Proceedings of the National Academy of Sciences U S A.* 102:7091-7096.

Folch J, Lees M, Sloane Stanley GH (1957) A simple method for the isolation and purification of total lipides from animal tissues. *Journal of Biological Chemistry.* 226:497-509.

Francis PJ, Hoh J, Dewan A, Klein ML, Zhang H (2008) Joint effects of polymorphisms in the HTRA1, LOC387715/ARMS2, and CFH genes on AMD in a Caucasian population. *Molecular Vision.* 14:1395-1400.

Fraser-Bell S, Azen SP, Varma R, Hooper C, Wu J, Klein R, Foong AWP (2008) Cardiovascular risk factors and age-related macular degeneration: the Los Angeles Latino Eye Study. *American Journal of Ophthalmology.* 145:308-316.

Fraunfelder FW (2005) Pegaptanib for wet macular degeneration. *Drugs Today (Barc).* 41:703-709.

Frey T (1995) Nucleic acid dyes for detection of apoptosis in live cells. *Cytometry.* 21:265-274.

Fritsche LG, Rivera A, Fisher SA, Weber BHF, Loenhardt T, Janssen A, Keilhauer CN (2008) Age-related macular degeneration is associated with an unstable ARMS2 (LOC387715) mRNA. *Nature Genetics.* 40:892-896.

Gaillard E, Avalle L, Dillon J (2004) The autooxidation of A2E, a component of human retinal lipofuscin. *Investigative Ophthalmology & Visual Science.* 45:U332-U332.

Gaillard ER, Atherton SJ, Eldred G, Dillon J (1995) Photophysical studies on human retinal lipofuscin. *Photochemistry and Photobiology.* 61:448-453.

Garnett MC, Kallinteri P (2006) Nanomedicines and nanotoxicology: some physiological principles. *Occupational Medicine (London).* 56:307-311.

Geiser M, Kreyling W, Heyder J, Schürch S, Semmler M, Rothen-Rutishauser B, Kapp N, Schulz H, Im Hof V (2005) Ultrafine particles cross cellular membranes by nonphagocytic mechanisms in lungs and in cultured cells. *Environmental Health Perspectives.* 113:1555-1560.

Gerth C, Keltner JL, Park SS, Zawadzki RJ, Choi SS, Werner JS (2007) Visualization of lipofuscin accumulation in Stargardt macular dystrophy by high-resolution

Fourier-domain optical coherence tomography. *Archives of Ophthalmology.* 125:575.

Godley BF, Shamsi FA, Liang FQ, Jarrett SG, Davies S, Boulton M (2005) Blue light induces mitochondrial DNA damage and free radical production in epithelial cells. *Journal of Biological Chemistry.* 280:21061-21066.

Gold B, Taiber AJ, Bergeron J, Hancox LS, Cramer K, Merriam JE, Zernant J, Gehrs K, Neel J (2006) Variation in factor B (BF) and complement component 2 (C2) genes is associated with age-related macular degeneration. *Nature Genetics.* 38:458-462.

Gonzalez-Fernandez F, Baer CA, Ghosh D (2007) Module structure of interphotoreceptor retinoid-binding protein (IRBP) may provide bases for its complex role in the visual cycle - structure/function study of Xenopus IRBP. *BMC Biochemistry.* 8:15.

Greenstein VC, Seiple W, Sparrow JR, Holopigian K, Chiosi F, Baker P, Braunstein RE (2007) Scotopic sensitivity and color vision with a blue-light-absorbing intraocular lens. *Journal of Cataract and Refractive Surgery.* 33:667-672.

Gu X, Hollyfield JG, Rayborn ME, Salomon RG, Meer SG, Miyagi M, Crabb JW (2003) Carboxyethylpyrrole protein adducts and autoantibodies, biomarkers for age-related macular degeneration. *Journal of Biological Chemistry.* 278:42027-42035.

Hageman GS, Johnson LV, Anderson DH, Luthert PJ, Victor Chong NH, Mullins RF (2001) An integrated hypothesis that considers drusen as biomarkers of immune-mediated processes at the RPE-Bruch's membrane interface in aging and age-related macular degeneration. *Progressive Retinal Eye Research.* 20:705-732.

Hageman GS, Taiber AJ, Borchardt JD, Hancox LS, Hageman JL, Anderson DH, Johnson LV, Hardisty LI, Stockman HA (2005) A common haplotype in the complement regulatory gene factor H (HF1/CFH) predisposes individuals to age-related macular degeneration. *Proceedings of the National Academy of Sciences U S A.* 102:7227-7232.

Hageman GS, Anderson DH, Richards A, Gehrs KM, Radeke MJ, Hancox LS, Taiber AJ, Johnson LV, Kavanagh D (2006) Extended haplotypes in the complement factor H (CFH) and CFH-related (CFHR) family of genes protect against age-related macular degeneration: characterization, ethnic distribution and evolutionary implications. *Annals of Medicine.* 38:592-604.

Haines JL, Olson LM, Noureddine M, Scott WK, Spencer KL, Hauser MA, Schmidt S, Gallins P, Kwan SY (2005) Complement factor H variant increases the risk of age-related macular degeneration. *Science.* 308:419-421.

Haines JL, Spencer KM, Pericak-Vance MA (2007) Bringing the genetics of macular degeneration into focus. *Proceedings of the National Academy of Sciences U S A.* 104:16725-16726.

Halliwell B, Zhao K, Whiteman M (1999) Nitric oxide and peroxynitrite. The ugly, the uglier and the not so good: a personal view of recent controversies. *Free Radical Research Communications.* 31:651-669.

Halliwell B (2001) Role of free radicals in the neurodegenerative diseases: therapeutic implications for antioxidant treatment. *Drugs Aging.* 18:685-716.

Hanifin JP, Brainard GC (2007) Photoreception for circadian, neuroendocrine, and neurobehavioral regulation. *Journal of Physiological Anthropology.* 26:87-94.

Hankins MW, Peirson SN, Foster RG (2008) Melanopsin: an exciting photopigment. *Trends in Neuroscience.* 31:27-36.

Haralampus-Grynaviski NM, Lamb LE, Simon JD, Krogmeier JR, Dunn RC, Pawlak A, Rozanowska M, Sarna T, Burke JM (2001) Probing the spatial dependence of the emission spectrum of single human retinal lipofuscin granules using near-field scanning optical microscopy. *Photochemistry and Photobiology.* 74:364-368.

Haralampus-Grynaviski NM, Lamb LE, Clancy CMR, Skumatz C, Burke JM, Sarna T, Simon JD (2003) Spectroscopic and morphological studies of human retinal lipofuscin granules. *Proceedings of the National Academy of Sciences USA.* 100:3179-3184.

Hardwicke J, Stephens P, Moseley R, Thomas DW, Ferguson EL, Duncan R (2008) Dextrin-rhEGF conjugates as bioresponsive nanomedicines for wound repair. *Journal of Controlled Release.*

Hashizume K, Noda S, Kurihara T, Shimizu T, Hirasawa M, Imamura Y, Ozawa Y, Shinoda K, Noda K (2008) Retinal dysfunction and progressive retinal cell death in SOD1-deficient mice. *American Journal of Pathology.* 172:1325-1331.

Hayashi K, Hayashi H (2006) Visual function in patients with yellow tinted intraocular lenses compared with vision in patients with non-tinted intraocular lenses. *British Journal of Ophthalmology.* 90:1019-1023.

Hollyfield JG, Bonilha VL, Rayborn ME, Yang XP, Shadrach KG, Lu L, Ufret RL, Salomon RG, Perez VL (2008) Oxidative damage-induced inflammation initiates age-related macular degeneration. *Nature Medicine.* 14:194-198.

Holz FG, Bellman C, Staudt S, Schutt F, Volcker HE (2001) Fundus autofluorescence and development of geographic atrophy in age-related macular degeneration. *Investigative Ophthalmology & Visual Science.* 42:1051-1056.

Holz FG, Kammerer E, Bindewald A, Kopitz J (2004) Effects of lipidperoxidation-related protein modifications on RPE lysosomal functions, ROS phagocytosis and their impact for lipofuscinogenesis. *Investigative Ophthalmology & Visual Science.* 45:U122-U122.

Holz FG, Bindewald-Wittich A, Fleckenstein M, Dreyhaupt J, Scholl HPN, Schmitz-Valckenberg S (2007) Progression of geographic atrophy and impact of fundus autofluorescence patterns in age-related macular degeneration. *American Journal of Ophthalmology.* 143:463-472.

Hoppe G, O'Neil J, Hoff HF, Sears J (2004) Accumulation of oxidized lipid-protein complexes in the RPE impedes phagosome maturation by blocking recruitment of phosphatidylinositol-3-kinase. *Investigative Ophthalmology & Visual Science.* 45:U332-U332.

Hreczuk-Hirst D, Duncan R, Chicco D, German L (2001) Dextrins as potential carriers for drug targeting: tailored rates of dextrin degradation by introduction of pendant groups. *International Journal of Pharmacy.* 230:57-66.

Hubscher SG, Harrison RF (1989) Portal lymphadenopathy associated with lipofuscin in chronic cholestatic liver-disease. *Journal of Clinical Pathology.* 42:1160-1165.

Hyman LG, Fine SL, Lilienfeld AM, Ferris FL (1983) Senile macular degeneration: a case-control study. *American Journal of Epidemiology.* 118:213-227.

Iyer RS, Ghosh S, Salomon RG (1989) Levuglandin E2 crosslinks proteins. *Prostaglandins.* 37:471-480.

Jahngen-Hodge J, Shang F, Abasi H, Nowell TR, Obin MS, Gong X, Taylor A, Gong J, Blumberg J (1997) Regulation of ubiquitin-conjugating enzymes by glutathione following oxidative stress. *Journal of Biological Chemistry.* 272:28218-28226.

Jarrett SG, Boulton ME (2005) Antioxidant up-regulation and increased nuclear DNA protection play key roles in adaptation to oxidative stress in epithelial cells. *Free Radical Biology and Medicine.* 38:1382-1391.

Jellinek D, Janji N, Green LS, Bell C (1994) Inhibition of receptor binding by high-affinity RNA ligands to vascular endothelial growth factor. *Biochemistry.* 33:10450-10456.

Jin M, Sun H, Travis GH, Li S, Moghrabi WN (2005) Rpe65 is the retinoid isomerase in bovine retinal pigment epithelium. *Cell.* 122:449-459.

Jin M, Travis GH, Yuan Q, Li S (2007) Role of LRAT on the retinoid isomerase activity and membrane association of Rpe65. *Journal of Biological Chemistry.* 282:20915-20924.

Johnson D, Lardy H (1967) Isolation of liver and kidney mitichondria. *Methods in Enzymology.* 10:363-371.

Jones AA (2007) Age related macular degeneration--should your patients be taking additional supplements? *Australian Family Physician.* 36:1026-1028.

Journet A, Louwagie M, Luche S, Chapel A, Kieffer S, Garin J (2000) Towards a human repertoire of monocytic lysosomal proteins. *Electrophoresis.* 21:3411-3419.

Journet A, Roux F, Garin J, Chapel A, Kieffer S (2002) Proteomic analysis of human lysosomes: application to monocytic and breast cancer cells. *Proteomics.* 2:1026-1040.

Justilien V, Crabb JW, Lewin AS, Zhan X, Sparrow JR, Pang J-J, Renganathan K, Kim SR, Hauswirth WW (2007) SOD2 knockdown mouse model of early AMD. *Investigative Ophthalmology and Visual Science.* 48:4407-4420.

Kaemmerer E, Schutt F, Krohne TU, Holz FG, Kopitz J (2007) Effects of lipid peroxidation-related protein modifications on RPE lysosomal functions and POS phagocytosis. *Investigative Ophthalmology & Visual Science.* 48:1342-1347.

Kanda A, Brooks M, Abecasis GR, Branham KEH, He S, Chen W, Othman M, Khanna R, Lyons R (2007) A variant of mitochondrial protein LOC387715/ARMS2, not HTRA1, is strongly associated with age-related macular degeneration. *Proceedings of the National Academy of Sciences U S A.* 104:16227-16232.

Kannan R, Spee CK, Hinton DR, Rodriguez A, Zhang N, Sreekumar PG, Barron E (2006) Stimulation of apical and basolateral VEGF-A and VEGF-C secretion by oxidative stress in polarized retinal pigment epithelial cells. *Molecular Vision.* 12:1649-1659.

Kanofsky JR, Sima PD, Richter C (2003) Singlet-oxygen generation from A2E. *Photochemistry and Photobiology.* 77:235-242.

Karan G, Lillo C, Yang Z, Cameron D, Locke K, Zhao Y, Thirumalaichary S, Li C, Birch D, Vollmer-Snarr H, Williams D, Zhang K (2005) Lipofuscin accumulation, abnormal electrophysiology, and photoreceptor degeneration in mutant ELOVL4 transgenic mice: a model for macular degeneration. *Proceedings of the National Acadamy of Sciences USA.* 102:4164-4169.

Katz ML (1985) Factors influencing lipofuscin accumulation in the retinal-pigment epithelium of the eye. *Archives of Biology.* 96:360-360.

Katz ML, Drea CM, Robison WG (1985) Relationship between dietary retinol and lipofuscin in the retinal-pigment epithelium. *Age.* 8:145-145.

Katz ML, Hess HH, Robison WG, Drea CM, Eldred GE (1986) Influence of early photoreceptor degeneration on lipofuscin in the retinal pigment epithelium. *Experimental Eye Research.* 43:561-573.

Katz ML, Eldred GE, Robison WG (1987) Lipofuscin autofluorescence - evidence for vitamin-a involvement in the retina. *Mechanisms of Ageing and Development.* 39:81-&.

Katz ML (1989) Incomplete proteolysis may contribute to lipofuscin accumulation in the retinal pigment epithelium. *Advances in Experimental Medical Biology.* 266:109-116.

Katz ML, Gao CL (1995) Vitamin A incorporation into lipofuscin-like inclusions in the retinal pigment epithelium. *Mechanisms of Ageing and Development.* 84:29-38.

Katz ML, Gao CL, Rice LM (1996) Formation of lipofuscin-like fluorophores by reaction of retinal with photoreceptor outer segments and liposomes. *Mechanisms of Ageing and Development.* 92:159-174.

Katz ML, Redmond TM (2001) Effect of Rpe65 knockout on accumulation of lipofuscin fluorophores in the retinal pigment epithelium. *Investigative Ophthalmology and Visual Science.* 42:3023-3030.

Katz ML (2002) Potential role of retinal pigment epithelial lipofuscin accumulation in age-related macular degeneration. *Archives of Gerontology and Geriatrics.* 34:359-370.

Katz ML, Robison WG (2002) What is lipofuscin? Defining characteristics and differentiation from other autofluoreseent lysosomal storage bodies. *Archives of Gerontology and Geriatrics.* 34:169-184.

Kawasaki A, Kardon RH (2007) Intrinsically photosensitive retinal ganglion cells. *Journal of Neuroophthalmology.* 27:195-204.

Kennedy CJ, Rakoczy P, Constable IJ (1993) Quantifying rod outer segment phagocytosis and digestion and lipofuscin accumulation in cultured human RPE cells. *Investigative Ophthalmology & Visual Science.* 34:867-867.

Kennedy CJ, Papadimitriou JM, Constable IJ, Rakoczy PE, Robertson TA (1994) Kinetic studies on phagocytosis and lysosomal digestion of rod outer segments by human retinal pigment epithelial cells in vitro. *Experimental Cell Research.* 210:209-214.

Kennedy CJ, Rakoczy PE, Constable IJ (1995) Lipofuscin of the retinal pigment epithelium: A review. *Eye.* 9:763-771.

Ketterer B, Meyer DJ (1989) Glutathione transferases: a possible role in the detoxication and repair of DNA and lipid hydroperoxides. *Mutatation Research.* 214:33-40.

Ketterer B (1998) Glutathione S-transferases and prevention of cellular free radical damage. *Free Radical Research Communications.* 28:647-658.

Kim IK, Connolly E, Hafezi-Moghadam A, Lane AM, Husain D, Michaud N, O'Neill CA, Durrani K, Gragoudas ES (2006) Effect of intravitreal injection of ranibizumab in combination with verteporfin PDT on normal primate retina and choroid. *Investigative Ophthalmology and Visual Science.* 47:357-363.

Kim SR, Jang YP, Jockusch S, Fishkin NE, Turro NJ, Sparrow JR (2007) The all-trans-retinal dimer series of lipofuscin pigments in retinal pigment epithelial cells in a recessive Stargardt disease model. *Proceedings of the National Academy of Sciences USA.* 104:19273-19278.

Kiss C, Michels S, Prager F, Geitzenauer W, Schmidt-Erfurth U (2007) Retinal pigment epithelium tears following intravitreal ranibizumab therapy. *Acta Ophthalmologica Scandinavica.* 85:902-903.

Klein R, Klein BE, Jensen SE (1997) The relation of cardiovascular disease and its risk factors to the 5 year incidence of age-related maculopathy: The Beaver Dam study. *Ophthalmology* 1804-1812.

Klein RJ, Sackler RS, Mane SM, Tsai J-Y, Henning AK, Zeiss C, Chew EY, Haynes C, SanGiovanni JP (2005) Complement factor H polymorphism in age-related macular degeneration. *Science.* 308:385-389.

Koeck T, Crabb JW, Stuehr DJ, Levison B, Hazen SL, Aulak KS (2004) Tyrosine nitration impairs mammalian aldolase A activity. *Molecular and Cellular Proteomics.* 3:548-557.

Kopitz J, Kammerer E, Schutt F, Holz FG (2004a) Lipid peroxidation damage contributes to the pathogenesis of age-related macular degeneration. *European Journal of Cell Biology.* 83:95-95.

Kopitz J, Schutt F, Holz FG, Kaemmerer E (2004b) Lipids and lipid peroxidation products in the pathogenesis of age-related macular degeneration. *Biochimie.* 86:825-831.

Kurz T, Terman A, Brunk UT (2007) Autophagy, ageing and apoptosis: the role of oxidative stress and lysosomal iron. *Archives of Biochemistry and Biophysics.* 462:220-230.

Kurz T, Brunk UT, Gustafsson B, Terman A (2008) Lysosomes and oxidative stress in aging and apoptosis. *Biochimica et Biophysica Acta.* 1780:1291-1303.

Lamb LE, Pawlak A, Rozanowska M, Wrona M, Simon JD, Sarna T (2001) The photophysics and aerobic photoreactivity of A2E. *Free Radical Biology and Medicine.* 31:S25-S25.

Lamb LE, Simon JD (2004) A2E: A component of ocular lipofuscin. *Photochemistry and Photobiology.* 79:127-136.

Landers J, Tan TH, Yuen J, Liu H (2007) Comparison of visual function following implantation of Acrysof Natural intraocular lenses with conventional intraocular lenses. *Clinical and Experimental Ophthalmology.* 35:152-159.

LaVail MM (1980) Circadian nature of rod outer segment disc shedding in the rat. *Investigative Ophthalmology and Visual Science.* 19:407-411.

LaVail MM (1983) Outer segment disc shedding and phagocytosis in the outer retina. *Transactions of the Ophthalmological Societies of the U K.* 103(Pt4):397-404.

Leske MC, Nemesure B, Schachat AP, Yang L, Wu S-Y, Hennis A, Hyman L (2006) Nine-year incidence of age-related macular degeneration in the Barbados Eye Studies. *Ophthalmology.* 113:29-35.

Levy J, Klemperer I, Pitchkhadze A, Rand D, Shneck M, Rosen S, Lifshitz T, Weinstein O, Belfair N (2008) Intravitreal bevacizumab (avastin) for subfoveal neovascular age-related macular degeneration. *International Ophthalmology.*

Liu J, Itagaki Y, Ben-Shabat S, Nakanishi K, Sparrow J (2000) The biosynthesis of A2E, a fluorophore of aging retina, involves the formation of the precursor, A2-PE, in the photoreceptor outer segment membrane. *Journal of Biological Chemistry* 275:29354-29360.

Lois N, Hopkins J, Fitzke FW, Owens SL, Coco R, Bird AC (2002) Fundus autofluorescence in patients with age-related macular degeneration and high risk of visual loss. *American Journal of Ophthalmology.* 133:341-349.

Lopez PF, Green WR, Maumenee IH, de la Cruz Z (1990) Autosomal-dominant fundus flavimaculatus. Clinicopathologic correlation. *Ophthalmology.* 97:798-809.

Lu L, Lai H, Campochiaro PA, Hackett SF, Mincey A (2006) Effects of different types of oxidative stress in RPE cells. *Journal of Cell Physiology.* 206:119-125.

Maeda A, Crabb JW, Palczewski K (2005) Microsomal Glutathione S-Transferase 1 in the Retinal Pigment Epithelium: Protection against Oxidative Stress and a Potential Role in Aging. *Biochemistry.* 44:480-489.

Mainster MA (1986) The spectra, classification, and rationale of ultraviolet-protective intraocular lenses. *American Journal of Ophthalmology.* 102:727-732.

Mainster MA (2005) Intraocular lenses should block UV radiation and violet but not blue light. *Archives of Ophthalmology.* 123:550-555.

Mainster MA (2006) Violet and blue light blocking intraocular lenses: photoprotection versus photoreception. *British Journal of Ophthalmology.* 90:784-792.

Margrain TH, Boulton M, Marshall J, Sliney DH (2004) Do blue light filters confer protection against age-related macular degeneration? *Progress in Retinal and Eye Research.* 23:523-531.

Marmor MF (1998) Structure, Function and disease of the retinal pigment epithelium. In: *The retinal pigemnt epithelium*, 1 Edition (Marmor MWT, ed), pp 3-13. New York: Oxford University Press.

Marmorstein A, Marmorstein L, Sakaguchi H, Hollyfield J (2002) Spectral profiling of autofluorescence associated with lipofuscin, Bruch's Membrane, and sub-RPE deposits in normal and AMD eyes. *Investigative Ophthalmology & Visual Science.* 43:2435-2441.

Marmorstein AD, Wang X, Hollyfield JG, Marmorstein LY, Rayborn M, Petrukhin K (2000) Bestrophin, the product of the Best vitelliform macular dystrophy gene (VMD2), localizes to the basolateral plasma membrane of the retinal pigment epithelium. *Proceedings of the National Academy of Sciences USA.* 97:12758-12763.

Marmorstein AD (2001) The polarity of the retinal pigment epithelium. *Traffic.* 2:867-872.

Marshall J (1987) The ageing retina: physiology or pathology. *Eye.* 1(Pt2):282-295.

Marshall J, Cionni RJ, Davison J, Ernest P, Lehmann R, Maxwell A, Solomon K (2005) Clinical results of the blue-light filtering AcrySof Natural foldable acrylic intraocular lens. *Journal of Cataract and Refractive Surgery.* 31:2319-2323.

Mata NL, Weng J, Travis GH (2000) Biosynthesis of a major lipofuscin fluorophore in mice and humans with ABCR-mediated retinal and macular degeneration. *Proceedings of the National Academy of Sciences U S A.* 97:7154-7159.

McGwin G, Xie A, Owsley C (2005) The use of cholesterol-lowering medications and age-related macular degeneration. *Ophthalmology.* 112:488-494.

Melamud A, Stinnett S, Fekrat S (2008) Treatment of neovascular age-related macular degeneration with intravitreal bevacizumab: efficacy of three consecutive monthly injections. *American Journal of Ophthalmology.* 146:91-95.

Meyers SM, Ostrovsky MA, Bonner RF (2004) A model of spectral filtering to reduce photochemical damage in age-related macular degeneration. *Transactions of the American Ophthalmological Society.* 102:83-85.

Miller SS, Steinberg RH (1977) Passive ionic properties of frog retinal pigment epithelium. *Journal Membrane Biology.* 36:337-372.

Moiseyev G, Redmond TM, Oatis J, Crouch RK, Goletz P, Ma J-x (2003) Retinyl esters are the substrate for isomerohydrolase. *Biochemistry.* 42:2229-2238.

Moiseyev G, Wu BX, Ma J-X, Chen Y, Takahashi Y (2005) RPE65 is the isomerohydrolase in the retinoid visual cycle. *Proceedings of the National Academy of Sciences U S A.* 102:12413-12418.

Moore MN, Allen JI, Somerfield PJ (2006) Autophagy: role in surviving environmental stress. *Marine Environmental Research.* 62Suppl:S420-425.

Muftuoglu O, Karel F, Duman R (2007) Effect of a yellow intraocular lens on scotopic vision, glare disability, and blue color perception. *Journal of Cataract and Refractive Surgery.* 33:658-666.

Murthi KK, Salomon RG, Friedman LR, Oleinick NL (1993) Formation of DNA-protein cross-links in mammalian cells by levuglandin E2. *Biochemistry.* 32:4090-4097.

Nandrot EF, Sheppard D, Huang X, Kim Y, Brodie SE, Finnemann SC (2004) Loss of synchronized retinal phagocytosis and age-related blindness in mice lacking alphavbeta5 integrin. *Journal of Experimental Medicine.* 200:1539-1545.

Nandrot EF, Sheppard D, Atabai K, Anand M, Almeida D, Finnemann SC (2007) Essential role for MFG-E8 as ligand for alphavbeta5 integrin in diurnal retinal phagocytosis. *Proceedings of the National Academy of Sciences U S A.* 104:12005-12010.

Newsome DA (1983) Retinal pigmented epithelium culture: current applications. *Transactions of the Ophthalmological Societies of the U K.* 103(Pt4):458-466.

Ng EWM, Cunningham ET, Guyer DR, Shima DT, Calias P, Adamis AP (2006) Pegaptanib, a targeted anti-VEGF aptamer for ocular vascular disease. *Nature Review of Drug Discovery.* 5:123-132.

Ng K-P, Gugiu B, Renganathan K, Davies MW, Gu X, Crabb JS, Kim SR, Rózanowska MB, Bonilha VL, Rayborn ME, Salomon RG, Sparrow JR, Boulton ME, Hollyfield JG, Crabb JW (2008) Retinal pigment epithelium lipofuscin proteomics. *Molecular and Cellular Proteomics.* 7:1397-1405.

Nilsson E, Yin D (1997) Preparation of artificial ceroid/lipofuscin by UV-oxidation of subcellular organelles. *Mechanisms of Ageing and Development.* 99:61-78.

Nilsson SEG, Sundelin SP, Wihlmark U, Brunk UT (2003) Aging of cultured retinal pigment epithelial cells: oxidative reactions, lipofuscin formation and blue light damage. *Documenta Ophthalmologica.* 106:13-16.

Nowak JZ (2006a) Pathogenesis and treatments of age-related macular degeneration (AMD). *Pharmacological Reports.* 58:283-284.

Nowak JZ (2006b) Age-related macular degeneration (AMD): pathogenesis and therapy. *Pharmacological Reports.* 58:353-363.

Ottonello S, Petrucco S, Maraini G (1987) Vitamin A uptake from retinol-binding protein in a cell-free system from pigment epithelial cells of bovine retina. Retinol transfer from plasma retinol-binding protein to cytoplasmic retinol-binding protein with retinyl-ester formation as the intermediate step. *Journal of Biological Chemistry.* 262:3975-3981.

Palczewski K, Crouch RK, Asson-Batres MA, Bredberg DL, Jäger S, Buczyko J, Hofmann KP, Saari JC (1994) Rod outer segment retinol dehydrogenase: substrate specificity and role in phototransduction. *Biochemistry.* 33:13741-13750.

Papermaster DS (1982) Preparation of retinal rod outer segments. *Methods in Enzymology.* 81:48-52.

Parish CA, Hashimoto M, Nakanishi K, Dillon J, Sparrow J (1998) Isolation and one-step preparation of A2E and iso-A2E, fluorophores from human retinal pigment epithelium. *Proceedings of the National Academy of Sciences of the USA.* 95:14609-14613.

Pawlak A, Wrona M, Rozanowska M, Zareba M, Lamb LE, Roberts JE, Simon JD, Sarna T (2003) Comparison of the aerobic photoreactivity of A2E with its precursor retinal. *Photochemistry and Photobiology.* 77:253-258.

Petrukhin K, Xie G, Holmgren G, Li W, Sandgren O, Koisti MJ, Bakall B, Marknell T, Forsman K (1998) Identification of the gene responsible for Best macular dystrophy. *Nature Genetics.* 19:241-247.

Pfeffer BA, Bok D, Clark VM, Flannery JG (1986) Membrane receptors for retinol-binding protein in cultured human retinal pigment epithelium. *Investigative Ophthalmology and Visual Science.* 27:1031-1040.

Philp NJ, Yoon H, Grollman EF (1998) Monocarboxylate transporter MCT1 is located in the apical membrane and MCT3 in the basal membrane of rat RPE. *American Journal of Physiology-Cell Physiology.* 274:R1824-1828.

Pieramici DJ, Rabena MD (2008) Anti-VEGF therapy: comparison of current and future agents. *Eye.* 28:976-980.

Poliakov E, Mesaros C, Salomon RG, Meer SG, Roy SC (2004) Iso[7]LGD2-protein adducts are abundant in vivo and free radical-induced oxidation of an arachidonyl phospholipid generates this D series isolevuglandin in vitro. *Chemical Research in Toxicology.* 17:613-622.

Pollack A, Oliver M, Marcovich A, Bukelman A (1996) Age-related macular degeneration after extracapsular cataract extraction with intraocular lens implantation. *Ophthalmology.* 103:1546-1554.

Pons A, Delgado D, Campos J (2007) Determination of the action spectrum of the blue-light hazard for different intraocular lenses. *Journal of the Optical Society of America a-Optics Image Science and Vision.* 24:1545-1550.

Quiram PA, Hassan TS, Williams GA (2007) Treatment of naïve lesions in neovascular age-related macular degeneration with pegaptanib. *Retina.* 27:851-856.

Rakoczy P, Sarks S, Daw N, Constable I (1999) Distribution of cathepsin D in human eyes with or without age-related maculopathy. *Experimental Eye Research.* 69:367-374.

Rakoczy PE, Di Grandi S, Fitton JH, Lai CM, Baines M, Constable IJ (1997) Modulation of cathepsin D activity in retinal pigment epithelial cells. *Biochemical Journal.* 324(Pt3):935-940.

Rakoczy PE, Barnett NL, Lai C-M, Papadimitriou J, Zhang D, Robertson T, Constable IJ (2002) Progressive age-related changes similar to age-related macular degeneration in a transgenic mouse model. *American Journal of Pathology.* 161:1515-1524.

Rando RR (2001) The biochemistry of the visual cycle. *Chemical Review.* 101:1881-1896.

Richardson SCW, Deacon SPE, Piper RC, Davies MW, Wallom K-L, Ferguson EL, Powell AJ, Duncan R (2008) The use of fluorescence microscopy to define polymer localisation to the late endocytic compartments in cells that are targets for drug delivery. *Journal of Controlled Release.* 127:1-11.

Rivera A, Lichtner P, Keilhauer CN, Weber BHF, Fisher SA, Fritsche LG, Meitinger T (2005) Hypothetical LOC387715 is a second major susceptibility gene for age-related macular degeneration, contributing independently of complement factor H to disease risk. *Human Molecular Genetics.* 14:3227-3236.

Roberts JE, Kukielczak BM, Hu DN, Miller DS, Bilski P, Sik RH, Motten AG, Chignell CF (2002) The role of A2E in prevention or enhancement of light damage in human retinal pigment epithelial cells. *Photochemistry and Photobiology.* 75:184-190.

Robison WG, Kuwabara T, Bieri JG (1980) Deficiencies of vitamins E and A in the rat. Retinal damage and lipofuscin accumulation. *Investigative Ophthalmology and Visual Science.* 19:1030-1037.

Rosenthal FS, Emmett EA, Strickland PT, West SK, Munoz B, Taylor HR (1991) Ocular and facial skin exposure to ultraviolet radiation in sunlight: a personal exposure model with application to a worker population. *Health Physics.* 61:77-86.

Rozanowska M, Jarvis-Evans J, Korytowski W, Boulton ME, Burke JM, Sarna T (1995) Blue light-induced reactivity of retinal age pigment. In vitro generation of oxygen-reactive species. *Journal of Biological Chemistry.* 270:18825-18830.

Rozanowska M, Boulton M, Korytowski W, Sarna T (1997) Photo-induced lipid peroxidation mediated by RPE lipofuscin. *Investigative Ophthalmology & Visual Science.* 38:4809-4809.

Rozanowska M, Wessels J, Boulton M, Burke JM, Rodgers MA, Truscott TG, Sarna T (1998) Blue light-induced singlet oxygen generation by retinal lipofuscin in non-polar media. *Free Radical Biology and Medicine.* 24:1107-1112.

Rozanowska M, Pawlak A, Rozanowski B, Skumatz C, Zareba M, Boulton ME, Burke JM, Sarna T, Simon JD (2004) Age-related changes in the photoreactivity of retinal lipofuscin granules: Role of chloroform-insoluble components. *Investigative Ophthalmology & Visual Science.* 45:1052-1060.

Rozanowska MB, Pawlak A, Rozanowska B, Boulton M, Burke JM, Sarna T, Simon J (2002) Role of chloroform soluble and insoluble components in photoreactivity of RPE lipofuscin. *Investigative Ophthalmology & Visual Science.* 43:U148-U148.

Rudolf M, Schmidt-Erfurth U, Ivandic B, Winkler J (2004) Accumulation of lipid particles in Bruch's membrane of LDL receptor knockout mice as a model of age-related macular degeneration. *Ophthalmology.* 101:715-719.

Salinas AE, Wong MG (1999) Glutathione S-transferases--a review. *Current Medicinal Chemistry.* 6:279-309.

Salomon RG, Schreiber MJ, Hazen SL, Sprecher DL, Penn MS, Batyreva E, Kaur K, Crabb JW, DiCorletoe AM (2000) Isolevuglandin-protein adducts in humans: products of free radical-induced lipid oxidation through the isoprostane pathway. *Biochimica et Biophysica Acta.* 1485:225-235.

Salomon RG (2005) Levuglandins and isolevuglandins: Stealthy toxins of oxidative injury. *Antioxidants & Redox Signaling.* 7:185-201.

SanGiovanni JP, Gensler G, Sperduto RD, Ferris FL, Milton RC, Chew EY, Clemons TE, Lindblad AS, Seddon JM (2007) The relationship of dietary carotenoid and vitamin A, E, and C intake with age-related macular degeneration in a case-control study: AREDS Report No. 22. *Archives of Ophthalmology.* 125:1225-1232.

Schacht E, Ruys L, Vermeersch J, Remon JP, Duncan R (1985) Use of polysaccharides as drug carriers. Dextran and inulin derivatives of procainamide. *Annals of the New York Academy of Sciences.* 446:199-212.

Schmidt-Erfurth U, Beckendorf A, Michels S, Schlötzer-Schrehard U, Cursiefen C, Naumann GOH (2003) Influence of photodynamic therapy on expression of vascular endothelial growth factor (VEGF), VEGF receptor 3, and pigment epithelium-derived factor. *Investigative Ophthalmology and Visual Science.* 44:4473-4480.

Schmitz-Valckenberg S, Bindewald-Wittich A, Dolar-Szczasny J, Dreyhaupt J, Wolf S, Scholl HPN, Holz FG (2006) Correlation between the area of increased autofluorescence surrounding geographic atrophy and disease progression in patients with AMD. *Investigative Ophthalmology & Visual Science.* 47:2648-2654.

Schutt F, Davies S, Kopitz J, Holz FG, Boulton ME (2000) Photodamage to human RPE cells by A2-E, a retinoid component of lipofuscin. *Investigative Ophthalmology & Visual Science.* 41:2303-2308.

Schutt F, Bergmann M, Holz FG, Kopitz J (2001) Effects of a major lipofuscin fluorophore, A2E, on the integrity of various membranes in human RPE cells. *Investigative Ophthalmology & Visual Science.* 42:S943-S943.

Schutt F, Holz FG, Bergmann M, Kopitz J (2002) Effect of A2-E on phagocytic capacity of human RPE-cells. *Investigative Ophthalmology & Visual Science.* 43:U600-U600.

Schutt F, Ueberle B, Schnolzer M, Holz FG, Kopitz J (2002a) Proteome analysis of lipofuscin in human retinal pigment epithelial cells. *Febs Letters.* 528:217-221.

Schutt F, Bergmann M, Holz FG, Kopitz J (2003a) Proteins modified by malondialdehyde, 4-hydroxynonenal, or advanced glycation end products in lipofuscin of human retinal pigment epithelium. *Investigative Ophthalmology & Visual Science.* 44:3663-3668.

Schutt F, Ueberle B, Schnoelzer M, Kopitz J, Holz R (2003b) Proteome analysis of lipofuscin and detection of posttranslational protein modifications in human retinal pigment epithelial cells. *Investigative Ophthalmology & Visual Science.* 44:U125-U125.

Schutt F, Bergmann M, Holz FG, Dithmar S, Volcker HE, Kopitz J (2007a) Accumulation of A2-E in mitochondrial membranes of cultured RPE cells. *Graefes Archive for Clinical and Experimental Ophthalmology.* 245:391-398.

Schutt F, Volcker HE, Dithmar S (2007b) N-acetylcysteine improves lysosomal function and enhances the degradation of photoreceptor outer segments in cultured RPE cells. *Klinische Monatsblatter Fur Augenheilkunde.* 224:580-584.

Seddon JM, Blair N, Haller J, Hiller R, Farber MD, Ajani UA, Sperduto RD, Burton TC, Gragoudas ES (1994) Dietary carotenoids, vitamins A, C, and E, and advanced age-related macular degeneration. Eye Disease Case-Control Study Group. *JAMA.* 272:1413-1420.

Seddon JM (2007) Multivitamin-multimineral supplements and eye disease: age-related macular degeneration and cataract. *American Journal of Clinical Nutrition.* 85:304S.

Shamsi F, McCarroll L, Hemingway J, Boulton M (2001) Effect of lipofuscin on expression and activity of lysosomal enzymes in the retinal pigment epithelium. *Free Radical Biology and Medicine.* 31:S97-S97.

Shang F, Taylor A (1995) Oxidative stress and recovery from oxidative stress are associated with altered ubiquitin conjugating and proteolytic activities in bovine lens epithelial cells. *Biochemical Journal.* 307(Pt1):297-303.

Shang F, Taylor A (2004) Function of the ubiquitin proteolytic pathway in the eye. *Experimental Eye Research.* 78:1-14.

Shepherd VL, Tarnowski BI, McLaughlin BJ (1991) Isolation and characterization of a mannose receptor from human pigment epithelium. *Investigative Ophthalmology and Visual Science.* 32:1779-1784.

Simon JD, Haralampus-Grynaviski NM, Lamb LE, Rozanowska M, Sarna T, Burke JM (2002) Examination of individual RPE lipofuscin granules as a function of donor age using optical and spatial microscopy. *Investigative Ophthalmology & Visual Science.* 43:U1299-U1299.

Singhal SS, Pandya U, Awasthi S, Jin GF, Godley BF, Chandra A, Saini MK, Awasthi YC (1999) Induction of glutathione S-transferase hGST 5.8 is an early response to oxidative stress in RPE cells. *Investigative Ophthalmology and Visual Science.* 40:2652-2659.

Snodderly DM (1995) Evidence for protection against age-related macular degeneration by carotenoids and antioxidant vitamins. *American Journal of Clinical Nutrition.* 62:1448S.

Solbach U, Wolf S, Keilhauer C, Knabben H (1997) Imaging of retinal autofluorescence in patients with age-related macular degeneration. *Retina.* 17:385-389.

Spaide RF (2003) Fundus autofluorescence and age-related macular degeneration. *Ophthalmology.* 110:392-399.

Sparrow JR, Parish C, Hashimoto M, Liu J, Nakanishi K (1999) The lipofuscin component A2-E: Effects on retinal pigmented epithelial (RPE) cells in culture. *Investigative Ophthalmology & Visual Science.* 40:S927-S927.

Sparrow JR, Parish C, Nakanishi K (2000) The lipofuscin fluorophore, A2E, mediates blue light-induced damage to retinal pigment epithelial (RPE) cells in culture. *Investigative Ophthalmology & Visual Science.* 41:S145-S145.

Sparrow JR, Cai B (2001) Blue light induced apoptosis of A2E-containing RPE: Involvement of caspase-3 and protection by Bcl-2. *Investigative Ophthalmology & Visual Science.* 42:S943-S943.

Sparrow JR, Zhou J, Ben-Shabat S, Vollmer H, Itagaki Y, Nakanishi K (2002) Involvement of oxidative mechanisms in blue-light-induced damage to A2E-laden RPE. *Investigative Ophthalmology & Visual Science.* 43:1222-1227.

Sparrow JR, Cai BL, Fishkin N, Jang YP, Krane S, Vollmer HR, Zhou JL, Nakanishi K (2003a) A2E, a fluorophore of RPE lipofuscin: Can it cause RPE degeneration? In: *Retinal Degenerations: Mechanisms and Experimental Therapy*, pp 205-211.

Sparrow JR, Fishkin N, Zhou JL, Cai BL, Jang YP, Krane S, Itagaki Y, Nakanishi K (2003b) A2E, a byproduct of the visual cycle. *Vision Research.* 43:2983-2990.

Sparrow JR, Vollmer-Snarr HR, Zhou JL, Jang YP, Jockusch S, Itagaki Y, Nakanishi K (2003c) A2E-epoxides damage DNA in retinal pigment epithelial cells - Vitamin E and other antioxidants inhibit A2E-epoxide formation. *Journal of Biological Chemistry.* 278:18207-18213.

Sparrow JR, Miller AS, Zhou JL (2004) Blue light-absorbing intraocular lens and retinal pigment epithelium protection in vitro. *Journal of Cataract and Refractive Surgery.* 30:873-878.

Sparrow JR, Boulton M (2005) RPE lipofuscin and its role in retinal-pathobiology. *Experimental Eye Research.* 80:595-606.

Stamer WD, Jaffe GJ, McKay BS, Bok D, Hu J (2003) Aquaporin-1 channels in human retinal pigment epithelium: role in transepithelial water movement. *Investigative Ophthalmology and Visual Science.* 44:2803-2808.

Starita C, Hussain AA, Marshall J (1995) Decreasing hydraulic conductivity of Bruch's membrane: relevance to photoreceptor survival and lipofuscinoses. *American Journal of Medical Genetics.* 57:235-237

Sternberg P, Hagen TM, Reed RL, Davidson PC, Jones DP, Drews-Botsch C (1993) Protection of retinal pigment epithelium from oxidative injury by glutathione and precursors. *Investigative Ophthalmology and Visual Science.* 34:3661-3668.

Strauss O (2005) The retinal pigment epithelium in visual function. *Physiological Reviews.* 85:845-881.

Sugano E, Isago H, Tamai M, Tomita H, Ishiguro S-i (2006) Nitric oxide-induced accumulation of lipofuscin-like materials is caused by inhibition of cathepsin S. *Current Eye Research.* 31:607-616.

Sun H, Molday RS, Nathans J (1999) Retinal stimulates ATP hydrolysis by purified and reconstituted ABCR, the photoreceptor-specific ATP-binding cassette transporter responsible for Stargardt disease. *Journal of Biological Chemistry.* 274:8269-8281.

Sun H, Nathans J (2001) Mechanistic studies of ABCR, the ABC transporter in photoreceptor outer segments responsible for autosomal recessive Stargardt disease. *Journal of Bioenergy and Biomembranes.* 33:523-530.

Sun MJ, Finnemann SC, Febbraio M, Shan L, Annangudi SP, Podrez EA, Hoppe G, Darrow R, Organisciak DT, Salomon RG, Silverstein RL, Hazen SL (2006) Light-induced oxidation of photoreceptor outer segment phospholipids generates ligands for CD36-mediated phagocytosis by retinal pigment epithelium - A potential mechanism for modulating outer segment phagocytosis under oxidant stress conditons. *Journal of Biological Chemistry.* 281:4222-4230.

Sundelin SP, Nilsson SE (2001) Lipofuscin-formation in retinal pigment epithelial cells is reduced by antioxidants. *Free Radical Biology and Medicine.* 31:217-225.

Szende B, Lapis K, Timar J, Schaff Z, Simon K, Jeney A, Divald A, Paku S, Timar F (1988) Glycosaminoglycan containing fat-storing cells in hepatic fibrogenesis. *Acta Morphologica Hungarica.* 36:241-251.

Szweda LI (1994) Age-related increase in liver retinyl palmitate. Relationship to lipofuscin. *Journal of Biological Chemistry.* 269:8712-8715.

Tan JSL, Rochtchina E, Smith W, Wang JJ, Flood V, Mitchell P (2008) Dietary antioxidants and the long-term incidence of age-related macular degeneration: the Blue Mountains Eye Study. *Ophthalmology.* 115:334-341.

Tanito M, Anderson RE, Elliott MH, Kotake Y (2005) Protein modifications by 4-hydroxynonenal and 4-hydroxyhexenal in light-exposed rat retina. *Investigative Ophthalmology and Visual Science.* 46:3859-3868.

Tanito M, Singh AK, Matsumoto H, Haniu H, Elliott MH, Anderson RE (2006) Identification of 4-hydroxynonenal-modified retinal proteins induced by photooxidative stress prior to retinal degeneration. *Free Radical Biology and Medicine.* 41:1847-1859.

Tarnowski BI, Shepherd VL, McLaughlin BJ (1988) Expression of mannose receptors for pinocytosis and phagocytosis on rat retinal pigment epithelium. *Investigative Ophthalmology and Visual Science.* 29:742-748.

Taylor HR, Bressler NM, Bressler SB, Muñoz B, West S, Rosenthal FS (1990) Visible light and risk of age-related macular degeneration. *Transactions of the American Ophthalmological Society.* 88:163-168.

Terman A, Brunk UT (2006) Oxidative stress, accumulation of biological 'garbage', and aging. *Antioxidant Redox Signalling.* 8:197-204.

Terman A, Gustafsson B, Brunk UT (2006) Mitochondrial damage and intralysosomal degradation in cellular aging. *Molecular Aspects of Medicine.* 27:471-482.

Terman A, Gustafsson B, Brunk UT (2007) Autophagy, organelles and ageing. *Journal of Pathology.* 211:134-143.

Thompson DA, Gal A (2003) Vitamin A metabolism in the retinal pigment epithelium: genes, mutations, and diseases. *Progress in Retinal and Eye Research.* 22:683-703.

Tirouvanziam R, Herzenberg LA, Moss RB, Conrad CK, Bottiglieri T, Herzenberg LA (2006) High-dose oral N-acetylcysteine, a glutathione prodrug, modulates inflammation in cystic fibrosis. *Proceedings of the National Academy of Sciences U S A.* 103:4628-4633.

Traboulsi EI (2005) The challenges and surprises of studying the genetics of age-related macular degeneration. *American Journal of Ophthalmology.* 139:908-911.

Tuo J, Bojanowski CM, Chan C-C (2004) Genetic factors of age-related macular degeneration. *Progressive Retinal Eye Research.* 23:229-249.

van de Kraats J, van Norren D (2007) Sharp cutoff filters in intraocular lenses optimize the balance between light reception and light protection. *Journal of Cataract and Refractive Surgery.* 33:879-887.

van den Berg TJ, Spekreijse H (1997) Near infrared light absorption in the human eye media. *Vision Research.* 37:249-253.

van der Schaft TL, Mulder PG, Pameyer JH, Mooy CM, de Bruijn WC, de Jong PT (1994) Increased prevalence of disciform macular degeneration after cataract extraction with implantation of an intraocular lens. *British Journal of Ophthalmology.* 78:441-445.

van Deurs B, Peterson OW, Olsnes S, Sandvig K (1989) The Ways of Endocytosis. *International Review of Cytology.* 131-177.

Verco SJ, Rodgers KE, Roda N, Peers EM, Brown CB, diZerega G (2000) Development of a novel glucose polymer solution (icodextrin) for adhesion prevention: pre-clinical studies. *Human Reproduction.* 15:1764-1772.

Wabbels B, Wegscheider E, Preising MN, Demmler A, Paunescu K, Lorenz B (2006) Fundus autofluorescence in children and teenagers with hereditary retinal diseases. *Graefes Archive of Clinical and Experimental Ophthalmology.* 244:36-45.

Wang N, Wiegand RD, Anderson RE (1992) Uptake of 22-carbon fatty acids into rat retina and brain. *Exprimental Eye Research.* 54:933-939.

Warburton S, Southwick K, Hardman RM, Secrest AM, Grow RK, Xin HJ, Woolley AT, Burton GF, Thulin CD (2005) Examining the proteins of functional retinal lipofuscin using proteomic analysis as a guide for understanding its origin. *Molecular Vision.* 11:1122-1134.

Wassell J, Boulton M (1997) A role for vitamin A in the formation of ocular lipofuscin. *British Journal of Ophthalmology.* 81:911-918.

Wassell J, Davies S, Bardsley W, Boulton M (1999) The photoreactivity of the retinal age pigment lipofuscin. *Journal of Biological Chemistry.* 274:23828-23832.

Wautier JL, Schmidt AM (2004) Protein glycation - A firm link to endothelial cell dysfunction. *Circulation Research.* 95:233-238.

Weale RA (1988) Age and the transmittance of the human crystalline lens. *Journal of Physiological Anthropology.* 395:577-587.

West S, Muñoz B, Bressler NM, Muller D, Vitale S, Hallfrisch J, Bressler S (1994) Are antioxidants or supplements protective for age-related macular degeneration? *Archives of Ophthalmology.* 112:222-227.

Wihlmark U, Wrigstad A, Roberg K, Brunk UT, Nilsson SEG (1996a) Formation of lipofuscin in cultured retinal pigment epithelial cells exposed to pre-oxidized photoreceptor outer segments. *Apmis.* 104:272-279.

Wihlmark U, Wrigstad A, Roberg K, Brunk UT, Nilsson SEG (1996b) Lipofuscin formation in cultured retinal pigment epithelial cells exposed to photoreceptor outer segment material under different oxygen concentrations. *Apmis.* 104:265-271.

Wihlmark U, Wrigstad A, Roberg K, Nilsson SEG, Brunk UT (1997) Lipofuscin accumulation in cultured retinal pigment epithelial cells causes enhanced sensitivity to blue light irradiation. *Free Radical Biology and Medicine.* 22:1229-1234.

Winkler B, Boulton M, Gottsch J, Sternberg P (1999) Oxidative damage and age-related macular degeneration. *Molecular Vision.* 5.

Yanagi Y, Inoue Y, Iriyama A, Jang WD (2006) Effects of yellow intraocular lenses on light-induced upregulation of vascular endothelial growth factor. *Journal of Cataract and Refractive Surgery.* 32:1540-1544.

Yang Z, Gibbs D, Pearson E, Tong Z, Chen H, Camp NJ, Sun H, Cameron DJ, Zhao Y (2006) A variant of the HTRA1 gene increases susceptibility to age-related macular degeneration. *Science.* 314:992-993.

Yin DZ (1992) Lipofuscin-like fluorophores can result from reactions between oxidized ascorbic acid and glutamine. Carbonyl-protein cross-linking may represent a common reaction in oxygen radical and glycosylation-related ageing processes. *Mechanisms of Ageing and Development.* 62:35-45.

Yin DZ, Yuan XM, Brunk UT (1995) Test-Tube Simulated Lipofuscinogenesis - Effect of Oxidative Stress on Autophagocytotic Degradation. *Mechanisms of Ageing and Development.* 81:37-50.

Yin DZ (1996) Biochemical basis of lipofuscin, ceroid, and age pigment-like fluorophores. *Free Radical Biology and Medicine.* 21:871-888.

Young R (1967) The renewal of photoreceptor cell outer segments. *Journal of Cell Biology.* 33:61-72.

Yu K, Xiao Q, Cui G, Lee A, Hartzell HC (2000) The Bests' Disease-linked Cl- Channel hBest1 Regulates Ca V 1 (L-type) Ca2+ Channels Via src-homology-binding domains *Proceedings of the National Academy of Sciences USA.* 23:12758-12763.

Zaidi FH, Wulff K, Brainard GC, Aeschbach D, Hull JT, Peirson SN, Rizzo JF, Gooley JJ, Gregory-Evans K (2007) Short-wavelength light sensitivity of circadian, pupillary, and visual awareness in humans lacking an outer retina. *Current Biology.* 17:2122-2128.

Zamora R, Hidalgo FJ (2001) Inhibition of proteolysis in oxidized lipid-damaged proteins. *Journal of Agricultiral Food Chemistry.* 49:6006-6011.

Zhao L, Sweet BV (2008) Lutein and zeaxanthin for macular degeneration. *American Journal of Health-System Pharmacy.* 65:1232-1238.

Zhou JL, Cai BL, Jang YP, Pachydaki S, Schmidt AM, Sparrow JR (2005) Mechanisms for the induction of HNE- MDA- and AGE-adducts, RAGE and VEGF in retinal pigment epithelial cells. *Experimental Eye Research.* 80:567-580.

Zhou JL, Jang YP, Kim SR, Sparrow JR (2006) Complement activation by photooxidation products of A2E, a lipofuscin constituent of the retinal pigment epithelium. *Proceedings of the National Academy of Sciences USA.* 103:16182-16187.

Appendices

Appendix 1

A.1.1 Phototoxicity of retinal lipofuscin

ANOVA result obtained from the results of the analysis of the determination of the phototoxicity of crude and washed retinal lipofuscin:
$p = <0.000001$.
The result is only significant if the p-value is less than 0.05

Post Hoc test using Tukey analysis

	Dark Control crude LF	Dark control washed LF	Light exposed no LF	Light exposed crude LF	Light exposed washed LF
Dark Control no LF	0.844575	0.934132	0.750515	<0.000001	<0.000001
Dark Control crude LF		0.427568	0.999968	<0.000001	<0.000001
Dark control washed LF			0.345919	<0.000001	<0.000001
Light exposed no LF				<0.000001	<0.000001
Light exposed crude LF					0.978901

The result is only significant if the p-value is less than 0.05. Those not significant have been highlighted in grey.
Table A.1 Statistical analysis of a comparison of the phototoxicity of crude and washed retinal lipofuscin. p-values displayed in this table relate to data displayed in Figure 3.5.

A.1.2 Identification of proteins present in crude retinal lipofuscin preparations

Swiss Prot Accession	Protein[a]	Calc. Mass[b] (KD)
P11488	Guanine nucleotide-binding protein G(t), alpha-1 subunit	40
P68871	Hemoglobin subunit beta	16
P68371	Tubulin beta-2C chain	50
P04406	Glyceraldehyde-3-phosphate dehydrogenase	36
P12277	Creatine kinase B-type	43
P12271	Cellular retinaldehyde-binding protein	36
P68363	Tubulin alpha-1B chain	50
P08100	Rhodopsin 39	35
P60709	Actin, cytoplasmic 1	42
P14618	Pyruvate kinase isozymes M1/M2	58
Q71U36	Tubulin alpha-1A chain	50
P62873	Guanine nucleotide-binding protein G(I)/G(S)/G(T) subunit beta 1	37
Q16518	Retinal pigment epithelium-specific 65 kDa protein	61
P06733	Alpha-enolase	47
P25705	ATP synthase subunit alpha, mitochondrial	60
P10745	Interphotoreceptor retinoid-binding protein	135
Q9BQE3	Tubulin alpha-1C chain	50
Q9BVA1	Tubulin beta-2B chain	50
P00505	Aspartate aminotransferase, mitochondrial	47
P07195	L-lactate dehydrogenase B chain	37
P07437	Tubulin beta chain	50
P05091	Aldehyde dehydrogenase, mitochondrial	56
P01009	Alpha-1-antitrypsin	47
Q16555	Dihydropyrimidinase-related protein 2	62
P09211	Glutathione S-transferase P	23
P11142	Heat shock cognate 71 kDa protein	71
P07900	Heat shock protein HSP 90-alpha	85
P69905	Hemoglobin subunit alpha	15
P01871	Ig mu chain C region	50
P00338	L-lactate dehydrogenase A chain	37
P10523	S-arrestin	45
P22695	Ubiquinol-cytochrome-c reductase complex core protein 2	48
Q92781	11-cis retinol dehydrogenase	35
P63104	14-3-3 protein zeta/delta	28
P09543	2',3'-cyclic-nucleotide 3'-phosphodiesterase	48
P10809	60 kDa heat shock protein, mitochondrial	61
P24752	Acetyl-CoA acetyltransferase, mitochondrial	45
Q99798	Aconitate hydratase, mitochondrial	85
P63261	Actin, cytoplasmic 2	42
O43707	Alpha-actinin-4	105
Q96NY7	Chloride intracellular channel 6	73

Table A.2 Identification of proteins isolated from crude retinal lipofuscin preparations after SDS-PAGE.

Swiss Prot Accession	Protein[a]	Calc.Mass[b] (KD)
Q00610	Clathrin heavy chain 1	191
P09622	Dihydrolipoyl dehydrogenase, mitochondrial	54
P49411	Elongation factor Tu, mitochondrial	50
P09104	Gamma-enolase	47
P06396	Gelsolin	86
P06744	Glucose-6-phosphate isomerase	63
P00367	Glutamate dehydrogenase 1, mitochondrial	61
P09471	Guanine nucleotide-binding protein G(o) subunit alpha 1	40
P08107	Heat shock 70 kDa protein 1	70
P19367	Hexokinase-1	102
P01876	Ig alpha-1 chain C region	38
P01857	Ig gamma-1 chain C region	36
P01834	Ig kappa chain C region	12
P40926	Malate dehydrogenase, mitochondrial	36
P28331	NADH-ubiquinone oxidoreductase 75 kDa subunit, mitochondrial	79
P23942	Peripherin-2	39
P30086	Phosphatidylethanolamine-binding protein 1	21
P00558	Phosphoglycerate kinase 1	45
P35243	Recoverin	23
Q02846	Retinal guanylyl cyclase 1	120
Q8TC12	Retinol dehydrogenase 11	35
P16499	Rod cGMP-specific 3',5'-cyclic phosphodiesterase subunit alpha	100
P35913	Rod cGMP-specific 3',5'-cyclic phosphodiesterase subunit beta	98
Q5TZA2	Rootletin	228
P02768	Serum albumin	69
Q9BT40	Skeletal muscle and kidney-enriched inositol phosphatase	51
P05023	Sodium/potassium-transporting ATPase subunit alpha-1	113
Q01082	Spectrin beta chain, brain 1	274
P38646	Stress-70 protein, mitochondrial	74
P29401	Transketolase	68
P40939	Trifunctional enzyme subunit alpha, mitochondrial	83
P60174	Triosephosphate isomerase	27
P38606	Vacuolar ATP synthase catalytic subunit A	68
P21281	Vacuolar ATP synthase subunit B, brain isoform	56
P49748	Very long-chain specific acyl-CoA dehydrogenase, mitochondrial	70

a. Proteins were identified by LC MS/MS following SDS-PAGE fractionation of crude lipofuscin preparation 1
b. Calculated mass based on sequence

Table A.2 Identification of proteins isolated from crude retinal lipofuscin preparations after SDS-PAGE (continued).

Accession[a]	Protein[b]	Calc Mass[c] (kD)	Peptide Matches
P07437	Tubulin beta	49.6	60
P05023	Na/K - transporting ATPase	112.8	43
P08100	Rhodopsin	38.9	41
P04406	Glyceraldehyde-3-phosphate dehydrogenase	36	35
P11488	Guanine nucleotide-binding protein	40	35
Q9BQE3	Tubulin alpha	49.9	29
P60709	Actin	41.7	27
P68871	Hemoglobin subunit beta	16	27
P14618	Pyruvate kinase isozymes M1/M2	57.9	23
P07339	Cathepsin D precursor	44.5	21
P60201	Myelin proteolipid protein	30.1	19
P02768	Serum albumin precursor	69.3	15
P12271	Cellular retinaldehyde-binding protein	36.5	14
P09543	2',3'-cyclic-nucleotide 3'-phosphodiesterase	47.5	13
P12277	Creatine kinase B-type	42.6	13
P62805	Histone H4	11.4	13
P78363	Retinal-specific ATP-binding cassette transporter	255.8	11
P00733	Alpha-enolase	47.1	10
P25705	ATP synthase subunit alpha	59.7	10
P13591	Neural cell adhesion molecule	93.3	10
Q16518	Retinal pigment epithelium-specific 65 kDa	60.9	10
P21796	Voltage-dependent anion-selective channel protein 1	30.6	10
O95639	Elongation factor 1-alpha 2	50.4	9
Q6QNW6	Histone H2B	13.9	9
P02686	Myelin basic protein	33.1	9
P80723	Brain acid soluble protein 1	22.7	8
Q00610	Clathrin heavy chain 1	191.6	8
Q03395	Rod outer segment membrane protein 1	37.2	8
P10523	S-arrestin	45.1	8
P23634	Plasma membrane calcium-transporting ATPase 4	137.8	7
Q92781	11-cis retinol dehydrogenase	35	6
Q13509	Dihydropyrimidinase-related protein	62.3	6
P07900	Heat shock protein HSP	84.6	6
P35913	Rod cGMP-specific 3',5'-cyclic phosphodiesterase	98.3	6
P11166	Solute carrier family 2	54	6
P07195	L-lactate dehydrogenase	36.6	5
P00558	Phosphoglycerate kinase 1	44.6	5
P35243	Recoverin	23.1	5
Q02846	Retinal guanylyl cyclase 1 precursor	120	5
P47804	RPE-retinal G protein-coupled receptor	31.9	5
P08133	Annexin	75.5	4
P62988	Ubiquitin	8.6	4
Q15836	Vesicle-associated membrane protein 3	11.3	4
P08237	6-phosphofructokinase	85.1	3
P02511	Alpha crystallin	20.1	3
P00505	Aspartate aminotransferase	47.4	3
P43320	Beta crystallin	23.4	3
P43003	Excitatory amino acid transporter 1	59.5	3
P09972	Fructose-bisphosphate aldolase C	39.4	3
P06737	Glycogen phosphorylase	97.1	3
P11142	Heat shock cognate 71 kDa protein	70.9	3
Q14108	Lysosome membrane protein 2	54.3	3
P35625	Metalloproteinase inhibitor 3 precursor	24.1	3
P30041	Peroxiredoxin-6	25	3
Q9H0U4	Ras-related protein Rab-1B	22.2	3
P60174	Triosephosphate isomerase	26.7	3
Q08752	40 kDa peptidyl-prolyl cis-trans isomerase	40.7	2
P08195	4F2 cell-surface antigen heavy chain	57.9	2
Q13510	Acid ceramidase precursor	44.6	2
P01009	Alpha-1-antitrypsin precursor	46.7	2
P29973	cGMP-gated cation channel alpha 1	79.1	2
P00403	Cytochrome c oxidase subunit 2	26.5	2
P09104	Gamma-enolase	47.2	2
P06744	Glucose-6-phosphate isomerase	63.1	2
P17066	Heat shock 70 kDa protein 6	71	2
Q12931	Heat shock protein 75 kDa	80.1	2
Q8P9F7	Leucine-rich repeat-containing protein 8B	92.3	2
Q14894	Mu-crystallin homolog	33.6	2
Q9P2S2	Neurexin-2-alpha precursor	184.9	2
Q00325	Phosphate carrier protein	40.1	2
P07602	Proactivator polypeptide precursor	58.1	2
Q5NOY7	Probable phosphoglycerate mutase 4	28.5	2
O43490	Prominin-1 precursor	97.1	2
Q8TC12	Retinol dehydrogenase 11	35.4	2
Q13813	Spectrin alpha chain, brain	284.4	2
P29401	Transketolase	67.8	2
P21281	Vacuolar ATP synthase subunit B	56.5	2

a. Swiss-Protein database accession numbers.
b. Proteins were identified by LC MS/MS following off-line SCX and RP-HPLC fractionation of a tryptic digest of crude lipofuscin
c. Based on protein sequence

Table.A.3 Proteins identified from crude lipofuscin after SCX chromatography.

Appendix 2.

Statistical analysis of work conducted in Chapter 4.

A.2.1 Identification of a lysosomal enriched fraction using lysosomal enzyme assays

A.2.1.1 Acid phosphatase

ANOVA results obtained from the analysis of a comparison of the Acid phosphatase activity in each cell fraction during the isolation of an enriched lysosomal fraction:
$p = 0.00001$
The result is only significant if the p-value is less than 0.05

Post Hoc test using Tukey analysis

	Fraction 2	Fraction 3	Fraction 4
Fraction 1	0.002032167	0.001544862	0.000353720
Fraction 2		0.000637654	0.000000669
Fraction 3			0.000000179

The result is only significant if the p-value is less than 0.05. Those not significant have been highlighted in grey.
Table A.2.1 Statistical analysis of a comparison of the Acid phosphatase activity in each sedimentation fraction during the isolation of an enriched lysosomal fraction. p- values displayed in this table relate to data displayed in Figure 4.2 a

A.2.1.2 N-acetlyl β-D glucuronidase

ANOVA results obtained from the analysis of a comparison of the N-acetlyl β-D glucuronidase activity in each cell fraction during the isolation of an enriched lysosomal fraction:
$p = 0.00061$
The result is only significant if the p-value is less than 0.05

Post Hoc test using Tukey analysis

	Fraction 2	Fraction 3	Fraction 4
Fraction 1	0.011877757	0.002523523	0.000036887
Fraction 2		0.000712261	0.000216566
Fraction 3	0.000712261		0.000397864

The result is only significant if the p-value is less than 0.05. Those not significant have been highlighted in grey.
Table A.2.2 Statistical analysis of a comparison of the N-acetlyl β-D glucuronidase activity in each sedimentation fraction during the isolation of an enriched lysosomal fraction. p-values displayed in this table relate to data displayed in Figure 4.2 b.

A2.1.3 Cathepsin D

ANOVA results obtained from the analysis of a comparison of the Cathepsin D activity in each cell fraction during the isolation of an enriched lysosomal fraction: p= 0.00003

The result is only significant if the p-value is less than 0.05

Post Hoc test using Tukey analysis

	Fraction 2	Fraction 3	Fraction 4
Fraction 1	0.002032167	0.001544862	0.00035372
Fraction 2		0.00063765	0.00000067
Fraction 3	0.000637654		0.00000018

The result is only significant if the p-value is less than 0.05. Those not significant have been highlighted in grey.

Table A.2.3 Statistical analysis of a comparison of the Cathepsin D activity in each sedimentation fraction during the isolation of an enriched lysosomal fraction. p-values displayed in this table relate to data displayed in Figure 4.2 c.

Appendix 3

Student's t-tests conducted in Excel (Microsoft, USA) were used to determine the significance of results containing only two test conditions. One way ANOVA was used with Tukey's post-hoc test in SPSS (USA) to compare cell viability when multiple conditions were used to identify any significant changes.

A.3.1 Optimisation of experimental conditions

t-test analysis of the means of cells, either exposed to retinal lipofuscin or not, were conducted using Excel (Microsoft, USA) to determine if there was a significant difference between the conditions.

	Mean	Variance	p value
Cell with retinal lipofuscin	67.5	156.9	0.003
Cells minus retinal lipofuscin	95.3	146.5	0.003

Table A.3.1 t-test results used to determine whether the cell viability of cells irradiated with blue-light (400-500 nm, 2.8 mW/cm^2) for 24 hours, plus or minus retinal lipofuscin, was significantly different. The p-values in this table refer to the data found in Figure 5.3.

	Mean	Variance	p value
Cell with retinal lipofuscin	43.9	108.6	0.00003
Cells minus retinal lipofuscin	84.0	30.9	0.00003

Table A.3.2 t-test results used to determine whether the cell viability of cells irradiated with blue-light (400-500 nm, 2.8 mW/cm^2) for 48 hours, plus or minus retinal lipofuscin, was significantly different. The p-values in this table refer to the data found in Figure 5.4.

A.3.2 Determination of the phototoxicity of lipofuscin as a function of the number of granules taken up by RPE cells

A.3.2.1 Blue-light studies

ANOVA result obtained from the analysis of the quantification of retinal lipofuscin phototoxicity as a function of granule number when irradiated with blue-light (400-500 nm, 2.8 mW/cm^2):

$p = 0.00000$

The result is only significant if the p value is less than 0.05.

Post Hoc test using Tukey analysis

	10 granules	50 granules	100 granules	300 granules	500 granules	700 granules
0 granules	0. 3708	0.000013	<0.000001	<0.000001	<0.000001	<0.000001
10 granules		0.039112	0.000023	<0.000001	<0.000001	<0.000001
50 granules			0.007779	<0.000001	<0.000001	<0.000001
100 granules				<0.000001	<0.000001	<0.000001
300 granules					0.251902	0.006063
500 granules						0.383741

The result is only significant if the p value is less than 0.05. Those not significant are highlighted in grey.

Table A.3.3 Statistical analysis of the quantification of retinal lipofuscin phototoxicity as a function of granule number when irradiated with blue-light (400-500 nm, 2.8 mW/cm^2). The p-values contained within this table relate to the data displayed in Figure 5.5 (A).

A.3.2.2 White-light studies

ANOVA result obtained from the analysis of the quantification of retinal lipofuscin phototoxicity as a function of granule number when irradiated with white-light (2.8 mW/cm^2):

p = 0.01

The result is only significant if the p value is less than 0.05.

Post Hoc test using Tukey analysis

	10 granules	50 granules	100 granules	300 granules	500 granules	700 granules
0 granules	0.9316878	0.9312835	0.9029033	0.0746920	0.0089449	0.0014719
10 granules		1.0000000	0.9999999	0.3860154	0.0601822	0.0096998
50 granules			0.9999999	0.3867314	0.0603350	0.0097253
100 granules				0.4331785	0.0707025	0.0114645
300 granules					0.8916429	0.3599983
500 granules						0.9434738

The result is only significant if the p value is less than 0.05. Those not significant are highlighted in grey.

Table A.3.4 Statistical analysis of the quantification of retinal lipofuscin phototoxicity as a function of granule number when irradiated with white-light (2.8 mW/cm^2). The p-values contained within this table relate to the data displayed in Figure 5.5 (B).

ANOVA result obtained from the analysis of the quantification of retinal lipofuscin phototoxicity as a function of granule number when irradiated with white-light (13 mW/cm^2):

p = <0.00001

The result is only significant if the p value is less than 0.05.

Post Hoc test using Tukey analysis

	10 granules	50 granules	100 granules	300 granules	500 granules	700 granules
0 granules	0.10372	<0.000001	<0.000001	<0.000001	<0.000001	<0.000001
10 granules		<0.000001	<0.000001	<0.000001	<0.000001	<0.000001
50 granules			<0.000001	<0.000001	<0.000001	<0.000001
100 granules				0.006	<0.000001	<0.000001
300 granules					0.035	<0.000001
500 granules						0.191000

The result is only significant if the p value is less than 0.05. Those not significant are highlighted in grey.

Table A.3.5 Statistical analysis of the quantification of retinal lipofuscin phototoxicity as a function of granule number when irradiated with white-light (13 mW/cm^2). The p-values contained within this table relate to the data displayed in Figure 5.5 (C).

A.3.3 Assessment of optical filters in reducing the lipofuscin phototoxicity to RPE cells

A.3.3.1 Blue-light studies

ANOVA result obtained from the analysis of the effect of blue-light (400-500 nm, 2.8 mW/cm^2) irradiation and lipofuscin-loading on the cell viability of ARPE-19 cells:
p = <0.00001
The result is only significant if the p value is less than 0.05.

.

Post Hoc test using Tukey analysis

	No filter plus LF	Control filter plus LF	Filter 1 plus LF	Filter 2 plus LF
Dark control plus LF	<0.0001	<0.0001	<0.0001	<0.0001
No filter plus LF		0.0038	<0.0001	<0.0001
Control filter plus LF			<0.0001	0.0001
Filter 1 plus LF				0.9869

The result is only significant if the p value is less than 0.05. Those not significant are highlighted in grey.

Table A.3.6 Statistical analysis of the effect of blue-light (400-500 nm, 2.8 mW/cm^2) irradiation and lipofuscin-loading on the cell viability of ARPE-19 cells. The p-values contained within this table relate to the data displayed in Figure 5.10

ANOVA result obtained from the analysis of the effect of blue-light (400-500 nm, 2.8 mW/cm^2) irradiation on the cell viability of ARPE-19 cells:
p = <0.00001
The result is only significant if the p value is less than 0.05.

Post Hoc test using Tukey analysis

	No filter	Control filter	Filter 1	Filter 2
Dark	<0.0001	<0.0001	0.0037	0.8146
No filter		0.9312	0.0002	<0.0001
Control filter			0.0005	<0.0001
Filter 1				0.0185

The result is only significant if the p value is less than 0.05. Those not significant are highlighted in grey.

Table A.3.7 Statistical analysis of the effect of blue-light (400-500 nm, 2.8 mW/cm^2) irradiation on the cell viability of ARPE-19 cells. The p-values contained within this table relate to the data displayed in Figure 5.10.

A.3.3.2 White-light studies

ANOVA result obtained from the analysis of the effect of white-light (2.8 mW/cm^2) irradiation and lipofuscin-loading on the cell viability of ARPE-19 cells:
p = <0.001
The result is only significant if the p value is less than 0.05.

Post Hoc test using Tukey analysis

	No filter plus LF	Control filter plus LF	Filter 1 plus LF	Filter 2 plus LF
Dark control plus LF	0.1396	0.2321	0.3974	0.9321
No filter plus LF		0.9961	0.9350	0.4023
Control filter plus LF			0.9930	0.5895
Filter 1 plus LF				0.8132

The result is only significant if the p value is less than 0.05. Those not significant are highlighted in grey.

Table A.3.8 Statistical analysis of the effect of white-light (2.8 mW/cm^2) irradiation and lipofuscin-loading on the cell viability of ARPE-19 cells. The p-values contained within this table relate to the data displayed in Figure 5.11.

ANOVA result obtained from the analysis of the effect of white-light (2.8 mW/cm^2) irradiation on the cell viability of ARPE-19 cells:
p = <0.001
The result is only significant if the p value is less than 0.05.

Post Hoc test using Tukey analysis

	No filter	Control filter	Filter 1	Filter 2
Dark control	0.7431	0.8252	0.6110	0.9981
No filter		0.9998	0.9992	0.5802
Control filter			0.9938	0.6720
Filter 1				0.4518

The result is only significant if the p value is less than 0.05. Those not significant are highlighted in grey.

Table A.3.9 Statistical analysis of the effect of white-light (2.8 mW/cm^2) irradiation on the cell viability of ARPE-19 cells. The p-values contained within this table relate to the data displayed in Figure 5.11.

ANOVA result obtained from the analysis of the effect of white-light (13 mW/cm^2) irradiation and lipofuscin-loading on the cell viability of ARPE-19 cells:
p = <0.001
The result is only significant if the p value is less than 0.05.

Post-Hoc test using Tukey analysis

	No filter plus LF	Control filter plus LF	Filter 1 plus LF	Filter 2 plus LF
Dark control plus LF	<0.0001	<0.0001	<0.0001	<0.0001
No filter plus LF		0.0020	<0.0001	<0.0001
Control filter plus LF			0.0033	0.0007
Filter 1 plus LF				0.7704

The result is only significant if the p value is less than 0.05. Those not significant are highlighted in grey.
Table A.3.10 Statistical analysis of the effect of white-light (13 mW/cm^2) irradiation and lipofuscin-loading on the cell viability of ARPE-19 cells. The p-values contained within this table relate to the data displayed in Figure 5.12.

ANOVA result obtained from the analysis of the effect of white-light (13 mW/cm^2) irradiation on the cell viability of ARPE-19 cells:
p = <0.001
The result is only significant if the p value is less than 0.05.

Post-Hoc test using Tukey analysis

	No filter	Control filter	Filter 1	Filter 2
Dark control	<0.0001	<0.0001	<0.0001	<0.0001
No filter		0.0243	0.0001	0.0001
Control filter			0.0064	0.0085
Filter 1				0.9996

The result is only significant if the p value is less than 0.05. Those not significant are highlighted in grey.
Table A.3.11 Statistical analysis of the effect of white-light (13 mW/cm^2) irradiation on the cell viability of ARPE-19 cells. The p-values contained within this table relate to the data displayed in Figure 5.12.

ANOVA result obtained from the analysis of the effect of white-light (19 mW/cm^2) irradiation and lipofuscin-loading on the cell viability of ARPE-19 cells:
p = <0.001
The result is only significant if the p value is less than 0.05.

Post-Hoc test using Tukey analysis

	No filter plus LF	Control filter plus LF	Filter 1 plus LF	Filter 2 plus LF
Dark control plus LF	<0.0001	<0.0001	<0.0001	<0.0001
No filter plus LF		0.8869	0.0115	0.0064
Control filter plus LF			0.0431	0.0252
Filter 1 plus LF				0.9938

The result is only significant if the p value is less than 0.05. Those not significant are highlighted in grey.

Table A.3.12 Statistical analysis of the effect of white-light (19 mW/cm^2) irradiation and lipofuscin-loading on the cell viability of ARPE-19 cells. The p-values contained within this table relate to the data displayed in Figure 5.12.

ANOVA result obtained from the analysis of the effect of white-light (19 mW/cm^2) irradiation on the cell viability of ARPE-19 cells:

p = <0.001

The result is only significant if the p value is less than 0.05.

Post-Hoc test using Tukey analysis

	No filter	Control filter	Filter 1	Filter 2
Dark control	<0.0001	<0.0001	<0.0001	<0.0001
No filter		0.9741	0.0065	0.0029
Control filter			0.0156	0.0068
Filter 1				0.9784

The result is only significant if the p value is less than 0.05. Those not significant are highlighted in grey.

Table A.3.13 Statistical analysis of the effect of white-light (19 mW/cm^2) irradiation on the cell viability of ARPE-19 cells. The p-values contained within this table relate to the data displayed in Figure 5.12.

Appendix 4

Student's t-tests conducted in Excel (Microsoft, USA) were used to determine the significance of results containing only two test conditions. One way ANOVA was used with Tukey's post-hoc test in SPSS (USA) to identify any significant differences in results when multiple conditions were used.

A.4.1 Succinoylated dextrin safety

t-test analyses were conducted using Excel software (Microsoft, USA) to compare the viability of cells maintained in basal medium or basal medium supplemented with succinoylated dextrin over a 21 day period.

The p-value given in table A.4.1 refers to the difference in mean cell viability between the control cells maintained in basal medium and those in basal medium supplemented with succinoylated dextrin at the corresponding time-points.

	p-value
BMSD Day 0	0.676
BMSD Day 7	0.591
BMSD Day 14	0.410
BMSD Day 21	0.160

The result is only significant if the p value is less than 0.05. Those not significant are highlighted in grey.

Table A.4.1 Shows a comparison of the means of cells maintained in basal medium or basal medium supplemented with succinoylated dextrin (BMSD) after 0, 7, 14 and 21 days.

A.4.2 Prevention of the accumulation of lipofuscin-like fluorescence in RPE cells

ANOVAs were used to determine whether the difference in the lipofuscin-like fluorescence of cells loaded with POS in the presence or absence of GST were significant.

A.4.2.1 7 day trial

ANOVA results obtained from the analysis of lipofuscin-like fluorescence of ARPE-19 cells after 7 days under each of the conditions;
$p = 0.0003$.
The result is only significant if the p value is less than 0.05.

Post Hoc test using Tukey analysis

	BM + SD	BM + POS	BM + POS + 10 units GST	BM + POS + 4 units GST	BM + POS + 1 unit GST
BM	0.9999999	0.0039157	0.010292345	0.006069	0.005387
BM + SD		0.004249	0.011194	0.006594	0.005850
BM + POS			0.990179	0.999759	0.999949
BM + POS + 10 units GST				0.99944463	0.998508551
BM + POS + 4 units GST					0.999999631

The result is only significant if the p value is less than 0.05. Results not significant are highlighted grey
Table A.4.2 Statistical analysis of the lipofuscin-like fluorescence of ARPE-19 cells after 7 days with or without POS and or GST. The p-values contained within this table relate to data displayed in Figure 6.12

A.4.2.2 14 day trial

ANOVA result obtained from analysis of the lipofuscin-like fluorescence of ARPE-19 cells after 14 days under each of the conditions;
p = 0.000102
The result is only significant if the p value is less than 0.05.

Post Hoc test using Tukey analysis

	BM + SD	BM + POS	BM + POS + 10 units GST	BM + POS + 4 units GST	BM + POS + 1 unit GST
BM	0.999993	0.0008882	0.004857382	0.003559367	0.001880
BM + SD		0.001085	0.006022	0.004403	0.002312
BM + POS			0.882398	0.943456	0.995873
BM + POS + 10 units GST				0.999954302	0.989793712
BM + POS + 4 units GST					0.998332466

The result is only significant if the p value is less than 0.05. Results not significant are highlighted grey
Table A.4.3 Statistical analysis of the lipofuscin-like fluorescence of ARPE-19 cells after 14 days with or without POS and or GST. The p-values contained within this table relate to data displayed in Figure 6.12

A.4.2.3 21 day trial

ANOVA result obtained from analysis of the lipofuscin-like fluorescence of ARPE-19 cells after 21 days under each of the conditions;
p = 0.00000010
The result is only significant if the p value is less than 0.05.

Post Hoc test using Tukey analysis

	BM + SD	BM + POS	BM + POS + 10 units GST	BM + POS + 4 units GST	BM + POS + 1 unit GST
BM	0.999956	0.000001	0.000044	0.000017	0.000006
BM + SD		0.000001	0.000056	0.000021	0.000008
BM + POS			0.013233	0.048889	0.196012
BM + POS + 10 units GST				0.966797	0.591144
BM + POS + 4 units GST					0.948258

The result is only significant if the p value is less than 0.05. Results not significant are highlighted grey

Table A.4.4 Statistical analysis of the lipofuscin-like fluorescence of ARPE-19 cells after 21 days with or without POS and or GST. The p-values contained within this table relate to data displayed in Figure 6.12

A.4.3 Assessment of the use of GST in degrading lipofuscin in RPE cells when in its free state or when conjugated to the dextrin polymer

A.4.3.1 Lipofuscin-like fluorescence of cells measured in cells with or without lipofuscin and/or free GST.

ANOVA result obtained from analysis of the lipofuscin-like fluorescence of ARPE-19 cells under each of the conditions;

$p = <0.0001$

The result is only significant if the p value is less than 0.05.

Post Hoc test using Tukey analysis

	BM + GST	BM + LF	BM + LF + GST
BM	0.999984	0.000003	0.000003
BM + GST		0.000002	0.000002
BM + LF			1.000000

The result is only significant if the p value is less than 0.05. Results not significant are highlighted grey

Table A.4.5 Statistical analysis of the lipofuscin-like fluorescence of ARPE-19 cells with or without lipofuscin and or GST. The p-values contained within this table relate to data displayed in Figure 6.14

A.4.3.2 Lipofuscin-like fluorescence of cells measured in cells with or without lipofuscin and/or dex-GST.

ANOVA result obtained from analysis of the lipofuscin-like fluorescence of ARPE-19 cells under each of the conditions;

$p = <0.000001$

The result is only significant if the p value is less than 0.05.

Post Hoc test using Tukey analysis

	BM + GST	BM + LF	BM + LF + dex-GST
BM	0.950195	<0.000001	<0.000001
BM + dex-GST		<0.000001	<0.000001
BM + LF			<0.000001

The result is only significant if the p value is less than 0.05. Results not significant are highlighted grey

Table A.4.6 Statistical analysis of the lipofuscin-like fluorescence of ARPE-19 cells with or without lipofuscin and or dex-GST. The p-values contained within this table relate to data displayed in Figure 6.15

	Mean	Variance	p value
BM and lipofuscin	0.72	0.023	0.001149
BM, lipofuscin and dex-GST	0.527	0.027	0.001149

The result is only significant if the p value is less than 0.05

Table A.4.7 t-test results used to determine whether the mean size of lipofuscin granules in cells maintained with or without dex-GST was significantly different. The p-values contained within this table relate to data displayed in Table 6.3

	Mean	Variance	p value
BM and lipofuscin	10.852	21.714	0.017
BM, lipofuscin and GST	6.021	29.016	0.017

The result is only significant if the p value is less than 0.05

Table A.4.8 t-test results used to determine whether the mean area of cell cytoplasm occupied by lipofuscin granules in cells maintained with or without dex-GST was significantly different. The p-values contained within this table relate to data displayed in Table 6.3

Appendix 5

Solutions

10 × PBS (1000 ml)

80.0g NaCl (Sodium Chloride):
2.0g KCl (Potassium Chloride):
14.4g Na_2PO_4 (di-Sodium Hydrogen Orthophosphate anhydrous)
2.4g KH_2PO_4 (Potassium dihydrogen orthophosphate)
Disolves in 800 ml dH_2O, adjusts pH to 7.4 (using HCl), add up to 1000 ml of dH2O, mix well for use. To make 1× PBS: dilute 10× PBS 1:10 in dH_2O, mix well for use.

Trypsin –EDTA solution

0.25% (m/v) trypsin
0.05% (m/v) EDTA
Disolve in 1 × PBS, mix thoroughly, filtered using 0.2 μm filter, store at -20°C in aliquots.

Sucrose solutions (2 M)

171 g Sucrose
250 ml ddH_2O.
Subsequent sucrose solutions were generated by diluting the stock solution with ddH_2O

Tris-acetate (40 mM, 1000 ml)

242 g Tris (Trizma) base
57.1 ml Glacial acetic acid
Make up to l L with ddH_2O. The stock Tris-acetate was diluted with ddH_2O according to the concentration needed.

SDS sample buffer (5x)

5 ml Glycerol
1 g SDS
2.56 ml 0.1 M DTT
2.13 ml 0.5 M Tris-HCl pH 6.8
Sample buffer was stored in 1 ml aliquots at -20°C until needed. Sample buffer was diluted to 1x using ddH_2O when needed.

DTT solution

A stock 1 M solution of DTT was created by dissolving 1.5425 g of DTT in 10 ml of ddH_2O. The stock solution was diluted according to the required concentration for experiments.

Gel solutions

	Resolving gel (10%) (10 ml)	Stacking gel (5%) (3 ml)
Distilled H2O	4.0 ml	2.1 ml
30% acrylamide mix	3.3 ml	500 µl
1.5 M Tris/HCl pH 8.8	2.5 ml	-
1.0 M Tris/HCl pH 6.8	-	380 µl
10% SDS	100 µl	30 µl
10% APS	100 µl	30 µl
TEMED	4 µl	3 µl

Appendix 6

Publications and Presentations

Publications:

Richardson SC, Wallom KL, Ferguson EL, Deacon SP, **Davies MW**, Powell AJ, Piper RC, Duncan R
The use of fluorescence microscopy to define polymer localisation to the late endocytic compartments in cells that are targets for drug delivery.
Journal of Controlled Release. 2008 Apr 7;127(1):1-11.

Ng KP, Gugiu B, Renganathan K, **Davies MW**, Gu X, Crabb JS, Kim SR, Rózanowska MB, Bonilha VL, Rayborn ME, Salomon RG, Sparrow JR, Boulton ME, Hollyfield JG, Crabb JW
Retinal pigment epithelium lipofuscin proteomics.
Molecular and Cellular Proteomics. 2008 Jul;7(7):1397-405.

Posters:

M.W. Davies and M.E. Boulton
Effect of antihypertensive drugs on lipofuscin accumulation the retinal pigment epithelium.
ISOCB. 2006. Cambridge, UK.

M.W. Davies, M.B. Rozanowska, J.W. Crabbe, M.E. Boulton
Preparation and proteomic analysis of an *in vitro* model of retinal lipofuscin.
ARVO. 2007. Fort Lauderdale, Florida USA.

P. Gupta, **M.W. Davies**, R. Jain, M. Mainster, M. Rozanowska, M. E. Boulton
Effect of Lipofuscin Density on Acute Phototoxicity in Retinal Pigment Epithelial Cells
ARVO. 2008. Fort Lauderdale, Florida, USA